AD-A042 672 PURDUE UNIV LAFAYETTE IND COMPUTATIONAL FLUID MECHAN--ETC F/G 20/4
COMPARISONS OF THEORETICAL PROFILES FOR A TWO-DIMENSIONAL TIME---ETC(U)
JUN 77 R K SCHARNHORST, J D WALKER AF-AFOSR-2707-74

UNCLASSIFIED CFMTR-77-1 AFOSR-TR-77-0877 NL

1 OF 3

ADA042-672

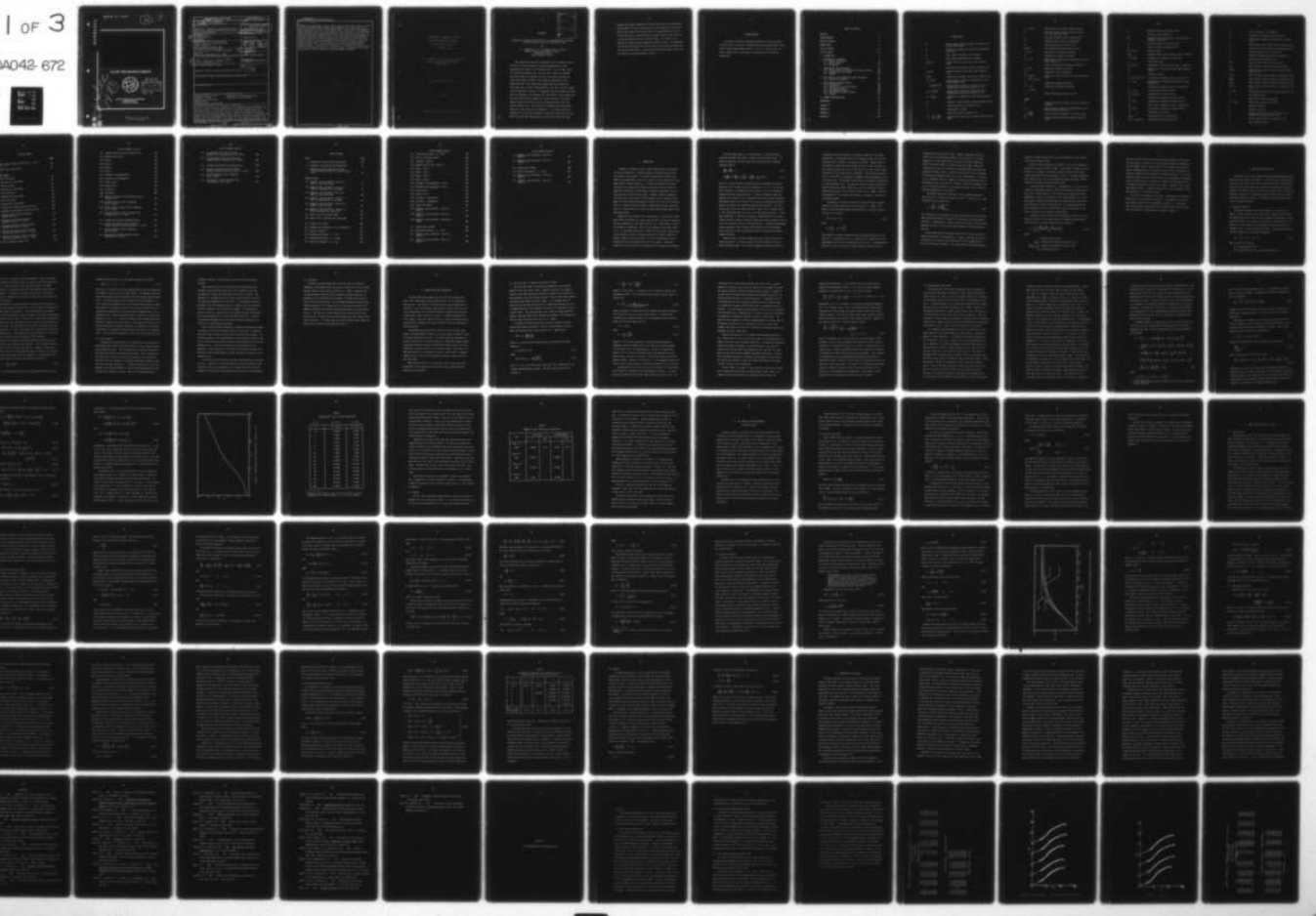

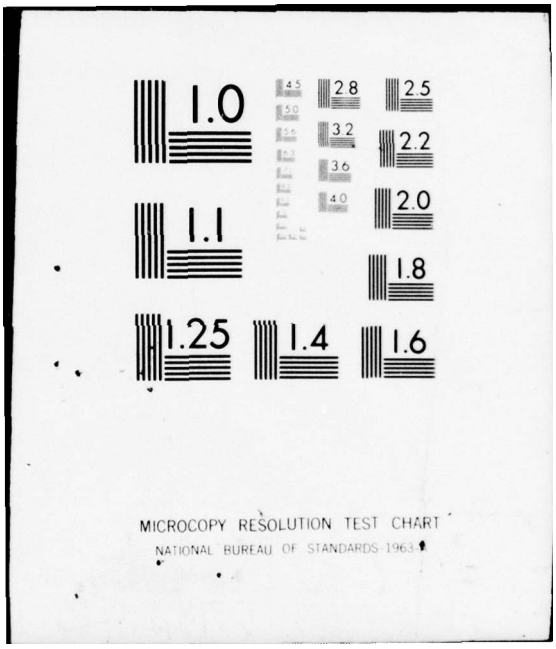
1.0
1.1
1.25
1.4
1.6
1.8
2.0
2.2
2.5
2.8
3.2
3.6
4.0
4.5
5.0
5.6
MICROCOPY RESOLUTION TEST CHART
NATIONAL BUREAU OF STANDARDS-1963

AFOSR-TR- 77-0877

12

2

Computational

FLUID MECHANICS GROUP

SCHOOL OF MECHANICAL ENGINEERING
PURDUE UNIVERSITY
LAFAYETTE, INDIANA

REPORT DOCUMENTATION PAGE

READ INSTRUCTIONS BEFORE COMPLETING FORM

1. REPORT NUMBER	2. GOVT ACCESSION NO.	3. RECIPIENT'S CATALOG NUMBER
AFOSR-TR- 77-0877		

4. TITLE (and Subtitle)

COMPARISONS OF THEORETICAL PROFILES FOR A TWO-DIMENSIONAL TIME-MEAN TURBULENT BOUNDARY LAYER WITH EXPERIMENTAL DATA.

5. TYPE OF REPORT & PERIOD COVERED

INTERIM ≠ rept.
1 Feb 76 — 31 Jan 77

6. PERFORMING ORG. REPORT NUMBER

CFMTR-77-1

7. AUTHOR(s)

R. K. SCHARNHORST
J. D. A. WALKER
D. E. ABBOTT

8. CONTRACT OR GRANT NUMBER(s)

AFOSR 74-2707

9. PERFORMING ORGANIZATION NAME AND ADDRESS

THERMAL SCIENCES & PROPULSION CENTER
PURDUE UNIVERSITY
WEST LAFAYETTE, INDIANA 47907

10. PROGRAM ELEMENT, PROJECT, TASK AREA & WORK UNIT NUMBERS

2307A2
61102F

11. CONTROLLING OFFICE NAME AND ADDRESS

AIR FORCE OFFICE OF SCIENTIFIC RESEARCH/NA
BLDG 410
BOLLING AIR FORCE BASE, D C 20332

12. REPORT DATE

June 1977

13. NUMBER OF PAGES

230

14. MONITORING AGENCY NAME & ADDRESS *(if different from Controlling Office)*

AF-AFOSR-2707-74

15. SECURITY CLASS. *(of this report)*

UNCLASSIFIED

15a. DECLASSIFICATION/DOWNGRADING SCHEDULE

16. DISTRIBUTION STATEMENT *(of this Report)*

Approved for public release; distribution unlimited.

233 p.

17. DISTRIBUTION STATEMENT *(of the abstract entered in Block 20, if different from Report)*

18. SUPPLEMENTARY NOTES

19. KEY WORDS *(Continue on reverse side if necessary and identify by block number)*

TURBULENT BOUNDARY LAYER
ASYMPTOTIC METHODS
UNSTEADY WALL LAYER MODEL
INCOMPRESSIBLE
TWO-DIMENSIONAL TIME-MEAN FLOW
COMPARISON WITH EXPERIMENTAL DATA
EVALUATION OF PROFILE MODELS

20. ABSTRACT *(Continue on reverse side if necessary and identify by block number)*

Four theoretical models are considered for the time-mean velocity profile in a constant property turbulent boundary which is two-dimensional and steady in the time-mean sense. For the inner region of a turbulent boundary layer, the Van Driest (1956) and extended Van Driest models are compared with the more recent unsteady wall layer model. (Walker & Abbott, 1977; Walker & Scharnhorst, 1977). Comparisons with inner region data suggest that the unsteady wall layer model gives a better representation of the data; for this reason and for theoretical reasons, it is suggested that the extended Van Driest model be abandoned. The

DD FORM 1 JAN 73 1473 EDITION OF 1 NOV 65 IS OBSOLETE

UNCLASSIFIED (cont on p 1473B)

SECURITY CLASSIFICATION OF THIS PAGE (When Data Entered)

409670

(cont'd p 1473A)

unsteady wall layer model is then coupled with two outer region models, namely the 'law of the wake' and an outer region similarity profile, to give two composite profiles for the entire boundary layer. Both profiles are compared with experimental data over a wide range of flow conditions. It is found that three parameter fits using the unsteady wall layer model and the 'law of the wake' give excellent representations of the data; however the data comparisons strongly suggest that the wall layer flow is not universal. One parameter fits were carried out with the unsteady wall layer model and the outer region similarity profile; the representation of equilibrium flow data is good and shows the proper trend to self-similarity in zero and favorable pressure gradient flows. This trend is not observed in adverse pressure gradient equilibrium flows. Two parameter fits carried out with the similarity profiles also show good representation of non-similar data. A discussion of how these results can be used to construct a prediction method is given.

(1473B)

COMPARISONS OF THEORETICAL PROFILES FOR A TWO-DIMENSIONAL TIME-MEAN TURBULENT BOUNDARY LAYER WITH EXPERIMENTAL DATA

by

R.K. Scharnhorst, J.D.A. Walker and D.E. Abbott
School of Mechanical Engineering
Thermal Sciences and Propulsion Center
Purdue University

Technical Report CFMTR-77-1

June 1977

ABSTRACT

Comparisons of Theoretical Profiles for a Two-Dimensional Time-Mean Turbulent Boundary Layer with Experimental Data

-by-

R. K. Scharnhorst, J. D. A. Walker and D. E. Abbott
Thermal Sciences and Propulsion Center
Purdue University
West Lafayette, Indiana

Four theoretical models are considered for the time-mean velocity profile in a constant property turbulent boundary which is two-dimensional and steady in the time-mean sense. For the inner region of a turbulent boundary layer, the Van Driest (1956) and extended Van Driest models are compared with the more recent unsteady wall layer model (Walker & Abbott, 1977; Walker & Scharnhorst, 1977). Comparisons with inner region data suggest that the unsteady wall layer model gives a better representation of the data; for this reason and for theoretical reasons it is suggested that the extended Van Driest model be abandoned. The unsteady wall layer model is then coupled with two outer region models, namely the "law of the wake" and an outer region similarity profile, to give two composite profiles for the entire boundary layer. Both profiles are compared with experimental data over a wide range of flow conditions. It is found that three parameter fits using the unsteady wall layer model and the "law of the wake" give excellent representations of the data; however the data

comparisons strongly suggest that the wall layer flow is not universal. One parameter fits were carried out with the unsteady wall layer model and the outer region similarity profile; the representation of equilibrium flow data is good and shows the proper trend to self-similarity in zero and favorable pressure gradient flows. This trend is not observed in adverse pressure gradient equilibrium flows. Two parameter fits carried out with the similarity profiles also show good representation of non-similar data. A discussion of how these results can be used to construct a prediction method is given.

ACKNOWLEDGMENTS

The authors gratefully acknowledge support of this work by the Air Force Office of Scientific Research under grant number AFOSR-74-2707. The Air Force Program Managers were Lt. Col. R. C. Smith and Lt. Col. Lowell Ormand; their encouragement and cooperation are gratefully appreciated.

TABLE OF CONTENTS

NOMENCLATURE

A^+	viscous damping length parameter associated with the Van Driest model
A_o	constant in unsteady wall layer model (equations 3.17, 3.23)
C_i	inner region logarithmic law "constant"
C_o	outer region logarithmic law "constant"
$f_1(x,y^+)$	stream function for the inner layer (equation 5.11)
F	Van Driest mixing length function (equation 3.2)
$F_1(x,\eta)$	stream function for the outer layer (equation 5.3)
$h_i(\vec{x})$	optimization parameter constraints (equation 2.3)
$H = y^+/2S$	scaled normal variable for unsteady wall layer model (equation 3.9)
$= y^+/2\sqrt{S^2 + t_o^+}$	scaled normal variable for preferred form of unsteady wall layer model (equation 3.16)
$H_o = y^+/2\sqrt{t_o^+}$	scaled normal variable for preferred form of unsteady wall layer model (equation 3.16)
$H_1 = y_1^+/2S$	parameter in unsteady wall layer model (equation 3.9)
K	constant in eddy viscosity formula (equation 5.36)
ℓ	mixing length function (equation 3.1)
L	representative length
L	Heaviside function (equation 3.9)
$p^+ = \frac{-\nu}{u_\tau^3} U_e \frac{dU_e}{dx^*}$	dimensionless inner layer pressure gradient parameter

$U_1 = \partial F_1/\partial \eta$	dimensionless outer region defect velocity
U^+	the inner region time-mean velocity profile (= $\bar{u}^+$ for the inner layer)
v'	fluctuating normal velocity (dimensional)
$\bar{v}^*$	time-mean normal velocity (dimensional)
W	function defined by equation (3.21)
$W(y/\delta)$	wake function defined by equation (4.5)
$x = x^*/L$	dimensionless streamwise coordinate
x^*	dimensional streamwise coordinate
$x^+ = x^*/\lambda$	dimensionless streamwise coordinate for the inner layer (section 3)
$\vec{x}$	vector of optimization parameters (section 2)
$y = y^*/L$	dimensionless normal coordinate
y^*	dimensional normal coordinate
$y^+ = u_\tau y^*/\nu$ $= Re\, u^* U_\infty(x) y$	scaled inner region normal coordinate (dimensionless)
z^*	dimensional spanwise coordinate
$z^+ = z^*/\lambda$ $= u_\tau z/\nu\lambda^+$	dimensionless spanwise coordinate
Z	function defined by equation (3.19)

Greek

α	constant defined in equation (5.9) for similarity analysis
α_i	small positive constants associated with penalty function method (section 2)
$\beta = \frac{-\Delta_0 U'_\infty}{u^* U_\infty}$	pressure gradient parameter in the outer layer
β_c	Clauser pressure gradient parameter (equation 5.30)

P	function defined by equation (3.20)
q	the ratio Δ_0/u^* (section 5)
$\vec{q}_j$	gradient vector with respect to the optimization parameters (section 2)
Q	function defined by equation (3.18)
R	function defined by equation (3.17)
$Re = U_0 L/\nu$	Reynolds number
Re_δ	Reynolds number based on boundary-layer thickness
$S = u_\tau\sqrt{T/\nu}$	parameter in unsteady wall layer model
t	time (dimensional)
$t^+ = u_\tau^2 t/\nu$	dimensionless time (for inner layer - section 3)
t_0^+	parameter in unsteady wall layer model (equation 3.16)
T	mean burst period
$u = u(x^+,y^+,z^+,t^+)$	instantaneous streamwise velocity (section 3)
$u^+ = u/u_\tau$	dimensionless instantaneous streamwise velocity (section 3)
u'	fluctuating streamwise velocity (dimensional)
$u_\tau = \tau_w/\rho$	friction velocity (dimensional)
$u^* = u_\tau/U_e(x)$	dimensionless friction velocity
$\overline{u}^*$	dimensional time-mean streamwise profile
$\overline{u} = \overline{u}^*/U_0$	dimensionless time-mean streamwise profile
$\overline{u}_0^*$	outer region streamwise velocity (dimensional)
$\overline{u}^+ = \overline{u}^*/u_\tau$	dimensionless time-mean streamwise profile
U_0	representative velocity
$U_e(x)$	mainstream velocity (dimensional)
$U_\infty(x) = U_e(x)/U_0$	dimensionless mainstream velocity

γ_0	Euler's constant, 0.5772156649...
δ	boundary-layer thickness (dimensionless)
δ^*	displacement thickness (dimensionless, equation 5.31)
Δ_0	dimensionless outer region length scale (section 5)
Δ_C	Clauser outer region length scale (equation 5.44)
ε	root-mean-square error (equation 1.5)
$\tilde{\varepsilon}$	modified root-mean-square error (equation 2.2)
$\bar{\varepsilon}$	average root-mean-square error
$\varepsilon(\eta)$	eddy viscosity function (equation 5.37)
ε_0	eddy viscosity function for the outer layer
$\varepsilon_M(\eta)$	eddy viscosity function (Mellor & Gibson (1966), equation 5.43)
$\varepsilon_S(\eta)$	eddy viscosity function defined in equation (5.45)
$\varepsilon_N(\eta)$	eddy viscosity function defined in equation (5.58)
$\varepsilon_0(\eta)$	eddy viscosity function defined in equation (5.55)
$\varepsilon_s(\eta)$	eddy viscosity function defined in equation (5.58) for N = 5
$\eta = y/\Delta_0$	scaled dimensionless outer variable (equation 5.5)
κ	von Kármán constant
λ	mean streak spacing (dimensional)
$\lambda^+ = u_\tau\lambda/\nu$	dimensionless mean streak spacing
μ	absolute viscosity
ν	kinematic viscosity
$\vec{\nu}_i$	the search direction at the i^{th} step in the optimization procedure (section 2)
Ξ	triple integral defined in equation (3.10)
Π	wake strength parameter

ρ	fluid density (constant)
σ	dimensionless stress function (equation 5.1)
σ_1	scaled stress function in the inner layer (equation 5.12)
Σ_1	scaled stress function in the outer layer (equation 5.4)
τ	total shear stress (dimensional)
$\tau_w = \mu \left.\frac{\partial \bar{u}^*}{\partial y^*}\right\|_{y^*=0}$	wall shear (dimensional)
$\tau^+ = \tau/\tau_w$	dimensionless total shear stress

Nomenclature and Units for Tables

In Appendices A, B, C and D in this report, experimental data are tabulated. The units for these data and definitions are given below.

Symbol	English	Metric
NU = ν	ft^2/sec	m^2/sec
XSTA = x^*	feet	meters
UE = $U_e(x^*)$	ft/sec	m/sec
UTAU = u_τ	ft/sec	m/sec
DUEDX = $U_e'(x^*)$	1/sec	1/sec
P+ = p^+	-	-
BETA = β	-	-
DELTA = $L\delta$	in.	cm.
DELTA* = $L\delta^*$	in.	cm.
THETA - momentum thickness	in.	cm.
EPSILON = ε	-	-
MEAN EPSILON = $\bar{\varepsilon}$	-	-
PI = Π	-	-

LIST OF FIGURES

LIST OF FIGURES (cont'd)

LIST OF FIGURES (cont'd)

LIST OF TABLES

LIST OF TABLES (cont'd)

LIST OF TABLES (cont'd)

1. INTRODUCTION

A number of time-mean velocity profile models have been proposed for the two-dimensional, constant property, turbulent boundary layer. The purpose of this report is to present comparisons of several such models with experimental data and to offer a critical evaluation of each model based on these comparisons. It should be stated at the outset that while poor comparisons with data constitute a strong reason for rejecting or modifying a given model, no amount of good data fits can ever prove the validity of that model. However, favorable agreement with data over a wide range of flow conditions gives a degree of confidence in a given theory and seems the logical first step in the development of a reliable prediction method. Consequently the main objective here is to observe how well several velocity profile models compare with experimental data.

Specifically four models will be considered. The Van Driest (1956) model (with and without its various modifications for pressure gradients) and the unsteady wall layer model (Walker et al., 1976; Walker & Abbott, 1977; Walker & Scharnhorst, 1977) will be compared in the inner region in §3. In the outer region Coles' (1956) "law of the wake" and an outer region similarity profile (discussed by Mellor and Gibson (1966) and Fendell (1972)) will be considered in §4 and §5 respectively, each in conjunction with the unsteady wall layer inner model. A detailed description of each model will be delayed until the appropriate section.

All four models apply to a two-dimensional, constant property, turbulent boundary layer which is steady in the time-mean sense. The governing equations are mass continuity and the streamwise momentum equation given by,

$$\frac{\partial \bar{u}^*}{\partial x^*} + \frac{\partial \bar{v}^*}{\partial y^*} = 0, \tag{1.1}$$

$$\bar{u}^* \frac{\partial \bar{u}^*}{\partial x^*} + \bar{v}^* \frac{\partial \bar{u}^*}{\partial y^*} = U_e \frac{dU_e}{dx^*} + \nu \frac{\partial^2 \bar{u}^*}{\partial y^{*2}} - \frac{\partial}{\partial y^*} (\overline{u'v'}), \tag{1.2}$$

Here (x^*, y^*) are Cartesian coordinates with corresponding time-mean velocities $(\bar{u}^*, \bar{v}^*)$ and fluctuating components (u', v'); ν is the kinematic viscosity. The Reynolds normal stresses in (1.2) are neglected thereby excluding relaminarization or incipient separation where the gradient with respect to x^* of these terms may possibly become important. The Reynolds shear stress term, $-\overline{u'v'}$, marks the distinguishing feature between the laminar and turbulent boundary-layer equations. The functional form of both the normal and shear stress terms is unknown and it is this information which is lost in the time averaging process. It has been traditional in the past to attempt to postulate the form of these unknown functions based on the belief that constitutive relations exist relating the Reynolds stresses to the mean profile. Alternative approaches, such as turbulent kinetic energy, obtain equations for the Reynolds stress terms but at the considerable expense of introducing additional unknown functions.

Before moving to the data comparisons there are two points which deserve attention. The first concerns a feature common to all four models mentioned above. Each contain independent parameters which can

be adjusted to alter the profile form and one objective of the data comparisons is to determine what set of parameter values best fits the given data and to discern, if possible, any trends. However there is one quantity, namely the time-averaged friction or shear velocity, u_τ, which appears either explicitly or implicitly in all the profile models and which will be treated here as a parameter. There may be some question as to why this is considered a parameter since experimental values are always given. The primary reason concerns the method of determining u_τ from experimental data. An excellent review of various techniques is given by Brown and Joubert (1969) and a critical discussion of those techniques and others can be found in Walker, et al. (1976). Basically the methods fall into three classifications: graphical, indirect and direct measurements.

The graphical techniques include the classical Clauser crossplot method and a secant method described by Kline et al. (1967). The Clauser crossplot method assumes the existence of a universal "law of the wall" or "log-law":

$$\bar{u}^+ = \frac{1}{\kappa} \ell n\, y^+ + C_i \,, \tag{1.3}$$

where

$$\bar{u}^+ \equiv \frac{\bar{u}^*}{u_\tau} \,, \quad y^+ \equiv \frac{u_\tau y^*}{\nu} \,.$$

This relation is used in conjunction with the measured data to plot $\bar{u}^*$ versus y^*. A determination of u_τ is made from the intersection of the experimental profile and the relation given by (1.3). To implement this technique κ and C_i are usually assumed constant, with 0.41 and 5.0,

respectively, being typical values. However, suggested values for κ vary from 0.39 by Schlichting (1968) to 0.44 by Kays et al. (1970). Suggested C_i values range from 4.9 by Cebeci and Smith (1974), and Mellor and Gibson (1966) to 5.56 by Schlichting (1968). Empirical relations for κ and C_i as functions of Reynolds number have even been proposed by Simpson (1970). Clearly such variations are not palatable if accurate and reliable values for u_τ are to be obtained. In general, C_i for a boundary layer will depend on the flow conditions and should be expected to be a function of x^* (Fendell, 1972); the assumption that C_i is a universal constant is not supported by Walker et al. (1976) or the data comparisons in this report.

The secant method uses the slope of a line through data points near the wall to estimate the slope at the wall. A value of u_τ is then calculated from its definition:

$$u_\tau \equiv \sqrt{\frac{\tau_w}{\rho}} = \sqrt{\nu \left.\frac{\partial \bar{u}^*}{\partial y^*}\right)_{y^*=0}} \quad . \tag{1.4}$$

This technique is questionable since near-wall data may not be reliable due to probe interference; moreover this technique is an extrapolation procedure. Extrapolation is always a dangerous procedure but would seem especially so here in view of the rapid variation of the profile near the wall.

Preston tubes and flush-mounted surface hot film probes represent indirect techniques for determining u_τ. However, they rely on the law of the wall for calibration and specifically on the assumption that κ and C_i are universal constants. Thus they have the same deficiencies as

Clauser's crossplot method and of course give nearly the same results (Strickland & Simpson, 1973).

The only direct measurement instrument is the floating element as described by Brown and Joubert (1969). Even though it appears to offer promise, it is subject to secondary pressure forces due to the gap around the element and flow through its cavity. This makes calibration very difficult but it has been attempted by Brown and Joubert (1969), Pierce and Zimmerman (1972) and Miller (1972).

In view of these uncertainties in determining u_τ, it will be considered an independent parameter which can be adjusted to generate the best fit to a given data set. At the same time, although the quoted experimental values are considered to be rough estimates of u_τ, large discrepancies between the experimental and optimized value obtained in this study would clearly be unacceptable. The tabulated data (to be given subsequently in this report) reveal that the differences in the two u_τ values are not large but are significant.

It remains to define the basis for determining a best fit and the best-fit criterion is the second point which deserves attention here. For this study a root-mean-square error was defined as:

$$\epsilon^2 = \frac{1}{N} \sum_{n=1}^{N} \left[\frac{\overline{u}^*_{Data}(y^*_n) - \overline{u}^*_{Analytical}}{U_e} \right] , \qquad (1.5)$$

where

$N \equiv$ number of data points,

$\overline{u}^*_{Data} \equiv$ experimentally measured velocity at y^*_n,

$\overline{u}^*_{Analytical} \equiv$ appropriate analytical profile at y^*_n,

$U_e \equiv$ freestream velocity.

An error criterion based on the normal distance between the data point and the analytical profile could be defined and indeed was attempted by York and Abbott (1973). However there is an iteration involved which was not implemented by York and Abbott (1973) and this resulted in an unnatural weighting being assigned to the near wall points. It is felt that the standard error criterion given by (1.5) represents an objective basis of comparison and in addition it parallels the technique used in the Stanford Conference (Coles & Hirst, 1969). The best fit to a given experimental profile is defined as that set of profile parameter values which minimizes ε as defined by (1.5).

The plan of the report is as follows. The particular optimization techniques will be discussed in Section 2. The comparison of the two inner region profiles will be presented in Section 3. In Sections 4 and 5 the two outer region models will be tested and a critical evaluation of each model will conclude this report in Section 6.

2. OPTIMIZATION TECHNIQUES

To minimize ε one of two different optimization techniques was used depending on the model to be tested. For the Van Driest, unsteady wall layer and Coles' models, the efficient Newton-Greenstadt gradient method was applied, since each model can be written as an analytical function. However, the similarity profile discussed by Fendell (1972) involves the numerical solution of a differential equation and here a direct search technique proved more feasible. The important features of each technique are summarized below.

2.1 Newton-Greenstadt

The Newton-Greenstadt minimization method is a variation of a general iterative technique and is described in detail by Bard (1974). The Newton nomenclature signifies that a quadratic approximation to the objective function (ε) is made at an estimate of the minimum at $\vec{x} = \vec{x}_i$. Here $\vec{x}$ is a vector which has as components, the parameters which are allowed to vary in the optimization procedure. The necessary condition for the existence of an extremum then becomes:

$$\vec{x}_{i+1} = \vec{x}_i - H_i^{-1} \vec{q}_i = \vec{x}_i + \vec{v}_i, \tag{2.1}$$

where for the i^{th} iteration:

$\vec{x}_i \equiv$ the parameter vector,

$H_i \equiv$ the Hessian (matrix of second derivatives of ε),

$\vec{q}_i \equiv$ the gradient vector, $\partial\varepsilon/\partial x_i$,

$\vec{v}_i \equiv$ the search direction.

Equation (2.1) is often referred to as Newton's method and in practice to assure convergence of the method, it is necessary for H_i to be positive definite. However this may not be the case in general, except as the minimum is approached; if there is a small negative eigenvalue associated with $H_i = H(\vec{x}_i)$ then the step given by (2.1) will be such that optimization search will be driven away from the minimum. On the other hand if H_i has a small positive eigenvalue, then equation (2.1) implies a large step in the parameter direction associated with that eigenvalue; this situation is often not desirable. The modification of Newton's method to overcome these difficulties that was used here is due to Greenstadt and is discussed by Bard (1974). The basis of the method is to expand the Hessian in terms of its eigenvalues and eigenvectors. If a negative eigenvalue is encountered it is made positive by taking the absolute value; if the ratio of the largest to the smallest eigenvalue is too large ($\gtrsim 10^5$), the smallest eigenvalue is arbitrarily increased. With these redefinitions of the eigenvalues of H_i (when the problem occurs), a revised Hessian may be calculated in terms of the old eigenvectors and new eigenvalues. The object of this modification is to ensure that the optimization will always proceed in the right direction and also that it will not be misled into taking too large a step in one of the parameter directions. The iteration prescription (2.1) can now be used safely to execute the algorithm. At any stage in the iterative procedure, the step indicated by (2.1) may be too large which can be rectified by reducing the magnitude of the

vector $\vec{\nu}_i$ until a successful step has been taken. Here a successful step is defined as one which leads to a smaller value of the objective function. Once a successful step was taken, a process of either interpolation or extrapolation was used to accelerate the progress of the algorithm. This general technique is described by Bard (1974, p. 112-113). Convergence occurs when the step size is less than some specified tolerance.

To implement the Newton-Greenstadt algorithm it was necessary to evaluate the gradient and Hessian for ε, and to compute the eigenvalues and eigenvectors of the Hessian. The gradient vector was computed directly from the analytical profile expression; the Gauss approximation to the Hessian (Bard, 1974, p. 96) was used. This latter approximation was chosen solely for convenience and has no effect on the accuracy of the final result since the Hessian is used only to indicate the proper search direction. In fact at any stage it is only necessary to have an approximation to H_i. The eigenvalues and eigenvectors of H_i were computed by two Purdue University Computer Center routines.

In practice the Newton-Greenstadt procedure performed very well. The Hessian H_i was always positive definite. Final gradient values on the order of 10^{-6} and smaller were typical. However in some cases, particularly those with large adverse pressure gradients, it was necessary to introduce penalty function techniques. Following Bard (1974, p. 159) the objective function was modified according to:

$$\tilde{\varepsilon} = \varepsilon + \sum_{i=1}^{N} \alpha_i / h_i(\vec{x}). \tag{2.2}$$

Here ε is the root-mean-square error as previously defined and $h_i(\vec{x})$

represents the constraints on the profile parameters such that:

$$h_i(\vec{x}) > 0, \quad i = 1, \ldots, N. \tag{2.3}$$

Here the α_i's are small positive constants whose values are dictated by the range of values of h_i and ε (Bard, 1974). The gradient vector and Hessian were appropriately altered with the Gauss approximation applied to H_i. The basic concept behind the penalty function approach is to force the profile parameters away from values which they cannot assume; for example in the present problem u_τ must always be positive and if a situation was encountered in the optimization procedure where u_τ was approaching zero, then the procedure given in equation (2.2) was implemented with say, $h_1 = u_\tau$. Once the minimum of the redefined objective function in equation (2.2) was found, α_1 was reduced by a factor of 10 and the optimization procedure continued. By continuing this process iteratively $\tilde{\varepsilon}$ is eventually reduced arbitrarily close to ε in equation (2.2). This technique performed very well in the more difficult cases.

2.2 Direct Search

To optimize the composite profile consisting of the unsteady wall layer model and the outer similarity profile, a direct search minimization procedure was used. This technique has the distinct advantage of only requiring values of the objective function. This is important in the case of the similarity profile since gradients of the objective function (which are required in the Newton-Greenstadt procedure) would have to be evaluated numerically. The basic procedure was to vary one parameter such that the objective function always decreased while holding the other parameters constant. When a local minimum had been

bracketed, quadratic interpolation was used to refine the minimum location.

More specifically an initial estimate of the optimum profile parameter values was made along with initial parameter step sizes. The objective function was evaluated at the initial location. One parameter was incremented by the initially specified step size while the remaining parameters were held fixed. If the objective function decreased, then the stepping process was repeated until the objective function increased; this bracketed the minimum. If the objective function initially increased, then the original estimate of the parameter was decreased by the initially specified step size. As before the remaining parameters were held constant and the process was continued until the minimum was bracketed.

Once a minimum had been bracketed, a quadratic interpolation scheme was applied to refine the parameter value at the minimum. A quadratic curve was fitted through the three points surrounding the minimum. The resulting expression was differentiated to determine the location of the curve's minimum and the objective function was evaluated at this refined parameter value. Since the objective function variation was not quadratic, it was necessary to continue the interpolation process until there was no appreciable change in either the objective function or the parameter value.

The direct search minimization procedure described above functioned very well. Typically less than 100 objective function evaluations were required for one and two parameter fits. However when more than two parameters are optimized, the procedure does become very time consuming.

2.3 Discussion

For both the Newton-Greenstadt and direct search minimization techniques, considerable effort was taken to assure that a valid minimum had been found for each velocity profile fit. After a candidate best-fit was obtained, different initial parameter estimates were made to determine if the same minimum was achieved. Different step sizes and error criteria were also used. For the Newton-Greenstadt procedure the results presented in this report are for a step size tolerance of 10^{-8}. However essentially the same fits were obtained when this was decreased to 10^{-10}. For the direct search technique the relatively small step sizes and error criteria that were used produced only very slight differences in the fits. In either case, the results given in this report are those with the smallest root-mean-square error, ε.

3. INNER REGION DATA COMPARISONS

The data comparisons between the Van Driest and unsteady wall layer inner region mean velocity profile models will be presented in this section. The reason for considering inner region comparisons is two-fold. First, and foremost, they provide a direct test of the two inner region models to be considered without introducing any question of which outer region profile is the best. A second and mainly practical reason is that the results of the inner region optimization serve as good initial estimates for the full profile fits to be presented in the next section.

To determine those points which truly lie within the wall layer region, the experimentally reported u_τ value was used to graph $\bar{u}^+$ versus y^+ on the standard semi-log plot. The inner region was considered to extend from the wall up to and including the logarithmic region; however, a practical difficulty exists in deciding which data points lie in the logarithmic region and which lie in the outer region. The exclusion of data points which are considered to be outer region points is somewhat subjective but in practice the uncertainty usually concerns one and at most two points.

Before moving directly to a discussion of the inner region data comparisons, a description of the two inner region velocity profile models will be presented.

3.1 The Van Driest and Modified Van Driest Profiles

The Van Driest model was originally proposed for zero pressure gradient flows (Van Driest, 1956). However, because of its apparent success it has been extensively modified to account for non-zero pressure gradients, and heat and mass transfer. Many of these modifications are discussed by Cebeci and Smith (1974). It is perhaps unfair to associate the name Van Driest with all of these modifications but this is common practice in the literature and thus it is convenient to do so in this report. The modified model forms a basis for many prediction methods including Cebeci-Smith, Patankar and Spalding, and Bradshaw and Ferris; these are detailed in Kline, et al. (1969).

In spite of the many variations, the basic concept of the Van Driest model remains unaltered. Prandtl's mixing length is used to model the Reynolds shear stress term in (1.2). Specifically:

$$-\overline{u'v'} = \ell^2 \left|\frac{\partial \bar{u}^*}{\partial y^*}\right| \frac{\partial \bar{u}^*}{\partial y^*} \quad .$$

Here ℓ is a mixing length function which is written for the inner region as:

$$\ell = \kappa y^+ F(y^+, \tau^+, A^+) \tag{3.1}$$

where

$$F(y^+, \tau^+, A^+) = 1 - \exp\left\{-\frac{y^+\sqrt{\tau^+}}{A^+}\right\} \quad . \tag{3.2}$$

Here $\tau^+ = \tau/\tau_w$ is the total shear stress and A^+ is referred to as the viscous damping length parameter. The total shear stress can be written as

$$\tau^+ = \frac{\partial \bar{u}^+}{\partial y^+} + \kappa^2 F^2 y^{+2} \left(\frac{\partial \bar{u}^+}{\partial y^+}\right)^2 . \tag{3.3}$$

where $\bar{u}^+ = \bar{u}^*/u_\tau(x,Re)$. If equation (3.3) is solved for $\partial\bar{u}^+/\partial y^+$ and integrated from $y^+ = 0$ to an arbitrary point within the wall layer, it follows that

$$U^+ = \int_0^{y^+} \frac{2\tau^+}{1 + \sqrt{1 + 4\kappa^2 F^2(\xi)\xi^2\tau^+}}\, d\xi , \tag{3.4}$$

where the capital U^+ notation has been introduced to denote the portion of $\bar{u}^+$ which is strictly an inner region profile. It follows from integrating the momentum equation (1.2) and neglecting the convective terms that the total shear stress is

$$\tau^+ = 1 + p^+ y^+ \tag{3.5}$$

where

$$p^+ = -\frac{\nu}{u_\tau^3} U_e \frac{dU_e}{dx^*} . \tag{3.6}$$

Equation (3.5) is often referred to as the Couette approximation (Patankar & Spalding, 1968) and it is of interest to briefly examine in what sense (3.5) is an approximation. For pipe or channel flow equation (3.5) is exact; for boundary-layer flow neglecting the convective terms does incur an error in (3.5) for any finite value of the Reynolds number. However in the limit $Re \to \infty$, the asymptotic analysis of Fendell (1972) suggests that to leading order equation (3.6) is correct.

Substitution of (3.5) and (3.6) into (3.4) results in an expression for U^+ which is a function of the two parameters A^+ and u_τ. For zero pressure gradient flow Van Driest (1956) found that a value of $A^+ = 26$

represented inner region data reasonably well; when (3.1) is used in prediction programs, various forms are used for A^+ to attempt to account for pressure gradient effects and heat and mass transfer. Because A^+ is not a physically measureable quantity the proposed forms for A^+ are often obtained indirectly in the following way. A correlation for A^+ is proposed with various adjustable constants which are then altered in a prediction program so that profile data are reproduced as well as possible. Of course there are many sources of error in such a procedure; the alternative that is adopted here is that both u_τ and A^+ are regarded as parameters and these are adjusted to best fit profile data. The result of this procedure is the best representation of the data that can be obtained by equation (3.4); the object of this is to gain some insight into how well the Van Driest and modified Van Driest profile can represent the inner region data.

Because the integral in (3.5) cannot be determined analytically, for a given value of A^+ and u_τ and at any stage in the optimization procedure, the profile was calculated numerically. The numerical quadrature used was one based on Simpson's rule and to achieve a good level of accuracy 500 intervals were taken between the wall and the first data point and then 250 intervals between subsequent data points. Although this integration procedure is somewhat time consuming, the main motivation here was to obtain at least four significant figures of accuracy in order to ensure a fair comparison.

At this stage, it is useful to point out that in spite of its wide use in connection with non-zero pressure gradient flows, there is an inherent contradiction between the extended Van Driest model and

experimental observation. First consider the case of zero pressure gradient flow and formally take $p^+ = 0$ in (3.5); a simple asymptotic expansion of the derivative of (3.4), for large y^+ yields

$$\frac{\partial U^+}{\partial y^+} \sim \frac{1}{\kappa y^+}\left\{1 - \frac{1}{2\kappa y^+} + \frac{1}{8\kappa^2 y^{+2}} - \cdots\right\} \quad \text{as } y^+ \to \infty, \text{ for } p^+ \equiv 0. \quad (3.7)$$

Consequently for $p^+ \equiv 0$, equation (3.7) implies a logarithmic behavior for U^+ as y^+ becomes large. This is consistent with all experimental measurements of the time-mean turbulent velocity profile for flows at constant pressure. Thus the Van Driest (1956) model performs correctly under the conditions for which it was originally proposed. However for any non-zero value of p^+ a similar analysis yields:

$$\frac{\partial U^+}{\partial y^+} \sim \frac{1}{\kappa}\sqrt{\frac{p^+}{y^+}}\left\{1 + \frac{1}{2p^+y^+} - \frac{1}{2\kappa^2 y^+\sqrt{p^+y^+}} + \cdots\right\}$$

$$\text{as } y^+ \to \infty, \; p^+ \neq 0. \quad (3.8)$$

Here p^+ is assumed to be no larger than $O(1)$, although perhaps small. Evidently from (3.8) the time-mean profile behaves as $\sqrt{y^+}$ for large y^+ and there is no logarithmic term in (3.4) either to leading order or to higher orders. However experiment confirms the existence of a logarithmic behavior for flows with non-zero pressure gradients. This fundamental contradiction with well-documented experimental observation of logarithmic behavior provides a valid reason for rejecting the modified Van Driest inner region model. The inability of the modified Van Driest profile to properly conform to flows with pressure gradient will be borne out in the subsequent data comparisons. First however a brief description of the unsteady wall layer model will be given.

3.2 Unsteady Wall Layer Model

The unsteady wall layer model incorporates the observations of several inner region flow visualization studies (Kline & Rundstadler, 1959; Kline et al., 1967; and Corino & Brodkey, 1969) with an analysis of the possible motions within the wall layer in the asymptotic limit $Re \to \infty$. Some main features of the model were proposed by Black (1968) based partially on the work of Einstein and Li (1956). Many of the assumptions behind Black's (1968) analysis and a number of features of his solution for the wall layer flow are not satisfactory. These are discussed in Walker, Abbott and Scharnhorst (1976) and Walker and Abbott (1977) where a complete discussion of the ideas behind the unsteady wall layer model is given. Only a brief discussion will be given here.

It is observed from experiment that the wall region flow is both three-dimensional and time-dependent but does possess a considerable degree of ordered structure. In particular two features dominate the wall layer flow. The first of these is the bursting phenomenon which can be regarded as a localized breakdown of the wall layer flow; it is characterized by rapid and violent ejection of wall layer fluid into the upper layer and is of relatively short duration. This event is followed almost simultaneously by inrushing fluid from the outer layer and this has been termed the sweep by Corino and Brodkey (1969). There then ensues a relatively long period of time, called the quiescent period. This is the second important feature of the wall layer flow and it is during this period of time that the streak structure is observed. The streaks are normally visualized with hydrogen bubble wire techniques and the tendency of the bubbles to collect into streaks

indicates surfaces across which there is no spanwise motion. Experiments indicate that the average spanwise spacing of the streaks, $\lambda^+ = \lambda u_\tau/\nu$, is a number on the order of 100; however most of the experiments that suggest a constant value of $\lambda^+ = 100$ are in a fairly limited Reynolds number range and the high Reynolds number results of Gupta, et al. (1971) suggest that λ^+ may become large as $Re \to \infty$. In either case, Walker and Abbott (1977) have argued that during the quiescent period (when the integrity of the wall layer is intact) the equations governing all three velocity components in the wall layer reduce to linear equations of the heat conduction type. The consequence of this is that the wall layer problem during the quiescent period is a linear one and the principle of superposition of solutions applies. Between two adjacent streaks the solutions for the velocity components may be written as a Fourier series in $z^+ = z/\lambda$; however over a long period of time and after a considerable number of cycles only that component of $u^+ = u(x^+,y^+,z^+,t^+)/u_\tau$ which is independent of z^+ during each quiescent period can contribute to the mean profile. Essentially this is because after each burst and subsequent quiescent period the streaks are observed to rearrange in different z^+ locations and over a long period of time the distribution appears random. In averaging the time-dependent solutions for u^+ over a single period, the average is to be interpreted essentially as an average over a large number of quiescent periods. Moreover it is also argued (Walker & Abbott, 1977) that the profile so obtained represents a good approximation to the total mean profile U^+ in the wall layer. The reason for this is associated with experimental observation; if attention is focused on

a fixed small area of the plate, the wall layer is observed to be in the quiescent state in excess of ninety percent of the total time. Thus it may be that in the limit $Re \to \infty$, the time scale associated with the bursting itself is small with respect to the time scale associated with the quiescent period. The main difficulty here is that to date there is no argument which remotely explains the presence of the streaks or the burst. The analytical difficulties in resolving these questions are formidable and at this stage neglecting the contribution to the mean profile from the burst itself is conjectural and motivated primarily from experiment.

In Walker, Abbott and Scharnhorst (1976) an initial condition for $u^+(x^+,y^+,z^+,t^+)$ was assumed which was selected to model the latter stages of the sweep. The following expression for the mean profile was obtained†:

$$
\begin{aligned}
U^+ = & -\frac{1}{\kappa}(1 + \gamma_0 + 2\log H_1)\left[\frac{1}{2}\,\mathrm{erf}H - H^2\,\mathrm{erfc}H + \frac{1}{\sqrt{\pi}}He^{-H^2}\right] \\
& + \frac{4}{\kappa\sqrt{\pi}}\left[\Xi(H) + H\Xi'(H) + \frac{\sqrt{\pi}}{4}\,\mathrm{erf}H + 2H^2\left\{\Xi(H) - \frac{\sqrt{\pi}}{4}\log H - \frac{\sqrt{\pi}}{8}\gamma_0\right\}\right] \\
& - 2p^+S^2\left[\frac{1}{4}\,\mathrm{erf}H - H^2\left(\frac{H^2}{3} + 1\right)\mathrm{erfc}H + \frac{H}{3\sqrt{\pi}}\left(H^2 + \frac{5}{2}\right)e^{-H^2}\right] \\
& + \frac{L(H_1 - H)}{\kappa}\left[2H^2\log(H/H_1) - \frac{1}{3H_1}(H - H_1)(2H^2 + 5HH_1 - H_1^2)\right] \\
& + \frac{H_1^2}{3\kappa}\,\mathrm{erfc}H + \frac{H_1^4}{30\kappa}\frac{He^{-H^2}}{\sqrt{\pi}} + O(H_1^6). \qquad (3.9)
\end{aligned}
$$

Here

$$H = y^+/2S, \quad H_1 = y_1^+/2S, \quad S = u_\tau\sqrt{T/\nu},$$

† In the expressions below and throughout this report $\log x$ denotes the natural logarithm.

and T is the mean period between bursts; L is the Heaviside function and γ_0 is Euler's constant. In addition the function Ξ appearing in (3.9) is defined as

$$\Xi(\eta) = \int_0^{\eta} e^{-z^2} \int_0^{z} e^{y^2} \int_0^{y} e^{-x^2} dxdydz. \tag{3.10}$$

A partial list of the properties of (3.10) is given in Walker, et al. (1976) and a subsequent report in this series will give a complete compilation.

The parameter y_1^+ appears in the assumed functional form of the initial condition; it can be related to the log-law constant C_i and S from two profile compatibility relations as follows. First, upon expanding (3.9) for large y^+ it follows that

$$C_i = \frac{1}{\kappa} (1 - \ell og\ y_1^+) - \frac{1}{2} p^+ S^2. \tag{3.11}$$

Second from the definition of the time-mean velocity profile

$$\left.\frac{\partial U^+}{\partial y^+}\right|_{y^+=0} = 1, \tag{3.12}$$

and it follows from (3.9) and (3.12) that

$$\frac{\sqrt{\pi}}{2} \kappa S + \frac{2}{3} p^+ \kappa S^2 = - \ell og H_1 - \frac{\gamma_0}{2} + \frac{\sqrt{\pi}}{2} H_1 - \frac{1}{6} H_1^2 + \frac{1}{120} H_1^4 + O(H_1^6). \tag{3.13}$$

Equations (3.11) and (3.13) can be used to determine values of C_i, S and y_1^+ given any one value; in practice it is the quantity C_i which is usually assigned. Thus equations (3.9), (3.11) and (3.13) define the unsteady wall layer time-mean velocity profile model for the inner region of a two-dimensional turbulent boundary layer.

In Walker, et al. (1976) two objections to the profile (3.9) were discussed; first the profile has a jump discontinuity in the fourth derivative at y_1^+. This was shown to be a direct consequence of the assumed initial condition; although the difficulty is of little consequence insofar as data comparisons are concerned (because y_1^+ is in general small), it is clearly unsatisfactory on a theoretical basis. The second difficulty is that (3.9) does not satisfy the wall compatibility condition

$$\left.\frac{\partial^3 U^+}{\partial y^{+3}}\right|_{y^+=0} = 0. \tag{3.14}$$

This condition can be demonstrated in a variety of ways (Rotta, 1962). A more satisfactory expression for U^+ may be obtained by means of a similarity analysis. The details of this are involved and are given by Walker and Scharnhorst (1977); only the final result will be quoted here. The main idea is to write the time-dependent normal coordinate as:

$$\eta = \frac{y^+}{2\sqrt{t^+ + t_0^+}} \tag{3.15}$$

rather than the corresponding coordinate selected in Walker, et al. (1976). The motivation for the introduction of t_0^+ in (3.15) is suggested by the rapid character of the wall layer breakdown (the burst) and almost immediate re-establishment of the streak structure; the non-linearities that are almost certainly present in the governing equations during the burst then must rapidly subside as the quiescent period commences at $t^+ = 0$ (by definition). In effect the parameter t_0^+ in (3.15) corresponds to an uncertainty in the origin of time.

An analysis described in Walker and Scharnhorst (1977) leads to the result:

$$U^+ = \left(1 + \frac{t_0^+}{S^2}\right)\left[R(S^2,t_0^+)Q(H) + Z(H) + P(S^2,t_0^+)W(H)\right]$$

$$- \frac{t_0^+}{S^2}\left[R(0,t_0^+)Q(H_0) + Z(H_0) + P(0,t_0^+)W(H_0)\right], \qquad (3.16)$$

where

$$H \equiv \frac{y^+}{2\sqrt{S^2 + t_0^+}}, \quad H_0 \equiv \frac{y^+}{2\sqrt{t_0^+}},$$

and

$$R(S^2,t_0^+) \equiv A_0 + \frac{a_0}{4}\log(S^2 + t_0^+), \qquad (3.17)$$

$$Q(H) \equiv (2H^2 + 1)\,erf H + \frac{2}{\sqrt{\pi}} He^{-H^2}, \qquad (3.18)$$

$$Z(H) \equiv \frac{4}{\kappa\sqrt{\pi}}\left[(2H^2 + 1)\Xi(H) + H\Xi'(H) - \frac{\sqrt{\pi}}{8}(6H^2 + 1)\,erf H - \frac{3}{4} He^{-H^2}\right], \qquad (3.19)$$

$$P(S^2,t_0^+) \equiv -\frac{2}{3}p^+(S^2 + t_0^+), \qquad (3.20)$$

$$W(H) \equiv \left(H^4 + 3H^2 + \frac{3}{4}\right) erf H + \frac{H}{\sqrt{\pi}}\left(H^2 + \frac{5}{2}\right)e^{-H^2} - 3H^2. \qquad (3.21)$$

It can be shown that for large y^+, the asymptotic form of the profile given by (3.16) is

$$U^+ \sim \frac{1}{\kappa}\log y^+ + C_i, \qquad (3.22)$$

where the constant A_0 in (3.17) is related to C_i by

$$C_i = A_0 + \frac{1}{\kappa}\left\{\frac{\gamma_0}{2} - \log 2\right\} - \frac{1}{2}p^+(S^2 + 2t_0^+). \qquad (3.23)$$

In addition it is insisted that (3.12) and (3.14) be satisfied and this leads to:

$$(S^2 + t_0^+)^{\frac{1}{2}}\left[R(S^2,t_0^+) - \frac{1}{\kappa} + P(S^2,t_0^+)\right]$$

$$- (t_0^+)^{\frac{1}{2}}\left[R(0,t_0^+) - \frac{1}{\kappa} + P(0,t_0^+)\right] = \frac{\sqrt{\pi}}{2} S^2 \qquad (3.24)$$

and

$$(S^2 + t_0^+)^{-\frac{1}{2}}\left[R(S^2,t_0^+) + 3P(S^2,t_0^+)\right]$$

$$- (t_0^+)^{-\frac{1}{2}}\left[R(0,t_0^+ + 3P(0,t_0^+)\right] = 0, \qquad (3.25)$$

respectively. Consequently with (3.23) the three parameters C_i, S, and t_0^+ in (3.16), can be determined given any one value, using (3.24) and (3.25). The profile (3.16) may easily be evaluated numerically and involves approximately the same amount of execution time as is necessary to perform the numerical integration in (3.4) to evaluate the Van Driest profile. A computer program to evaluate (3.16) is available from the authors upon request.

The profile (3.16) is the preferred profile since the objections discussed by Walker, et al. (1976) to (3.9) are removed. However for all practical purposes both profiles are essentially the same. In Figure 1, both profiles are plotted for $C_i = 5.0$ and $\kappa = 0.41$ and appear as a single curve. For (3.9), equations (3.11) and (3.13) yield S = 10.52 and $y_1^+ = 0.350$ while (3.24) and (3.25) give S = 10.50 and $t_0^+ = 8.01 \times 10^{-3}$. Although there is a slight difference in S the profiles themselves are identical in most cases to three significant figures as demonstrated in Table 1. In this report the inner region fits and the

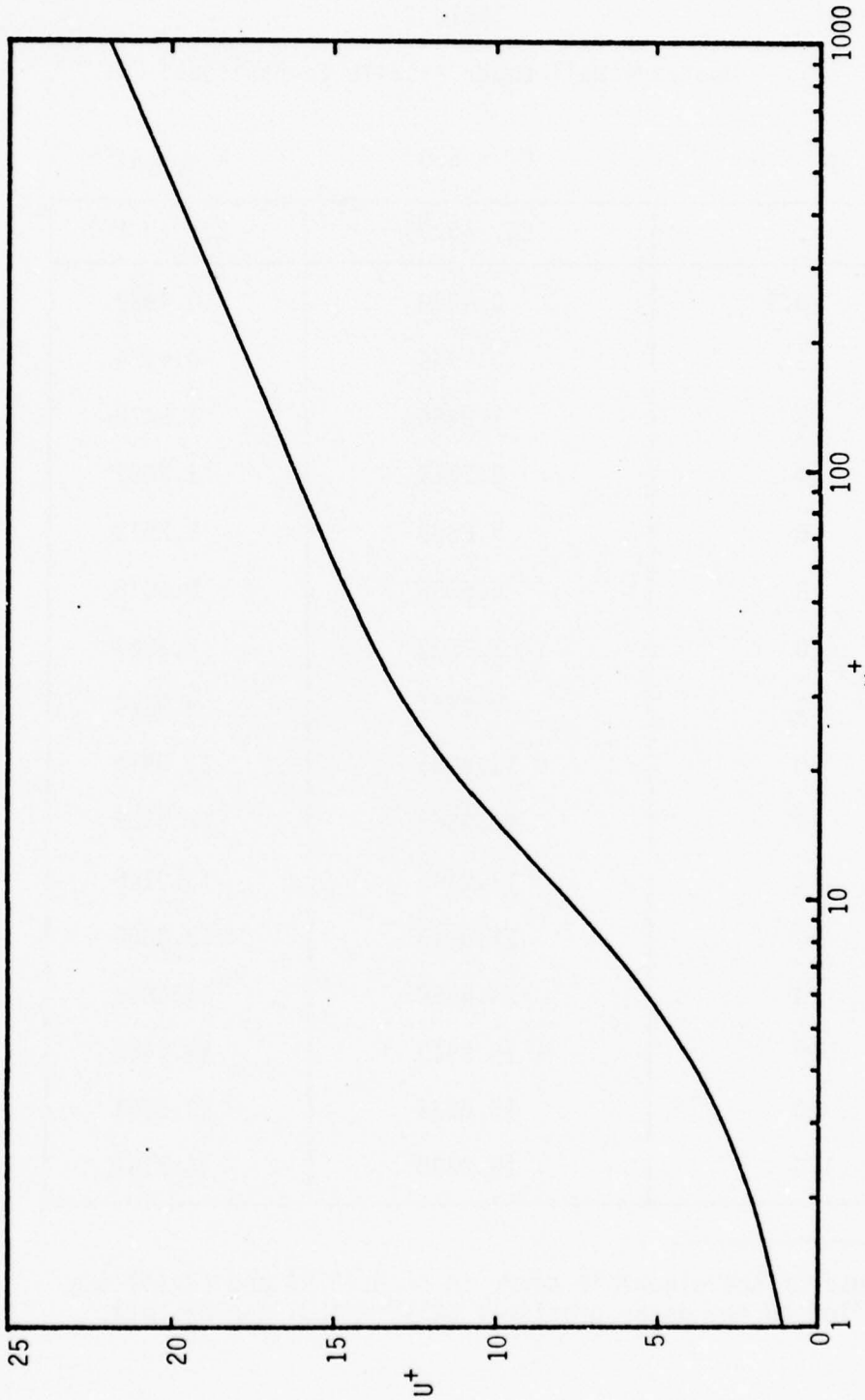

Figure 1. Inner region velocity profile for $\kappa = 0.41$, $C_i = 5.0$.

Table 1

Unsteady Wall Layer Profile Comparisons†

$p^+ = 0$ $C_i = 5.0$ $\kappa = 0.41$

y^+	Eq. (3.9)	Eq. (3.16)
0.5	0.4999	0.4992
1	0.9934	0.9924
2	1.9494	1.9478
4	3.7111	3.7087
6	5.2609	5.2579
8	6.6055	6.6018
10	7.7607	7.7567
15	9.9521	9.9474
20	11.3965	11.3914
25	12.3563	12.3512
30	13.0199	13.0146
40	13.8913	13.8860
50	14.4858	14.4805
60	14.9513	14.9460
80	15.6714	15.6661
100	16.2236	16.2184

† Because of the algebraic decay in both (3.9) and (3.16) the profiles do not agree precisely at $y^+ = 100$, for example.

full profile fits with Coles "law of the wake" were carried out with (3.9); the improved inner region profile (3.16) was used with the outer region similarity profile (Fendell, 1972) for the full profile fits to be described in Section 5. Since it has been demonstrated in Table 1 that for practical purposes the two inner region profiles (3.9) and (3.16) are essentially equivalent, the fact that two different forms of the unsteady wall layer model were used should have no effect on the final results and conclusions.

Comparisons with inner region data were made with the data sets grouped according to pressure gradient. The three non-transpiring flows of Andersen, Kays and Moffatt (1972) were considered; these flows are at zero, mild adverse and strong adverse pressure gradients, respectively, and are particularly attractive data sets because there are a considerable number of inner region data points. Comparisons were also made with the Fraser Flow A from the Stanford Conference (Coles & Hirst, 1969). Although there are not as many inner region data points, the pressure gradient is more severe than in the Andersen, et al. (1972) flows.

The detailed comparisons are presented in tabular and graphical form in Appendix A, to which the reader is referred. For convenience, a detailed discussion of the results for each data set is also included in Appendix A.

3.3 Summary

The four inner region data comparisons are discussed in detail in Appendix A and are summarized in Table 2. It is seen from the values of the average root-mean-square error, $\bar{\varepsilon}$, that the extended Van Driest

Table 2

Summary of Inner Region Data Comparisons

Flow	Van Driest		Unsteady Model	
	$\bar{\varepsilon}$	A^+_{avg}	$\bar{\varepsilon}$	S_{avg}
Zero P.G.				
8100	0.0072	31.6	0.0073	10.70
Mild P.G.				
8200	0.0076	-	0.0058	-
Strong P.G.				
8300	0.0070	-	0.0062	-
Fraser A				
5000	0.0181	-	0.0066	-

model fails to conform to velocity profiles in adverse pressure gradients. In view of the analysis of §3.1, and particularly equation (3.8), the result is not surprising. Current boundary-layer prediction schemes do not do particularly well in predicting flows where the pressure gradient is important; one reason to expect difficulty from predictive schemes that use a modified Van Driest model as a basis for the wall region is evident from (3.8). It is thus reasonable to suggest that the modified Van Driest model should be abandoned, although it is so firmly entrenched that this suggestion is not likely to be readily accepted. It should also be noted that even for the zero pressure gradient case for which the original model was developed, the arithmetic average value A^+_{avg} varies substantially from the value $A^+ = 26.0$ suggested by Van Driest (1956).

Referring again to Appendix A and Table 2 it is shown that the unsteady wall layer model exhibits no difficulties in fitting inner region data in flows with pressure gradient. In fact, it is seen that with increasing adverse pressure gradient, the average error $\bar{\epsilon}$ remains essentially unchanged from case to case. It should also be noted that for the zero pressure gradient case, the arithmetic average value S_{avg} is in good agreement with the theoretical value of 10.50 discussed in §3.2.

Finally it should be mentioned that the four data comparisons presented in this report are only representative of those obtained with a large number of other flow cases.

In the next two sections, the unsteady wall layer model will be combined with two different outer region models to form a composite velocity profile over the entire boundary layer; in this way complete profile data may be compared.

4. FULL PROFILE DATA COMPARISONS (LAW OF THE WAKE)

In order to obtain an expression for the velocity profile across the entire turbulent boundary layer it is necessary to couple an inner region profile discussed in section 3 with a model for the outer region. In this report two outer region models will be considered; in this section Coles' (1956) "law of the wake" will be considered and in section 5 a similarity profile, described originally by Mellor and Gibson (1966), will be investigated. For reasons discussed in section 3, the modified Van Driest profile for the inner region will not be considered further since both outer region profiles considered in this report require that the inner region profile behave logarithmically for large y^+. Also, in view of the results in section 3 both outer region profiles will be coupled with the unsteady wall layer model rather than the Van Driest (1956) model.

The majority of the incompressible data considered here is taken directly from Coles and Hirst (1969); in addition the more recent non-transpired data of Andersen, et al. (1972) and the adverse pressure gradient data of Samuel and Joubert (1974) will be considered. The values of mainstream velocity gradient dU_e/dx^* were taken directly from Coles and Hirst (1969) and from the appropriate reports for the more recent data.

A major objective of this and the following section is to decide which outer region model best represents the experimental data; in addition an important goal is to decide which profile model is best suited for a prediction method. These points will be considered subsequently in section 6.

4.1 The Law of the Wake

Coles' (1956) "law of the wake" is a simple formula for the outer region profile and is an empirical correlation based on the observation of data in a wide variety of flows, with and without pressure gradients. Coles (1956) postulated that the velocity deviation in the outer region from the law of the wall, when normalized with respect to the maximum deviation at the boundary layer edge, should be a single-valued function of y/δ. Here δ is the boundary-layer thickness. When several data sets were reduced to this form, hey appeared to exhibit a common behavior which was correlated as a numerical wake function $w(y/\delta)$. It was demonstrated by Hinze (1959) that the wake function could be closely approximated by

$$w(y/\delta) = 2 \sin^2 \left(\frac{\pi y}{2\delta}\right), \tag{4.1}$$

and this simple analytical expression was subsequently used by Coles and Hirst (1969). The law of the wake was then proposed as a linear combination of a logarithm and the wake function, according to,

$$\frac{\overline{u}_0^*}{u_\tau} = \frac{1}{\kappa} \log y^+ + C_i + \frac{2\Pi}{\kappa} \sin^2 \left(\frac{\pi y}{2\delta}\right). \tag{4.2}$$

Here $\overline{u}_0$ denotes the time-mean velocity profile in the outer region of the boundary layer and Π is the so-called wake strength parameter.

It should be emphasized that (4.2) is not a physical law in the usual sense but simply a good experimental correlation. The main focus in this section will be on how well (4.2) represents experimental data when coupled with the unsteady wall layer model; we return to a critical evaluation of this model in section 6.

If κ and C_i are assumed to be universal constants, equation (4.2) contains the three parameters Π, δ, and u_τ. The boundary-layer thickness δ is normally defined as that physical location where the boundary-layer profile reaches a specified percentage of the mainstream value with 99% and 99.5% being typical experimental definitions. The definition of δ makes this quantity a somewhat nebulous quantity and in (4.2) δ is generally regarded as a parameter. By insisting that $\overline{u_0^+} = U_o$ at $y = \delta$, where U_o is the local mainstream velocity, the so-called skin friction relation

$$\Pi = \frac{\kappa}{2}\left\{\frac{U_o}{u_\tau} - \frac{1}{\kappa}\,\ell og\,\frac{\delta u_\tau}{\nu} - C_i\right\}, \tag{4.3}$$

is obtained. Equation (4.3) is a relation connecting the three parameters u_τ, Π and δ; consequently for assumed values of κ and C_i, equation (4.2) is a two-parameter expression for the outer region profile.

In preparation for the Stanford Conference, Coles and Hirst (1969) assumed that the values of $\kappa = 0.41$ and $C_i = 5.0$ were universal constants and optimized on the two parameters u_τ and δ; the best fit to the data was defined as in equation (1.5). Both values of κ and C_i are questionable and other values are often quoted in the literature. The main difficulty in deciding whether or not κ and C_i are universal constants is that there is as yet, no direct method for measuring u_τ in a boundary-

layer flow. The above values of κ and C_i are essentially extrapolated from pipe flow data where u_τ can be measured directly. Nevertheless in this report, a value of $\kappa = 0.41$ will be assigned tentatively.

A composite profile consisting of the unsteady wall layer model and the law of the wake (4.2) is defined by:

$$\overline{u}^+ = U^+ + W(y/\delta), \tag{4.4}$$

where

$$W(y/\delta) = \begin{cases} \dfrac{2\Pi}{\kappa} \sin^2 \left(\dfrac{\pi y}{2\delta}\right) & \text{for } \dfrac{y}{\delta} \leq 1, \\ \dfrac{2\Pi}{\kappa} & \text{for } y > \delta. \end{cases} \tag{4.5}$$

The additional definition in the second part of (4.5) is made so that all measured data points can be reasonably included in the fitting procedure. In Coles and Hirst (1969), data points near the mainstream and in some cases well within the boundary layer were omitted; the motivation for this was that the slope of the profile defined by (4.2) does not approach zero as $y \to \delta$. In addition, some data near the wall were also omitted on the grounds that it may be in error. The rejection of data points is rather subjective and in this report all measured data points were included in the comparisons.

The composite profile (4.4) contains the three independent parameters u_τ, δ and C_i; one main difference from the fitting procedure carried out by Coles and Hirst (1969) is that (4.4) contains an adjustable log-law "constant." At any stage in the optimization procedure, given a value of C_i, values of t_0^+ and S may be determined from (3.23),

(3.24) and (3.25) and the current form of U^+ is completely determined from (3.16).

The data fits are given in graphical and tabular form in Appendix B to which the reader is referred. The data sets are arranged and numbered in the same order as in Coles and Hirst (1969). The last two data sets of Samuel and Joubert (1974) and Andersen, et al. (1972) have been labelled as 7000 and 8000 series respectively. For convenience, brief comments about each data set and the corresponding fit are included in Appendix B.

5. OUTER REGION SIMILARITY PROFILE

5.1 Introduction

The existence of self-similar profiles for two-dimensional time-mean turbulent boundary layers is a subject which has attracted a good deal of attention in the literature. It is important here to make a distinction between the terms equilibrium and self-similar which are often used interchangeably. The term equilibrium is understood to apply to a turbulent boundary layer for which the mainstream velocity is such that either $U_\infty(x) \sim x^\alpha$ or $U_\infty(x) \sim e^{\beta x}$ where α and β are constants. In order for self-similar profiles to exist equilibrium is a necessary but by no means a sufficient condition.

To investigate this point further, consider the case of laminar boundary layers where similar solutions satisfy the well known Falkner-Skan equation. The existence of such solutions in laminar flows has been discussed by Brown and Stewartson (1965) who argue that similar solutions may be expected in two physical situations. The first of these is at an x station where the velocity profile is an initiator of the boundary-layer flow downstream; such a situation occurs physically at the front stagnation point of a bluff body or the leading edge of a flat plate, for example. In these cases the Falkner-Skan profile gives the proper laminar boundary-layer solution at a point of attachment of the mainstream and provides the initial condition to initiate a boundary-layer calculation downstream. For turbulent boundary layers there would

appear to be no analogue of this physical situation. Generally the flow at a point of attachment of the mainstream is observed to be laminar and when the downstream boundary-layer flow is turbulent, there is a transition zone in between. Moreover, a wide variety of experimental conditions can lead to transition and an eventual fully developed turbulent boundary layer downstream for the same mainstream velocity distribution. Consequently, there would appear to be no reason to expect that the flow in the outer region of an equilibrium boundary layer will be self-similar at the initial stations of a fully developed turbulent flow.

For laminar boundary layers, the other case discussed by Brown and Stewartson (1965) is that where a similarity solution becomes what may be described as a terminator of a more general boundary-layer flow and two cases of this behavior are considered by Brown and Stewartson (1965). A physical case where this can occur is at a point of detachment of the inviscid flow; examples of such behavior are known in magnetohydrodynamic flow (Leibovich, 1967a, 1967b) and in rotating flows (Walker & Stewartson, 1972) at the rear stagnation point of symmetrical and two-dimensional bluff bodies. Another case is flat plate flow and here if the initial velocity profile at any arbitrary location on the plate is not given by the Blasius solution, then the Blasius profile can only become the relevant solution at an infinite distance downstream. For turbulent boundary-layer flows an analogous type of situation is expected; that is similarity solutions are only anticipated as terminators and usually at an infinite distance downstream from wherever the boundary layer is created.

In practice, one would expect to be able to measure turbulent boundary-layer profiles, at large distances downstream of the transition zone, which become arbitrarily close to being self-similar; however, near the transition zone there is no reason to expect the same behavior. In zero and favorable pressure gradients, measured profiles in an equilibrium flow should increasingly approach self-similarity at subsequent data stations downstream. In adverse pressure gradient flows, boundary-layer separation will often occur before similarity is achieved.

5.2 Similarity in the Outer Region

An ordinary differential equation for the outer region similarity profile has been obtained by a number of authors, most notably Mellor and Gibson (1966), Yajnik (1970) and Fendell (1972). The approaches used by these authors differ somewhat but the end result is essentially the same. In this section, the spirit of the approach of Fendell (1972) will be adopted (although the notation is slightly different).

Fendell (1972) considered the asymptotic structure of the time-mean turbulent boundary-layer equations in the limit as $Re \to \infty$ and showed, on the basis of a few reasonable assumptions, that the boundary layer is a composite double layer. It was assumed that the turbulence could be modelled as an additive stress term σ so that the time-mean momentum equation is,

$$\bar{u}\frac{\partial \bar{u}}{\partial x} + \bar{v}\frac{\partial \bar{u}}{\partial y} = U_\infty \frac{dU_\infty}{dx} + \frac{\partial \sigma}{\partial y} + \frac{1}{Re}\frac{\partial^2 \bar{u}}{\partial y^2} \,. \tag{5.1}$$

Here all velocities and lengths have been made dimensionless with respect to U_0 and L, a representative velocity and length respectively

and $Re = U_0 L/\nu$ is the Reynolds number. For practical purposes the function σ may be related to the $\overline{u'v'}$ product by

$$\sigma = -\frac{\overline{u'v'}}{U_0^2} \quad . \tag{5.2}$$

Implicit in (5.2) is the notion that the intensities $\overline{u'^2}$ and $\overline{v'^2}$ and the $\overline{u'v'}$ product are of the same order of magnitude; consequently the intensities that are often included in equation (5.1) may reasonably be neglected since they are differentiated on x and will be of lower relative order.

Fendell (1972) assumed that in the outer region the velocity profile may be written as a linearization about the mainstream value; it can be shown that this assumption gives rise to a consistent asymptotic structure and in fact becomes the experimentally determined defect law. For the outer region,

$$\overline{u} = U_\infty(x)\left\{1 + u^*(x;Re)\,\frac{\partial F_1}{\partial \eta}\,(\eta,x) + \cdots\right\} \tag{5.3}$$

$$\sigma = U_\infty^2(x)\left\{u^{*2}(x;Re)\,\Sigma_1(\eta,x) + \cdots\right\} \tag{5.4}$$

Here

$$\eta = y/\Delta_0(x;Re) \ , \tag{5.5}$$

is the scaled normal coordinate in the outer region and Δ_0 is the dimensionless outer region length scale. In addition, $u^* = u_\tau(x;Re)/U_e(x)$ is an important parameter which emerges from Fendell's (1972) analysis and can be shown to be $O(1/\ell og\ Re_\delta)$ where Re_δ is the Reynolds number based on the local boundary-layer thickness; also it emerges that Δ_0 is $O(u^*)$ as $Re \to \infty$. It is worthwhile to note that (5.4) is equivalent

to assuming that $\overline{u'v'}$ is $O(u_\tau^2)$. This assumption as well as equations (5.2) and (5.3) are not expected to apply immediately upstream of a point of time-mean separation.

The equation for $\partial F_1/\partial\eta$ is obtained by substitution of (5.3) and (5.4) into (5.1). To leading order the laminar shear term in (5.1) is negligible and the dominant terms are the convection and Reynolds stress terms. Consequently

$$\frac{\partial \Sigma_1}{\partial \eta} = \frac{\Delta_0}{u^{*2}U_\infty^2}\,(u^*U_\infty^2)'\,\frac{\partial F_1}{\partial \eta} - \frac{1}{u^*U_\infty}\,(U_\infty\Delta_0)'\,\eta\,\frac{\partial^2 F_1}{\partial \eta^2} + \frac{\Delta_0}{u^*}\,\frac{\partial^2 F_1}{\partial \eta \partial x} \tag{5.6}$$

with

$$F_1(x,\eta) \to 0 \qquad \text{as} \qquad \eta \to 0, \tag{5.7}$$

and

$$\frac{\partial F_1}{\partial \eta}\,(x,\eta) \to 0 \qquad \text{as} \qquad \eta \to \infty. \tag{5.8}$$

In equation (5.6) a prime denotes differentiation with respect to x.

The necessary conditions for similarity follow from (5.6) and are that

$$\frac{\Delta_0}{u^{*2}U_\infty^2}\,(u^*U_\infty^2)' = -2\beta = \text{constant}, \tag{5.9}$$

and

$$\frac{1}{u^*U_\infty}\,(\Delta_0 U_\infty)' = \alpha = \text{constant}. \tag{5.10}$$

In order to make further progress, it is necessary to discuss the nature of the inner region.

The expansion given in (5.3) is not uniformly valid and in order for the no slip condition to be satisfied, an inner layer is required. In the inner region the leading terms in the expansions for velocity profile and stress are (Fendell, 1972),

$$\overline{u} = u^* U_\infty(x) \frac{\partial f_1}{\partial y^+}(x,y^+) + \cdots , \tag{5.11}$$

and

$$\sigma = u^{*2} U_\infty^2(x)\, \sigma_1(x,y^+) + \cdots , \tag{5.12}$$

where

$$y^+ = \frac{u_\tau L}{\nu} y = \mathrm{Re}\, u^* U_\infty(x) y , \tag{5.13}$$

is the conventionally defined inner region variable. Matching of (5.3) and (5.11) takes place in the limits $y^+ \to \infty$ and $\eta \to 0$ for fixed x; in order that both the vorticity and velocity profile merge smoothly, both profiles must behave logarithmically according to,

$$\frac{\partial F_1}{\partial \eta} \sim \frac{1}{\kappa(x)} \log \eta + C_0(x) , \qquad \text{as} \qquad \eta \to 0 , \tag{5.14}$$

and

$$\frac{\partial f_1}{\partial y^+} \sim \frac{1}{\kappa(x)} \log y^+ + C_i(x) , \qquad \text{as} \qquad y^+ \to \infty . \tag{5.15}$$

Here C_0 and C_i are in general functions of x; κ is analogous to the von Kármán "constant." It is often assumed on the basis of extrapolation from pipe flow data that κ is constant and equal to about 0.41. Whether or not this extrapolation is valid or not is conjectural; from a mathematical standpoint, whether or not κ depends on x depends on the particular constitutive model adopted for $\overline{u'v'}$. One additional feature

worth noting is that it also follows from the analysis (Fendell, 1972) that

$$\Sigma_1 \to 1 \qquad \text{as} \qquad \eta \to 0 \ , \tag{5.16}$$

and

$$\sigma_1 \to 1 \qquad \text{as} \qquad y^+ \to \infty \ , \tag{5.17}$$

where again flows in the immediate vicinity of a point of time-mean separation are excluded.

As yet the function $\Delta_0(x,Re)$ has not been specified other than to remark that it is $O(u^*)$ as $Re \to \infty$. A relation connecting u^* and Δ_0 follows from matching (5.3) and (5.11), using (5.14) and (5.15) and is

$$\frac{1}{u^*} = \frac{1}{\kappa(x)} \ell og \left\{ \Delta_0 Re u^* U_\infty(x) \right\} + C_i - C_0 \ . \tag{5.18}$$

To leading order as $Re \to \infty$, equation (5.18) implies that

$$u^* \sim \frac{\kappa(x)}{\ell og \ Re_\delta} \ , \tag{5.19}$$

which is a result referred to earlier.

We are now in a position to return to the question of self-similarity; in order to assess the magnitude of the ratio $u^{*'}/u^*$ which appears in (5.9) and (5.10), equation (5.18) is differentiated with respect to x, to obtain,

$$-\frac{u^{*'}}{u^{*2}} = -\frac{\kappa'}{\kappa^2} \ell og \left\{ \Delta_0 Re \, u^* U_\infty(x) \right\} + \frac{1}{\kappa} \left\{ \frac{\Delta_0'}{\Delta_0} + \frac{u^{*'}}{u^*} + \frac{U_\infty'}{U_\infty} \right\} + C_i' - C_0' \tag{5.20}$$

Using (5.18) to eliminate the first term on the right side of (5.20), it follows that,

$$\frac{u^{*\prime}}{u^*} = \frac{\kappa'}{\kappa} - \frac{u^*}{\kappa}\left\{\frac{\Delta_0'}{\Delta_0} + \frac{u^{*\prime}}{u^*} + \frac{U_\infty'}{U_\infty} + \kappa'(C_i - C_0) + \kappa(C_i - C_0)'\right\}. \qquad (5.21)$$

Although κ may in general be a function of x, it must become constant for a self-similar flow and it follows from (5.21) that

$$\frac{u^{*\prime}}{u^*} = O(u^*) \ . \qquad (5.22)$$

Thus terms containing this ratio may be neglected to leading order in (5.9) and (5.10) which become, respectively,

$$q\,\frac{U_\infty'}{U_\infty} = -\beta \ , \qquad (5.23)$$

and

$$q' + \frac{U_\infty'}{U_\infty}\,q = \alpha. \qquad (5.24)$$

Here the quantity q is defined by $q = \Delta_0/u^*$. Combining these two equations gives

$$q' = \alpha + \beta. \qquad (5.25)$$

Consequently only two types of mainstream velocity distributions can lead to self-similar solutions and these are:

(a) $\quad U_\infty(x) = D_1(x - x_0)^{\alpha_1} \ , \quad$ for $\quad \alpha + \beta \neq 0 \qquad (5.26)$

where

$$\alpha_1 = -\frac{\beta}{\alpha + \beta} \ , \quad q = \frac{\Delta_0}{u^*} = (\alpha + \beta)(x - x_0), \qquad (5.27)$$

with D_1 and x_0 arbitrary constants.

(b) $\quad U_\infty(x) = D_2 e^{-\alpha_2 x}, \quad$ for $\quad \alpha + \beta = 0 \qquad (5.28)$

where

$$\alpha_2 = \frac{\beta}{x_0}, \qquad q = \frac{\Delta_0}{u^*} = x_0, \tag{5.29}$$

with D_2 and x_0 arbitrary constants.

Equilibrium boundary layers have received a good deal of experimental attention and have been defined in this context as flows in which the dimensionless velocity defect $(U_e - \overline{u}^*)/u_\tau$, when expressed as a function of y/δ, becomes close to being invariant with downstream distance. This type of behavior is expected mathematically as a solution approaches self-similarity. Clauser (1954, 1956) suggested that the criterion for equilibrium should be a constant value of the parameter β_c defined as

$$\beta_c = -\frac{\delta^*}{u_\tau^2} U_e \frac{dU_e}{dx}. \tag{5.30}$$

Here δ^* is the dimensionless displacement thickness defined as

$$\delta^* = \int_0^\infty \left\{1 - \frac{\overline{u}}{U_\infty(x)}\right\} dy. \tag{5.31}$$

In view of (5.3) and (5.5), to leading order,†

$$\delta^* = -\Delta_0 u^* F_1(x,\infty) + \cdots \tag{5.32}$$

As a condition of self-similarity is approached $F_1(x,\infty)$ must approach a constant value, say $F_1(\infty)$; thus equation (5.30) becomes

$$\beta_c = \frac{\Delta_0 F_1(\infty)}{u^* U_\infty} \frac{dU_\infty}{dx} = -\beta F_1(\infty). \tag{5.33}$$

---

† Because (5.3) is a defect law, $\partial F_1/\partial\eta$ and $F_1(x,\infty)$ are in general negative.

Clearly both types of mainstream velocity distributions (5.26) and (5.28) give a constant value of β_c which again is a necessary condition for self-similarity.

5.3 The Eddy Viscosity

In order to define an outer region profile it is necessary to select a constitutive relation for the $\overline{u'v'}$ product in the outer region. It has traditionally been assumed that there exists some unknown functional relation between the $\overline{u'v'}$ product and the mean velocity field. This view will also be adopted here; however, it must be recognized that no such general functional relationship has ever been shown to exist and for the present any such hypothesis must be regarded as no more than a useful and convenient approximation. The major difficulty in resolving this point is that the time-dependent dynamics of the outer layer are not understood. From experiment it has become increasingly evident in recent times that the burst-sweep sequence provides the major contribution to the $\overline{u'v'}$ product for both the inner and outer layer. Consequently, it would appear necessary to analyze a typical burst-sweep sequence in order to either demonstrate or deny the existence of a general functional relationship between $\overline{u'v'}$ and $\bar{u}$. However, the burst-sweep sequence is a time-dependent viscous-inviscid interaction between the inner and outer layer caused by some unknown physical mechanism in the outer layer. Moreover even if the cause of the burst were known, the mathematical difficulties associated with such a problem are formidable. Consequently for the present, it will be assumed that some constitutive relation does exist.

The particular relation that will be adopted here is that of an eddy viscosity model for the outer layer. The main reasons for this choice are simplicity and the relative degree of success that this type of assumption has enjoyed in prediction methods. Indeed, at present it is far from clear that the increasing variety of much more involved second-order closure schemes offer any significant advantage in connection with predicting turbulent boundary-layer flows. A good discussion of the eddy viscosity assumption is given by Saffman (1970) which is quoted directly below:

> The assumption of an eddy viscosity has been severely criticized by some writers, who also regard it as harmful. The author regards this view as extreme and unjustified. The eddy viscosity hypothesis is equivalent to retaining the leading term in an expansion of the (unknown) functional relation between Reynolds stress and the mean velocity distribution.

Consequently for the outer region, define

$$-\overline{u'v'} = \varepsilon_0 \frac{U_0}{L} \frac{\partial \bar{u}}{\partial y} = U_0^2 \, \sigma. \tag{5.34}$$

From equations (5.4) and (5.5),

$$\Sigma_1' = \frac{\varepsilon_0}{\Delta_0 U_0 U_\infty(x) L u^*} \frac{\partial^2 F_1}{\partial \eta^2}. \tag{5.35}$$

In selecting a functional form for ε_0, the same type of model that is used in the Cebeci-Smith (1969) and Mellor and Herring (1969) prediction methods will be adopted. This particular type of model is discussed by Mellor and Gibson (1966) and is credited to Clauser (1954, 1956) by these authors.

One main feature of this model is that for fixed x and in the outermost regions of the outer layer, ε_0 is selected to approach a constant value. Specifically,

$$\varepsilon_0 \to KU_e(x)\delta^*L. \tag{5.36}$$

Here δ^* is the dimensionless displacement thickness defined in equation (5.31) and K is an empirically determined constant; Cebeci and Smith (1969) take K equal to 0.0168 while Mellor and Herring (1969) choose 0.016. For small η, equation (5.36) is clearly not appropriate in view of (5.16) since Σ_1 must approach one as $\eta \to 0$. Thus the stress function is defined according to

$$\Sigma_1 = \frac{\delta^*}{u^*\Delta_0}\,\varepsilon(\eta)\,\frac{\partial^2 F_1}{\partial\eta^2}, \tag{5.37}$$

where the function $\varepsilon(\eta)$ must be such that,

$$\varepsilon \to K \qquad \text{as} \qquad \eta \to \infty, \tag{5.38}$$

and

$$\varepsilon \to \kappa\eta \left\{\frac{u^*\Delta_0}{\delta^*}\right\} \qquad \text{as} \qquad \eta \to 0. \tag{5.39}$$

From (5.32), to leading order

$$\frac{\delta^*}{u^*\Delta_0} = -F_1(x,\infty) \tag{5.40}$$

and therefore (5.37) and (5.39) become

$$\Sigma_1 = -F_1(x,\infty)\,\varepsilon(\eta)\,\frac{\partial^2 F_1}{\partial\eta^2}, \tag{5.41}$$

$$-F_1(x,\infty)\varepsilon \to \kappa\eta \qquad \text{as} \qquad \eta \to \infty. \tag{5.42}$$

In general the functional form of $\varepsilon(\eta)$ is not known; however the limit (5.38) is assumed known from experiment while the limit (5.42) is known from theoretical considerations. A simple form is to assume two straight line variations according to,

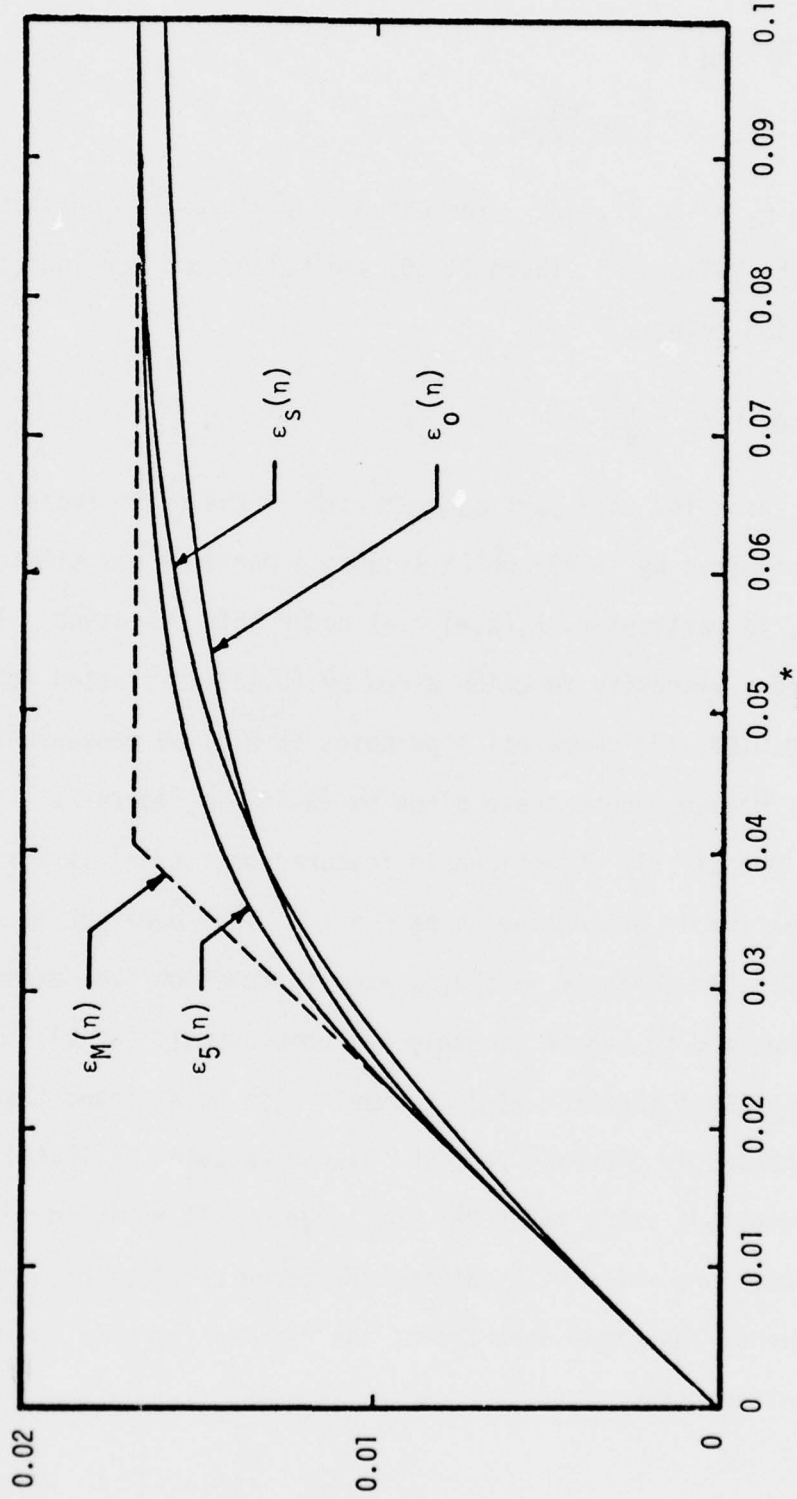

Figure 2. Eddy Viscosity Functions (The labels correspond to those in the text).

$$\varepsilon = \varepsilon_M = \begin{cases} K & \text{for} \quad \eta \geq \eta_1, \\ \dfrac{\kappa\eta}{-F_1(x,\infty)} & \text{for} \quad \eta < \eta_1, \end{cases} \tag{5.43}$$

where $\eta_1 = -KF_1(x,\infty)/\kappa$. The above eddy viscosity formulation is that used by Mellor and Gibson (1966) and Mellor and Herring (1969) who in addition select,

$$\Delta_0 = \Delta_c = \frac{\delta^*}{u^*} . \tag{5.44}$$

The reason for this particular choice of the outer region length scale is motivated by (5.42) which assumes a particularly simple form in this case; in particular, $F_1(x,\infty) = -1$ under this selection. In Figure 2, the eddy viscosity function given by (5.43) is plotted for $\kappa = 0.41$ and $K = 0.0168$; for comparative purposes it will be convenient to use the outer region length scale given by (5.44) in Figure 2.

One clearly objectionable feature about $\varepsilon_M(\eta)$ is that the first derivative is discontinuous at $\eta = \eta_1$. This behavior is rather unpalatable since if an eddy viscosity function does exist, it should be expected to behave smoothly and continuously for all η. In selecting a functional form for $\varepsilon(\eta)$ it should also be expected that $\varepsilon(\eta)$ will monotonically increase from the linear behavior in (5.42) near $\eta = 0$ to the constant value in (5.38) for large η. There is an endless variety of functions which will satisfy the above requirements and although a number of functions were tried, the results for only two will be discussed here.

The first of these is given by,

$$\varepsilon_s(\eta) = K \, erf\left\{\frac{-\sqrt{\pi}}{2}\frac{\kappa\eta}{KF_1(x,\infty)}\right\}, \tag{5.45}$$

which approaches the proper limits as $\eta \to 0$ and as $\eta \to \infty$. This function is representative of a class of functions which were tried, which approach K exponentially fast for large η and for which the approach to the linear variation as $\eta \to 0$ is algebraic. In the case of (5.45)

$$\varepsilon_s \to \kappa\eta + O\left(\frac{\kappa^3\eta^3}{K^3}\right) \qquad \text{as} \qquad \eta \to 0. \tag{5.46}$$

This function is also plotted in Figure 2. Discussion of the second form used for $\varepsilon(\eta)$ will be deferred until §5.5.

5.4 The Composite Profile

Substitution of (5.41) into (5.6) leads to

$$-F_1(x,\infty)\frac{\partial}{\partial\eta}\left\{\varepsilon(\eta)\frac{\partial U_1}{\partial\eta}\right\} + \frac{(U_\infty\Delta_0)'}{u^*U_\infty}\eta\frac{\partial U_1}{\partial\eta}$$

$$-\frac{\Delta_0(u^*U_\infty^2)'}{u^{*2}U_\infty^2}U_1 = \frac{\Delta_0}{u^*}\frac{\partial U_1}{\partial x} \tag{5.47}$$

where $U_1 = \partial F_1/\partial\eta$. For similarity (and using (5.22)), equation (5.47) becomes the ordinary differential equation

$$-F_1(\infty)\frac{d}{d\eta}\left\{\varepsilon(\eta)\frac{dU_1}{d\eta}\right\} + \left\{\frac{\Delta_0'}{u^*} - \beta\right\}\eta\frac{dU_1}{d\eta} + 2\beta U_1 = 0, \tag{5.48}$$

where β is defined by (5.23). Once a particular form for $\varepsilon(\eta)$ and an outer length scale Δ_0 are selected equation (5.48) may be solved numerically. In particular with (5.44) and (5.45), $F_1(x,\infty) = F_1(\infty) = -1$ and equation (5.48) becomes

$$\frac{d}{d\eta}\left\{\varepsilon_s \frac{dU_1}{d\eta}\right\} + \left\{\frac{\delta^{*\prime}}{u^{*2}} - \beta_c\right\} \eta \frac{dU_1}{d\eta} + 2\beta_c U_1 = 0 \tag{5.49}$$

where β_c is obtained from (5.33) and $\beta_c = -\delta^* U_\infty'/(u^{*2} U_\infty)$. Equation (5.47) may be integrated across the outer layer to obtain

$$\frac{\delta^{*\prime}}{u^{*2}} = 1 + 3\beta_c$$

and consequently (5.49) becomes

$$\frac{d}{d\eta}\left[\varepsilon_s \frac{dU_1}{d\eta}\right] + (1 + 2\beta_c)\,\eta \frac{dU_1}{d\eta} + 2\beta_c U_1 = 0. \tag{5.50}$$

Equation (5.50) contains three parameters, namely u*, K and κ. Setting K = 0.0168 and κ = 0.41 completely specifies the eddy viscosity and for a given value of u*, the solution of (5.50) may be calculated.

A composite profile for the entire boundary layer consisting of the unsteady wall layer model and the solution of (5.50) may be defined according to,

$$\frac{U_0 \bar{u}}{u_\tau} = \frac{\bar{u}}{u^* U_\infty(x)} = U^+ + U_1(\eta) - \frac{1}{\kappa} \log \eta - C_0, \tag{5.51}$$

where U^+ is defined by (3.16). The match condition (5.18) is

$$\frac{1}{u^*} = \frac{1}{\kappa} \log \left\{\delta^* \mathrm{Re}\, U_\infty(x)\right\} + C_i - C_0, \tag{5.52}$$

and C_i is related to the inner region parameter S through (3.23). At the data station (x = 0) where the fit is to be performed, take the representative velocity U_0 equal to the local mainstream value so that $U_\infty(0) = 1$; in addition at the data station being fit the measured displacement thickness $\delta^* L$ is taken from experiment. Thus with κ, K specified and the displacement thickness taken from experiment,

equation (5.51) is one parameter family of profiles with the single parameter being u_τ.

Because U_1 behaves logarithmically for small η, the accurate numerical solution of (5.50) is non-trivial and it is worthwhile to briefly discuss how this was carried out. Near $\eta = 0$ the solution for U_1 was written as a series,

$$U_1 = \frac{1}{\kappa} \log \eta + C_0 + \sum_1^\infty \eta^n (a_n \log \eta + c_n) . \tag{5.53}$$

Substitution into (5.50) yields a set of algebraic equations for the a_n and c_n; however, because the boundary condition (5.8) has not been applied at this stage, the series solution (5.53) is not uniquely determined and contains the arbitrary constant C_0. A value was first guessed for C_0 and the series evaluated at a non-zero value of $\eta = \eta_0$, say. In view of the singular behavior of (5.53) near $\eta = 0$, the value of η_0 must be selected large enough so that finite difference approximations to (5.50) may be made with good accuracy for $\eta > \eta_0$; on the other hand η_0 must be small enough so that the series (5.53) converges. In practice, a value of $\eta_0 = 0.02$ was found to be adequate for this purpose. A solution for $\eta \geq \eta_0$ was then calculated numerically using a method similar to that described by Keller (1969). This method is a boundary value technique which was implemented by defining a non-uniform numerical mesh in the range $\eta_0 \leq \eta \leq L$. Here L is a large but finite value of η; the value of L, on which condition (5.8) was imposed as an approximation, must be increased until there is no significant change in the computed solution. The numerical mesh that was used employed a telescoping spacing, wherein the mesh spacing was selected

as initially small and uniform near $\eta = \eta_0$; the mesh spacing was then successively increased by a factor of 1.02. It can be shown that the result of this procedure is a set of tridiagonal difference equations which are easily solved by a direct method.

Having computed a solution with one arbitrarily selected value of C_0, another solution was calculated with another arbitrarily selected value of C_0. Both solutions computed in this way do not have a continuous first derivative at η_0 but may be combined in such a way that both U_1 and $dU_1/d\eta$ are continuous at $\eta = \eta_0$. The essential features of this type of procedure are discussed by Walker and Stewartson (1974). Approximately 350 mesh points were used on the interval $\eta_0 \leq \eta \leq L$ and this was found to be sufficient to guarantee at least three significant figures of accuracy in the computed numerical solution.

Before moving to the data comparisons, it is necessary to discuss one further point. In the analysis leading to (5.47) it has been implicitly assumed that the inner region pressure gradient parameter p^+ (defined by equation (3.7)) is small as $Re \to \infty$. This assumption was not necessary in section 3 and the inner region profile given by (3.16) is also valid when p^+ is O(1). However, for the outer layer, when p^+ is O(1) the structure of the asymptotic expansions must be altered and (5.3) and (5.4) are no longer appropriate. It is worthwhile to briefly consider the physical situation when

$$p^+ = -\frac{\nu U_e(x)}{L u_\tau^3(x,Re)} \frac{dU_e}{dx} = -\frac{1}{Re\, u^{*3}} \frac{1}{U_\infty} \frac{dU_\infty}{dx} \quad , \tag{5.54}$$

is O(1) and this occurs for

$$U_\infty'/U_\infty = O(Re\, u^{*3}). \tag{5.55}$$

With x fixed, the right side of (5.55) becomes infinite as $Re \to \infty$ and it is clearly unacceptable for p^+ to become O(1) in this limit process. However, with Re large and fixed, a situation may be envisaged where p^+ becomes O(1) as x approaches a point of time-mean separation, specifically when $u^* = O(Re^{-1/3})$. When this situation occurs it appears that the expansions in the outer layer for both the velocity and additive stress in (5.3) and (5.4) respectively, are no longer complete. In addition, the constitutive relation defined by (5.35) and (5.45) is no longer adequate. This difficulty has been briefly mentioned by Yajnik (1970) and Fendell (1972) but the proper way to handle the near-separation problem is not resolved at present. Consequently, in this and the following section, p^+ is regarded as a lower order term for the inner layer and the inner region profile (3.16) was taken with p^+ formally set equal to zero. (Note that the log-law "constant" C_i in (3.16) is still variable though through the parameter S.) In view of the above discussion and that in §5.1, attention will be restricted here to flows which are not close to separation.

The data comparisons for a number of equilibrium flows using the composite profile defined by (5.51) are given in Appendix C to which the reader is referred. Detailed descriptions of each case are also given in Appendix C and only the main results will be summarized here.

Generally the one-parameter (u_τ) fits to the constant pressure and favorable pressure gradient equilibrium flows give good representations of the experimental data; in accordance with the discussion in §5.1, the representation of the data improves at the downstream stations as the flows presumably approach self-similar conditions. In the adverse

equilibrium flow considered in Appendix C, the representation of the data is fair but the trend to self-similar behavior was not observed; this is the expected result since self-similarity is not anticipated in an adverse pressure gradient flow.

5.5 An Alternative Eddy Viscosity

One property of the smoothly varying eddy viscosity formula used in §5.4 is that $\varepsilon_s(\eta)$ approaches the required linear behavior (equation (5.42)) algebraically as $\eta \to 0$. An alternative formula may be defined such that $\varepsilon(\eta)$ approaches the linear behavior near $\eta = 0$ exponentially quickly. It was found that such an eddy viscosity relation produced slightly better data fits and consequently this form of the eddy viscosity will be briefly considered here.

One possible choice, satisfying the above requirement, would be

$$\varepsilon_0(\eta) = -\frac{\kappa\eta}{F_1(x,\infty)} \operatorname{erf}(a_0/\eta). \tag{5.56}$$

As $\eta \to \infty$, ε must conform to (5.38) and to satisfy this requirement define

$$a_0 = -\frac{\sqrt{\pi}}{2}\frac{K}{\kappa} F_1(x,\infty). \tag{5.57}$$

The eddy viscosity defined by (5.56) and (5.57) effectively reverses the behavior inherent in (5.45); in this case the limit (5.42) is approached exponentially quickly but the decay to (5.38) is algebraic. In data comparisons using (5.56) it was found that the relatively slow decay of (5.56), for large η, tended to degrade the quality of the fits. Consequently an alternative form was defined according to

$$\varepsilon_N(\eta) = \frac{-\kappa\eta}{F_1(x,\infty)} \left\{ erf\ (a_0/\eta) + \sum_{j=1}^{N} a_j Q_j(a_0/\eta) \right\}. \tag{5.58}$$

Here the Q_j are a set of functions (to be selected) which decay exponentially to zero as $\eta \to 0$. The sum of terms in (5.58) is added solely to increase the rate of decay to the limit (5.38) for large η and the constants a_j are to be selected for this purpose. There is a wide variety of functions Q_j which will suit the above purpose and it was arbitrarily decided to take solutions of the equation

$$y'' + 2xy' - 2(j - 1)y = 0, \tag{5.59}$$

for the Q_j. These solutions are parabolic cylinder functions and may be related to repeated integrals of the error function. They represent a complete set of functions and the first few Q_j are defined by:

$$\left.\begin{aligned}
Q_1(x) &= erf\ x - 1, \\
Q_2(x) &= x(erf\ x - 1) + \frac{e^{-x^2}}{\sqrt{\pi}}, \\
Q_3(x) &= (2x^2 + 1)(erf\ x - 1) + \frac{2x}{\sqrt{\pi}} e^{-x^2}, \\
Q_4(x) &= (2x^3 + 3x)(erf\ x - 1) + \frac{2}{\sqrt{\pi}} (x^2 + 1)e^{-x^2}, \\
Q_5(x) &= (4x^4 + 12x^2 + 3)(erf\ x - 1) + \frac{2}{\sqrt{\pi}} (2x^3 + 5x)e^{-x^2}.
\end{aligned}\right\} \tag{5.60}$$

In Table 3, the coefficients associated with retaining an increasing number of terms in the sum in (5.58) is given as well as the rate of decay to the limit (5.38). In Figure 2 the functions $\varepsilon_0(\eta)$ and $\varepsilon_5(\eta)$ are plotted. It is clear that by taking additional terms in (5.58) the rate of decay to the limit (5.38) may be accelerated; however the quality of the fits obtained using $\varepsilon_5(\eta)$ did not improve substantially

Table 3

Coefficients Associated with the Eddy Viscosity Formula (5.58) for Various Values of N

N	0, 1, 2	3	4	5
$a_0\kappa/K$	0.886227	1.032408	1.163729	1.282963
a_1	0	1	3.476918	9.702465
a_2	0	3.544908	18.488031	74.728587
a_3	0	1	10.430755	68.268486
a_4	0	0	3.081339	43.304199
a_5	0	0	0	4.351232
Rate of decay to (5.38)	$O(\eta^{-2})$	$O(\eta^{-3})$	$O(\eta^{-4})$	$O(\eta^{-5})$

over that obtained using $\varepsilon_4(\eta)$. Consequently, formulae for $\varepsilon_N(\eta)$ for $N > 5$ were not considered.

The data comparisons using $\varepsilon_5(\eta)$ are given in Appendix D for the same data sets considered in Appendix C; the fits described in Appendix D are one-parameter optimizations on the parameter u_τ and may be compared with the corresponding cases in Appendix C. Overall for zero and favorable pressure gradients, use of $\varepsilon_5(\eta)$ produces slightly better results than use of equation (5.45). For the mild adverse pressure gradient equilibrium flow of Andersen, et al. (1972), there is a significant improvement in the quality of the fits. Thus it appears that maintaining the strictly linear behavior in $\varepsilon(\eta)$ near $\eta = 0$ is worthwhile.

5.6 Summary

It has been demonstrated in this section that the one-parameter composite profile consisting of the unsteady wall layer model and an outer region similarity profile gives a good representation of equilibrium flow data. In zero and favorable pressure gradient flows, the quality of the fits improves downstream, as expected from theoretical considerations. In the adverse pressure gradient flow this trend is not observed. By varying the eddy viscosity parameter K as well as u_τ, the quality of the fits (at data stations where the flow is not self-similar) may be significantly improved. Lastly, the eddy viscosity formula used in §5.5 (wherein an essentially linear variation is imposed near $\eta = 0$) appears to be somewhat preferable to the form used in §5.4.

One final point is worthy of note here. In carrying out the profile fits, the outer region length scale was selected as δ^*/u^* according to equation (5.44). The main reason for this choice is that the eddy viscosity formulae (5.45) and (5.58) assume a simple form with $F_1(x,\infty) = -1$. However an equally valid choice for Δ_0 would be the boundary-layer thickness which is also $O(u^*)$. Define the boundary-layer thickness as that ordinate where the velocity profile achieves some fixed and consistent fraction θ of the mainstream value; typical definitions of θ are 0.99 or 0.995. From equation (5.3)

$$u^* \frac{\partial F_1}{\partial \eta} \left(\frac{\delta}{\Delta_0}\right) = -(1 - \theta). \tag{5.61}$$

With Δ_0 selected according to

$$\Delta_0 = \delta \tag{5.62}$$

equations (5.18) and (5.40) become, respectively,

$$\frac{1}{u^*} = \frac{1}{\kappa} \log\left\{Re_\delta \, u^* U_\infty(x)\right\} + C_i - C_0, \tag{5.63}$$

$$F_1(x,\infty) = \frac{-\delta^*}{u^*\delta}. \tag{5.64}$$

An analysis similar to that leading to (5.50) leads to,

$$\frac{\delta^{*2}}{u^{*2}\delta^2} \frac{d}{d\eta^*}\left\{\varepsilon \frac{dU_1}{d\eta^*}\right\} + (1 + 2\beta)\eta^* \frac{dU_1}{d\eta^*} + 2\beta U_1 = 0 \tag{5.65}$$

where $\eta^* = y/\delta$ and β is the same as in equation (5.50). The fitting procedure described in §5.4 and §5.5 was also carried out using equation (5.65). To initiate the procedure a value of δ was first guessed and a solution of (5.65) computed; the value of δ was refined in an iterative procedure subject to the constraint (5.61). In this way results identical to those described in §5.4 and §5.5 were obtained. Clearly the two approaches are equivalent since (5.50) may be obtained from (5.65) by a transformation of η^*.

6. SUMMARY AND CONCLUSIONS

The stated objective of this report was to present data comparisons for four models for the velocity profile in a two-dimensional, time-mean, constant property turbulent boundary layer. The primary motivation for this was to ascertain how well each model represents experimental data and to offer a critical evaluation of each model on this basis. A secondary goal was to search for any obvious trends in the profile parameters which might prove useful in a boundary layer prediction method.

In section 3, the Van Driest (1956) and extended Van Driest models for the inner layer were compared with the more recent unsteady wall layer model (Walker & Abbott, 1977, Walker & Scharnhorst, 1977). To provide a direct test of the two models only inner region data was considered and the results are described in Appendix A. The data comparisons and the analysis in section 3 show the failure of the extended Van Driest model in flows with pressure gradient and for this reason, it was recommended that this model be abandoned. On the other hand, the unsteady wall layer model represents the data very well even in severe pressure gradients and generally gives a much closer representation of the data; of course this does not prove the validity of the assumptions behind the unsteady wall layer model (Walker & Abbott, 1977 and Walker & Scharnhorst, 1977) but does provide a good degree of confidence in the resulting profile.

From a practical standpoint a number of points in connection with the unsteady wall layer model deserve brief consideration. First

the unsteady wall layer model contains the parameters T and u_τ which are physically observeable quantities of the flow; this is in contrast to the parameter A^+, in the Van Driest (1956) and extended Van Driest models, which is simply an adjustable constant with no physical significance. At present there are substantial experimental problems in measuring the quantities T and u_τ directly but it may be expected that these difficulties will be resolved at some future date. In the second place, the theoretical basis of the unsteady wall layer model is somewhat more satisfactory than for the Van Driest (1956) model. At the same time, there are a number of unresolved features surrounding the theoretical development of the unsteady wall layer model which are discussed in Walker & Scharnhorst (1977). Further work in this area is clearly needed with particular reference to obtaining a good theoretical understanding of the dynamics of the outer layer and the observed inviscid-viscous interactions with the inner layer. For the present, the profile (3.16) must be regarded as only a useful model. Finally equation (3.16) appears more complicated than the Van Driest (1956) model; however the computation time necessary to perform the quadrature in (3.16) accurately is comparable to that necessary to evaluate (3.4). In addition a program to evaluate (3.16) is available from the authors upon request. In summary, for the above reasons the unsteady wall layer model is believed to be a preferred and useful formula for the mean profile in the wall region.

Additional verification of the unsteady wall layer model was considered in sections 4 and 5, where (3.16) was coupled with Coles' (1956)

"law of the wake" and an outer region similarity profile respectively, to form a composite profile for the entire boundary layer. We first consider the results of section 4 and discuss the "law of the wake".

The three parameter fits using (4.4), have been shown to yield a close representation of data under a wide range of experimental conditions. In this context equation (4.4) may be considered to be very useful and the results described in Appendix B provide additional confidence in the unsteady wall layer model. Moreover, the data fits also suggest that assuming that C_i has a universal value of 5.0 (or some other value) is not justified.

However, any conclusions based on use of the "law of the wake" must be regarded with some caution since a number of legitimate objections may be raised to Coles (1956) model. The first of these is that the model contains the ill-defined boundary layer thickness δ; in data comparisons in this report as well as in Coles & Hirst (1969) this quantity must be treated as a parameter to obtain good representations of the data. However, the optimized values of δ do not appear to correspond to a consistent definition of the boundary layer thickness from data set to data set. A second theoretical deficiency is that the slope and all higher derivatives of (4.4) are not continuous at the boundary layer dege. The third and most serious difficulty with the "law of the wake" is the notion that the velocity profile in the outer layer may be written as a linear combination of a logarithm and a wake function; this deficiency has been recently discussed by Fendell (1972) and is now recognized to be a flaw in the original

formulation. In zero and adverse pressure gradient flows the wake strength parameter assumes relatively large values which tends to mask this basic problem. However, in favorable pressure gradient flows, the wake strength parameter becomes small and it is in these situations where the improper formulation is most evident.

Although there are a number of well known disadvantages inherent in momentum integral prediction methods, the composite profile (4.4) could in principle be used for this purpose. One of the better integral methods is due to Alber (1968) which has been recently described by White (1974, p.289). This method has achieved a fair degree of success and is based on Coles (1956) model. Alber (1968) ignores the inner layer and assumes a universal value for C_i; the "law of the wake" thus provides a two parameter expression for the velocity profile in the outer layer. However, it is clear from Appendix B that a universal value of C_i will not provide a close representation of profile data in every situation. The effect of the inner layer could be included through use of (4.4); however, (4.4) is a three parameter expression and this means that at least two experimental correlations of the parameters are required. As White (1974, p.482) has shown the wake strength parameter Π can be correlated as a function of the Clauser parameter β_c (defined in equation, 5.30) and such a correlation could be obtained using the results of Appendix B. However, the form of the required second correlation relating the profile parameters is not evident at this time. It is also worthwhile to remark that there is serious question about the validity of the type of approach used by

Alber (1968). The so-called mechanical energy equation or its integrated form (containing the dissipation integral) is not a relation which is independent from the momentum equation. For these reasons and because of the difficulties discussed in connection with the "law of the wake" it is not clear that this momentum integral approach can be pursued with profit.

In summary, we regard the "law of the wake" as an interesting correlation; because it represents outer region data well, it is a useful expression to examine the validity of the unsteady wall layer model. Given profile data, equation (4.4) may be used, through a three parameter optimization, to closely represent the data at that station. However, because of various deficiencies in the "law of the wake" any attempt to use the formula in a prediction method should be exercised with caution.

In section 5, a similarity profile was used for the outer region. The theoretical foundation for this profile is somewhat firmer than for the "law of the wake" and good representations of equilibrium flow data were obtained with a <u>one</u> parameter (u_τ) optimization procedure. As expected the profiles in zero and favorable pressure gradients are successively represented better at subsequent stations downstream; the adverse pressure gradient flow does not exhibit this trend suggesting that in this environment similarity is not being approached. It was also shown that in situations where the flow is not similar; a closer representation of the data could be achieved by varying the eddy viscosity constant K as well as u_τ. This is important for a differential

prediction method, where the data at some initial station must be represented in order to initiate a numerical marching scheme downstream. A prediction method based on solving equation (5.6) numerically in the outer layer whilst matching to the inner profile (3.16) is currently under consideration and will be reported in due course.

REFERENCES

Alber, I.E. 1969 "Application of an exact expression for the equilibrium dissipation integral to the calculation of turbulent nonequilibrium flows", in Kline et al. (1969), 126-135.

Andersen, P.S., Kays, W.M. & Moffat, R.J. 1972 "The turbulent boundary layer on a porous plate: an experimental study of the fluid mechanics for adverse free-stream pressure gradients", Mech. Engrg. Rept. HMT-15, Stanford Univ.

Bard, Y. 1974 Nonlinear Parameter Estimation, Academic Press, New York.

Black, T.J. 1968 "An analytical study of the measured wall pressure field under supersonic boundary layers", NASA CR-888.

Brown, K.C. & Joubert, P.N. 1969 "The measurement of skin friction in turbulent boundary layers with adverse pressure gradients", J. Fluid Mech. 35, 737-757.

Brown, S.N. & Stewartson, K. 1965 "On similarity solutions of the boundary layer equations with algebraic decay", J. Fluid Mech. 23, 673-687.

Cebeci, T. & Smith, A.M.O. 1969 "A finite-difference solution of the incompressible turbulent boundary-layer equations by an eddy-viscosity concept", in Kline, et al. (1969), 346-355.

Cebeci, T. & Smith, A.M.O. 1974 Analysis of Turbulent Boundary Layers, Academic Press, New York.

Clauser, F.H. 1954 "Turbulent boundary layers in adverse pressure gradients", J. Aeronaut. Sci. 21, 91-108.

Clauser, F.H. 1956 "The turbulent boundary layer", Adv. Appl. Mech. 4, 1-51.

Coles, D.E. 1956 "The law of the wake in the turbulent boundary layer", J. Fluid Mech. 1, 191-226.

Coles, D.E. & Hirst, E.A. 1969 Proceedings, Computation of Turbulent Boundary Layers - 1968, AFOSR-IFP-Stanford Conference, Volume II, Mech. Engrg., Stanford Univ.

Corino, E.R. & Brodkey, R.S. 1969 "A visual investigation of the wall region in turbulent flow", J. Fluid Mech. 37, 1-30.

Einstein, H.A. & Li, H. 1956 "The viscous sublayer along a smooth boundary", Proc. Amer. Soc. Civil Engrs., paper 945.

Fendell, F.E. 1972 "Singular perturbation and turbulent shear flow near walls", J. Astronaut. Sci. 20, 129-165.

Gupta, A.K., Laufer, J. & Kaplan, R.E. 1971 "Spatial structure in the viscous sublayer", J. Fluid Mech. 50, 493-512.

Hinze, J.O. 1959 Turbulence, McGraw-Hill, New York.

Kays, W.B., Moffat, R.J. & Thielbahr, W.H. 1970 "Heat transfer to the highly accelerated turbulent boundary layer with and without mass addition", J. Heat Transfer 92, 499.

Keller, H.B. 1969 "Accurate difference methods for linear ordinary differential equations subject to linear constraints", SIAM J. Numer. Anal. 6, 8-30.

Kline, S.J., Morkovin, M.V., Sovran, G. & Cockrell, D.J. 1969 Proceedings, Computation of Turbulent Boundary Layers - 1968, AFOSR-IFP-Stanford Conference, Volume I, Mech. Engrg., Stanford Univ.

Kline, S.J., Reynolds, W.C., Schraub, F.A. & Runstadler, P.W. 1967 "The structure of turbulent boundary layers", J. Fluid Mech. 30, 741-773.

Kline, S.J. & Runstadler, P.W. 1959 "Some preliminary results of visual studies of the flow model of the wall layers of the turbulent boundary layer", Trans. ASME, (Ser. E) 2, 166-170.

Leibovich, S. 1967a "On the differential equation governing the rear stagnation point in magnetohydrodynamics and Goldstein's 'backward' boundary layers", Proc. Camb. Phil. Soc. 63, 1327-1330.

Leibovich, S. 1967b "Magnetohydrodynamic flow at a rear stagnation point", J. Fluid Mech. 29, 401-413.

Mellor, G.L. & Gibson, D.M. 1966 "Equilibrium turbulent boundary layers", J. Fluid Mech. 24, 225-253.

Mellor, G.L. & Herring, H.J. 1969 "A method for calculating compressible turbulent boundary layers", NASA CR-1144. (see also Kline et al. (1969).)

Miller, B.L.P. 1972 "The measurement of wall shearing stress in turbulent boundary layers", Ph.D. Thesis, Univ. of Leicester.

Patankar, S.V. & Spalding, D.B. 1968 Heat and Mass Transfer in Boundary Layers, C.R.C. Press, Cleveland.

Pierce, F. & Zimmerman, D.B. 1972 "Wall shear stress inference from two and three-dimensional turbulent boundary layer velocity profiles", ASME paper 72-WA/FE-4.

Rotta, J.C. 1962 "Turbulent boundary layers in incompressible flow", Prog. in Aero. Sci., Vol. 2., Boundary-Layer Problems, Pergamon Press, New York, 1-219.

Saffman, P.G. 1970 "A model for inhomogeneous turbulent flow", Proc. Roy. Soc. Lond., A.317, 417-433.

Samuel, A.E. & Joubert, P.N. 1974 "A boundary layer developing in in an increasingly adverse pressure gradient", J. Fluid Mech. 66, 481-505.

Schlichting, H. 1968 Boundary-Layer Theory, McGraw-Hill, New York.

Simpson, R.L. 1970 "Characteristics of turbulent boundary layers at low Reynolds numbers with and without transpiration", J. Fluid Mech. 42, 769.

Strickland, J.H. & Simpson, R.L. 1973 "The separating turbulent boundary layer: an experimental study of an airfoil type flow", Tech. Rept. WT-2, Southern Methodist Univ.

Van Driest, E.R. 1956 "On turbulent flow near a wall", J. Aeronaut. Sci. 23, 1007-1012.

Walker, J.D.A. & Abbott, D.E. 1977 "Implications of the structure of the viscous wall layer", Turbulence in Internal Flows, SQUID Workshop Proc., S.N.B. Murthy, Ed., Plenum Press.

Walker, J.D.A., Abbott, D.E. & Scharnhorst, R.K. 1976 "On the nominally steady two-dimensional time-mean turbulent boundary layer", Tech. Rept. CFMTR-76-1, Purdue Univ.

Walker, J.D.A. & Scharnhorst, R.K. 1977 "Solutions of the time-dependent wall layer flow in a turbulent boundary layer", to appear in Proc. of the 14th Annual Meeting of the Society of Engineering Science, held at Lehigh University, Bethlehem, Pa., Nov. 14-17, 1977.

Walker, J.D.A. & Stewartson, K. 1972 "The flow past a circular cylinder in a rotating frame", Z. Angew. Math. Phys. 23, 745-752.

Walker, J.D.A. & Stewartson, K. 1974 "Separation and the Taylor column problem for a hemisphere", J. Fluid Mech. 66, 767-789.

White, F.M. 1974 Viscous Flow Theory, McGraw-Hill, New York.

Yajnik, K.S. 1970 "Asymptotic theory of turbulent shear flows", J. Fluid Mech. 42, 411-427.

York, R.E. & Abbott, D.E. 1973 "The effects of pressure gradient on velocity profiles in turbulent boundary layers", Tech. Rept., CFMTR-73-2, Purdue Univ.

APPENDIX A

DATA COMPARISONS FOR THE INNER REGION

Introduction

Data comparisons between the Van Driest inner region model given by equation (3.4) and the unsteady wall layer model given by equation (3.16) are discussed in this appendix. The data sets are grouped according to pressure gradient and a few comments are presented below.

A.1 Zero Pressure Gradient Data

The Van Driest and unsteady wall layer fits to the constant pressure data of Andersen, et al. (1972) are detailed in Table A.1 and Figure A.1 and Table A.2 and Figure A.2, respectively. Visually there appears to be little to choose between the two models. However from the tables $\bar{\varepsilon}$ = 0.0072 for the Van Driest model while $\bar{\varepsilon}$ = 0.0073 for the unsteady wall layer profile; here $\bar{\varepsilon}$ is the average root-mean-square error over the nine data stations. Thus on average the Van Driest profile appears to fit the profiles very slightly better; however the difference is not significant and no conclusions can be drawn. For example, both profiles do not fit the sixth data station very well and if this data station is omitted $\bar{\varepsilon}$ for the unsteady wall layer model is slightly lower ($\bar{\varepsilon}$ = 0.0065) than that for the Van Driest model ($\bar{\varepsilon}$ = 0.0066). It should be noted that in Table A.1 the optimum value for A^+ varies substantially about the value of A^+ = 26.0 suggested by Van Driest (1956). It may also be observed that the optimum value of u_τ is appreciably different from the quoted experimental value for the Van Driest model than for the unsteady wall layer model. However because of the uncertainties that have already

been discussed in connection with the methods of determining u_τ from experimental data, no definite conclusions can be made here.

A.2 Mild Adverse Pressure Gradient Data

The fits of the two inner region models to a mildly adverse gradient flow are shown in Figures A.3 and A.4 and the numerical values of the parameters are given in Tables A.3 and A.4. A close inspection of Figures A.3 and A.4 reveals that the unsteady wall layer model appears to give a closer representation of the data than the extended Van Driest profile and this is borne out from the tables where $\bar{\varepsilon} = 0.0058$ for the unsteady wall layer profile and $\bar{\varepsilon} = 0.0076$ for the extended Van Driest model. The extended Van Driest profile only gives a better fit on the fifth data station although it is evident from the tables that both profiles encounter difficulty for this station. For this data set the unsteady wall layer model is superior and the difference is significant.

A.3 Strong Adverse Pressure Gradient Data

The results of the two profile fits to inner region data for strongly adverse gradient flows are shown in Figures A.5 to A.8 and Tables A.5 to A.8; these include the third Andersen, et al. (1972) flow and Fraser Flow A (Coles & Hirst, 1969).

The data fits for the Andersen, et al. (1972) flow are given in Figures A.5 and A.6; this flow has been referred to as a strong adverse pressure gradient flow by the originators since the values of p^+ are about twice as large as for their second flow (discussed in A.2). On average the unsteady wall layer model fits the data ($\bar{\varepsilon} = 0.0062$) better than the extended Van Driest model ($\bar{\varepsilon} = 0.0070$). The extended Van Driest

model gives a better fit on only the fourth and sixth data stations.

The data comparisons for Fraser Flow A are given in Figures A.7 and A.8; for this flow the values of p^+ are larger than in the previous case and in fact this flow is proceeding toward separation. At the first two stations the value of p^+ is small; both profile models give a good representation of the data although ε is smaller for the unsteady wall layer model. At subsequent data stations downstream as p^+ increases, the extended Van Driest model begins to deviate drastically from the data. Recall that the result of the optimization procedure is the optimum performance for a model (according to the fitting criterion (1.5)). Clearly there is no correspondence between the extended Van Driest model and these data; the algebraic behavior of the profile (discussed in §3.1) is clearly evident in Figure A.7 and the result of this is that the data can only skew through the data points. On the other hand, the unsteady wall layer model conforms to the latter data stations quite well as is apparent in Figure A.8; there is no drastic deviation from the data as in Figure A.7. The $\bar{\varepsilon}$ for the extended Van Driest model is almost three times as large as that for the unsteady wall layer model (0.0181 versus 0.0066).

TABLE A.1: ANDERSEN, KAYS AND MOFFAT - ZERO P. G. - 120771-1
(ENGLISH UNITS)

NU= 1.590000E-04

EXPERIMENTAL VALUES

ID	XSTA	UE	UTAU	DUEDX	P+	DELTA	DELTA*	THETA
8101	.167	31.21	1.557	.01	-.00001	.2871	.0504	.0328
8102	.833	31.13	1.467	.01	-.00001	.4225	.0772	.0521
8103	1.833	31.14	1.400	.01	-.00001	.6242	.1135	.0768
8104	2.833	31.05	1.353	.00	-.00001	.7654	.1412	.0977
8105	3.833	31.04	1.321	.00	-.00000	.9590	.1709	.1185
8106	4.833	31.13	1.296	-.00	.00000	1.1065	.1968	.1375
8107	5.833	31.04	1.272	-.01	.00001	1.2755	.2255	.1584
8108	6.833	31.07	1.254	-.01	.00002	1.4808	.2533	.1794
8109	7.500	31.06	1.246	-.01	.00003	1.5810	.2670	.1902

VAN DRIEST MODEL - INNER REGION FIT

ID	P+	UTAU	A+	EPSILON
8101	-.00001	1.551	27.915	.007246
8102	-.00001	1.564	19.550	.004434
8103	-.00001	1.270	35.032	.009342
8104	-.00001	1.252	33.161	.006499
8105	-0.00000	1.220	32.348	.004517
8106	.00001	1.157	38.676	.011817
8107	.00002	1.203	29.955	.007676
8108	.00003	1.141	35.359	.007668
8109	.00004	1.164	32.242	.005744

MEAN EPSILON= .007216

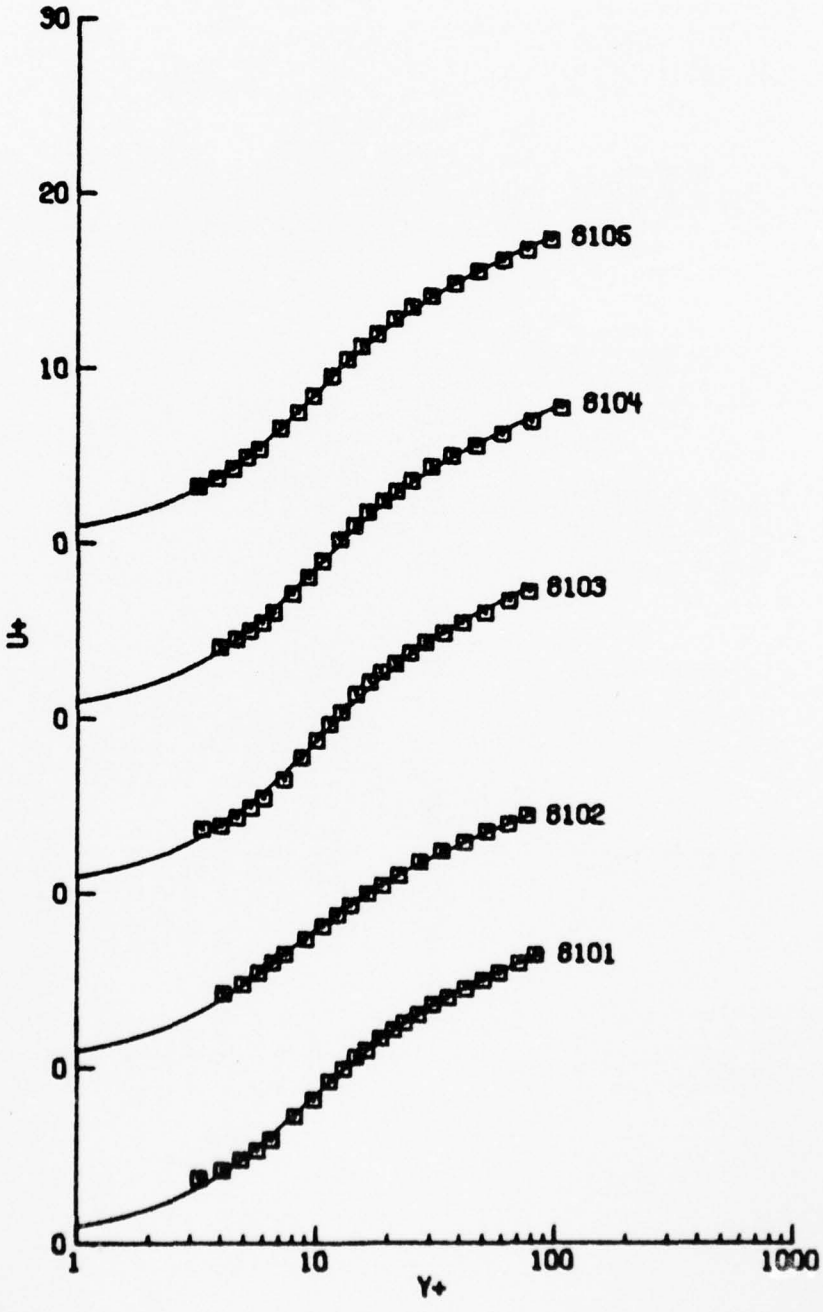

Figure A.1. Van Driest Model. (note shifted origins on the U^+ axis.)

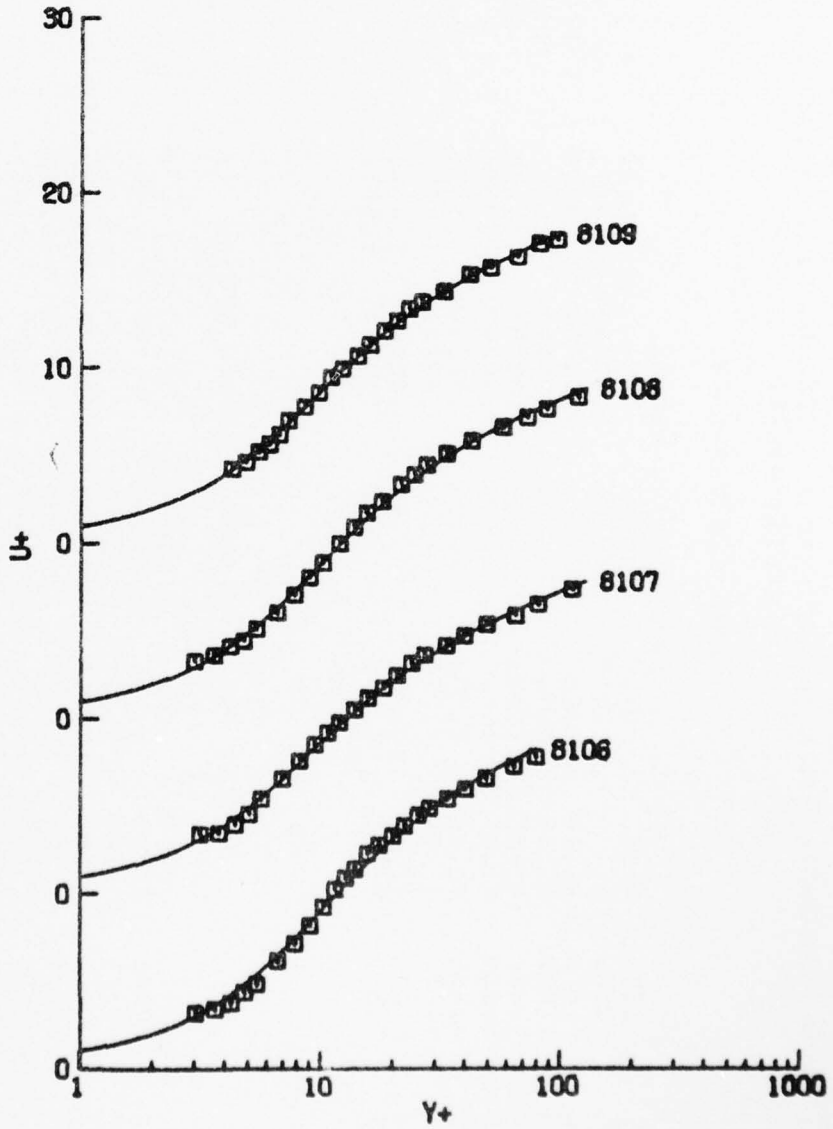

Figure A.1. (Continued).

TABLE A.2: ANDERSEN, KAYS AND MOFFAT - ZERO P. G. - 120771-1
(ENGLISH UNITS)

NU= 1.590000E-04

EXPERIMENTAL VALUES

ID	XSTA	UE	UTAU	DUEDX	P+	DELTA	DELTA*	THETA
8101	.167	31.21	1.557	.01	-.00001	.2871	.0504	.0328
8102	.833	31.13	1.467	.01	-.00001	.4225	.0772	.0521
8103	1.833	31.14	1.400	.01	-.00001	.6242	.1135	.0768
8104	2.833	31.05	1.353	.00	-.00001	.7854	.1412	.0977
8105	3.833	31.04	1.321	.00	-.00000	.9590	.1709	.1185
8106	4.833	31.13	1.298	-.00	.00000	1.1065	.1968	.1375
8107	5.833	31.04	1.272	-.01	.00001	1.2755	.2255	.1584
8108	6.833	31.07	1.254	-.01	.00002	1.4608	.2553	.1794
8109	7.500	31.06	1.246	-.01	.00003	1.5810	.2670	.1902

UNSTEADY WALL LAYER MODEL - INNER REGION F11

ID	P+	UTAU	S	EPSILON	Y1+	Ci
8101	-.00001	1.639	9.906	.006120	.4136	4.593
8102	-.00001	1.644	7.597	.004022	.7524	3.133
8103	-.00001	1.350	11.462	.009768	.2697	5.636
8104	-.00001	1.327	11.137	.005753	.2953	5.415
8105	-0.00000	1.291	11.010	.005053	.3058	5.329
8106	.00001	1.233	12.161	.013414	.2213	6.117
8107	.00001	1.273	10.413	.008732	.3602	4.929
8108	.00003	1.209	11.702	.006874	.2518	5.801
8109	.00003	1.235	10.907	.005999	.3143	5.260

MEAN EPSILON= .007304

AD-A042 672 PURDUE UNIV LAFAYETTE IND COMPUTATIONAL FLUID MECHAN--ETC F/G 20/4
COMPARISONS OF THEORETICAL PROFILES FOR A TWO-DIMENSIONAL TIME---ETC(U)
JUN 77 R K SCHARNHORST, J D WALKER AF-AFOSR-2707-74

UNCLASSIFIED CFMTR-77-1 AFOSR-TR-77-0877 NL

2 OF 3

ADA042-672

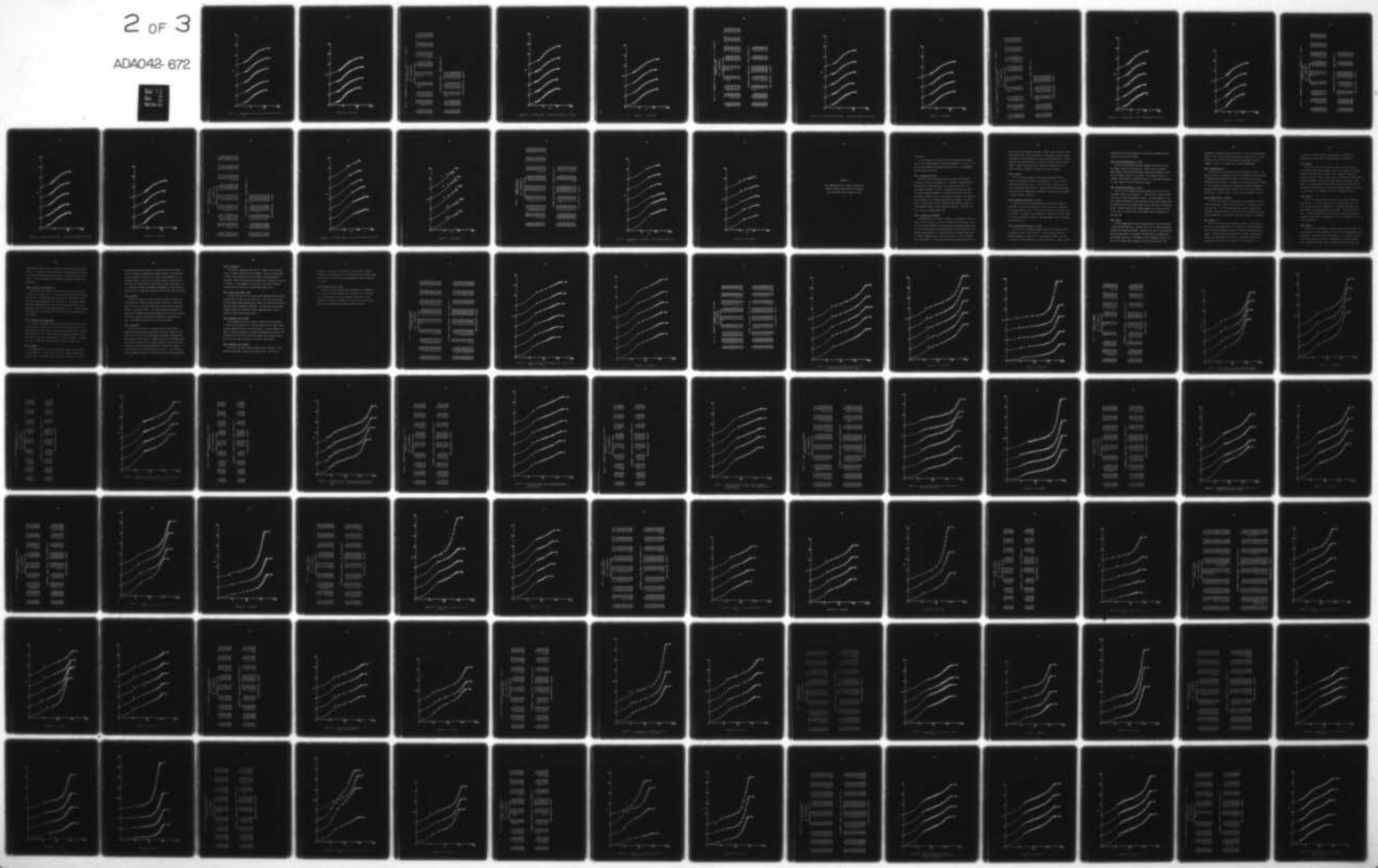

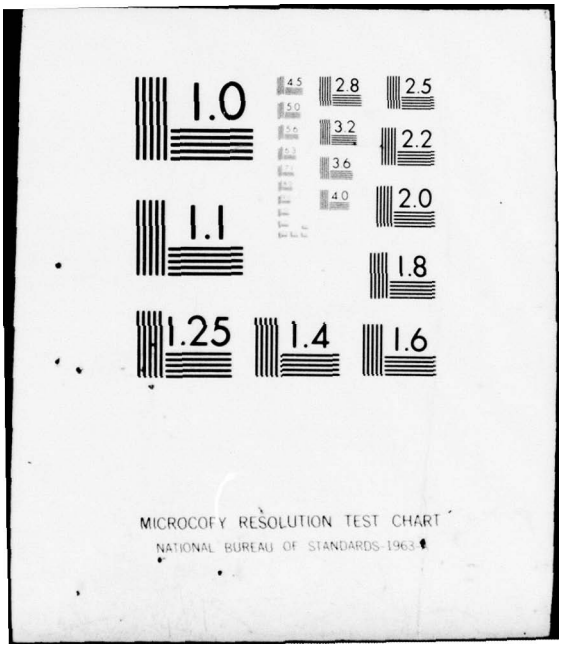
1.0
1.1
1.25
1.4
1.6
1.8
2.0
2.2
2.5
2.8
3.2
3.6
4.0
4.5
5.0
5.6
MICROCOPY RESOLUTION TEST CHART
NATIONAL BUREAU OF STANDARDS-1963-A

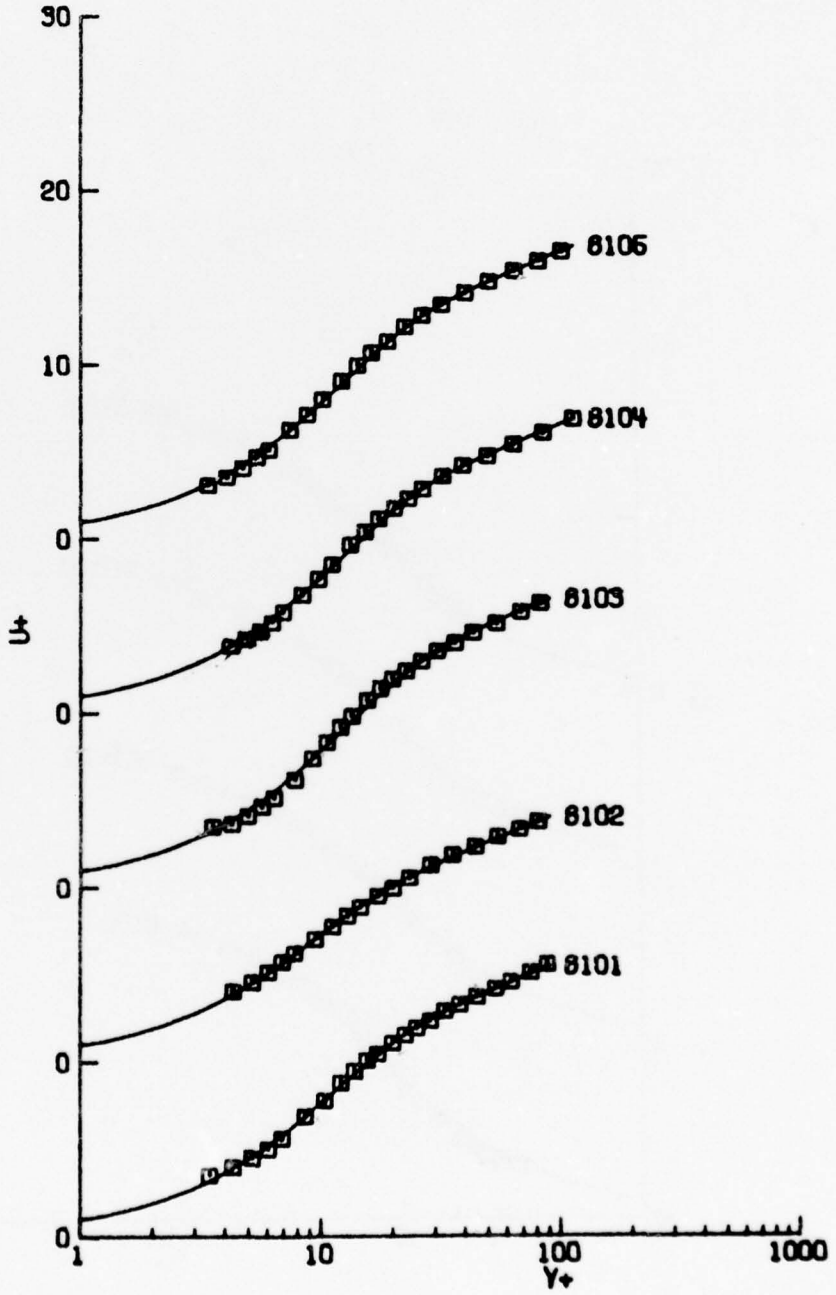

Figure A.2. Unsteady wall layer model. (Note shifted origins on U^+ axis).

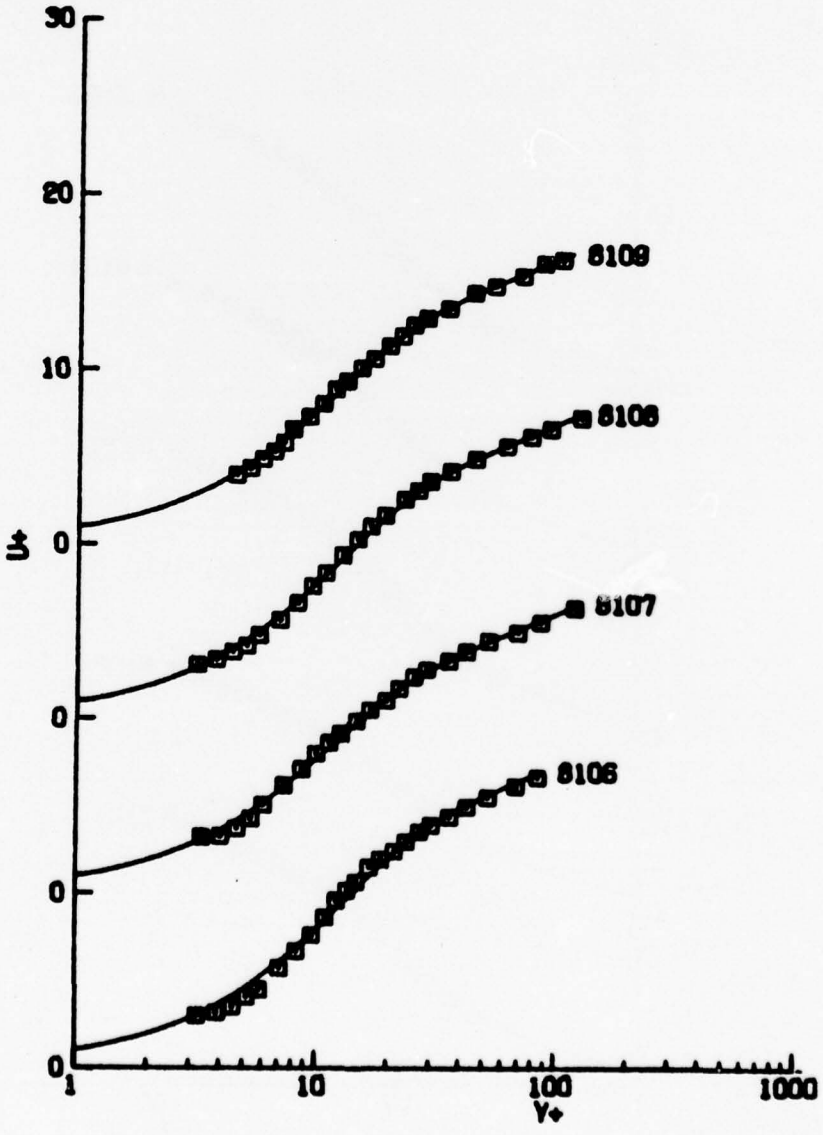

Figure A.2. (Continued).

TABLE A.3: ANDERSEN, KAYS AND MOFFAT - ...ILD P. G. - 071571-5
(ENGLISH UNITS)

NU= 1.660000E-04

EXPERIMENTAL VALUES

ID	XSTA	UE	UTAU	DUEDX	P+	DELTA	DELTA*	THETA
8201	.167	29.69	1.546	-2.44	.00325	.3081	.0556	.0357
8202	.833	26.93	1.198	-3.79	.00985	.5179	.1138	.0718
8203	1.833	24.57	1.010	-1.76	.00697	.8628	.1936	.1238
8204	2.833	23.26	.910	-1.13	.00579	1.1752	.2616	.1700
8205	3.833	22.27	.848	-.82	.00497	1.5029	.3356	.2176
8206	4.833	21.36	.799	-.63	.00438	1.7870	.3934	.2592
8207	5.833	20.74	.765	-.51	.00392	2.1211	.4610	.3049
8208	6.833	20.35	.742	-.43	.00356	2.4043	.5108	.3419
8209	7.500	20.05	.726	-.41	.00357	2.5701	.5449	.3656

VAN DRIEST MODEL - INNER REGION FIT

ID	P+	UTAU	A+	EPSILON
8201	.00384	1.463	25.868	.008821
8202	.01137	1.142	22.928	.008393
8203	.00779	.973	23.562	.008025
8204	.00632	.884	24.985	.008270
8205	.00696	.758	33.341	.006958
8206	.00478	.776	26.205	.007580
8207	.00426	.744	25.230	.007162
8208	.00362	.737	25.534	.005060
8209	.00342	.736	23.162	.006518

MEAN EPSILON= .007643

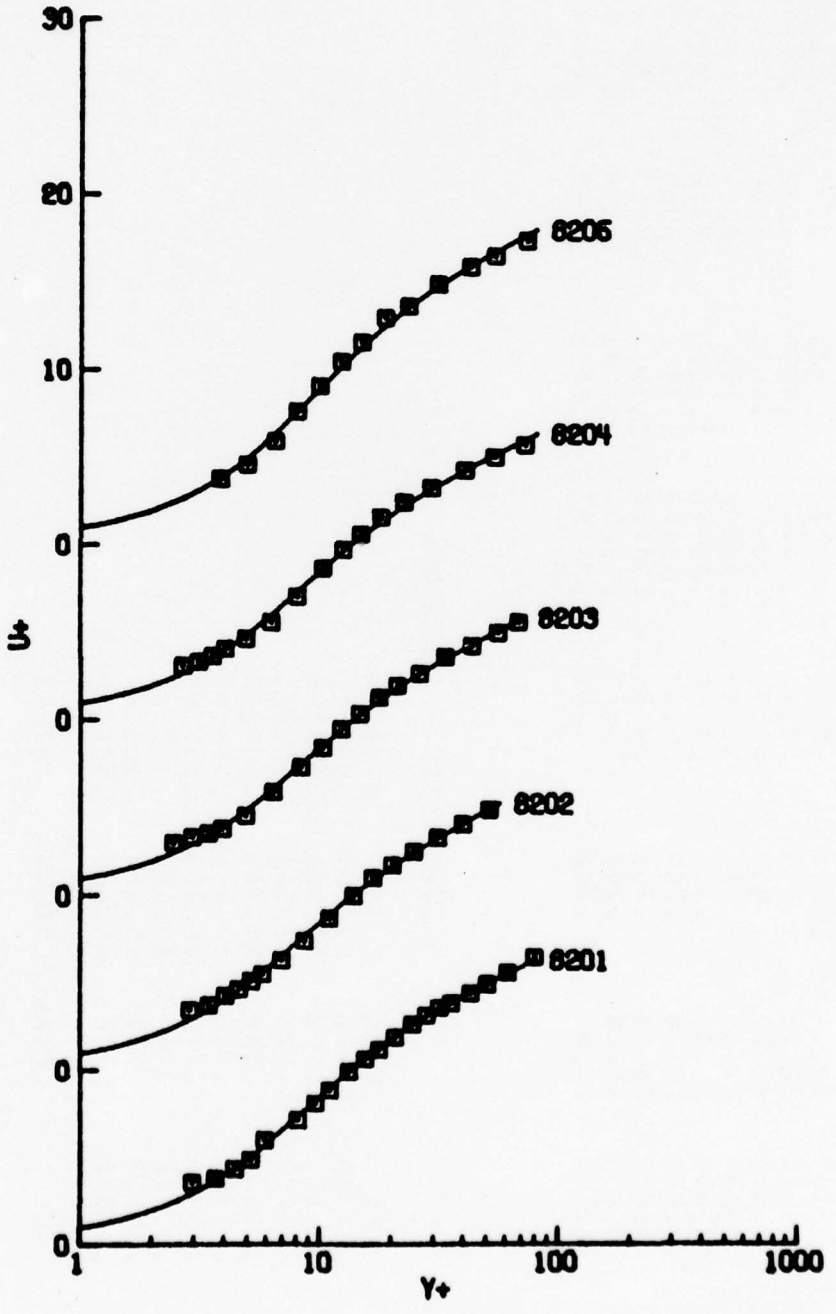

Figure A.3. Van Driest Model. (Note shifted origins on U^+ axis).

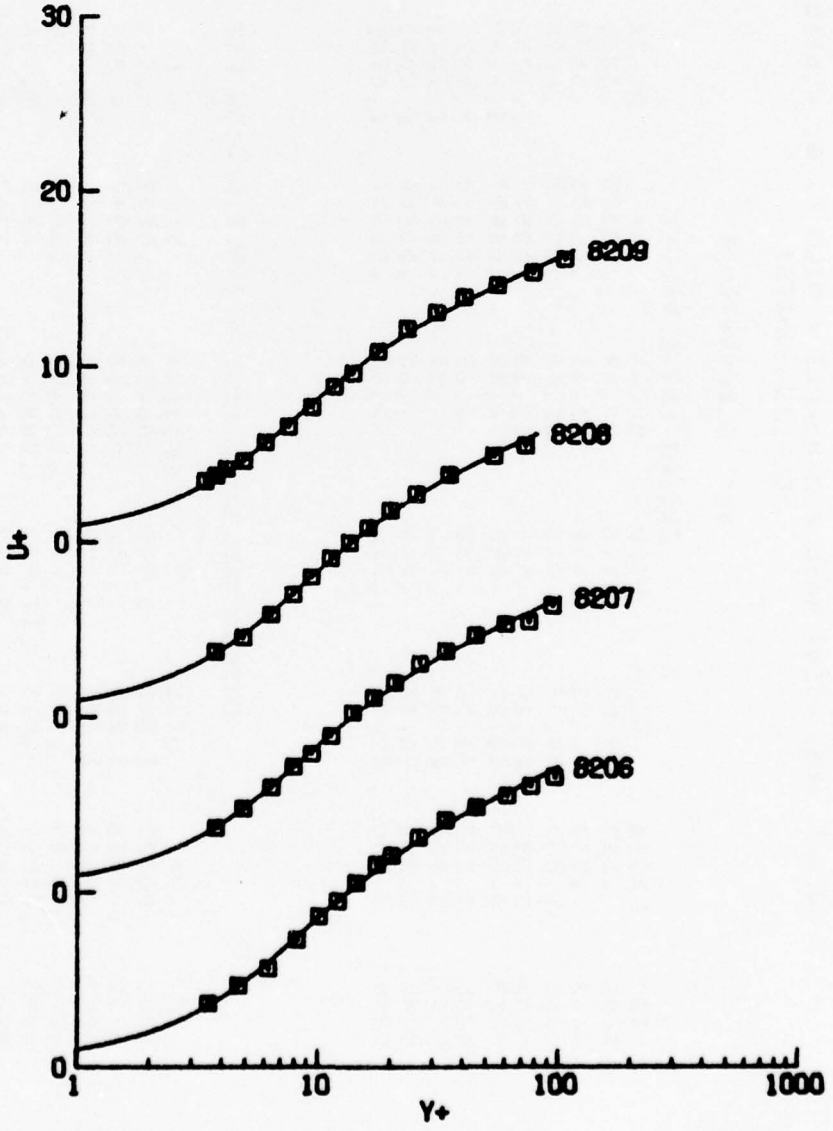

Figure A.3. (Continued).

TABLE A.4: ANDERSEN, KAYS AND MOFFAT - MILD P. G. - 071571-5
(ENGLISH UNITS)

NU= 1.660000E-04

EXPERIMENTAL VALUES

ID	XSTA	UE	UTAU	DUEDX	P+	DELTA	DELTA*	THETA
8201	.167	29.69	1.546	-2.44	.00325	.3081	.0556	.0357
8202	.833	26.93	1.198	-3.79	.00985	.5179	.1136	.0718
8203	1.833	24.57	1.010	-1.76	.00697	.6628	.1936	.1238
8204	2.833	23.26	.910	-1.13	.00579	1.1752	.2616	.1700
8205	3.833	22.27	.848	-.82	.00497	1.5029	.3356	.2176
8206	4.833	21.36	.799	-.63	.00468	1.7870	.3934	.2592
8207	5.833	20.74	.765	-.51	.00392	2.1211	.4610	.3049
8208	6.833	20.35	.742	-.43	.00356	2.4043	.5108	.3419
8209	7.500	20.05	.726	-.41	.00357	2.5701	.5449	.3656

UNSTEADY WALL LAYER MODEL - INNER REGION FIT

ID	P+	UTAU	S	EPSILON	Y1+	Ci
8201	.00327	1.543	9.703	.008454	.4007	4.515
8202	.00968	1.205	9.232	.005412	.3930	4.305
8203	.00668	1.025	9.357	.005915	.4066	4.342
8204	.00539	.932	9.639	.005699	.3863	4.509
8205	.00569	.811	11.420	.009346	.2223	5.736
8206	.00405	.820	9.892	.004646	.3717	4.655
8207	.00362	.786	9.593	.004926	.4097	4.449
8208	.00305	.781	9.492	.003903	.4277	4.373
8209	.00297	.772	9.147	.003927	.4720	4.146

MEAN EPSILON= .005825

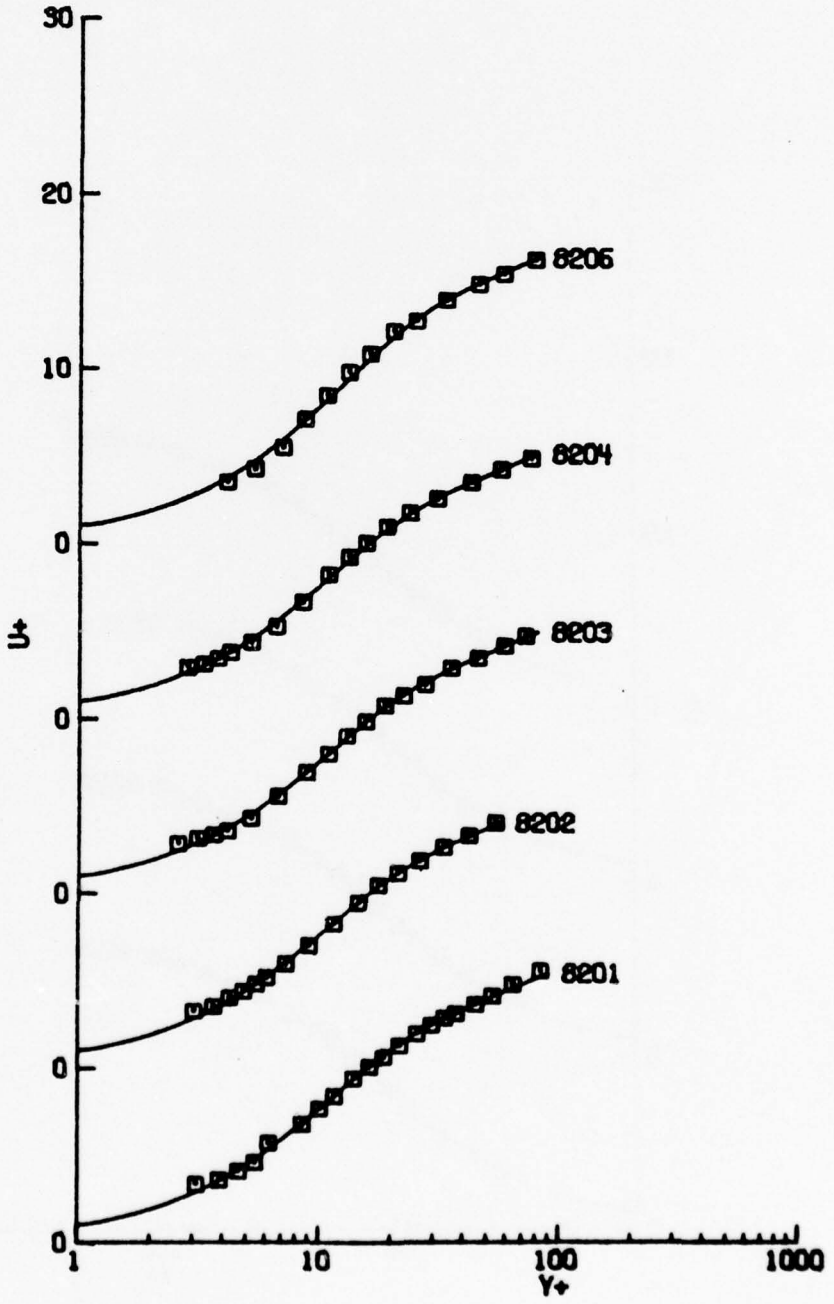

Figure A.4. Unsteady wall layer model. (Note shifted origins on U^+ axis).

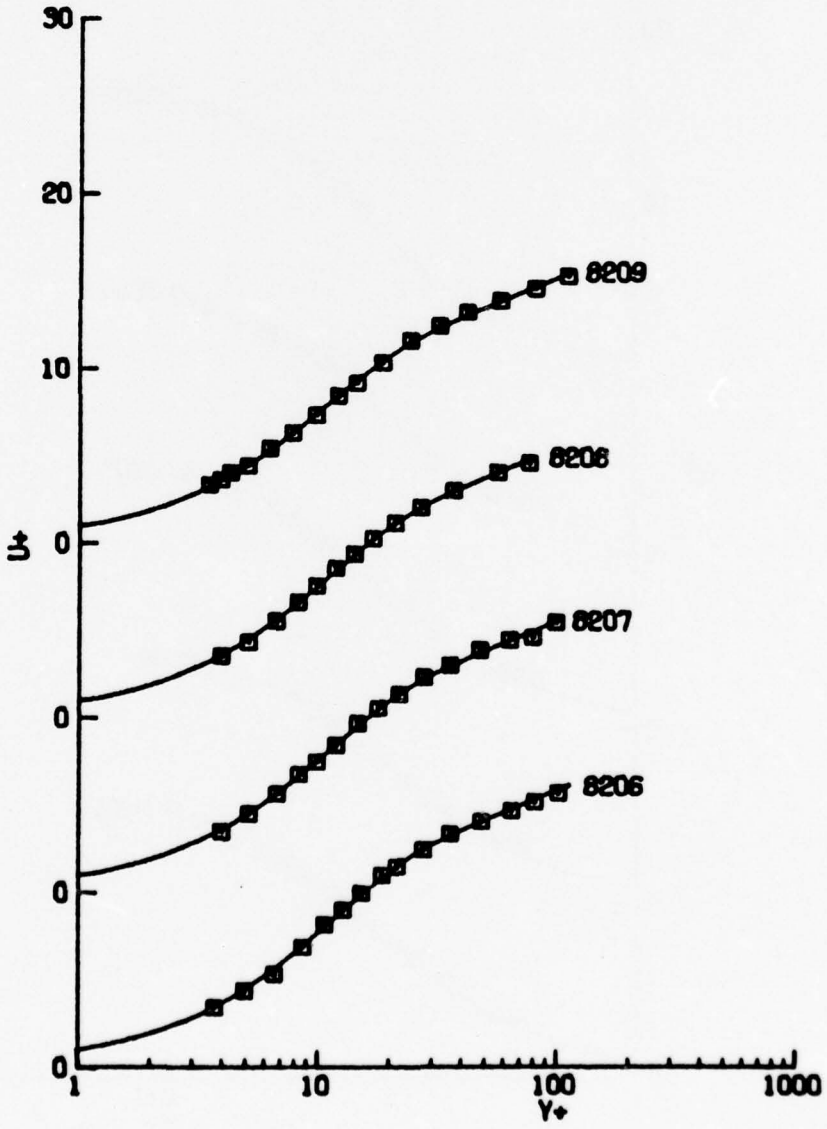

Figure A.4. (Continued).

TABLE A.5: ANDERSEN, KAYS AND MOFFAT - STRONG P. G. - 110971
(ENGLISH UNITS)

NU= 1.610000E-04

EXPERIMENTAL VALUES

ID	XSTA	UE	UTAU	DUEDX	P+	DELTA	DELTA*	THETA
8301	.167	29.13	1.511	-3.68	.00501	.3064	.0561	.0359
8302	.833	25.70	1.072	-5.21	.01750	.5366	.1237	.0770
8303	1.833	22.31	.801	-2.17	.01515	.9542	.2478	.1496
8304	2.833	20.53	.708	-1.32	.01227	1.3935	.3628	.2195
8305	3.833	19.39	.655	-.93	.01029	1.8038	.4663	.2836
8306	4.833	18.55	.615	-.70	.00899	2.1736	.5497	.3406
8307	5.833	17.97	.588	-.57	.00806	2.5570	.6291	.3951
8308	6.833	17.42	.559	-.47	.00753	2.9793	.7263	.4591
8309	7.500	17.10	.543	-.44	.00755	3.3669	.8244	.5174

VAN DRIEST MODEL - INNER REGION FIT

ID	P+	UTAU	A+	EPSILON
8301	.00608	1.416	26.029	.008167
8302	.01683	1.086	19.499	.005642
8303	.01650	.779	24.848	.005369
8304	.01426	.673	26.910	.007848
8305	.01350	.598	30.100	.005804
8306	.01077	.579	29.979	.007828
8307	.00811	.587	25.207	.006513
8308	.00808	.546	29.290	.007960
8309	.00793	.535	25.622	.007609

MEAN EPSILON= .006971

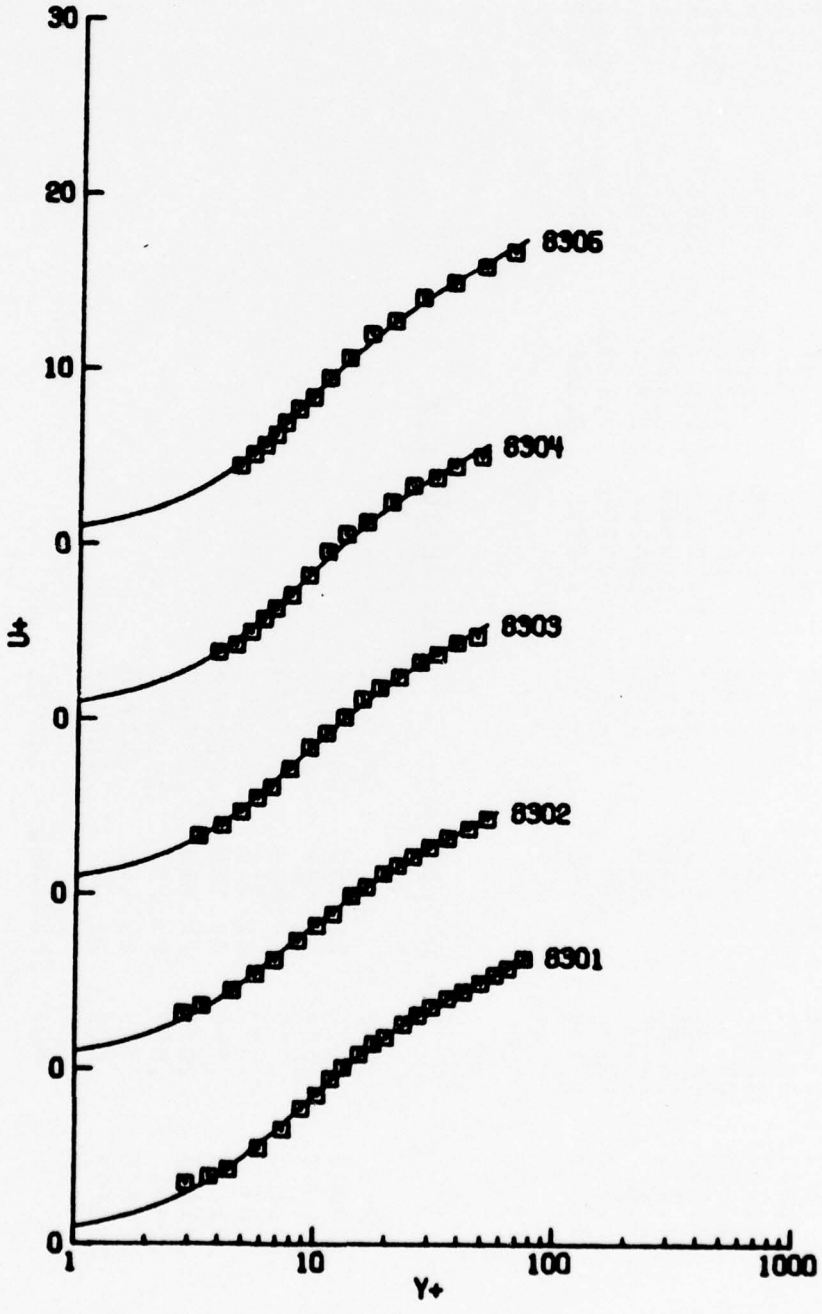

Figure A.5. Van Driest Model. (Note shifted origins on U^+ axis).

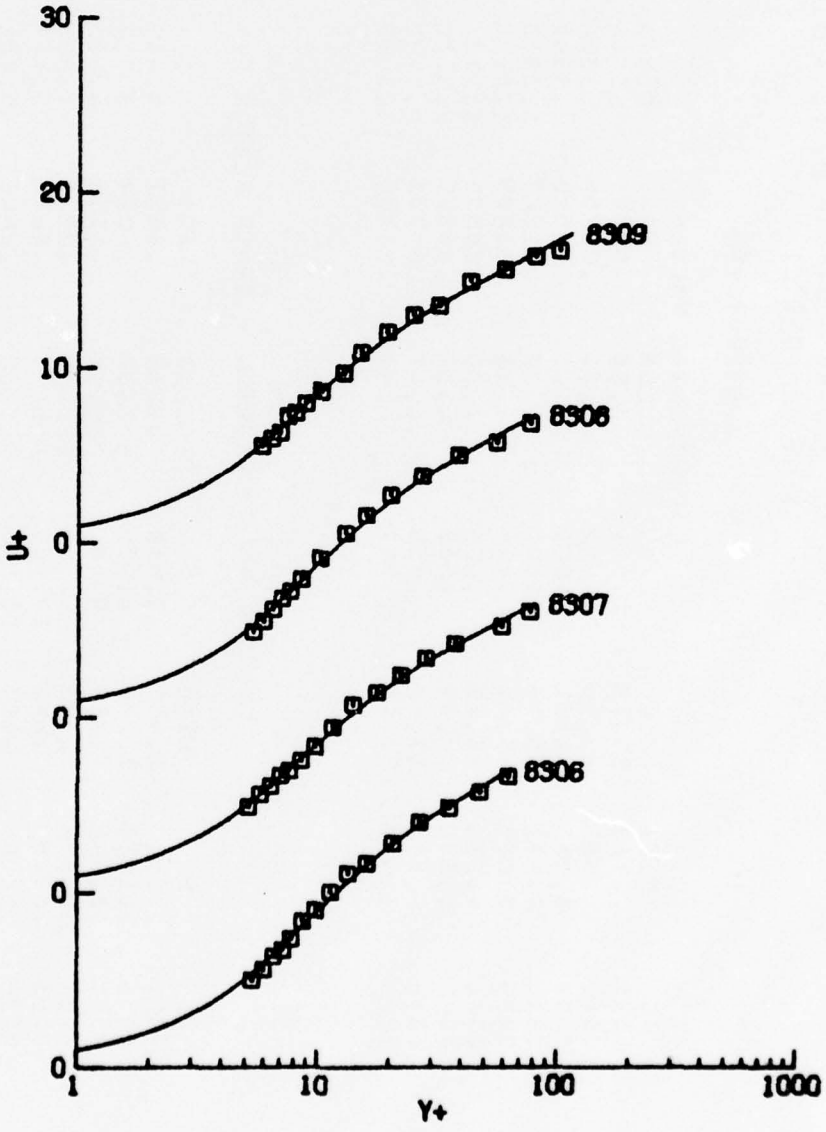

Figure A.5. (Continued).

TABLE A.6: ANDERSEN, KAYS AND MOFFAT - STRONG P. G. - 110971
(ENGLISH UNITS)

NU= 1.610000E-04

EXPERIMENTAL VALUES

ID	XSTA	UE	UTAU	DUEDX	P+	DELTA	DELTA*	THETA
8301	.167	29.13	1.511	-3.68	.00501	.3064	.0561	.0359
8302	.833	25.70	1.072	-5.21	.01750	.5366	.1237	.0770
8303	1.833	22.31	.801	-2.17	.01515	.9542	.2476	.1496
8304	2.833	20.53	.708	-1.32	.01227	1.3935	.3626	.2195
8305	3.833	19.39	.655	-.93	.01029	1.8038	.4663	.2836
8306	4.833	18.55	.615	-.70	.00899	2.1736	.5497	.3406
8307	5.833	17.97	.588	-.57	.00806	2.5570	.6291	.3951
8308	6.833	17.42	.559	-.47	.00753	2.9793	.7263	.4591
8309	7.500	17.10	.543	-.44	.00755	3.3669	.8244	.5174

UNSTEADY WALL LAYER MODEL - INNER REGION FIT

ID	P+	UTAU	S	EPSILON	Y1+	Ci
8301	.00513	1.499	9.810	.007332	.3697	4.619
8302	.01435	1.145	8.432	.003683	.4574	3.837
8303	.01346	.833	9.586	.005113	.3193	4.605
8304	.01154	.723	9.948	.008042	.2977	4.823
8305	.01090	.642	10.881	.005543	.2218	5.467
8306	.00865	.623	10.618	.008432	.2600	5.236
8307	.00671	.625	9.543	.004731	.3843	4.466
8308	.00660	.584	10.517	.007285	.2861	5.126
8309	.00658	.569	9.790	.005379	.3579	4.630

MEAN EPSILON= .006171

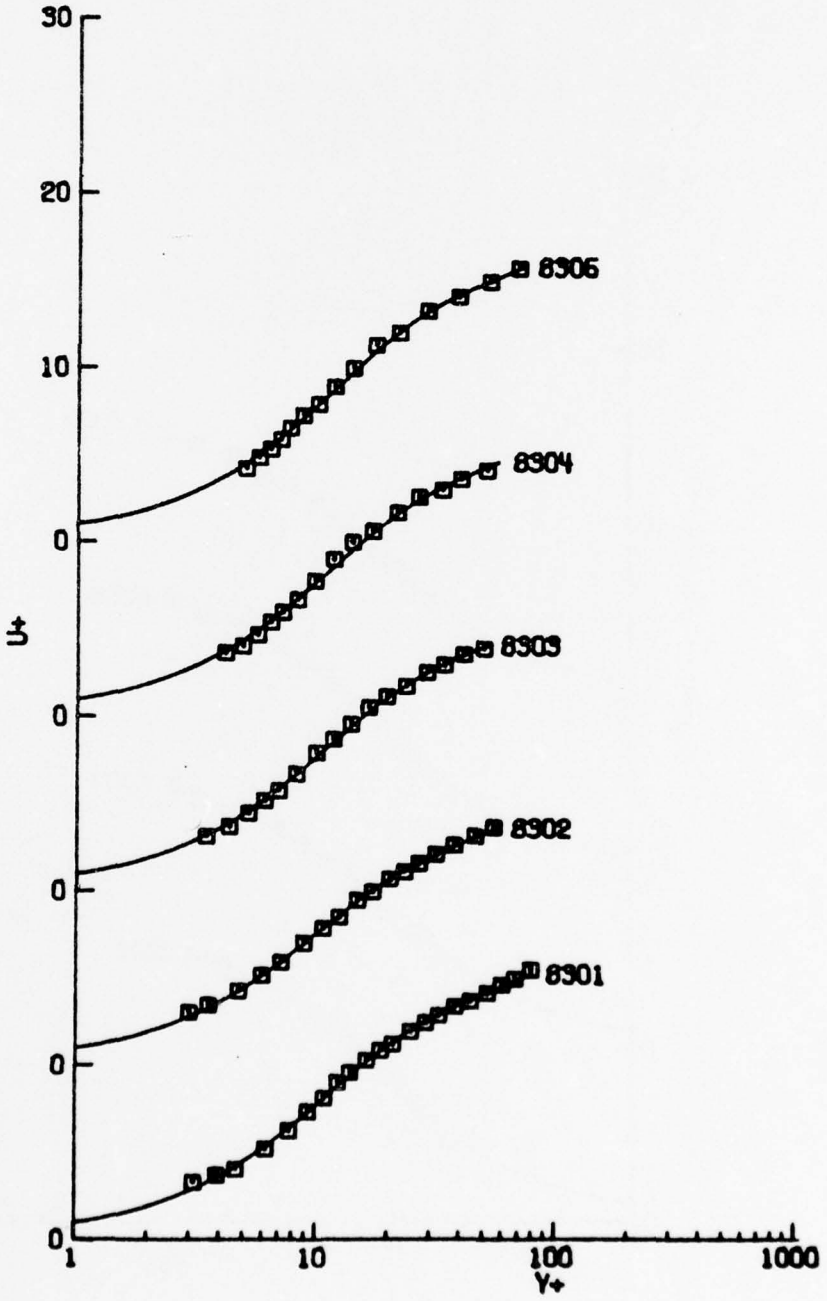

Figure A.6. Unsteady wall layer model. (Note shifted origins on U^+ axis).

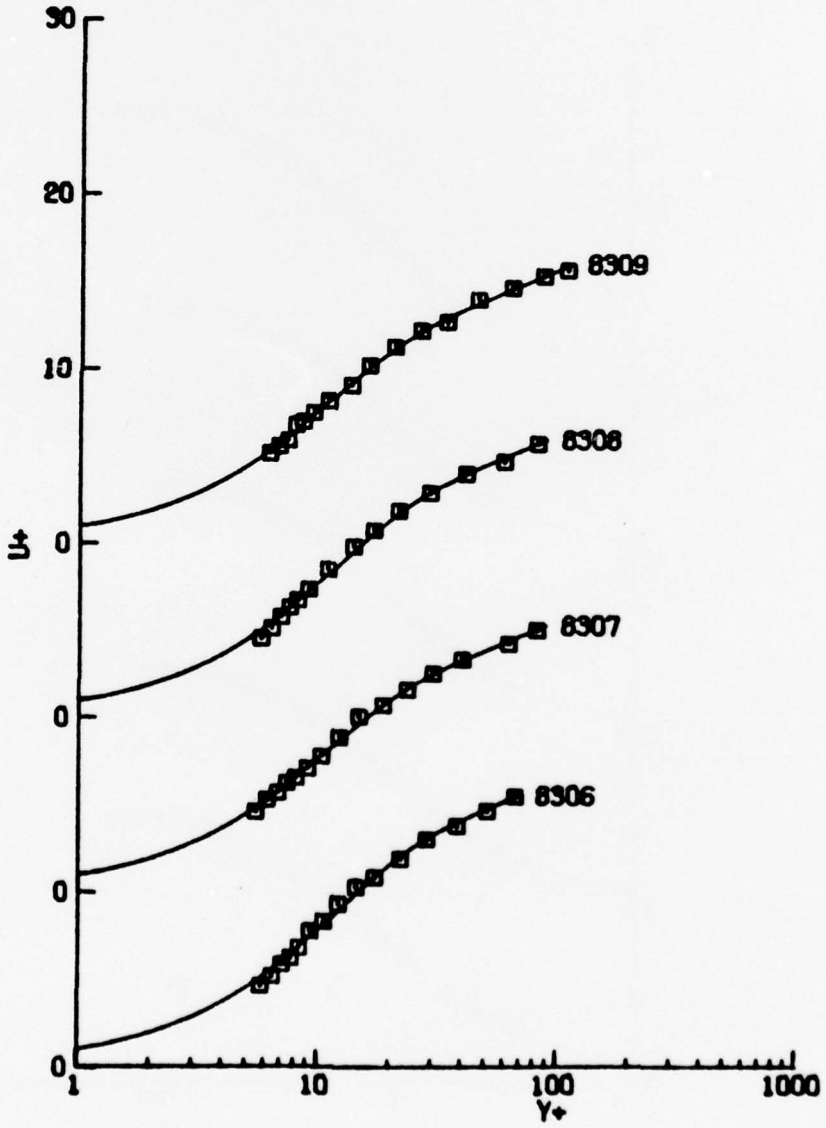

Figure A.6. (Continued).

TABLE A.7: FRASER FLOW A
(ENGLISH UNITS)

NU= 1.690000E-04

EXPERIMENTAL VALUES

ID	XSTA	UE	UTAU	DUEDX	P+	DELTA	DELTA*	THETA
5001	.383	170.00	7.098	10.50	-.00084	.4600	.0519	.0371
5002	.519	171.00	7.092	-15.00	.00122	.5000	.0547	.0395
5003	.691	161.00	6.089	-98.00	.01181	.5800	.0739	.0513
5004	.776	153.00	5.063	-85.50	.01703	.6300	.0948	.0623
5005	.984	138.00	3.730	-56.00	.02517	.7600	.1517	.0887
5006	1.251	126.00	2.598	-37.00	.04493	.9300	.2501	.1255
5007	1.438	120.00	2.096	-29.00	.06387	1.0500	.3408	.1542
5008	1.537	117.00	1.958	-26.50	.06980	1.1700	.3779	.1674
5009	1.715	113.00	1.475	-20.50	.12200	1.3800	.4970	.1931
5010	1.895	110.00	1.270	-17.00	.15428	1.7000	.6068	.2209
5011	2.107	106.00	1.001	-13.00	.23218	1.9500	.7412	.2491

VAN DRIEST MODEL - INNER REGION FIT

ID	P+	UTAU	A+	EPSILON
5001	-.00086	7.047	26.608	.006381
5002	.00173	6.310	36.897	.010626
5003	.01854	5.240	29.777	.014002
5004	.02024	4.780	22.847	.010194
5005	.02702	3.643	18.673	.014384
5006	.04292	2.638	14.764	.018437
5007	.06370	2.098	12.699	.025746
5008	.07904	1.879	12.561	.027440
5009	.19853	1.254	9.413	.022591
5010	.26016	1.067	8.133	.025011
5011	.34584	.876	6.728	.024181

MEAN EPSILON= .018090

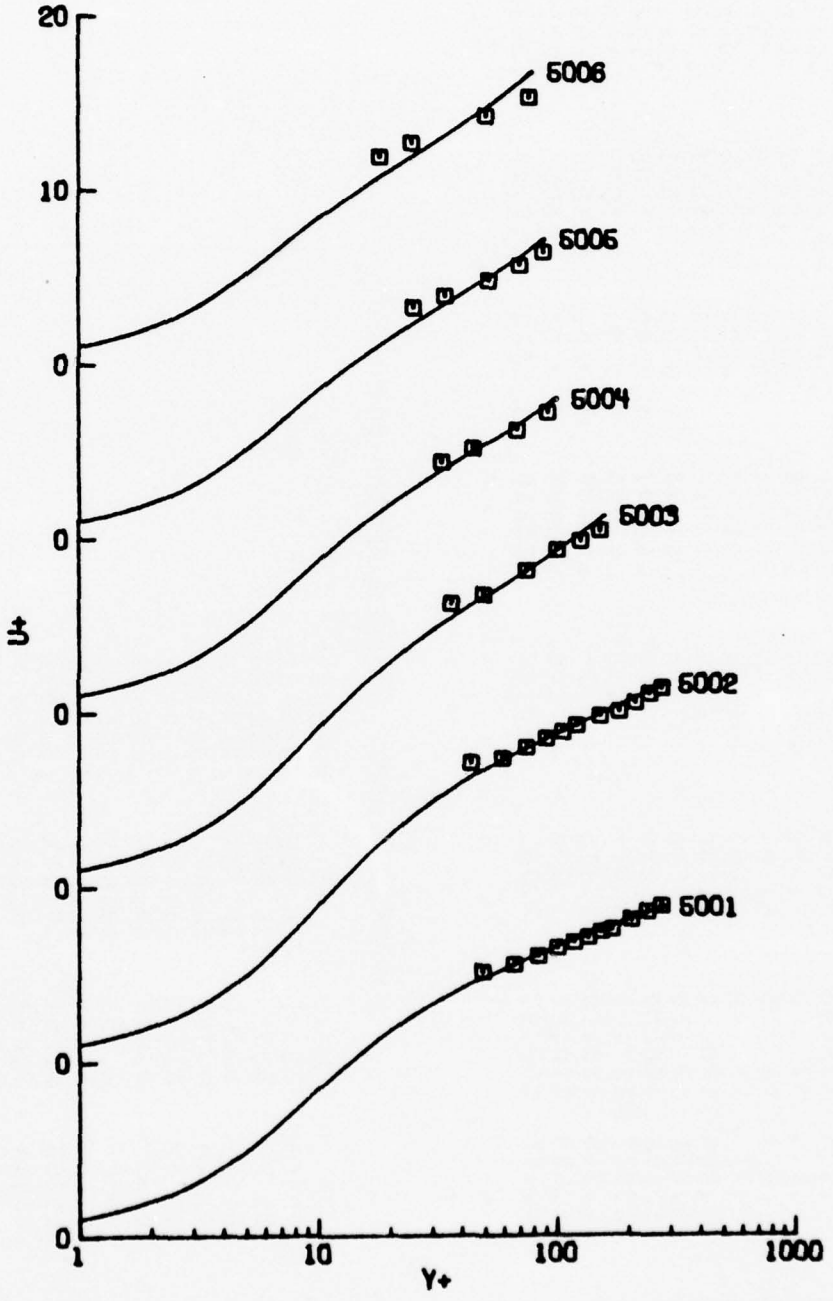

Figure A.7. Van Driest Model. (Note shifted origins on U^+ axis).

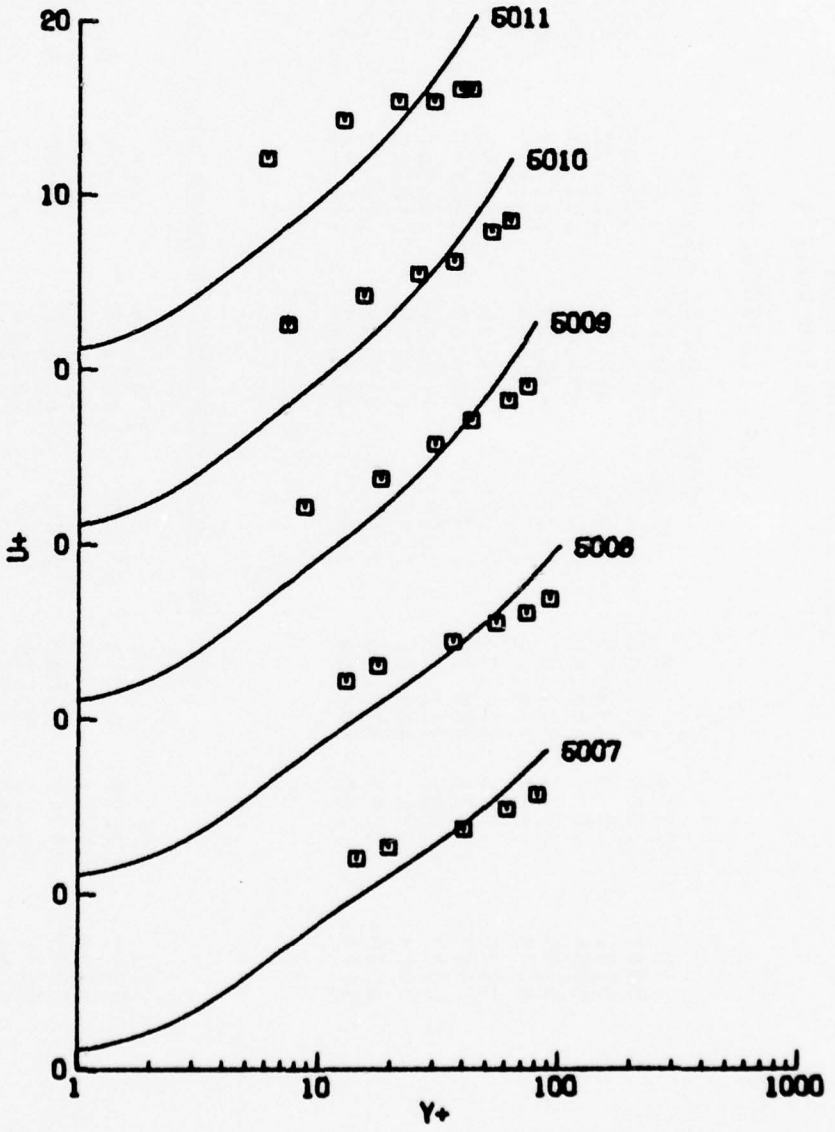

Figure A.7. (Continued).

TABLE A.8: FRASER FLOW A
(ENGLISH UNITS)

NU= 1.690000E-04

EXPERIMENTAL VALUES

ID	XSTA	UE	UTAU	DUEDX	P+	DELTA	DELTA*	THETA
5001	.383	170.00	7.098	10.50	-.00084	.4600	.0519	.0371
5002	.519	171.00	7.092	-15.00	.00122	.5000	.0547	.0395
5003	.691	161.00	6.069	-98.00	.01181	.5800	.0739	.0513
5004	.776	153.00	5.063	-85.50	.01703	.6300	.0946	.0625
5005	.984	138.00	3.730	-56.00	.02517	.7600	.1517	.0887
5006	1.251	126.00	2.598	-37.00	.04493	.9300	.2501	.1255
5007	1.438	120.00	2.096	-29.00	.06387	1.0500	.3408	.1542
5008	1.537	117.00	1.958	-26.50	.06980	1.1700	.3779	.1674
5009	1.715	113.00	1.475	-20.50	.12200	1.3800	.4970	.1931
5010	1.895	110.00	1.270	-17.00	.15428	1.7000	.6068	.2209
5011	2.107	106.00	1.001	-13.00	.23218	1.9500	.7412	.2491

UNSTEADY WALL LAYER MODEL - INNER REGION FIT

ID	P+	UTAU	S	EPSILON	Y1+	C_i
5001	-.00109	6.511	13.299	.005500	.1684	6.881
5002	.00167	6.380	13.890	.006686	.1230	7.389
5003	.00948	6.552	8.145	.004651	.5489	3.567
5004	.01503	5.279	9.105	.002213	.3613	4.299
5005	.02125	3.946	8.624	.004816	.3725	4.057
5006	.03175	2.917	7.342	.006151	.4926	3.310
5007	.03990	2.452	6.412	.011231	.6232	2.772
5008	.04385	2.286	6.388	.009421	.6005	2.788
5009	.06258	1.843	4.272	.004401	1.1101	1.613
5010	.07844	1.591	4.175	.007775	1.0534	1.628
5011	.10300	1.313	3.790	.010274	1.0816	1.508

MEAN EPSILON= .006647

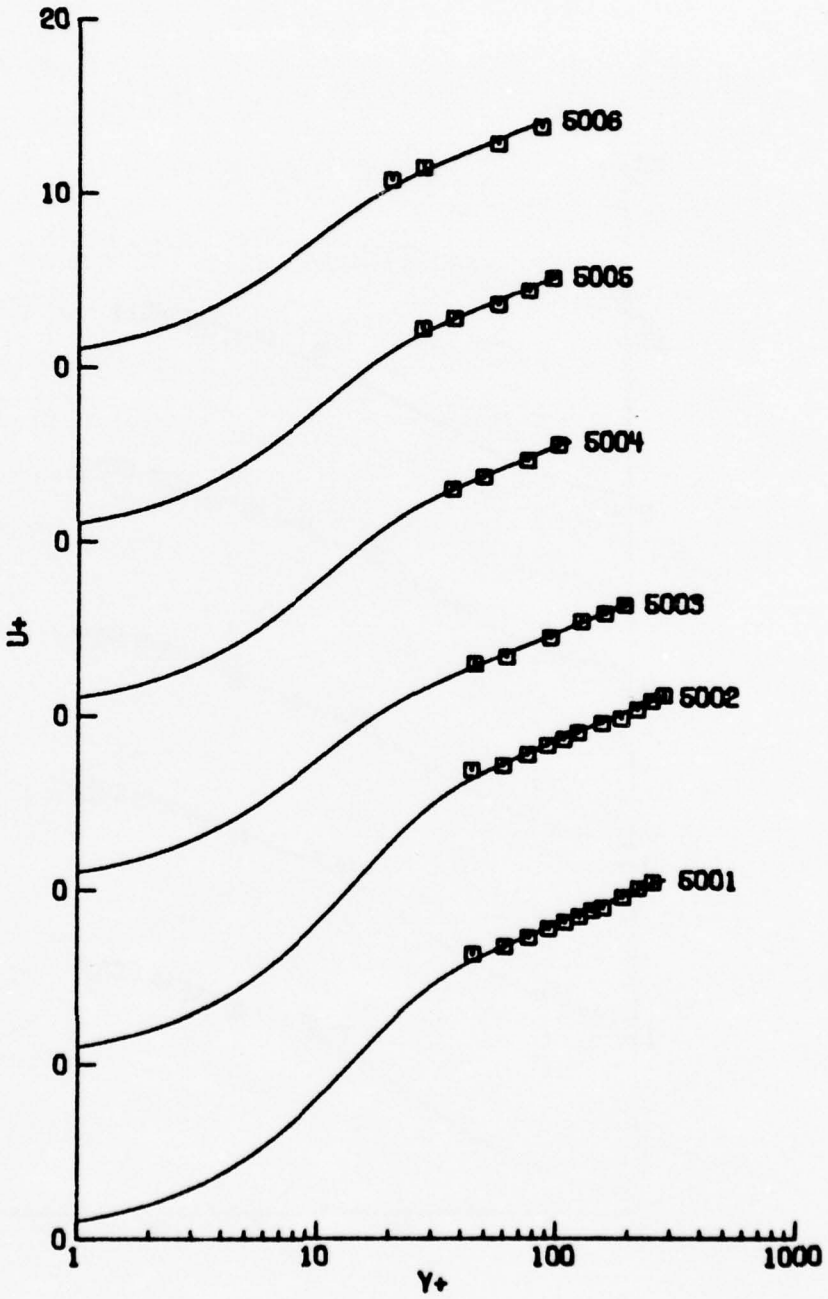

Figure A.8. Unsteady wall layer model. (Note shifted origins on U^+ axis).

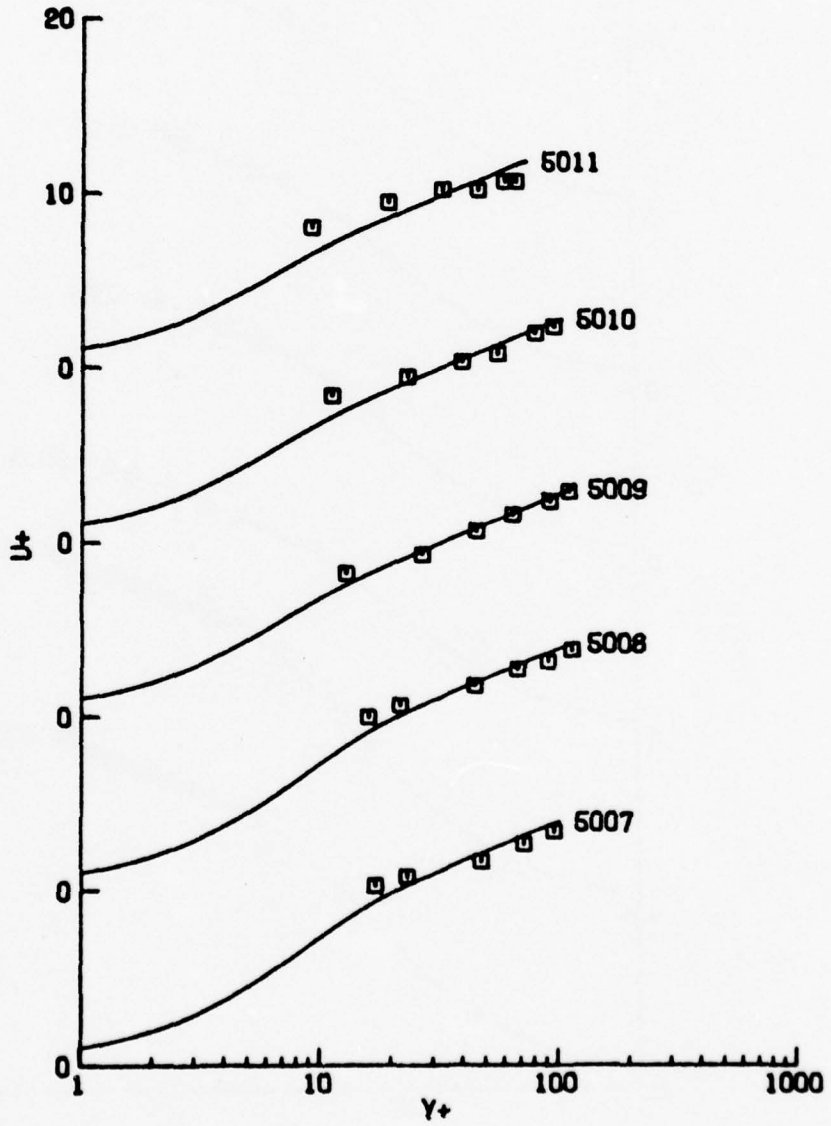

Figure A.8. (Continued).

APPENDIX B

DATA COMPARISONS FOR FULL PROFILE DATA USING A COMPOSITE PROFILE CONSISTING OF THE UNSTEADY WALL LAYER MODEL AND THE LAW OF THE WAKE

Introduction

In this appendix, full profile data are considered and equation (4.4) is fit by optimization of the three parameters u_τ, δ and C_i. The results are presented in graphical and tabular form. A few comments about each data set follow.

1300 - Ludwieg and Tillman

The fits to the accelerating flow of Ludwieg and Tillman are described in Table B.1 and Figure B.1. The overall representation of the data by the composite model is very good with the worst fits occurring at stations 2, 3 and 9. The negative and near zero values of the wake strength parameter Π influence the quality of the fits adversely at stations 2 and 3. As stated by Coles and Hirst (1969) the data at station 9 are distorted and may not be reliable. The flow is nearly in equilibrium so that Π should be approximately constant; a fair estimate is about 0.2 over the middle stations. Note the trend for C_i and S to increase downstream.

2100 - Schubauer and Klebanoff

The comparisons to the data of Schubauer and Klebanoff, taken on a large airfoil-like body, are given in Table B.2 and Figure B.2. Only the last fifteen stations are considered here since they represent that part of the flow where the pressure gradient is most severe as the flow proceeds toward separation. Examination of the root-mean-square error in Table B.2 suggests that the fits are only fair. This is believed due to two reasons. In some cases there are not enough data points to

clearly define the boundary-layer edge. Second, some of the data points near the wall show an erratic behavior at some stations, which adversely influences the fitting procedure and the root-mean-square error. Indeed the quality of some of the data is suspect as stated in Coles and Hirst (1969). However, note the trend of the profile parameters; as the pressure gradient parameter increases both δ and C_i decrease.

2300 - Clauser 2

The fits to the moderately adverse pressure gradient flow of Clauser are described in Table B.3 and Figure B.3. The fits to this equilibrium flow are only fair. Part of this may be due to a lack of inner region points near the wall. Coles and Hirst (1969) also remark that this flow is slightly three dimensional. Note that the Π parameter is roughly constant at about 4.

2500 - Bradshaw Equilibrium, a = -0.15

The fits to this mildly adverse gradient, equilibrium flow are described in Table B.4 and Figure B.4. The fits are fair. Note that Π is roughly equal to about 1.3 for all four profiles, while both δ and C_i decrease. It appears, upon examination of Figure B.4, that the slope of a line through the data points in the logarithmic region is somewhat different from 0.41.

2600 - Bradshaw Equilibrium, a = -0.255

The fits to this moderately adverse gradient, equilibrium flow are described in Table B.5 and Figure B.5. The fits are not very good. Note the tendency of the profile to skew through the data in the "law of the wall" region suggesting a κ different from 0.41. There are some

unresolved difficulties discussed by Coles and Hirst (1969) with this data set and also with flow 2500.

2700 - Herring and Norbury, $\beta = -0.35$

The fits to this mildly favorable gradient equilibrium flow are described in Table B.6 and Figure B.6. Overall the fits are good. Note, however, that as with flow 1300, a near zero or negative Π value does not produce a good fit to the data. This situation occurs at stations 3 and 4 where the quality of the fit is significantly degraded. The inner region data are fit quite well though.

2800 - Herring and Norbury, $\beta = -0.53$

The fits to this strongly favorable gradient equilibrium flow are described in Table B.7 and Figure B.7. The fits are all excellent even in the case of small and negative Π values. The wake component of the outer profile diminished as Π decreases and the fact that Π becomes small and negative at the latter data stations may be indicative of relaminarization. Indeed, Coles and Hirst (1969) suggest this may have occurred in this flow. In spite of this, the composite profile represents the data very well.

2900 - Perry

The data comparisons for this diverging channel flow are described in Table B.8 and Figure B.8. Overall the fits to this adverse gradient diffuser-like flow are very good. The worst fits occur at the third and fourth stations where it is apparent that the data are incomplete near the boundary-layer edge. The composite profile represents the data very well as p^+ increases even through the last two stations where flow

separation is imminent; observe the trend for S and C_i to decrease downstream. Also it may be observed from Figure B.8 that there is a slight tendency for the profile to skew through the logarithmic zone which suggests a value of κ different from 0.41 may be appropriate.

3300 - Bradshaw Layer C

The fits for this case are given in Table B.9 and Figure B.9. The flow is initially at constant pressure and is developing into equilibrium in a moderate adverse pressure gradient. The fits for this case are excellent with the smallest ε recorded in this report achieved at station 2. The Π parameter increases at the downstream stations and appears to be approaching an approximately constant value as the flow approaches equilibrium. A similar trend for S and C_i may be observed in Table B.9.

3500 - Newman Airfoil - Series 2

The fits to this airfoil boundary-layer flow proceeding to separation are described in Table B.10 and Figure B.10. In general the fits are quite good. As p^+ increases downstream S and C_i decrease and Π increases. Note that at the last station, which is believed to be very close to separation, the logarithmic region has apparently disappeared.

3600 - Moses 1

The fits to this flow are described in Table B.11 and Figure B.11. This case is the boundary layer on a cylinder in an axially symmetric flow. The rate of pressure increase is initially slow but then quite abrupt. In general the quality of the fits is good. The sparseness of the inner region makes it difficult to judge the inner model fit; however the Coles' model fits the data well. Observe that C_i is

significantly different from 5.0 and decreases as separation is approached; the last station is evidently close to separation.

3700 - Moses 2

The fits for this case are given in Table B.12 and Figure B.12. This case corresponds to the boundary layer on a cylinder in an axially symmetric flow; the rate of pressure rise is moderate. The overall quality of the fits is fair. Again there is a sparseness of inner region points which makes it difficult to assess the wall layer model. Note that C_i is significantly different from 5.0 and also that for the first few stations, the analytical profile skews slightly through the logarithmic region data. This suggests a value of κ different from 0.41.

3800 - Moses 3

The fits to the third Moses cylinder flow are given in Table B.13 and Figure B.13. For this case there is a strong pressure rise. The last two data stations are apparently in a separated flow region and were omitted from consideration for this reason. The fits are fair, at best. For the last three profiles fitted, the analytical curve skews through the logarithmic zone suggesting a value of κ different from 0.41 may be appropriate.

4000 - Moses 5

The fits for the fifth Moses cylinder flow are given in Table B.14 and Figure B.14. In this case there is an initially strong pressure rise followed by a relaxation at constant pressure. It is apparent that the fits are not good for this flow. The sparseness of the inner region data, coupled with the fact that the data points that are in the inner

region appear suspect, makes it difficult to draw any conclusions about the fits. In actuality, smaller values of ε were obtained for this data set but the optimal boundary-layer thickness δ took on unusually large values. The fits presented here are those which appear to be the most reasonable.

4400 - Schubauer and Spangenberg A

The fits to this strong positive pressure gradient flow are given in Table B.15 and Figure B.15. It is evident that the fits are not good for this case. The same problem that occurred for flow 4000 in connection with δ was encountered in this case as well. There are not enough points to properly define the inner region and possible errors in the data points near the wall may adversely affect the fits. Another possible difficulty here is the truncation of the profiles discussed by Coles and Hirst (1969).

4500 - Schubauer and Spangenberg B

The fits to this moderate positive pressure gradient flow are given in Table B.16 and Figure B.16. The fits for this case are fair. Some of the data near the wall appears somewhat suspect which tends to degrade the quality of the fit. The composite model represents the data reasonably well up to the last station which is close to separation. The trend for S and C_i to decrease downstream may be observed in Table B.16.

5000 - Fraser A

The comparisons for this conical diffuser flow are given in Table B.17 and Figure B.17. Overall the fits to this adverse gradient flow are quite good. The largest values of ε occur at stations 4, 5 and 10.

The mainstream velocity gradient is changing rapidly at the fourth and fifth stations; consequently the quoted values of the mainstream velocity gradient (in Coles & Hirst, 1969) may be somewhat in error. The major portion of the error at the tenth station derives from the first two inner region points and the last few outer layer points. It is interesting to observe the gradual disappearance of the logarithmic region as the flow approaches separation shortly after the last station.

5100 - Fraser B

The fits to Fraser's B flow are similar to those of flow A discussed above as evident from Table B.18 and Figure B.18. Again the worst fits occur at the fourth and fifth stations where the velocity gradient is changing rapidly. The pressure gradient parameter, p^+, continuously increases and eventually becomes O(1) at the last station. This profile exhibits no logarithmic region and is essentially all wake. The composite profile fits it fairly well though.

5200 - Stratford 5

The fits to this flow (in a channel with an abrupt onset of moderate positive pressure gradient) are described in Table B.19 and Figure B.19. At first the results appear disturbing, especially for the second and third stations. However, Coles and Hirst (1969) remark that the flow at these stations cannot be made to conform to the law of the wall, the profiles being essentially inviscid in character. If these two profiles are discarded the fits are fair. Note that these data also suggest a value of κ different from 0.41 may be appropriate.

5300 - Stratford 6

This flow is a boundary-layer flow in a channel with the abrupt onset of a severe positive pressure gradient. The fits are described in Table B.20 and Figure B.20 and are similar to those obtained for flow 5200. Again the second and third profiles are essentially inviscid in character. The raggedness of the data at the sixth and seventh stations contribute greatly to the root-mean-square error.

7000 - Samuel and Joubert (1974)

The fits for this flow in an increasingly adverse pressure gradient are described in Table B.21 and Figure B.21. The fits are quite good with the largest root-mean-square error obtained at the last two stations where the flow is undergoing relaxation. The analytical profile skews slightly through the logarithmic region suggesting that a value of κ different from 0.41 may be appropriate.

8100 - Andersen, et al. (1972)

The excellent fits to this constant pressure flow are described in Table B.22 and Figure B.22. The large number of inner region points provide a good definition of the inner region. It may be observed that there is negligible skewing of the profile through the logarithmic zone and that all but the first two profiles appear close to being similar. Both S and Π are nearly constant for the last seven stations.

8200 - Andersen, et al. (1972)

The fits to the mildly adverse gradient flow of Andersen, et al. (1972) are described in Table B.23 and Figure B.23. The fits are

excellent although again the analytical profile skews slightly through the logarithmic region. The fact that this is a nearly equilibrium flow is indicated by the approximately constant values of S, C_i and Π.

8300 - Andersen, et al. (1972)

The fits for the strongly adverse gradient flow of Andersen, et al. (1972) are given in Table B.24 and Figure B.24. Again the fits are excellent but a slight skewing of the profile in the logarithmic zone may be observed. The flow is near equilibrium as suggested by the essentially constant values of Π and S.

TABLE B.1: LUDWIEG AND TILLMANN
(METRIC UNITS)

NU= 1.540000E-05

EXPERIMENTAL VALUES

ID	XSTA	UE	UTAU	DUEDX	P+	DELTA	DELTA*	THETA
1301	.782	11.52	.553	3.65	-.00383	1.5000	.1920	.1347
1302	1.282	13.38	.628	4.00	-.00333	1.6750	.2047	.1488
1303	1.782	15.61	.711	4.33	-.00290	1.8000	.2168	.1581
1304	2.282	17.85	.796	4.68	-.00255	2.0000	.2356	.1732
1305	2.782	20.20	.875	4.90	-.00228	2.0000	.2586	.1890
1306	3.132	22.07	.939	5.00	-.00205	2.0000	.2668	.1958
1307	3.332	22.90	.975	5.00	-.00190	2.3000	.2656	.1960
1308	3.532	23.70	1.000	4.96	-.00181	2.3000	.2730	.2027
1309	3.732	25.13	1.070	4.86	-.00154	2.3000	.2622	.1963
1310	3.932	25.80	1.060	4.60	-.00153	2.4000	.2961	.2188
1311	4.132	26.40	1.080	4.13	-.00133	2.5000	.3052	.2268
1312	4.332	27.50	1.130	3.50	-.00103	2.5000	.3050	.2274

UNSTEADY + COLES MODEL - FULL PROFILE FIT

ID	P+	UTAU	S	DELTA	EPSILON	Y1+	C_i	PI
1301	-.00340	.575	9.657	1.3122	.009677	.4829	4.373	.1103
1302	-.00276	.668	9.323	1.6710	.015360	.5165	4.170	-.0437
1303	-.00252	.744	9.770	1.7850	.016827	.4587	4.461	.0040
1304	-.00261	.790	11.133	1.9489	.007241	.3232	5.355	.0790
1305	-.00218	.888	10.194	1.9868	.004072	.4073	4.743	.1698
1306	-.00211	.931	11.005	2.0780	.003622	.3286	5.281	.2113
1307	-.00196	.965	11.061	2.1143	.002846	.3222	5.321	.1785
1308	-.00194	.977	11.652	2.2062	.006734	.2749	5.721	.1775
1309	-.00175	1.025	12.293	2.2904	.011738	.2293	6.163	.0997
1310	-.00154	1.058	10.823	2.2849	.004788	.3385	5.171	.2577
1311	-.00135	1.075	10.967	2.3863	.003168	.3237	5.272	.2462
1312	-.00137	1.026	13.587	2.3714	.003420	.1574	7.075	.3612

MEAN EPSILON= .007458

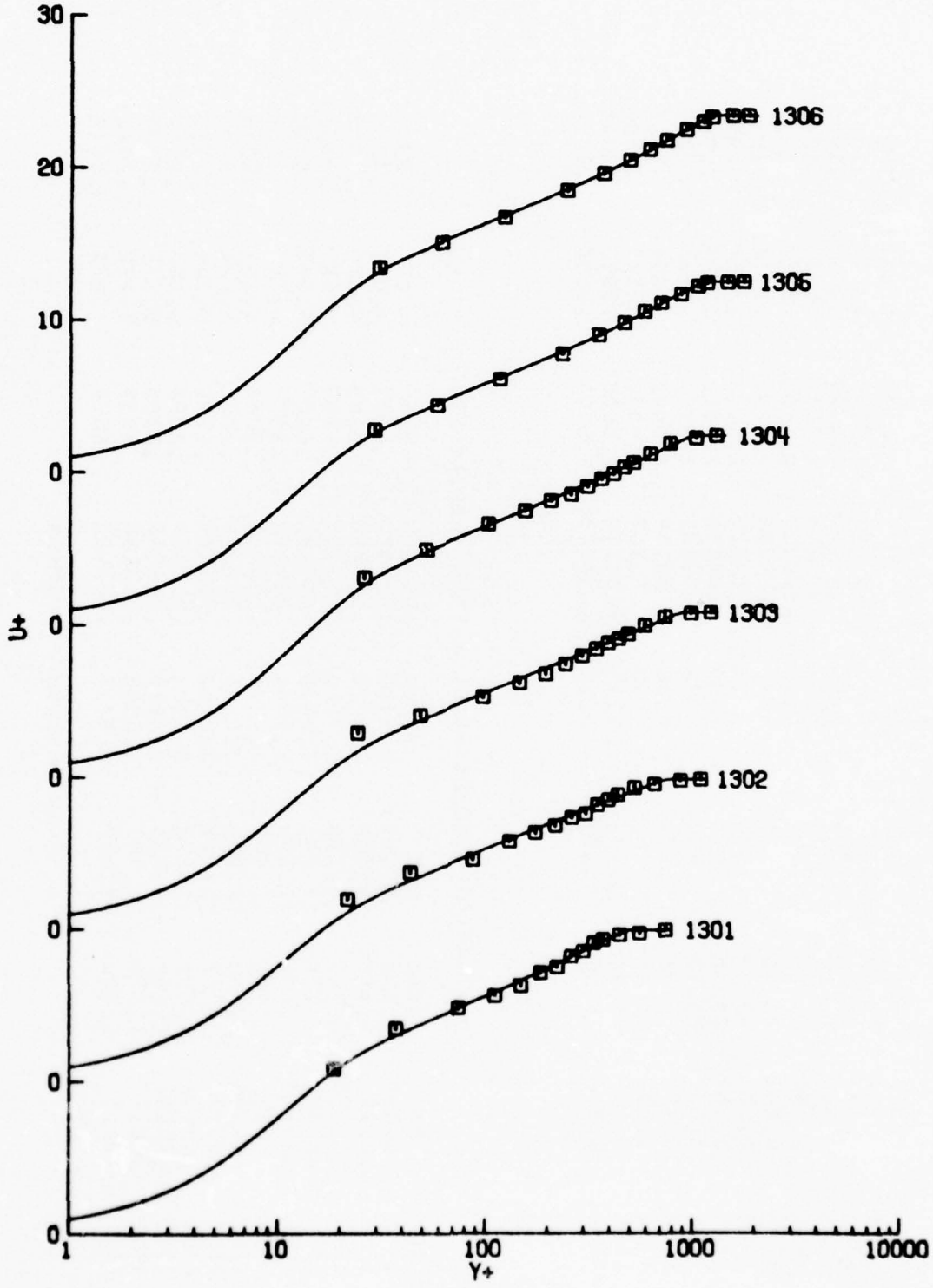

Figure B.1. Ludweig and Tillman accelerating flow. (Note shifted origins on U^+ axis).

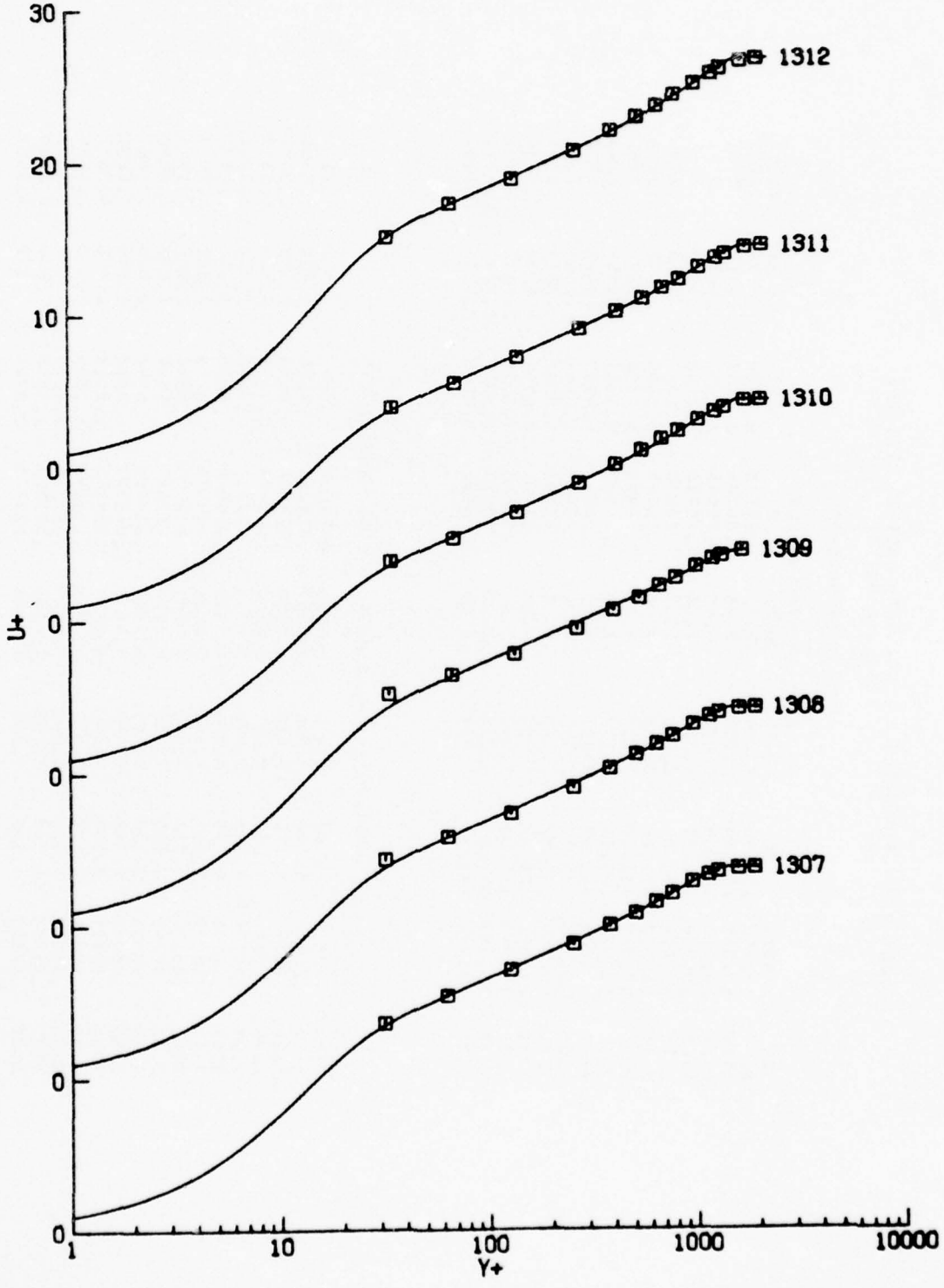

Figure B.1. (Continued).

TABLE B.2: SCHUBAUER + KLEBANOFF, LAST 15 STATIONS
(ENGLISH UNITS)

NU= 1.600000E-04

EXPERIMENTAL VALUES

ID	XSTA	UE	UTAU	DUEDX	P+	DELTA	DELTA*	THETA
2124	19.000	154.05	4.994	-5.70	.00113	2.5798	.3751	.2836
2125	19.500	150.94	4.757	-6.40	.00144	2.6117	.3949	.2967
2126	20.000	147.69	4.601	-6.80	.00165	2.7033	.4376	.3221
2127	20.500	144.27	4.208	-7.05	.00218	3.0145	.5053	.3666
2128	21.000	141.04	3.920	-7.25	.00272	3.1327	.5618	.3983
2129	21.500	137.64	3.689	-7.45	.00327	3.2885	.6442	.4406
2130	22.000	133.58	3.415	-7.55	.00405	3.7164	.7679	.5181
2131	22.500	129.89	3.197	-7.35	.00467	4.3351	.9754	.6263
2132	23.000	126.49	2.853	-6.80	.00593	4.4280	1.0626	.6732
2133	23.500	122.79	2.545	-6.20	.00739	4.6454	1.1964	.7246
2134	24.000	119.52	2.049	-5.30	.01178	5.3960	1.5818	.8721
2135	24.500	116.37	1.782	-4.50	.01481	5.8701	1.8636	.9693
2136	25.000	113.93	1.261	-3.80	.03455	7.1019	2.6172	1.1499
2137	25.400	112.57	1.213	-3.00	.03027	7.5077	2.8441	1.2076
2138	25.770	111.77	.880	-2.55	.06692	8.7760	3.7203	1.3403

UNSTEADY + COLES MODEL - FULL PROFILE FIT

ID	P+	UTAU	S	DELTA	EPSILON	Y1+	C	PI
2124	.00103	5.148	9.386	2.4687	.014280	.4631	4.271	.8598
2125	.00142	4.771	11.038	2.5756	.014686	.2892	5.378	1.0007
2126	.00156	4.692	9.852	2.6560	.009405	.4022	4.585	1.1228
2127	.00174	4.543	8.593	2.8710	.017318	.5638	3.772	1.3251
2128	.00209	4.275	8.456	2.9632	.020878	.5805	3.690	1.6091
2129	.00239	4.094	7.867	3.2164	.015976	.6744	3.326	1.7933
2130	.00295	3.796	7.168	3.5341	.025455	.8002	2.907	2.1916
2131	.00349	3.525	7.464	4.3270	.012901	.7354	3.092	2.4294
2132	.00411	3.223	6.666	4.2856	.016798	.8943	2.620	3.0686
2133	.00466	2.968	6.596	4.5549	.013331	.9038	2.584	3.5226
2134	.00629	2.526	4.993	5.2617	.014143	1.3083	1.705	4.9277
2135	.00876	2.122	5.492	5.6966	.014948	1.1369	1.990	6.4584
2136	.01512	1.661	1.608	7.0119	.013726	2.3100	.377	9.6303
2137	.01423	1.560	1.545	7.4735	.011217	2.3256	.363	10.3600
2138	.04571	.999	1.396	8.7251	.012875	2.2726	.392	18.6401

MEAN EPSILON= .015196

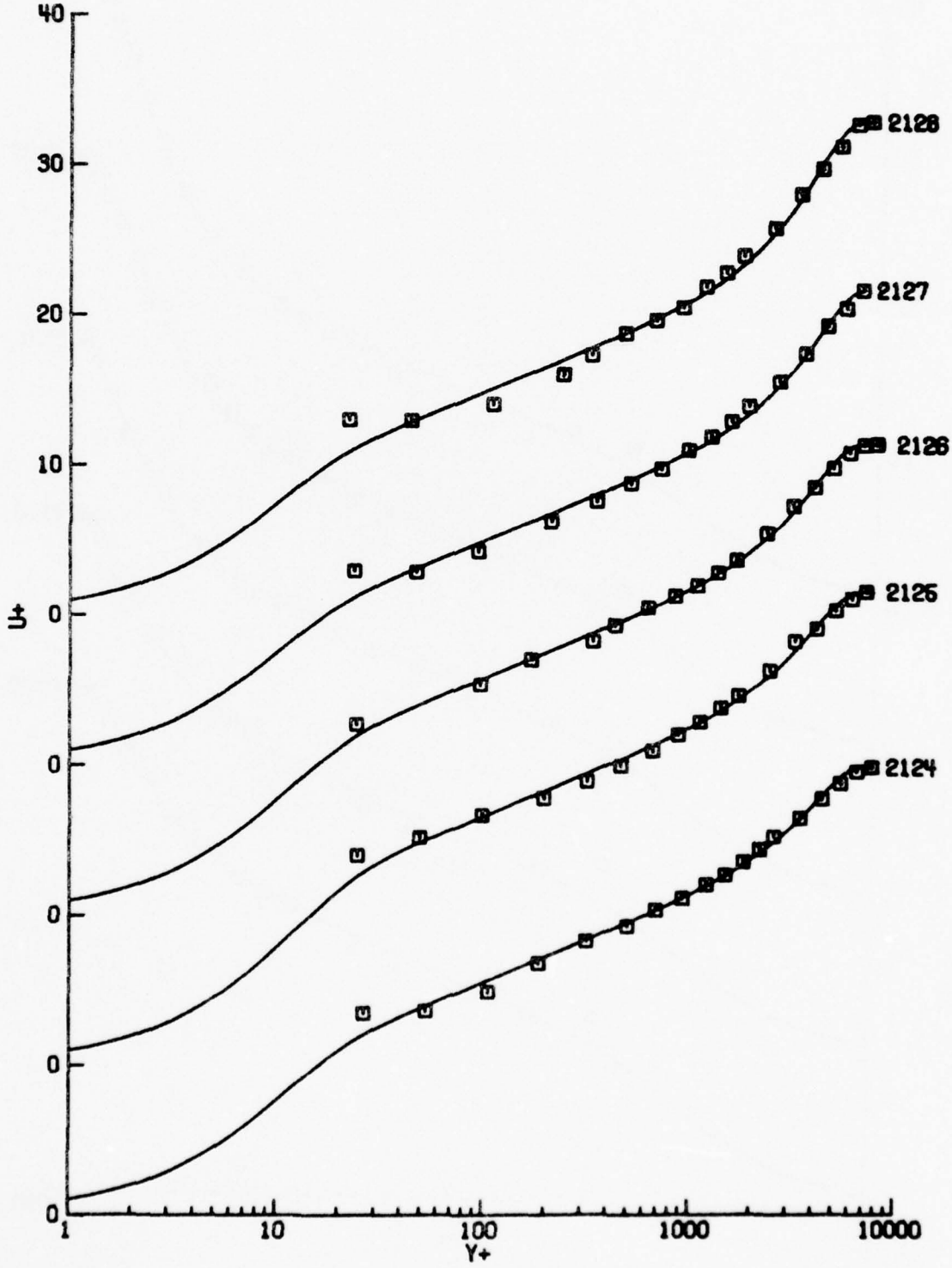

Figure B.2 Schubauer and Klebanoff airfoil-like flow.
(Note shifted origins on the U^+ axis).

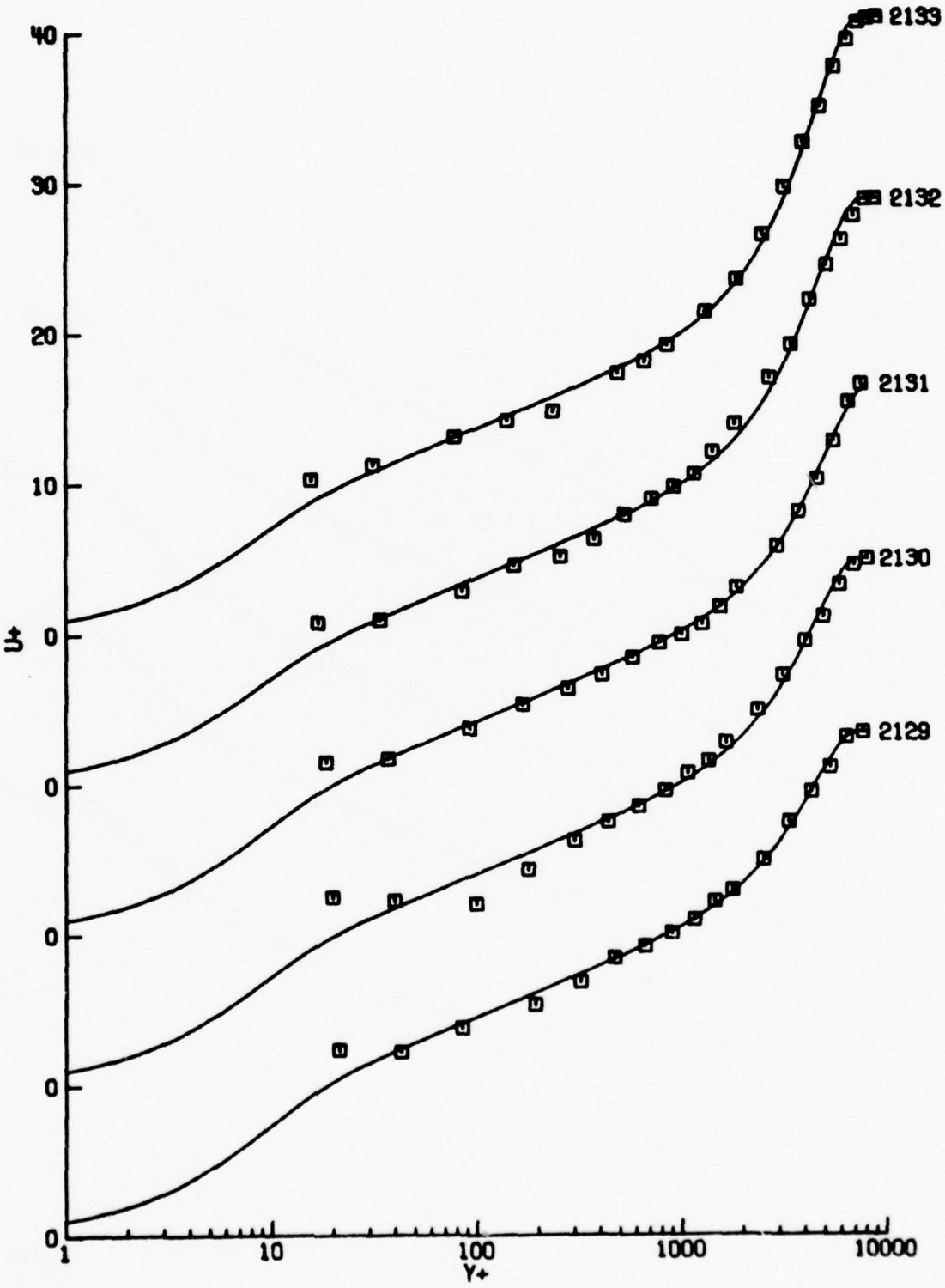

Figure B.2. (Continued).

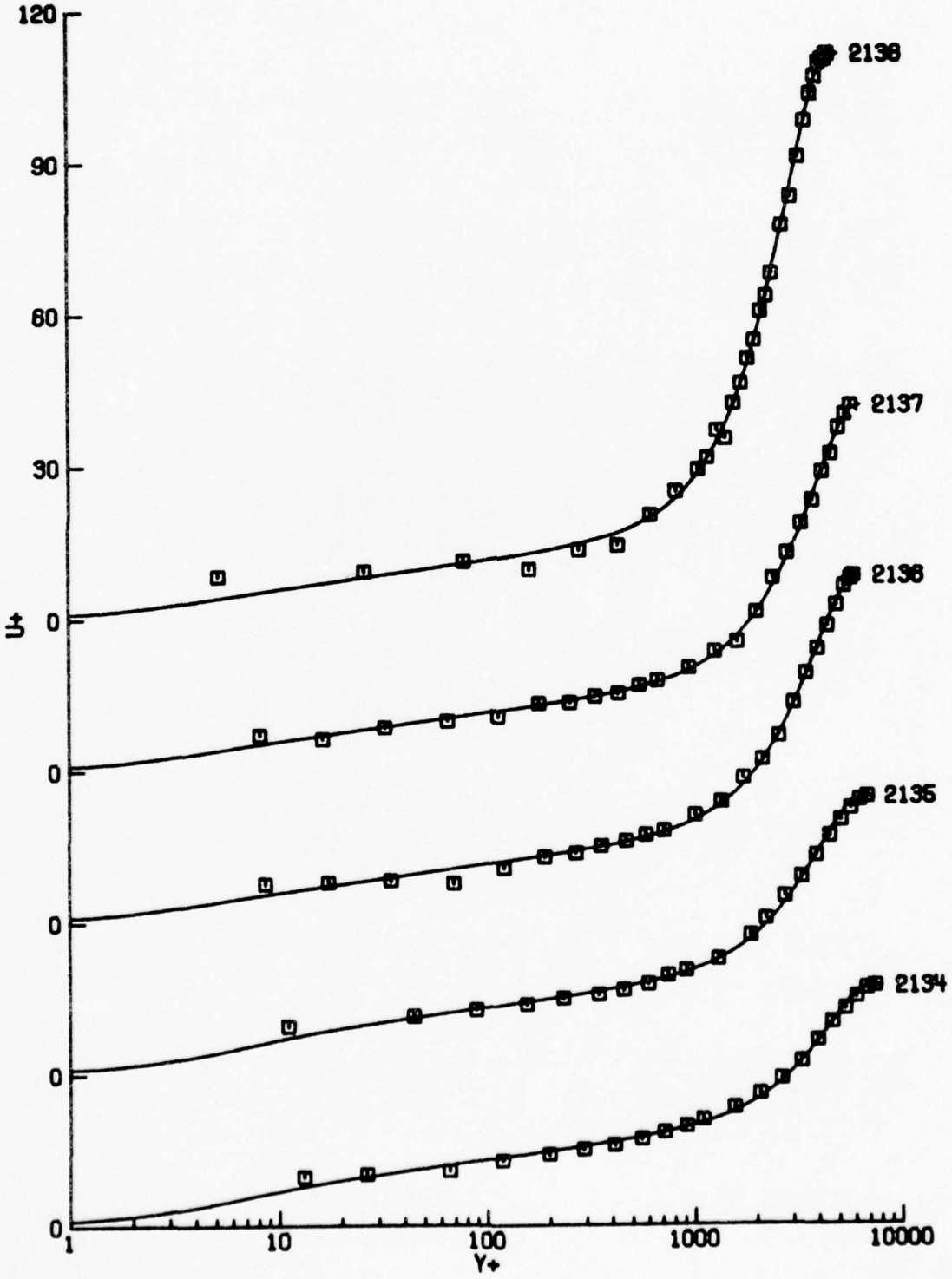

Figure B.2. (Continued).

TABLE B.3: CLAUSER - NUMBER 2
(ENGLISH UNITS)

NU= 1.650000E-04

EXPERIMENTAL VALUES

ID	XSTA	UE	UTAU	DUEDX	P+	DELTA	DELTA*	THETA
2301	7.500	26.10	.659	-.85	.01279	3.7500	1.0893	.6093
2302	9.000	24.80	.595	-.68	.01321	4.6000	1.3899	.7563
2303	11.000	23.50	.552	-.54	.01245	5.8000	1.7082	.9499
2304	12.670	22.80	.526	-.45	.01163	7.2000	2.0248	1.1288
2305	16.170	21.30	.492	-.36	.01062	10.3000	2.8531	1.6254
2306	19.170	20.20	.466	-.31	.01021	12.5000	3.6202	2.0503
2307	23.920	18.90	.414	-.27	.01187	17.5000	4.8660	2.7697
2308	26.670	18.10	.379	-.26	.01426	21.5000	5.9636	3.3931

UNSTEADY + COLES MODEL - FULL PROFILE FIT

ID	P+	UTAU	S	DELTA	EPSILON	Y1+	G_1	PI
2301	.01477	.628	11.369	3.8792	.006106	.1635	5.902	3.7511
2302	.01238	.608	9.183	4.7851	.010486	.3746	4.312	3.8311
2303	.01003	.593	8.188	6.0030	.010579	.5364	3.622	3.6318
2304	.00783	.600	7.032	7.1774	.012614	.7727	2.874	3.3559
2305	.01012	.500	9.793	10.1842	.007064	.3254	4.692	3.8432
2306	.01135	.450	10.316	13.0121	.014941	.2648	5.076	4.1699
2307	.01178	.415	10.115	17.2821	.010777	.2797	4.944	4.2241
2306	.01158	.406	8.699	21.0584	.012134	.4449	3.977	4.1315

MEAN EPSILON= .010588

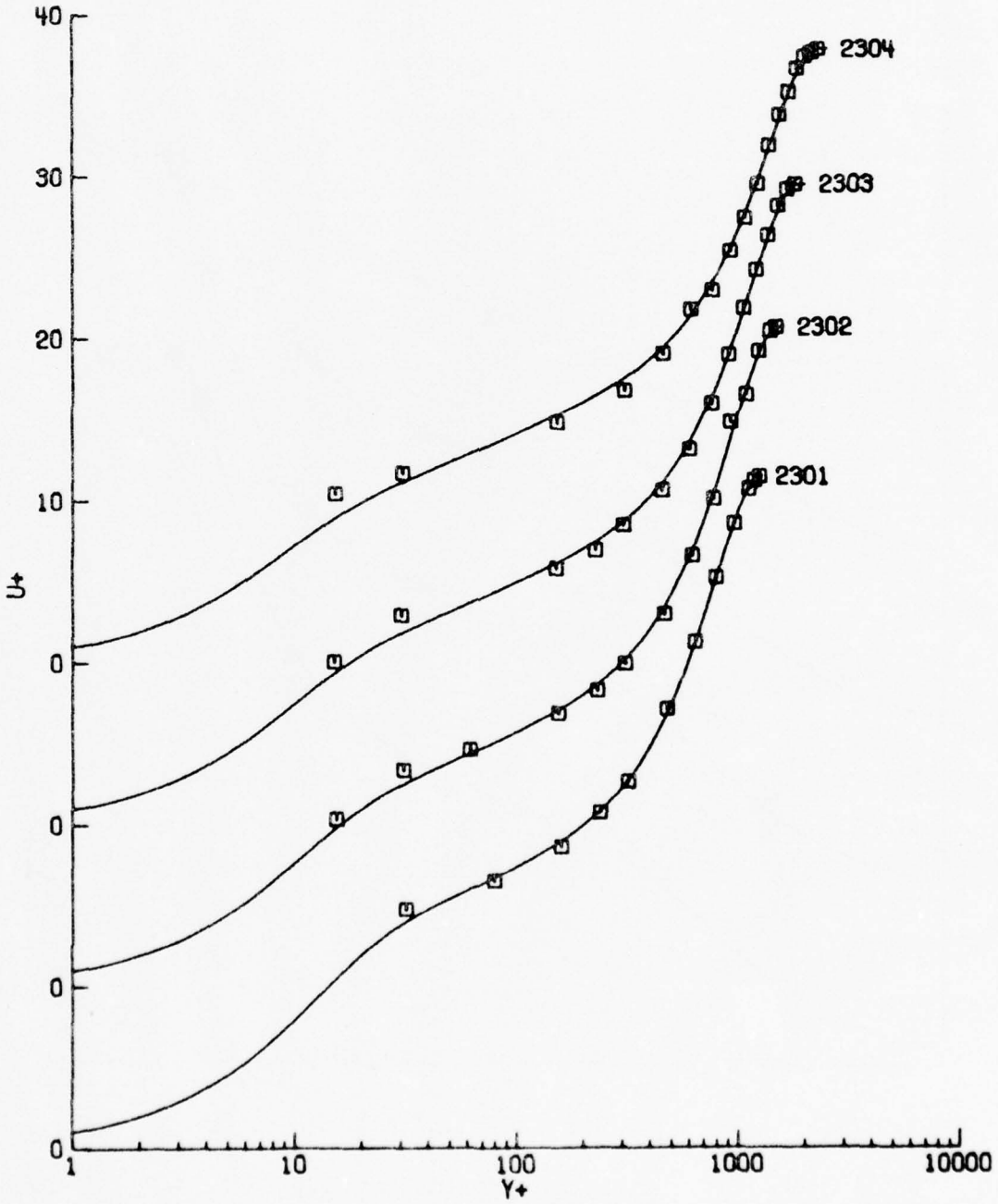

Figure B.3 Clauser adverse pressure gradient equilibrium flow. (Note shifted origins on the U^+ axis).

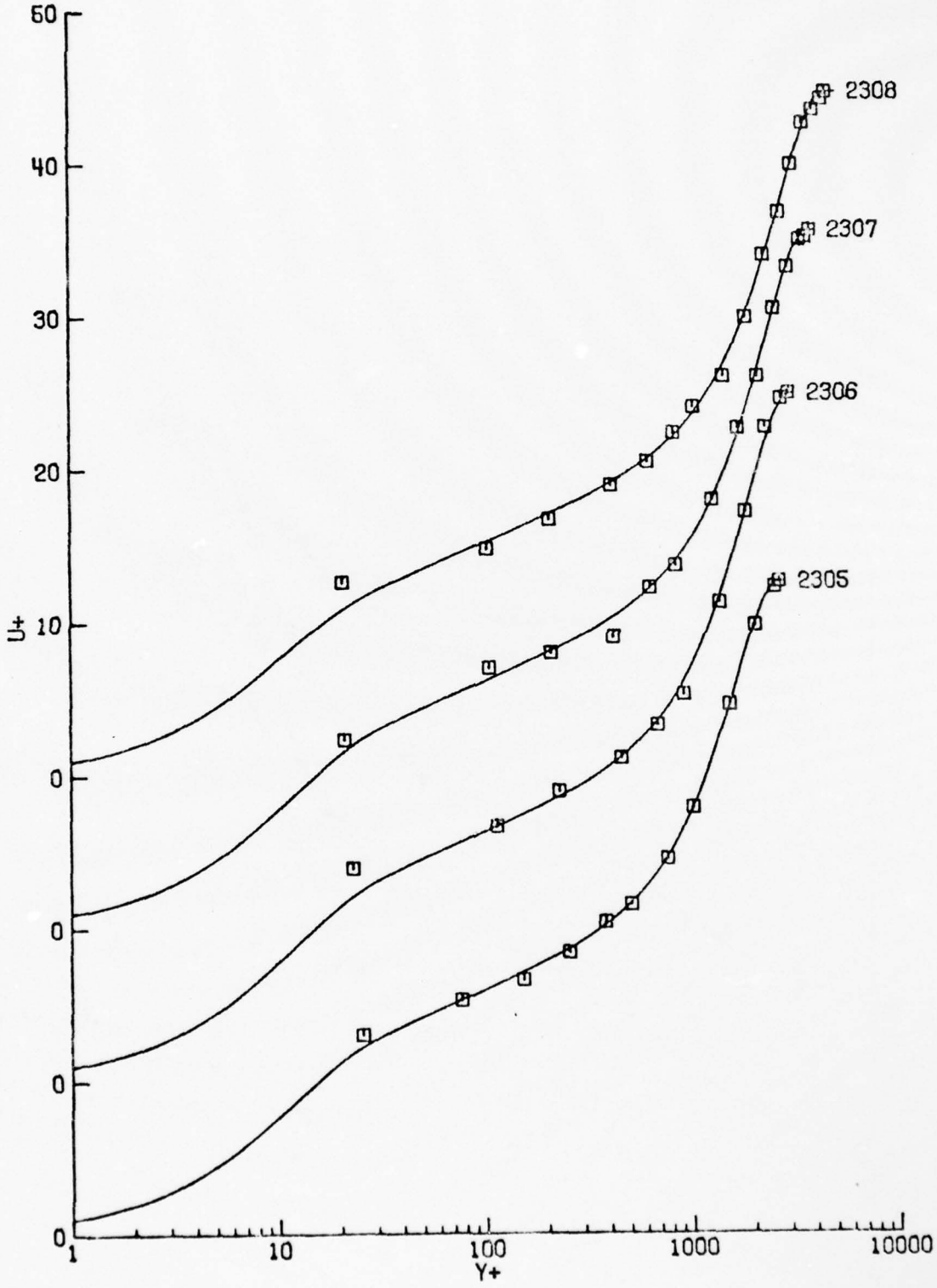

Figure B.3. (Continued).

TABLE B.4: BRADSHAW EQUILIBRIU.. - A= -0.15
(ENGLISH UNITS)

NU= 1.549000E-04

EXPERIMENTAL VALUES

ID	XSTA	UE	UTAU	DUEDX	P+	DELTA	DELTA*	THETA
2501	2.000	143.40	4.866	-9.25	.00178	1.0000	.1860	.1305
2502	4.000	129.10	4.264	-4.50	.00116	1.8000	.3093	.2231
2503	5.500	123.50	3.956	-3.25	.00100	2.3000	.4012	.2884
2504	7.000	119.00	3.720	-2.75	.00098	2.8000	.4936	.3529

UNSTEADY + COLES MODEL - FULL PROFILE FIT

ID	P+	UTAU	S	DELTA	EPSILON	Y1+	C_i	PI
2501	.00272	4.228	15.212	1.1055	.012054	.0765	8.394	1.3165
2502	.00165	3.795	14.336	1.8692	.007942	.1074	7.711	1.2701
2503	.00137	3.570	14.030	2.3965	.007998	.1198	7.480	1.3402
2504	.00129	3.401	13.567	2.8864	.008068	.1384	7.145	1.4234

MEAN EPSILON= .009015

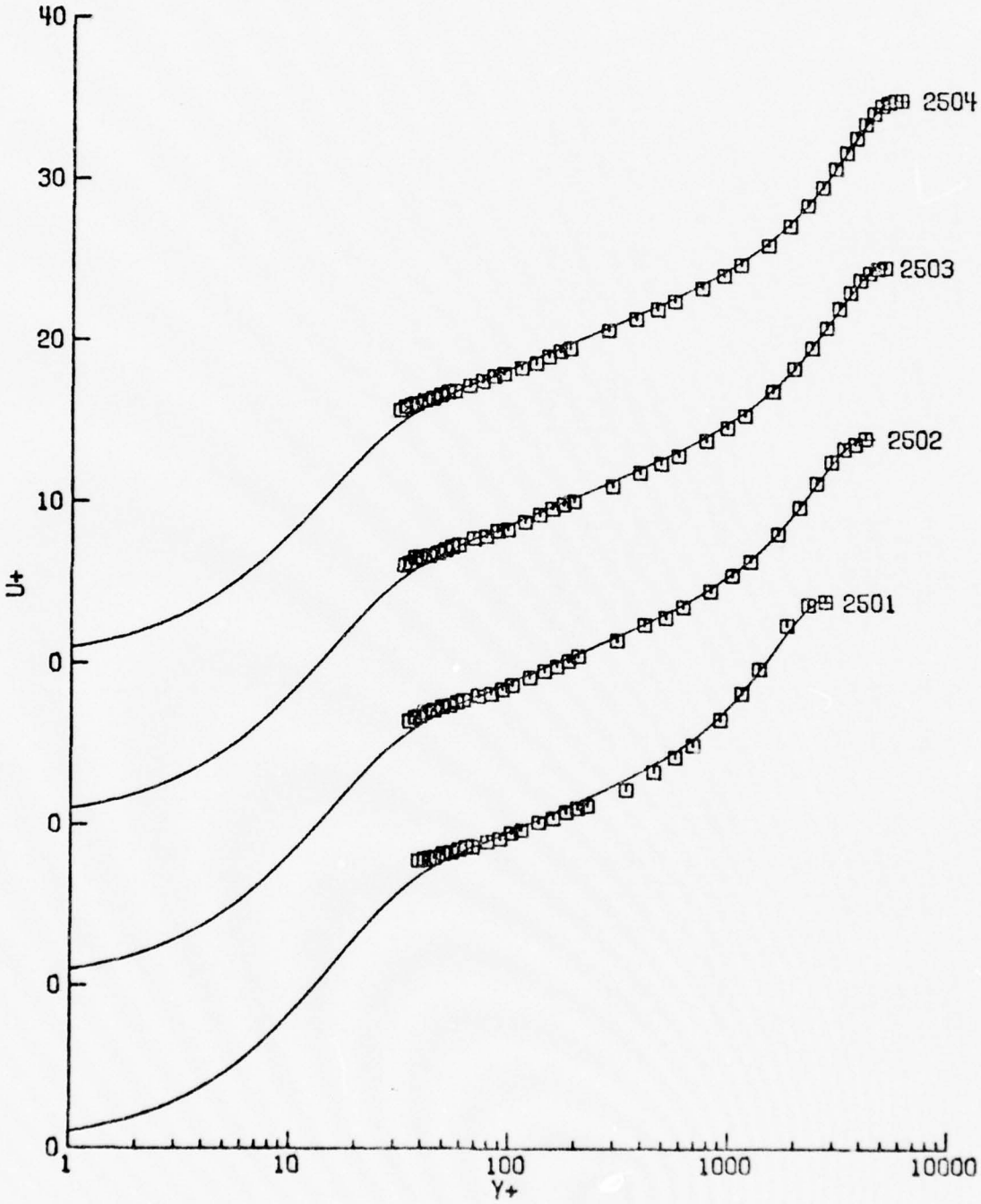

Figure B.4. Bradshaw mildly adverse gradient equilibrium flow, a = -0.15. (Note shifted origins on the U^+ axis).

TABLE B.5: BRADSHAW EQUILIBRIU - A= -0.255
(ENGLISH UNITS)

NU= 1.549000E-04

EXPERIMENTAL VALUES

ID	XSTA	UE	UTAU	DUEDX	P+	DELTA	DELTA*	THETA
2601	1.917	136.51	3.633	-18.50	.00816	1.2500	.3330	.2000
2602	3.917	113.78	2.982	-7.30	.00485	2.7000	.6710	.4210
2603	5.417	104.93	2.767	-4.50	.00345	3.6500	.8560	.5460
2604	6.917	98.39	2.525	-3.70	.00350	4.4000	1.0810	.7010

UNSTEADY + COLES MODEL - FULL PROFILE FIT

ID	P+	UTAU	S	DELTA	EPSILON	Y1+	Ci	PI
2601	.00594	4.038	7.927	1.3743	.024252	.6232	3.406	2.2307
2602	.00381	3.233	8.380	2.9239	.020092	.5727	3.665	2.1969
2603	.00257	3.052	7.851	3.9030	.020638	.6750	3.318	1.9845
2604	.00268	2.762	8.149	4.9792	.019245	.6228	3.505	2.1297

MEAN EPSILON= .021057

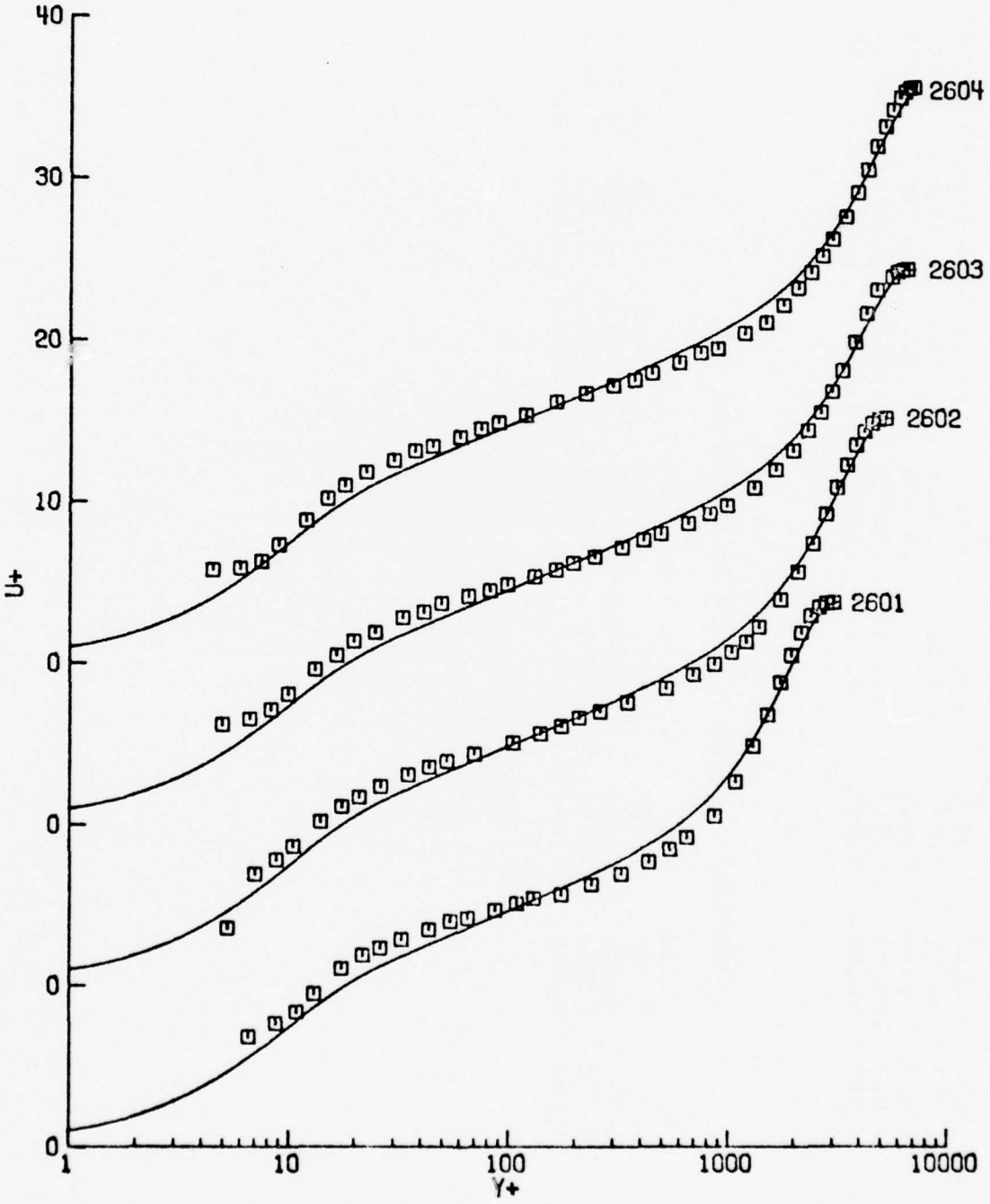

Figure B.5. Bradshaw moderately adverse gradient equilibrium flow, a = -0.255. (Note shifted origins on the U^+ axis).

TABLE B.6: HERRING AND NORBURY - DELTA= -0.35
(ENGLISH UNITS)

NU= 1.730000E-04

EXPERIMENTAL VALUES

ID	XSTA	UE	UTAU	DUEDX	P+	DELTA	DELTA*	THETA
2701	0.000	76.50	3.149	2.65	-.00112	.8500	.1239	.0921
2702	1.000	79.80	3.280	4.90	-.00192	.9000	.1282	.0960
2703	2.000	84.60	3.550	6.13	-.00201	1.0000	.1136	.0875
2704	3.000	90.50	3.798	6.20	-.00177	1.0000	.1110	.0856
2705	4.000	97.10	4.041	6.25	-.00159	1.0000	.1102	.0845
2706	5.000	103.60	4.270	6.25	-.00144	1.0000	.1124	.0860

UNSTEADY + COLES MODEL - FULL PROFILE FIT

ID	P+	UTAU	S	DELTA	EPSILON	Y1+	C_f	PI
2701	-.00094	3.346	8.854	.9375	.008751	.5578	3.900	.2270
2702	-.00182	3.335	10.207	.9928	.008041	.4018	4.758	.2422
2703	-.00175	3.714	9.629	1.0444	.016045	.4660	4.383	.0046
2704	-.00153	3.986	9.429	1.0111	.015760	.4878	4.258	-.0044
2705	-.00154	4.083	10.412	.9477	.006598	.3775	4.899	.1060
2706	-.00168	4.054	12.166	.9264	.004483	.2367	6.078	.2421

MEAN EPSILON= .009913

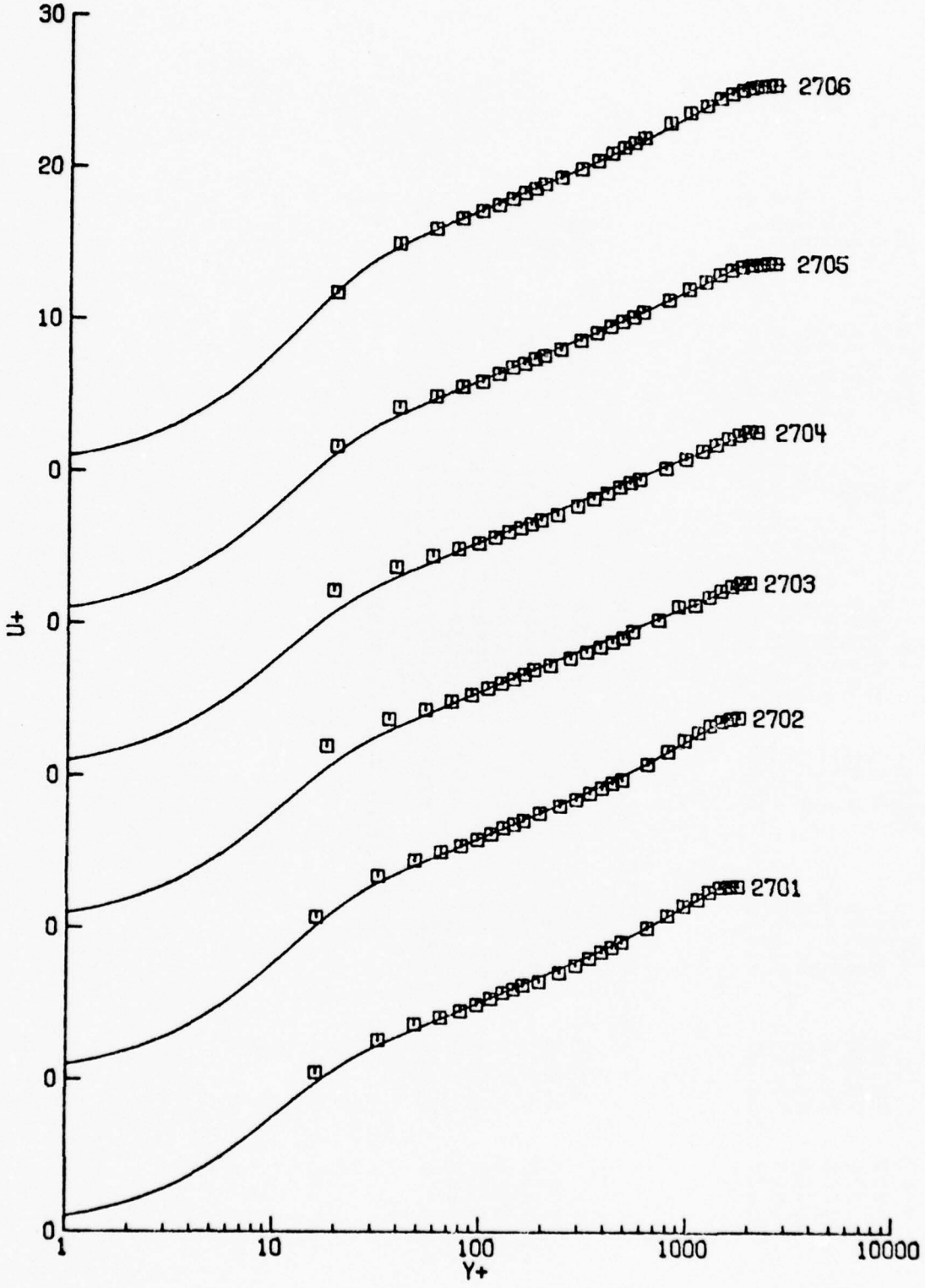

Figure B.6. Herring and Norbury mildly favorable gradient equilibrium flow, β=-0.35. (Note shifted origins on the U^+ axis).

TABLE B.7: HERRING AND NORBURY - BETA= -0.53
(ENGLISH UNITS)

NU= 1.680000E-04

EXPERIMENTAL VALUES

ID	XSTA	UE	UTAU	DUEDX	P+	DELTA	DELTA*	THETA
2801	0.000	76.90	3.110	5.00	-.00215	1.1000	.1477	.1077
2802	1.000	62.60	3.370	7.30	-.00265	1.1000	.1433	.1060
2803	2.000	90.80	3.801	9.50	-.00264	1.1000	.1241	.0929
2804	3.000	101.40	4.341	12.00	-.00250	.9000	.0978	.0725
2805	4.000	115.40	5.000	17.00	-.00264	.7500	.0832	.0607

UNSTEADY + COLES MODEL - FULL PROFILE FIT

ID	P+	UTAU	S	DELTA	EPSILON	Y1+	C1	PI
2801	-.00322	2.718	15.000	1.0845	.004672	.1181	8.011	.5133
2802	-.00412	2.907	15.568	1.1279	.004209	.1074	8.380	.4100
2803	-.00354	3.448	13.939	1.1307	.003644	.1600	7.252	.1286
2804	-.00343	3.907	14.229	.9626	.002776	.1472	7.459	.0256
2805	-.00329	4.644	13.072	.8417	.002656	.1990	6.657	-.0558

MEAN EPSILON= .003591

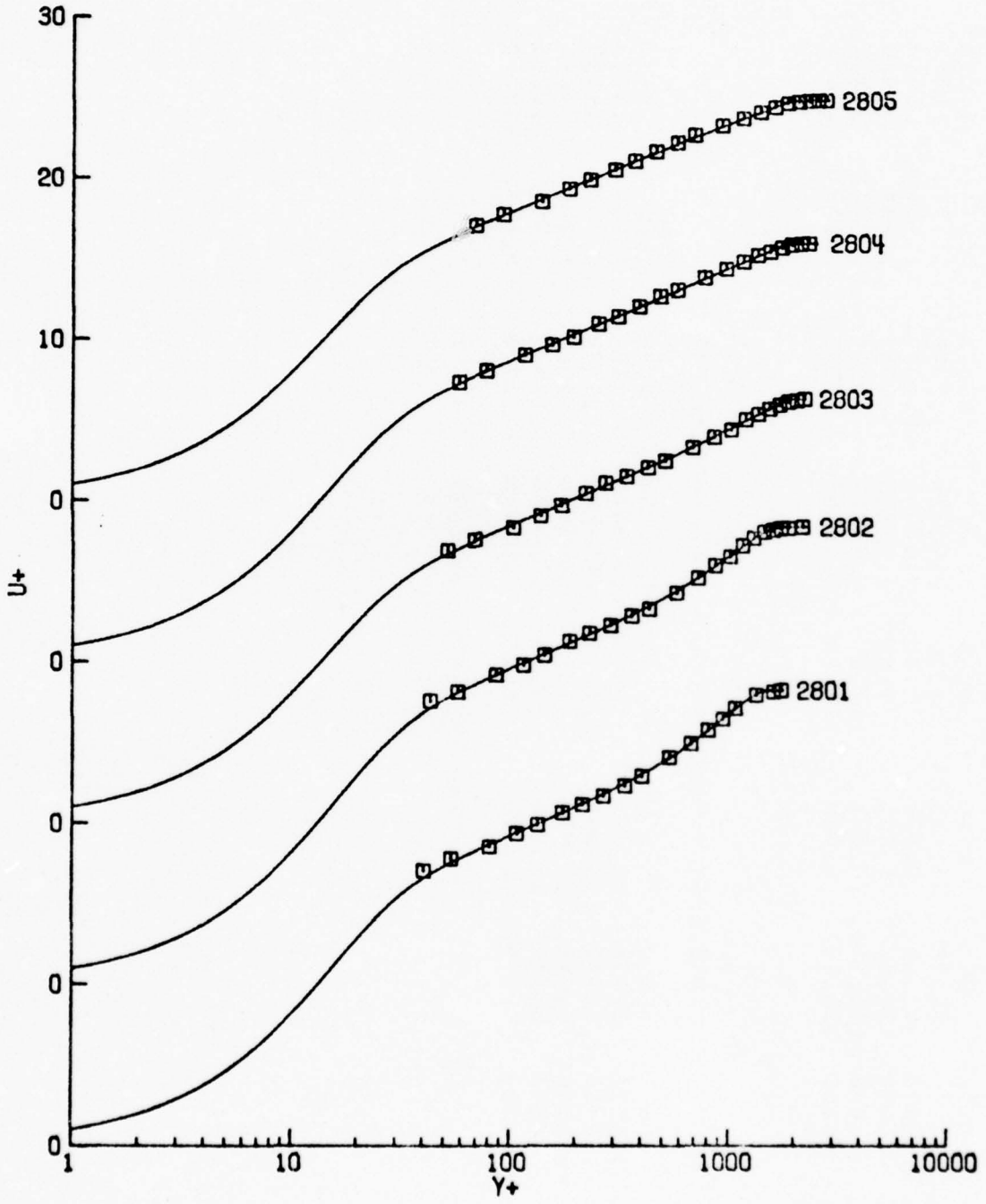

Figure B.7. Herring and Norbury strongly favorable gradient equilibrium flow, $\beta = -0.53$. (Note shifted origins on the U^+ axis).

TABLE B.8: PERRY - DIVERGING CHANNEL
(ENGLISH UNITS)

NU= 1.570900E-04

EXPERIMENTAL VALUES

ID	XSTA	UE	UTAU	DUEDX	P+	DELTA	DELTA*	THETA
2901	2.500	122.09	3.919	-9.50	.00303	2.3000	.3583	.2528
2902	4.000	109.18	3.249	-7.65	.00383	2.8000	.5645	.3876
2903	5.500	100.98	2.733	-5.60	.00435	3.8000	.8675	.5704
2904	7.000	92.96	2.198	-3.85	.00529	5.3000	1.3620	.8365
2905	8.500	88.67	1.887	-2.80	.00580	6.7000	1.9105	1.1182
2906	10.000	84.55	1.686	-2.20	.00610	9.1000	2.5308	1.4415
2907	11.000	82.16	1.449	-1.85	.00785	10.3000	3.1394	1.6796
2908	12.500	79.94	1.230	-1.55	.01046	10.9000	3.9009	1.9295
2909	14.000	77.27	.979	-1.30	.01682	13.3000	5.1334	2.3242
2910	15.000	76.04	.816	-1.20	.02638	14.8000	5.9677	2.4794

UNSTEADY + COLES MODEL - FULL PROFILE FIT

ID	P+	UTAU	S	DELTA	EPSILON	Y1+	Cj	PI
2901	.00564	3.184	16.715	1.9238	.005992	.0375	9.657	1.8372
2902	.00698	2.659	16.426	2.8385	.006536	.0377	9.495	2.3232
2903	.01090	2.012	19.845	3.8657	.010889	.0068	12.467	3.5680
2904	.01244	1.653	19.111	5.3040	.010609	.0080	11.951	4.8553
2905	.00592	1.874	10.716	7.1238	.004746	.2747	5.251	4.1901
2906	.00627	1.671	10.780	9.0320	.005646	.2664	5.301	4.7943
2907	.00791	1.445	10.637	10.2641	.005354	.2645	5.235	6.0978
2908	.01026	1.238	10.195	11.8156	.003903	.2845	4.972	7.7414
2909	.01329	1.059	8.214	14.3744	.008270	.5004	3.680	9.7053
2910	.02709	.809	9.802	15.5238	.005167	.2067	4.983	13.8494

MEAN EPSILON= .006711

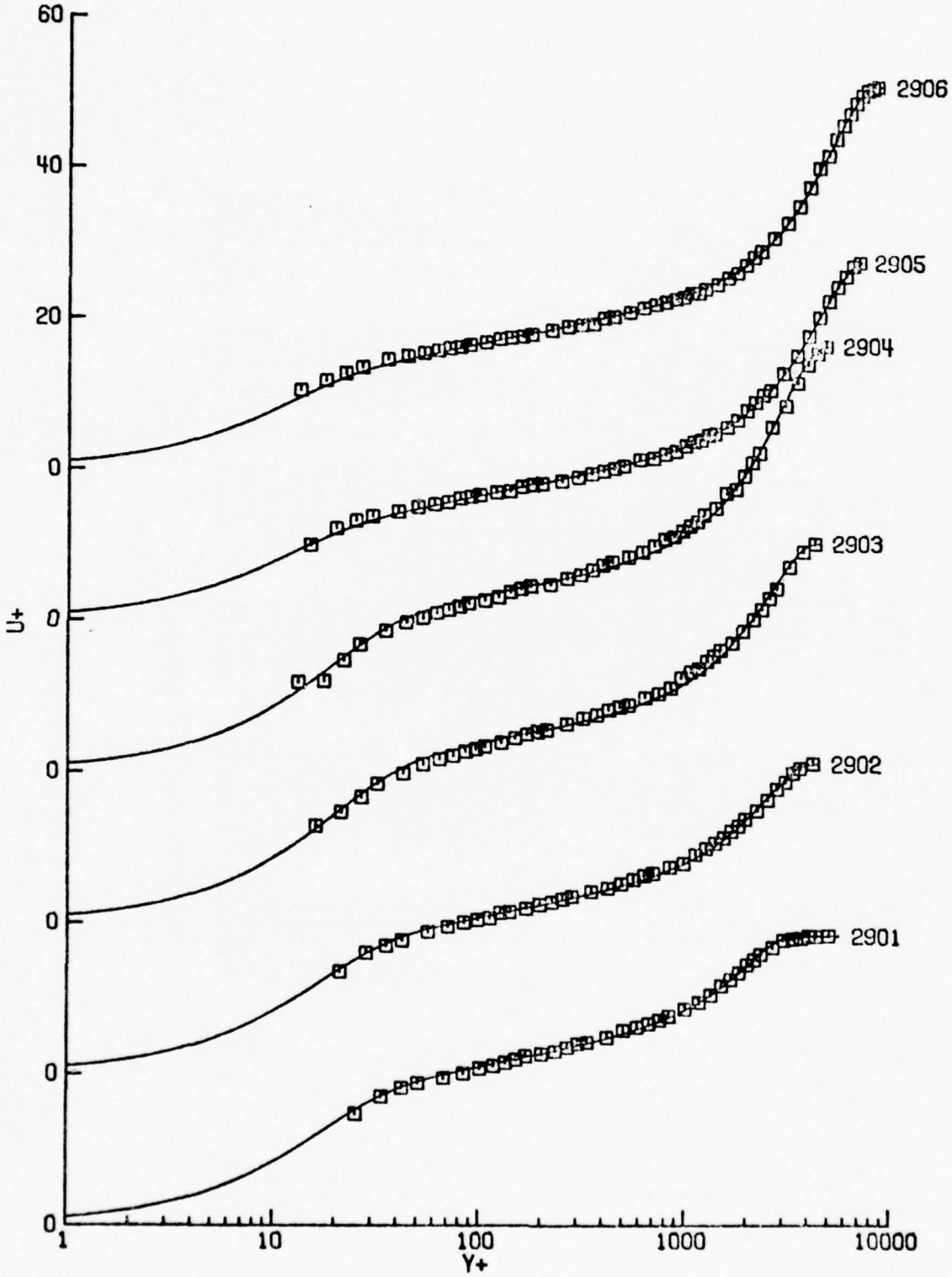

Figure B.8. Perry diverging channel flow. (Note shifted origins on the U^+ axis).

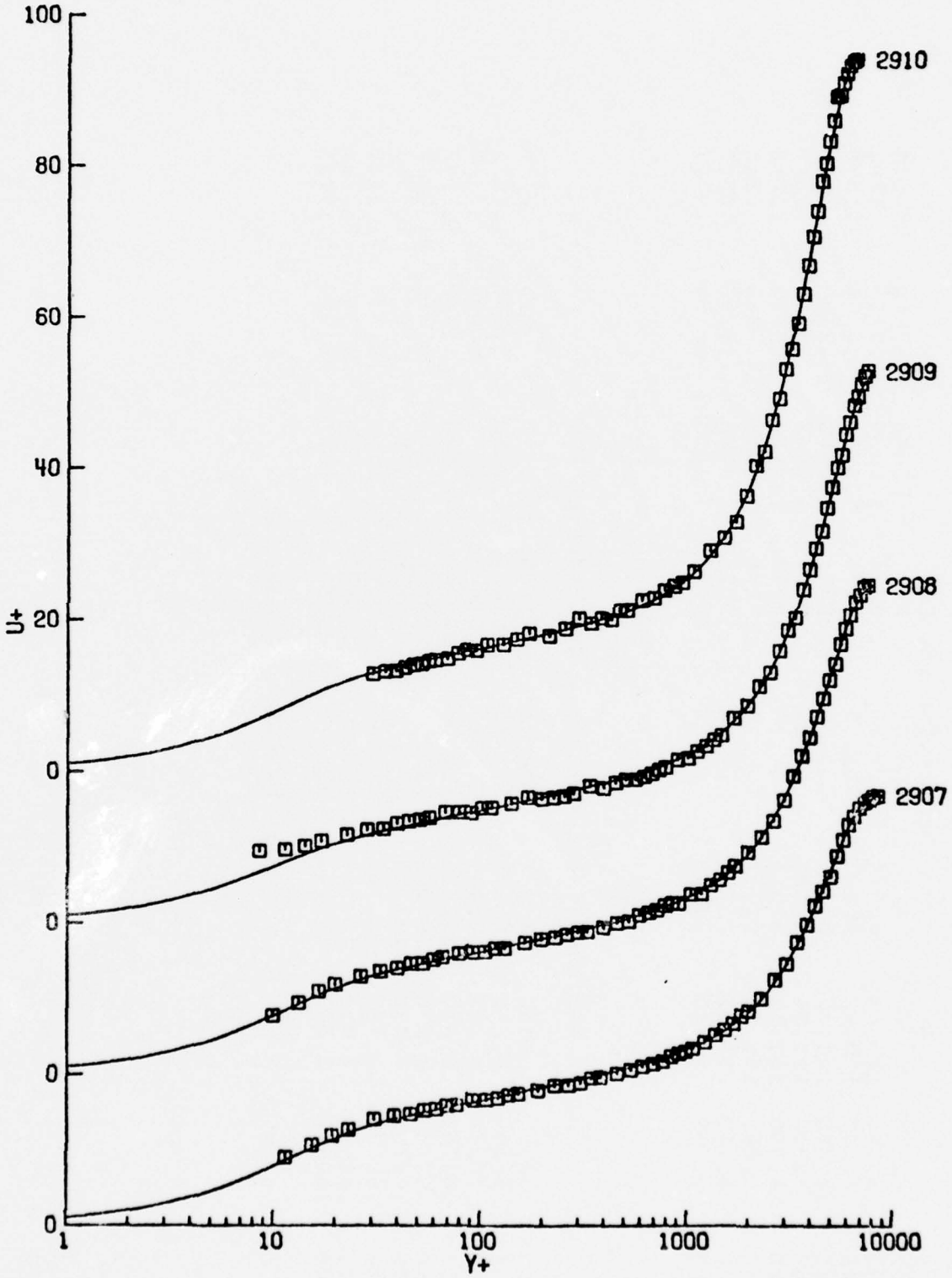

Figure B.8. (Continued).

TABLE B.9: BRADSHAW - LAYER C
(ENGLISH UNITS)

NU= 1.560000E-04

EXPERIMENTAL VALUES

ID	XSTA	UE	UTAU	DUEDX	P+	DELTA	DELTA*	THETA
3301	2.000	125.63	4.577	-11.40	.00233	1.1439	.1760	.1291
3302	2.500	120.48	4.213	-11.00	.00276	1.3429	.2108	.1540
3303	3.000	114.85	3.784	-9.30	.00308	1.5476	.2700	.1920
3304	3.500	110.77	3.505	-7.50	.00301	1.7571	.3262	.2263
3305	4.000	107.13	3.312	-6.38	.00293	1.9424	.3717	.2552
3306	5.000	101.40	2.991	-5.00	.00296	2.3650	.4863	.3268
3307	6.000	96.82	2.747	-4.19	.00305	2.7793	.5980	.3923
3308	7.000	92.95	2.596	-3.68	.00305	3.1858	.6968	.4527

UNSTEADY + COLES MODEL - FULL PROFILE FIT

ID	P+	UTAU	S	DELTA	EPSILON	Y1+	C_1	PI
3301	.00391	3.851	15.675	1.1477	.002289	.0608	8.788	1.0035
3302	.00278	4.203	10.444	1.3369	.001820	.3284	5.003	.8468
3303	.00343	3.650	11.488	1.5327	.003738	.2363	5.732	1.2747
3304	.00361	3.298	12.251	1.7354	.003883	.1858	6.272	1.5862
3305	.00362	3.088	12.728	1.9238	.005576	.1602	6.612	1.7243
3306	.00386	2.737	13.143	2.3526	.005089	.1391	6.917	2.1045
3307	.00400	2.510	13.124	2.7676	.003437	.1390	6.907	2.3808
3308	.00402	2.367	13.143	3.2041	.003500	.1380	6.922	2.4781

MEAN EPSILON= .003666

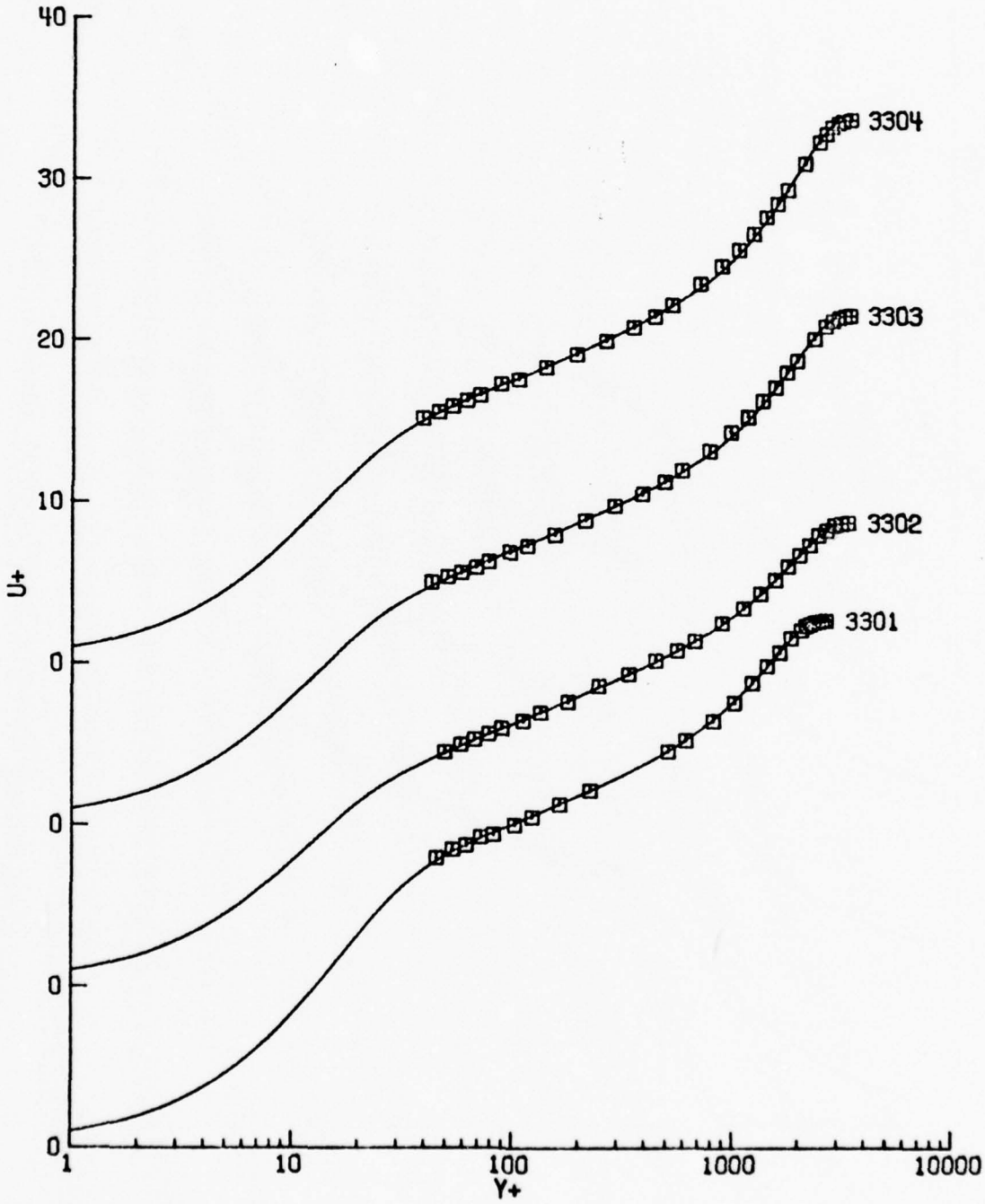

Figure B.9. Bradshaw adverse pressure gradient flow. (Note shifted origins on the U^+ axis).

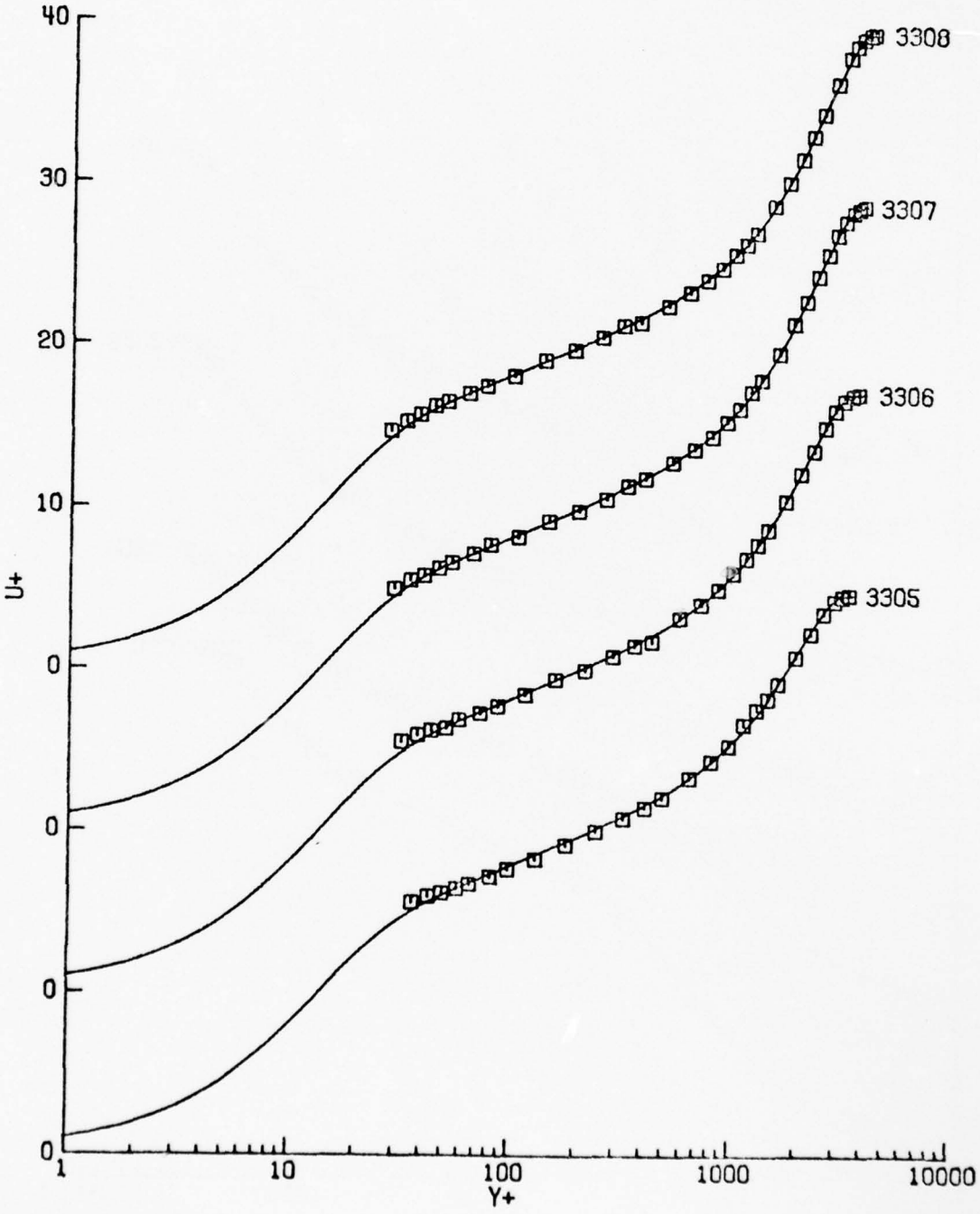

Figure B.9. (Continued).

TABLE B.10: NEWMAN AIRFOIL FLOW SERIES 2
(ENGLISH UNITS)

NU= 1.560000E-04

EXPERIMENTAL VALUES

ID	XSTA	UE	UTAU	DUEDX	P+	DELTA	DELTA*	THETA
3501	2.009	152.60	4.495	-47.60	.01248	.4366	.1081	.0656
3502	2.759	134.90	3.752	-19.00	.00757	.8383	.2148	.1277
3503	3.509	119.40	2.881	-16.50	.01285	1.3236	.3667	.2080
3504	4.009	111.60	2.377	-16.50	.02139	1.7966	.5260	.2879
3505	4.509	103.90	1.919	-16.50	.03784	2.3423	.7186	.3794
3506	4.759	100.80	1.420	-16.50	.09062	2.7174	.9120	.4449
3507	4.926	99.60	.954	-16.50	.29527	3.1212	1.1588	.5085

UNSTEADY + COLES MODEL - FULL PROFILE FIT

ID	P+	UTAU	S	DELTA	EPSILON	Y1+	Ci	PI
3501	.01489	4.238	11.514	.4330	.004966	.1542	6.011	2.7054
3502	.00728	3.801	9.401	.8626	.011595	.3954	4.381	2.6433
3503	.01220	2.932	9.246	1.3495	.007669	.3685	4.353	3.6292
3504	.01538	2.653	6.864	1.8092	.005369	.7300	2.844	4.1156
3505	.02247	2.283	5.545	2.3397	.003474	.9919	2.114	4.9175
3506	.04495	1.794	4.704	2.6764	.009169	1.0733	1.769	7.2318
3507	.17384	1.138	7.089	3.0492	.015096	.0745	4.403	13.2730

MEAN EPSILON= .008191

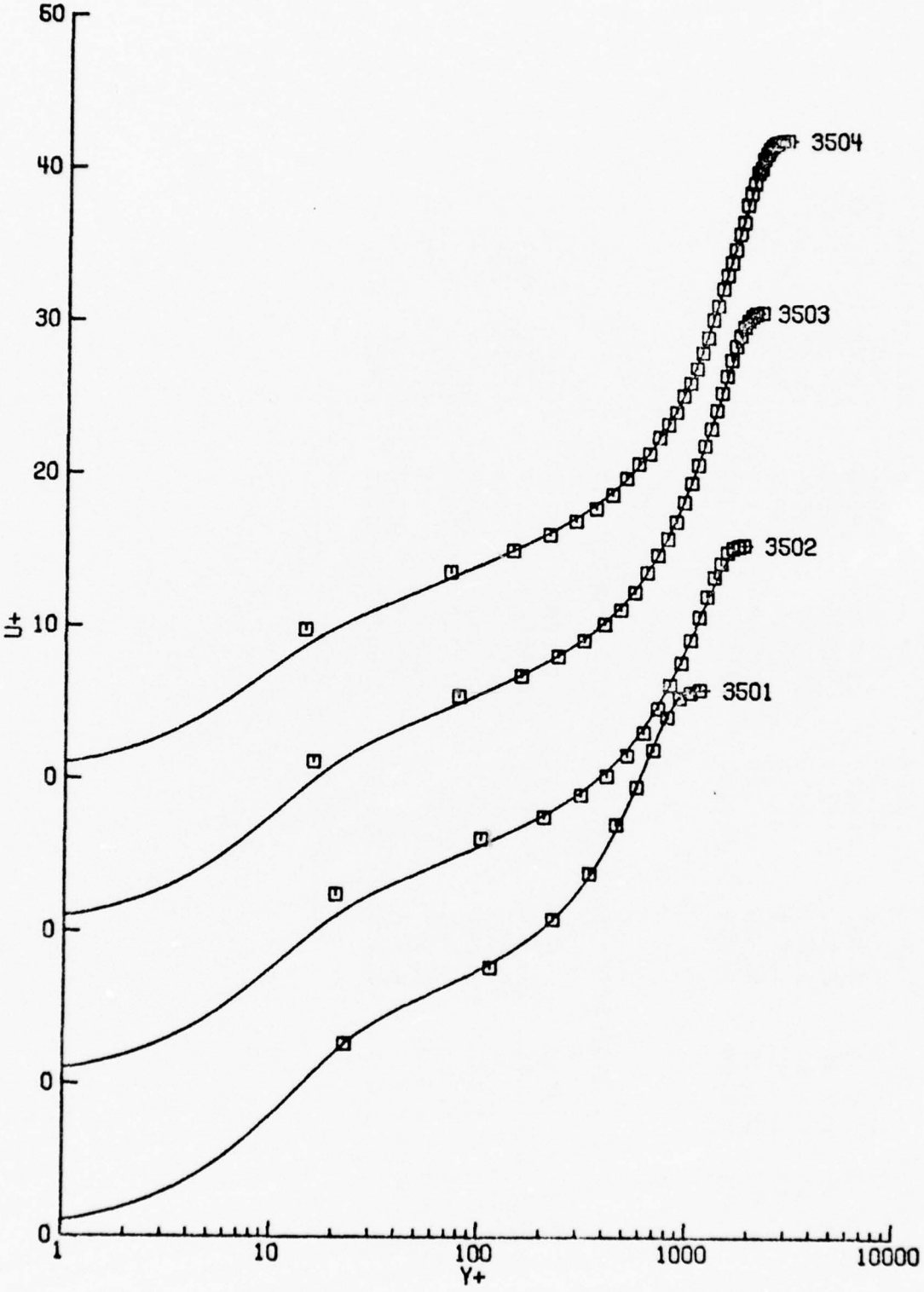

Figure B.10 Newman airfoil flow. (Note shifted origins on the U^+ axis).

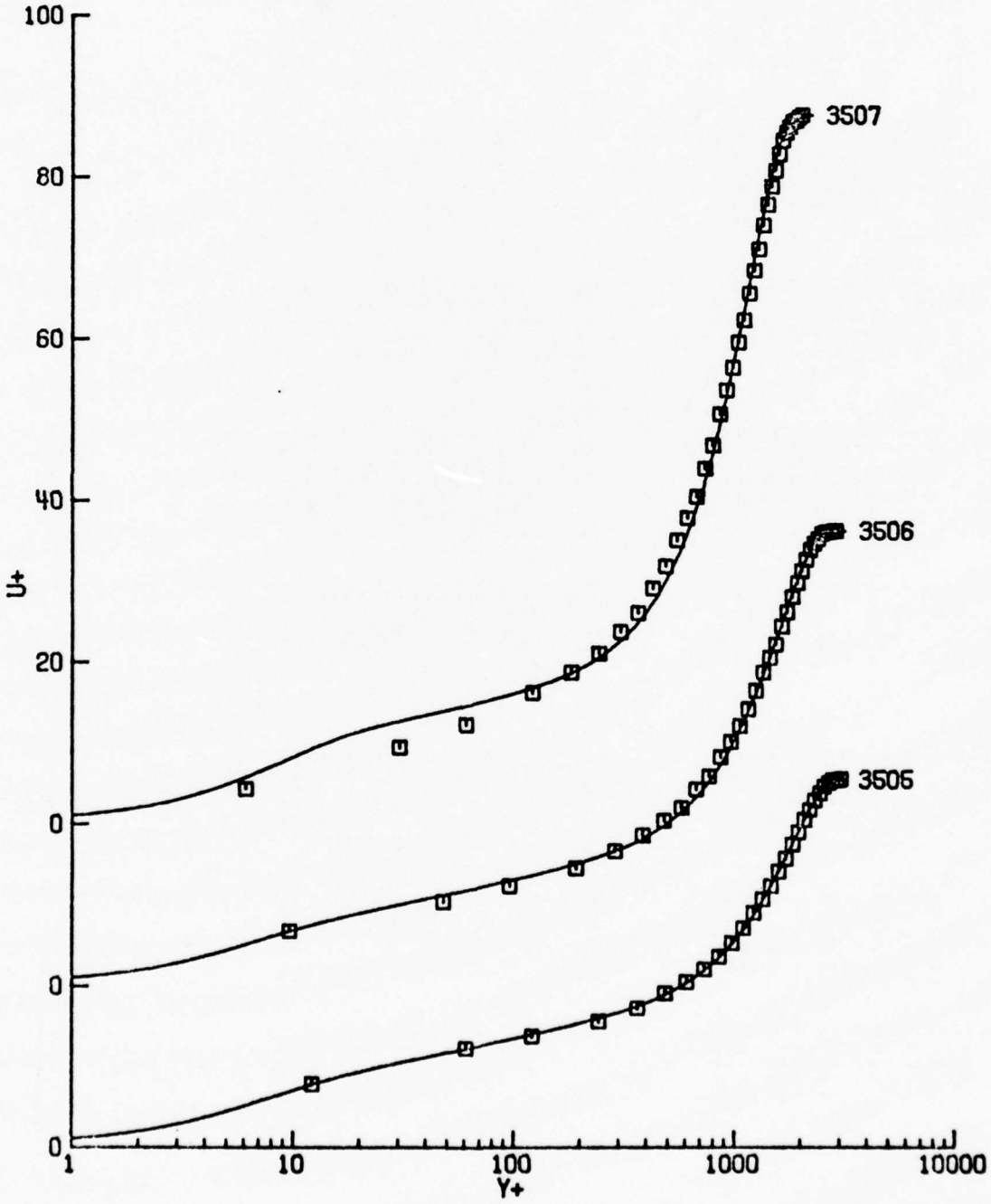

Figure B.10. (Continued).

TABLE B.11: MOSES - CASE 1
(ENGLISH UNITS)

NU= 1.660000E-04

EXPERIMENTAL VALUES

ID	XSTA	UE	UTAU	DUEDX	P+	DELTA	DELTA*	THETA
3601	0.000	105.00	5.412	-2.10	.00023	.1200	.0187	.0092
3602	.323	104.40	5.056	-2.10	.00028	.1800	.0279	.0165
3603	.646	103.80	4.794	-2.10	.00033	.2300	.0369	.0233
3604	.969	103.10	4.686	-2.10	.00035	.2900	.0429	.0284
3605	1.292	102.60	4.530	-2.70	.00049	.3500	.0517	.0350
3606	1.615	101.80	4.397	-5.70	.00113	.4100	.0598	.0407
3607	1.938	99.39	4.176	-12.60	.00285	.4700	.0727	.0503
3608	2.261	98.03	3.537	-28.60	.01052	.6300	.1103	.0756
3609	2.583	79.27	1.453	-19.00	.08150	1.0000	.3705	.1840

UNSTEADY + COLES MODEL - FULL PROFILE FIT

ID	P+	UTAU	S	DELTA	EPSILON	Y1+	Ci	PI
3601	.00032	4.836	13.355	.1028	.003916	.1546	6.964	.2639
3602	.00041	4.453	13.977	.1795	.004912	.1281	7.410	.2904
3603	.00048	4.231	14.045	.2335	.005859	.1252	7.461	.3972
3604	.00053	4.086	14.684	.2936	.007756	.1031	7.924	.3480
3605	.00071	4.014	14.219	.3446	.007640	.1173	7.594	.4118
3606	.00157	3.947	13.643	.3831	.005446	.1333	7.207	.4933
3607	.00391	3.760	13.447	.4499	.005084	.1260	7.139	.5829
3608	.01116	3.468	12.252	.5748	.008841	.1361	6.466	1.0144
3609	.05365	1.670	6.991	.9698	.015991	.4141	3.278	5.7061

MEAN EPSILON= .007272

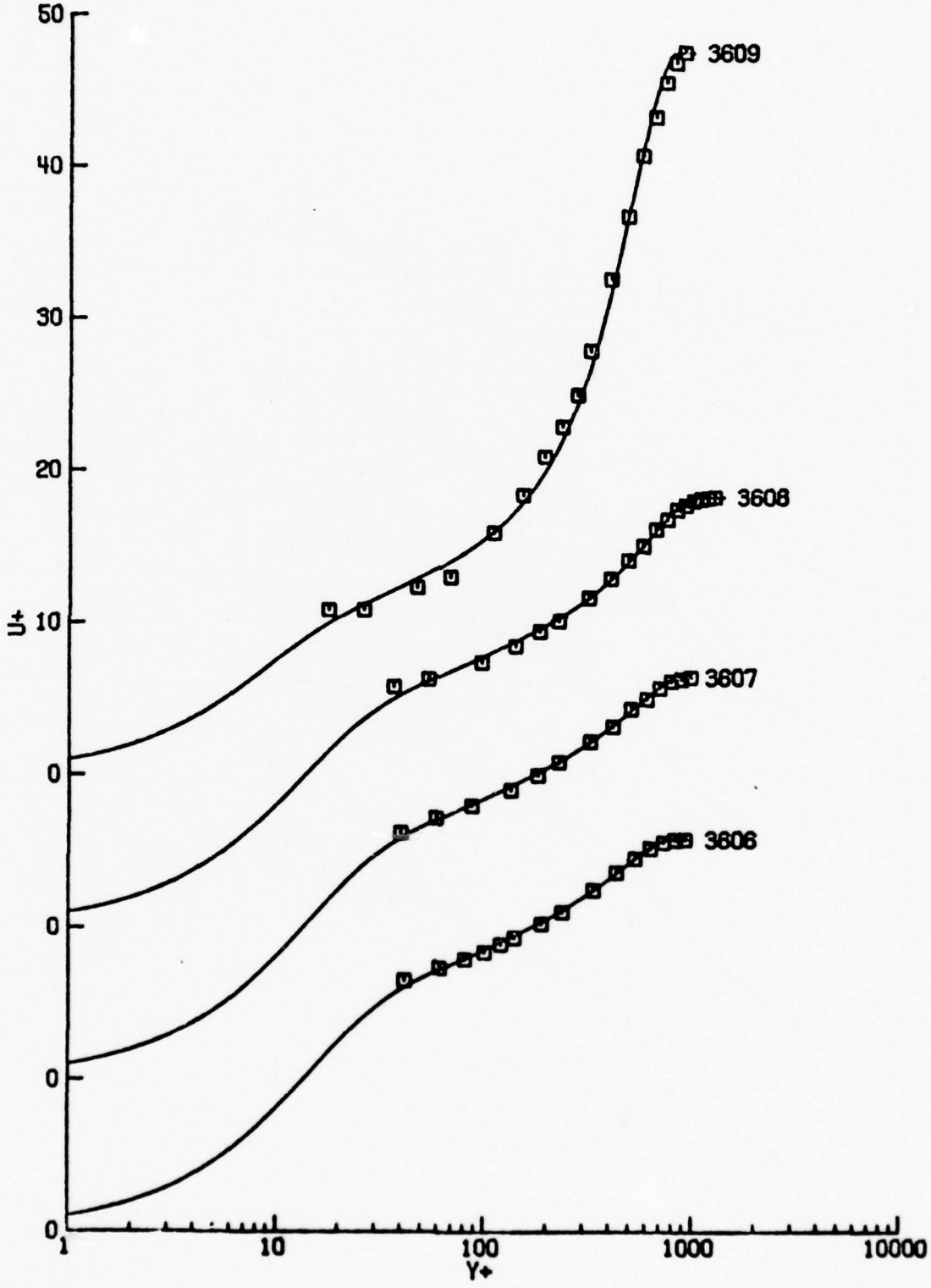

Figure B.11. Moses I (Note shifted origins on the U^+ axis).

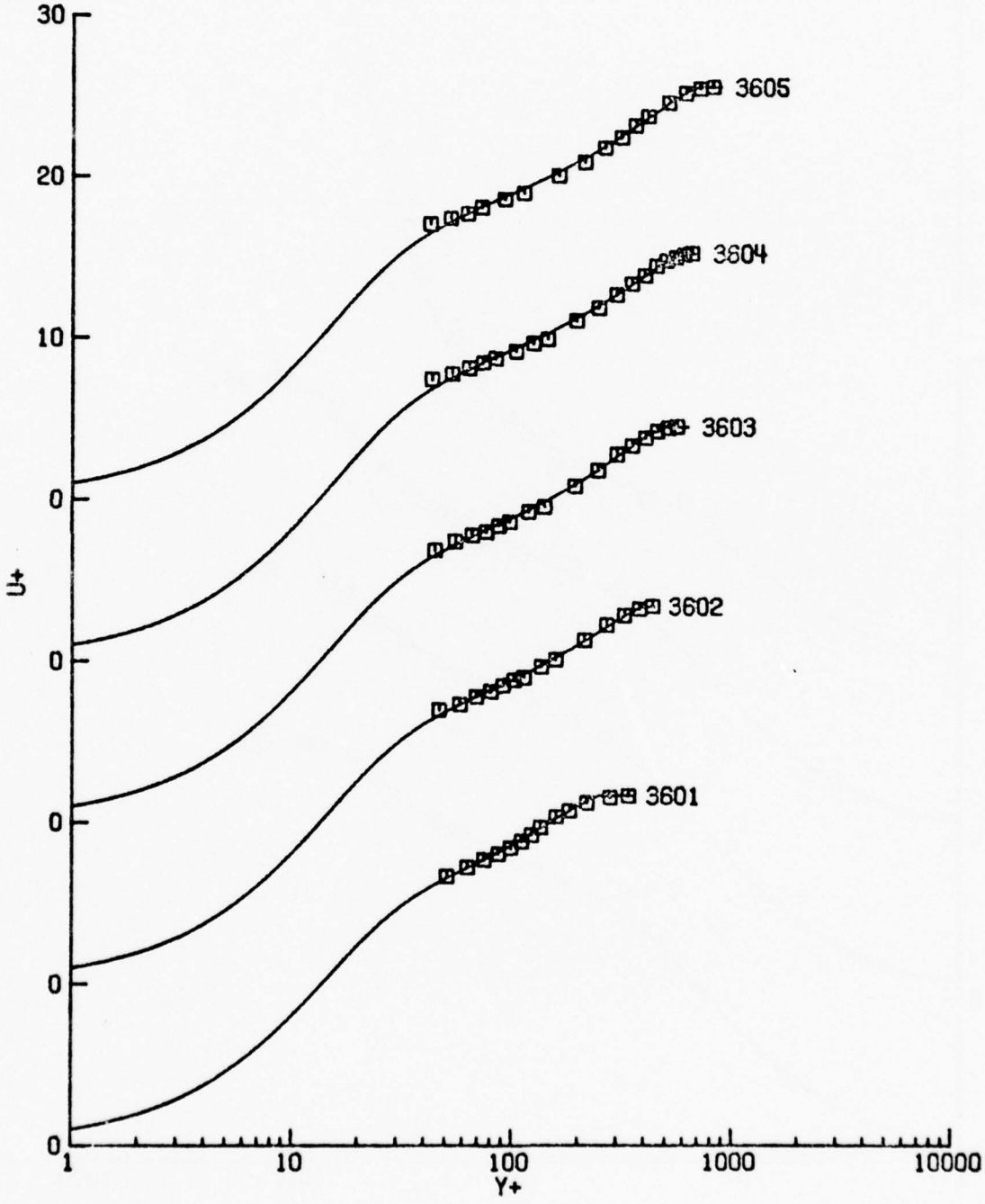

Figure B.11. (Continued).

TABLE B.12: MOSES - CASE 2
(ENGLISH UNITS)

NU= 1.660000E-04

EXPERIMENTAL VALUES

ID	XSTA	UE	UTAU	DUEDX	P+	DELTA	DELTA*	THETA
3701	0.000	86.00	4.388	-10.90	.00184	.1100	.0191	.0116
3702	.167	84.22	4.118	-11.45	.00229	.1600	.0261	.0171
3703	.407	81.41	3.760	-12.20	.00310	.2250	.0382	.0260
3704	.657	78.35	3.429	-13.20	.00426	.2900	.0531	.0364
3705	.917	75.17	3.158	-14.00	.00555	.3750	.0688	.0472
3706	1.167	71.64	2.900	-14.90	.00727	.4400	.0862	.0590
3707	1.407	68.21	2.536	-15.70	.01090	.5400	.1190	.0788
3708	1.657	64.07	2.221	-16.50	.01602	.6400	.1572	.1018
3709	1.917	59.83	1.734	-17.40	.03315	.8400	.2394	.1481
3710	2.167	55.13	1.276	-18.10	.07973	1.0500	.3460	.1896
3711	2.417	51.81	.715	-8.50	.20000	1.3000	.3786	.2433

UNSTEADY + COLES MODEL - FULL PROFILE FIT

ID	P+	UTAU	S	DELTA	EPSILON	Y1+	G	PI
3701	.00147	4.728	8.035	.1014	.005115	.6562	3.419	.2863
3702	.00189	4.393	8.894	.1641	.008434	.5185	3.966	.1710
3703	.00265	3.960	9.262	.2428	.012654	.4606	4.216	.2604
3704	.00355	3.642	8.967	.3200	.012868	.4896	4.038	.3969
3705	.00438	3.417	8.474	.4016	.012827	.5517	3.732	.4767
3706	.00587	3.113	8.705	.4798	.012950	.5011	3.902	.6081
3707	.00685	2.960	6.260	.5696	.009917	.9585	2.408	.8596
3708	.00933	2.660	5.919	.7018	.012637	1.0179	2.232	1.0590
3709	.01606	2.208	4.111	.8718	.011608	1.5016	1.312	1.8501
3710	.05074	1.483	6.369	1.0233	.011078	.5585	2.830	3.7203
3711	.06898	1.020	1.887	1.3058	.011031	2.0562	.558	7.0508

MEAN EPSILON= .011011

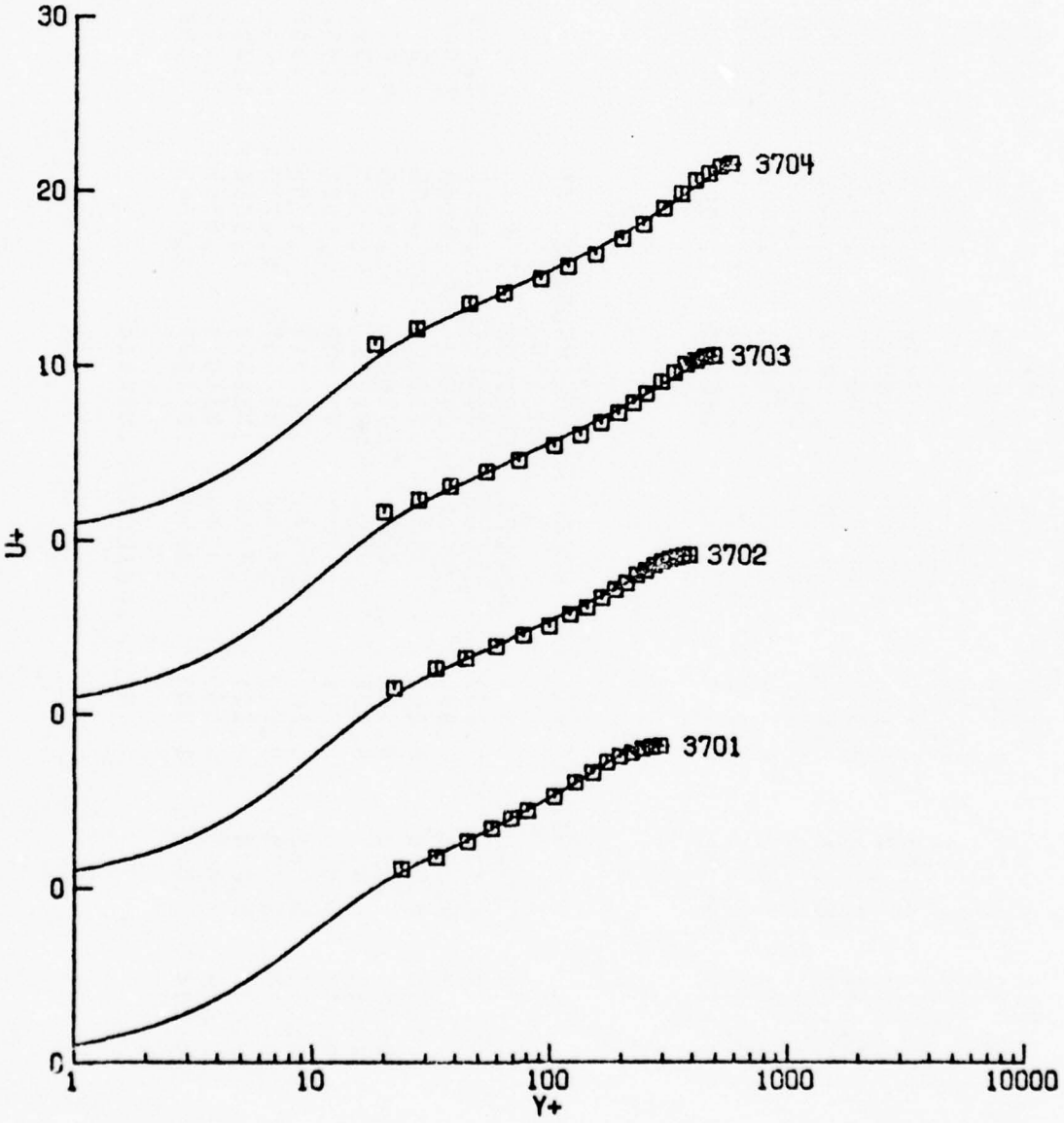

Figure B.12. Moses 2. (Note shifted origins on the U^+ axis).

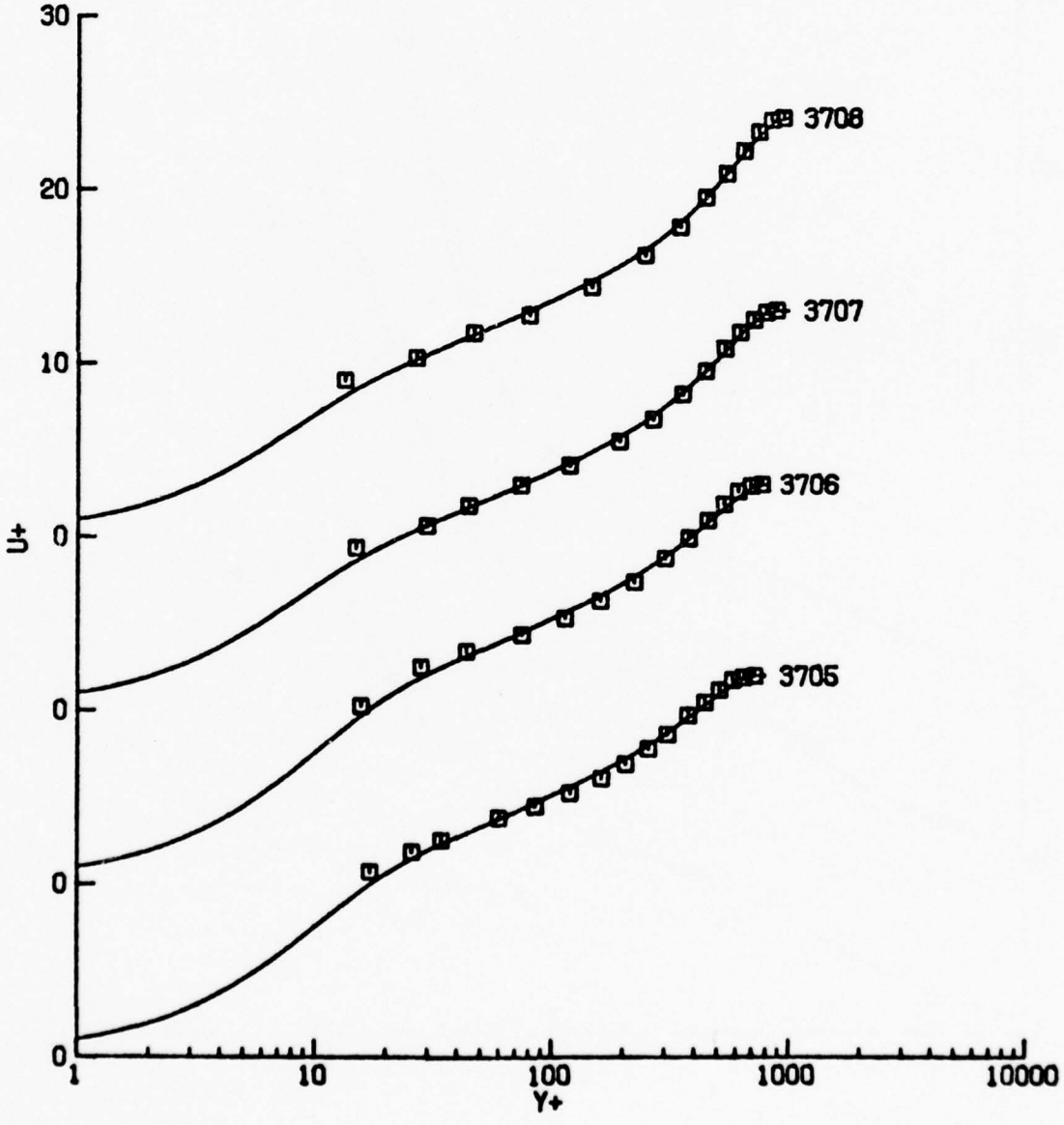

Figure B.12. (Continued)

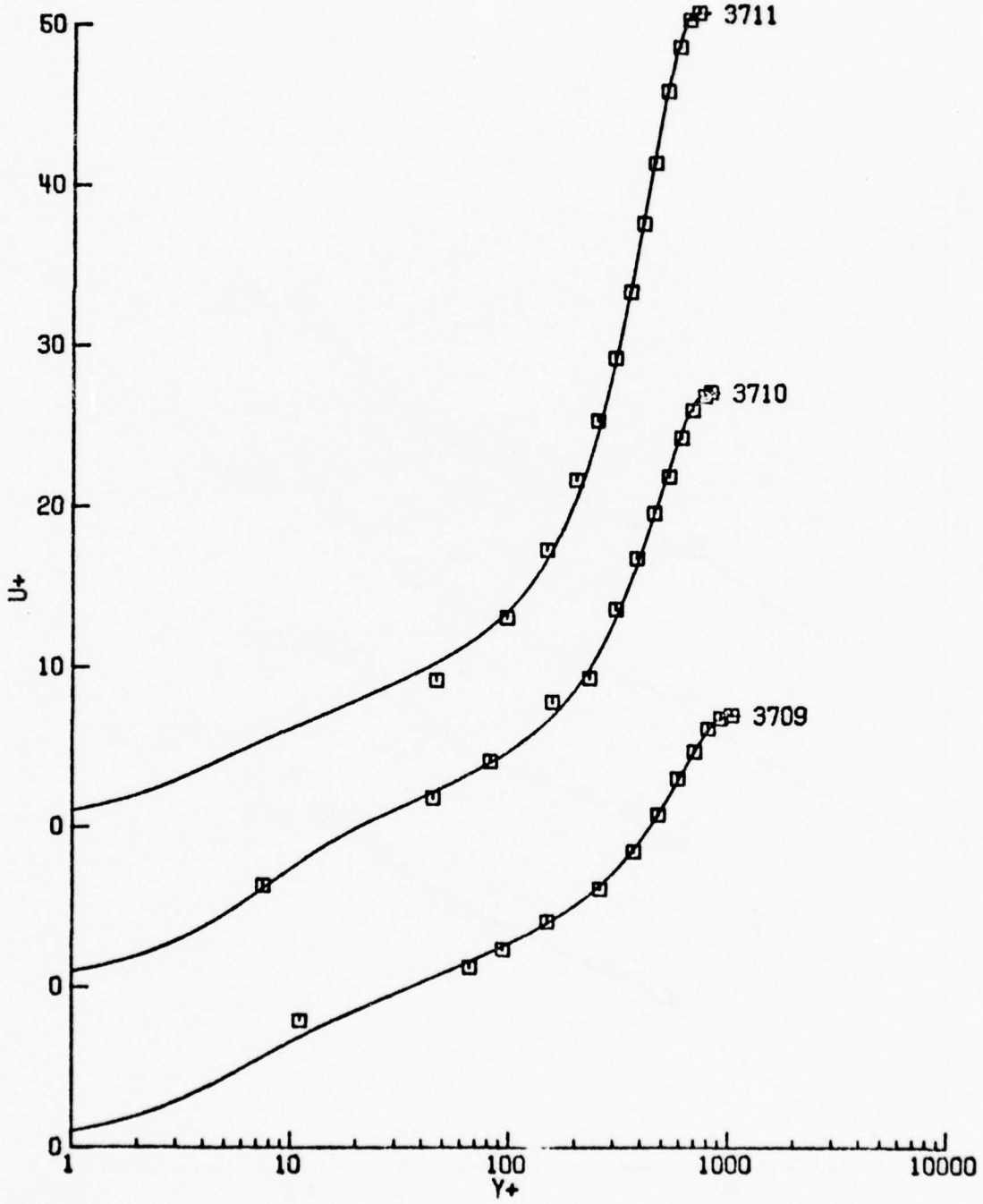

Figure B.12. (Continued).

TABLE B.13: MOSES - CASE 3
(ENGLISH UNITS)

NU= 1.660000E-04

EXPERIMENTAL VALUES

ID	XSTA	UE	UTAU	DUEDX	P+	DELTA	DELTA*	THETA
3801	0.000	78.00	3.814	-39.40	.00920	.1300	.0220	.0136
3802	.250	69.90	3.135	-34.50	.01299	.2350	.0422	.0277
3803	.521	60.87	2.396	-29.20	.02145	.3000	.0795	.0514
3804	.844	52.21	1.639	-22.20	.04370	.6400	.1815	.1066
3805	1.198	45.75	.790	-14.00	.21565	1.0000	.4375	.1917

UNSTEADY + COLES MODEL - FULL PROFILE FIT

ID	P+	UTAU	S	DELTA	EPSILON	Y1+	C_i	PI
3801	.00576	4.459	6.574	.1153	.007210	.8963	2.582	.2804
3802	.00863	3.593	6.866	.2296	.011175	.7994	2.782	.4053
3803	.01286	2.841	6.262	.3913	.021758	.8944	2.459	.7251
3804	.02283	2.035	4.507	.6725	.022649	1.3116	1.546	1.6768
3805	.09128	1.052	1.528	1.0636	.011733	2.1201	.500	5.6459

MEAN EPSILON= .014905

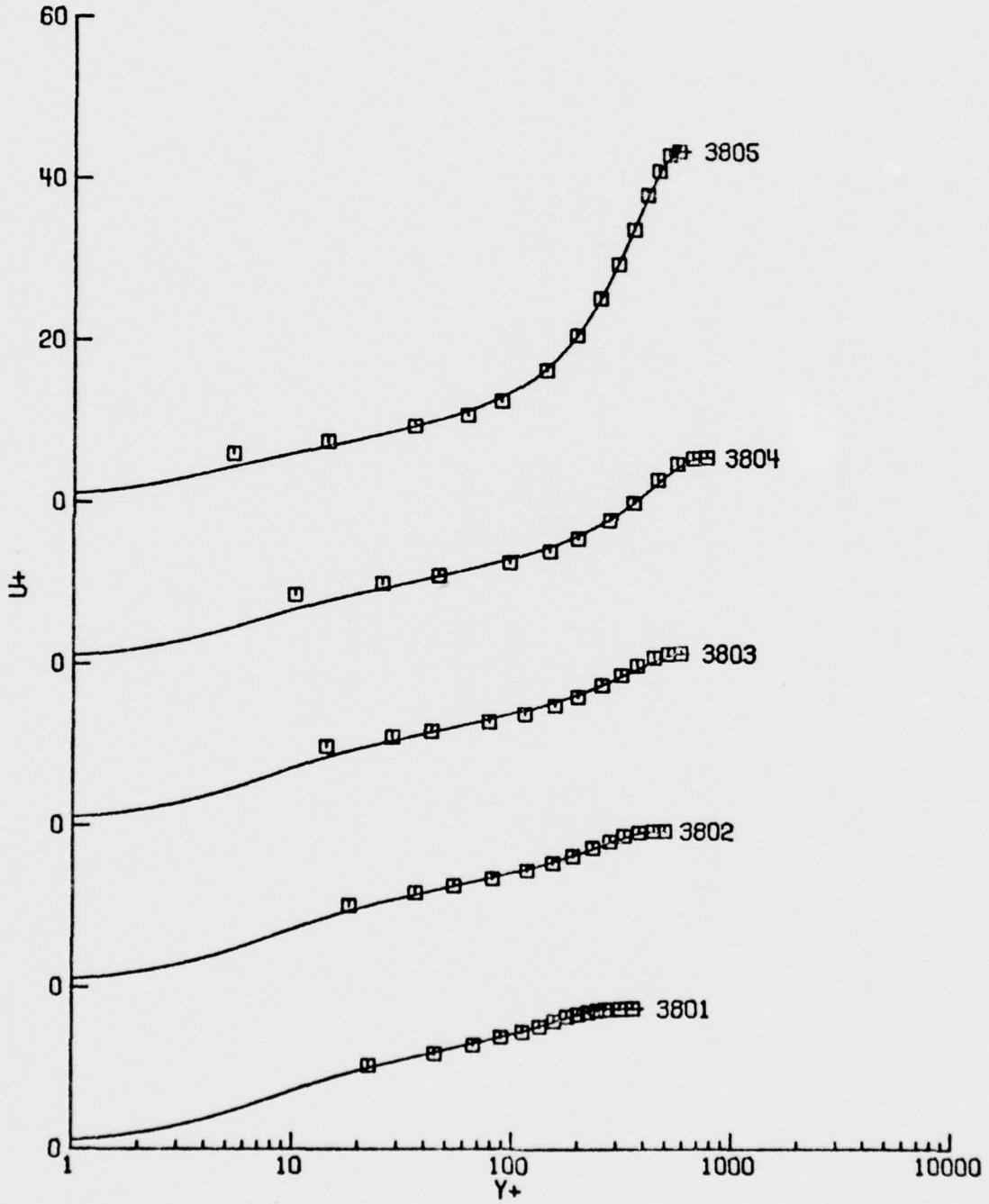

Figure B.13. Moses 3. (Note shifted origins on the U^+ axis).

TABLE B.14: MOSES - CASE 5
(ENGLISH UNITS)

NU= 1.660000E-04

EXPERIMENTAL VALUES

ID	XSTA	UE	UTAU	DUEDX	P+	DELTA	DELTA*	THETA
4001	0.000	82.00	3.981	-39.90	.00861	.1250	.0222	.0137
4002	.162	76.26	3.531	-40.20	.01156	.1800	.0336	.0221
4003	.323	69.09	2.879	-42.00	.02019	.2600	.0553	.0356
4004	.484	61.36	2.094	-47.00	.05214	.3700	.1029	.0608
4005	.646	55.49	1.498	-27.50	.07536	.5900	.1829	.0973
4006	.865	51.14	1.085	-14.00	.09305	.7800	.3118	.1466
4007	1.058	49.54	1.050	-6.20	.04404	.8600	.3526	.1687
4008	1.303	48.93	1.369	0.00	-0.00000	.9800	.3150	.1868
4009	1.516	48.65	1.595	0.00	-0.00000	.9800	.2800	.1849
4010	1.734	48.79	1.730	0.00	-0.00000	1.1000	.2743	.1916
4011	1.979	48.86	1.823	0.00	-0.00000	1.2000	.2632	.1920
4012	2.198	48.51	1.813	0.00	-0.00000	1.3100	.2743	.2035
4013	2.438	48.86	1.872	0.00	-0.00000	1.3000	.2602	.1969
4014	2.683	49.13	1.923	-2.90	.00333	1.4200	.2645	.2036
4015	2.928	48.16	1.881	-10.00	.01201	1.4500	.2880	.2190

UNSTEADY + COLES MODEL - FULL PROFILE FIT

ID	P+	UTAU	S	DELTA	EPSILON	Y1+	C_i	PI
4001	.00583	4.533	7.146	.1186	.009463	.7715	2.923	.3105
4002	.00799	3.994	7.419	.1960	.013601	.6933	3.112	.2895
4003	.01394	3.257	7.176	.2746	.011306	.6793	3.023	.6746
4004	.03420	2.410	6.401	.4024	.011046	.6691	2.719	1.5679
4005	.03788	1.884	4.590	.5924	.027721	1.1643	1.669	2.5313
4006	.04966	1.338	3.992	.8462	.026868	1.2994	1.405	4.3786
4007	.02164	1.331	3.435	.9516	.015469	1.6981	1.020	4.1951
4008	-0.00000	1.693	4.690	1.0831	.023621	1.4621	1.513	2.2039
4009	-0.00000	1.889	5.572	1.1680	.032766	1.2118	1.970	1.3717
4010	-0.00000	2.016	5.984	1.3202	.031366	1.1048	2.196	.9131
4011	-0.00000	2.070	6.681	1.4150	.026475	.9397	2.591	.6621
4012	-0.00000	2.081	6.535	1.5405	.029976	.9726	2.507	.5722
4013	-0.00000	2.131	6.773	1.5525	.026936	.9192	2.644	.4512
4014	.00231	2.171	6.634	1.6467	.029346	.9225	2.585	.3627
4015	.00862	2.101	6.476	1.7214	.024223	.8877	2.549	.4234

MEAN EPSILON= .022679

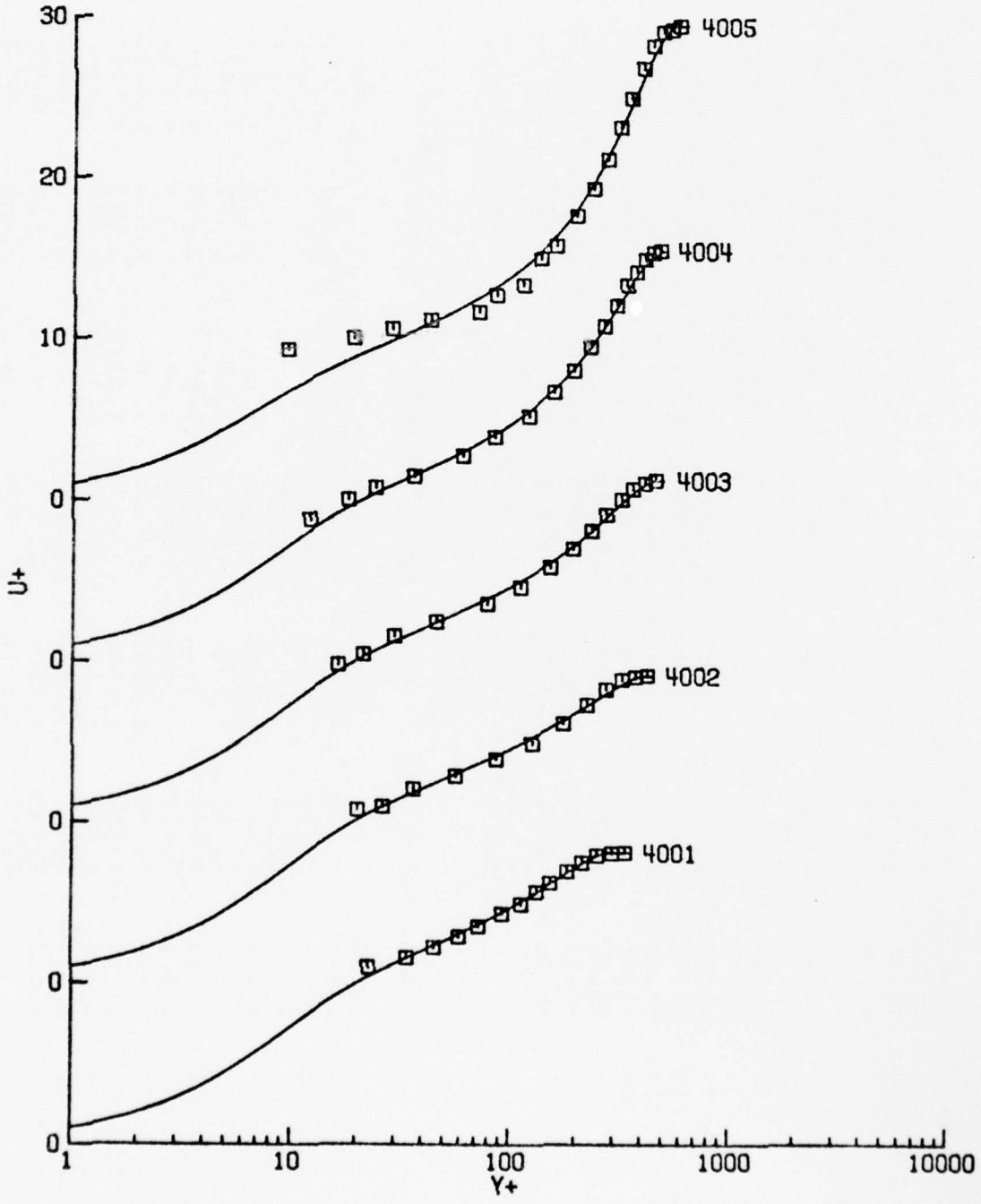

Figure B.14. Moses 5. (Note shifted origins on the U^+ axis).

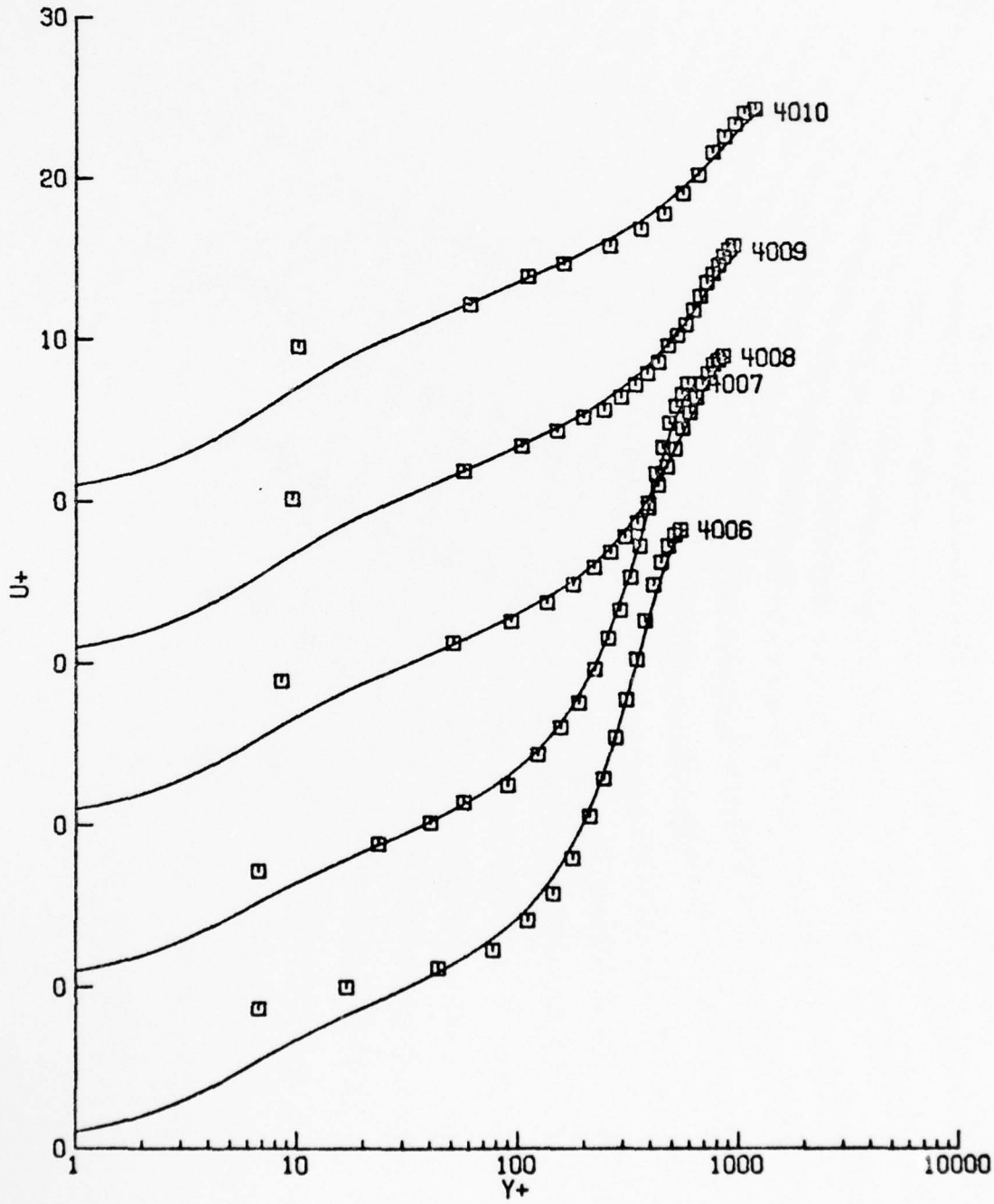

Figure B.14. (Continued).

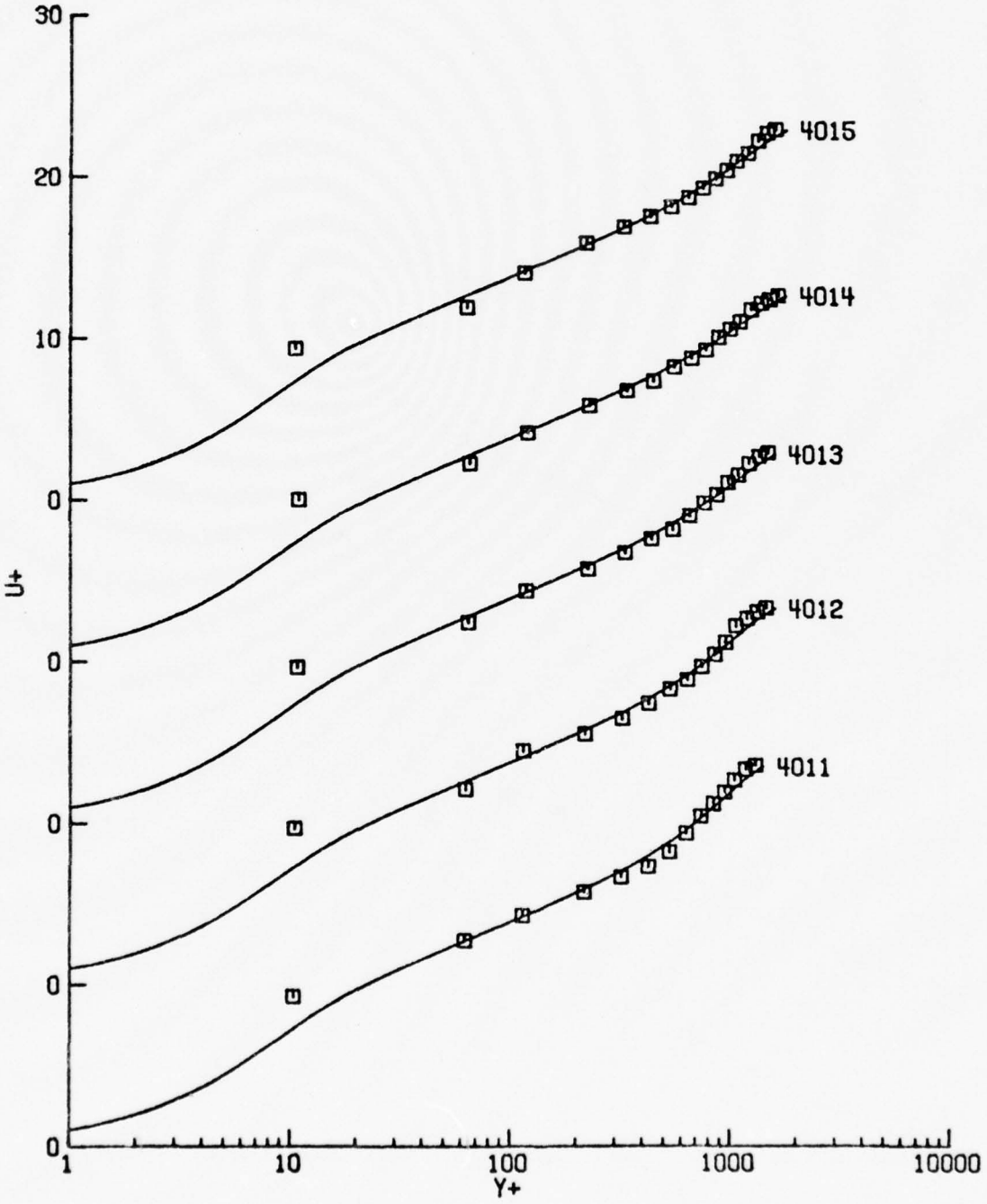

Figure B.14. (Continued).

TABLE B.15: SCHUBAUER AND SPANGENBERG - FLOW A
(ENGLISH UNITS)

NU= 1.680000E-04

EXPERIMENTAL VALUES

ID	XSTA	UE	UTAU	DUEDX	P+	DELTA	DELTA*	THETA
4401	-.833	82.10	3.386	0.00	-0.00000	.6999	.1048	.0758
4402	0.000	80.34	3.201	-1.35	.00056	.8653	.1288	.0930
4403	.833	79.45	3.128	-2.60	.00113	.9840	.1512	.1096
4404	1.667	76.30	2.885	-4.20	.00224	1.1620	.1849	.1333
4405	2.500	72.80	2.510	-5.87	.00454	1.3986	.2599	.1799
4406	3.333	69.01	2.163	-7.18	.00823	1.7240	.3632	.2401
4407	4.167	63.02	1.622	-7.42	.01841	2.3103	.5796	.3536

UNSTEADY + COLES MODEL - FULL PROFILE FIT

ID	P+	UTAU	S	DELTA	EPSILON	Y1+	C_i	PI
4401	0.00000	3.650	9.547	.8142	.035016	.4551	4.359	.0695
4402	.00044	3.454	9.381	.9560	.029713	.4705	4.258	.1941
4403	.00092	3.350	9.207	1.1007	.029120	.4873	4.153	.2550
4404	.00151	3.291	7.490	1.2715	.023958	.7540	3.085	.3018
4405	.00546	2.360	12.037	1.3766	.004940	.1844	6.167	1.3678
4406	.00563	2.454	7.140	1.7694	.012011	.7749	2.918	1.3282
4407	.00998	1.989	5.403	2.3138	.013271	1.1518	1.949	2.2282

MEAN EPSILON= .021147

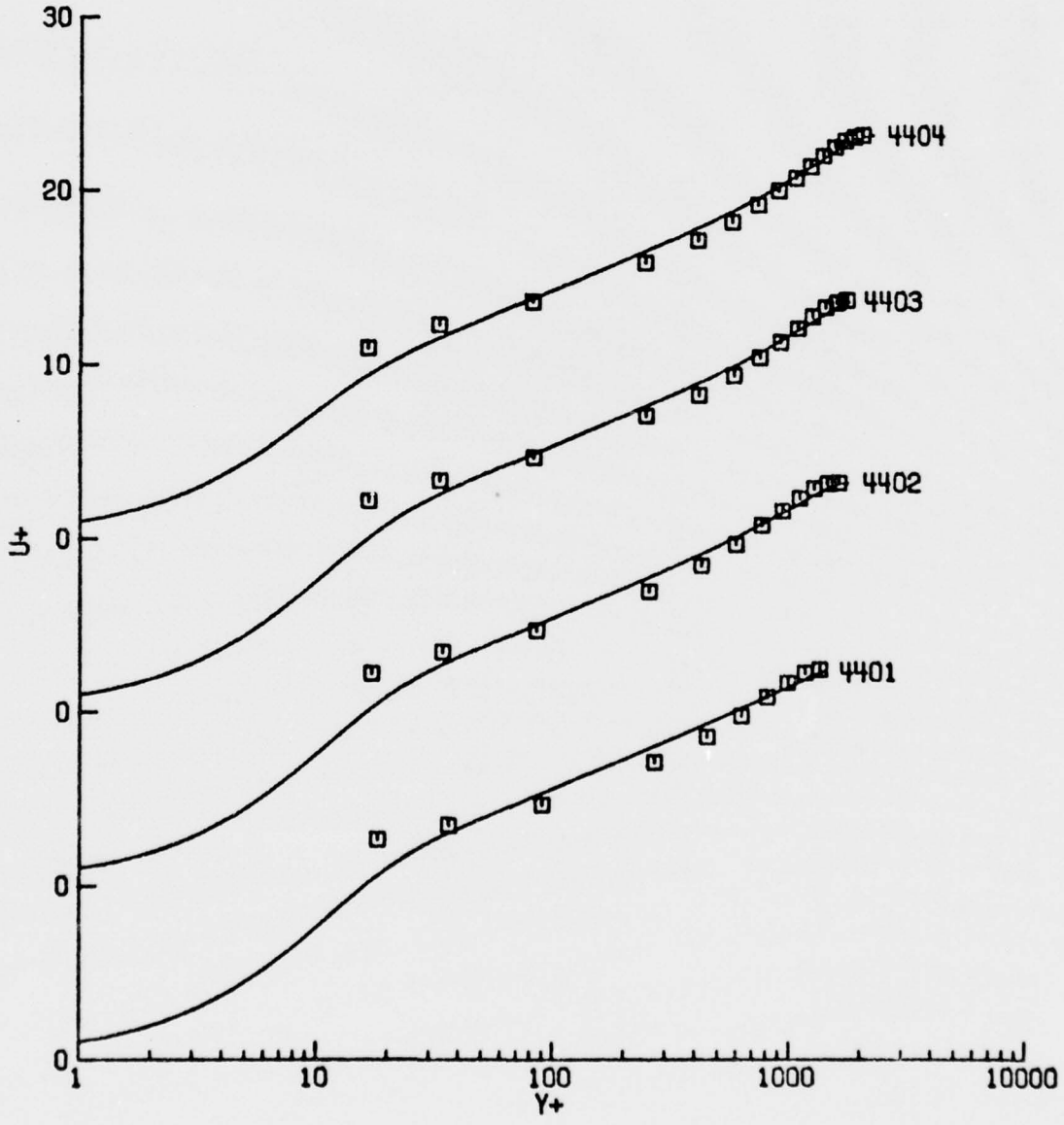

Figure B.15. Schubauer and Spangenberg A. (Note shifted origins on U^+ axis).

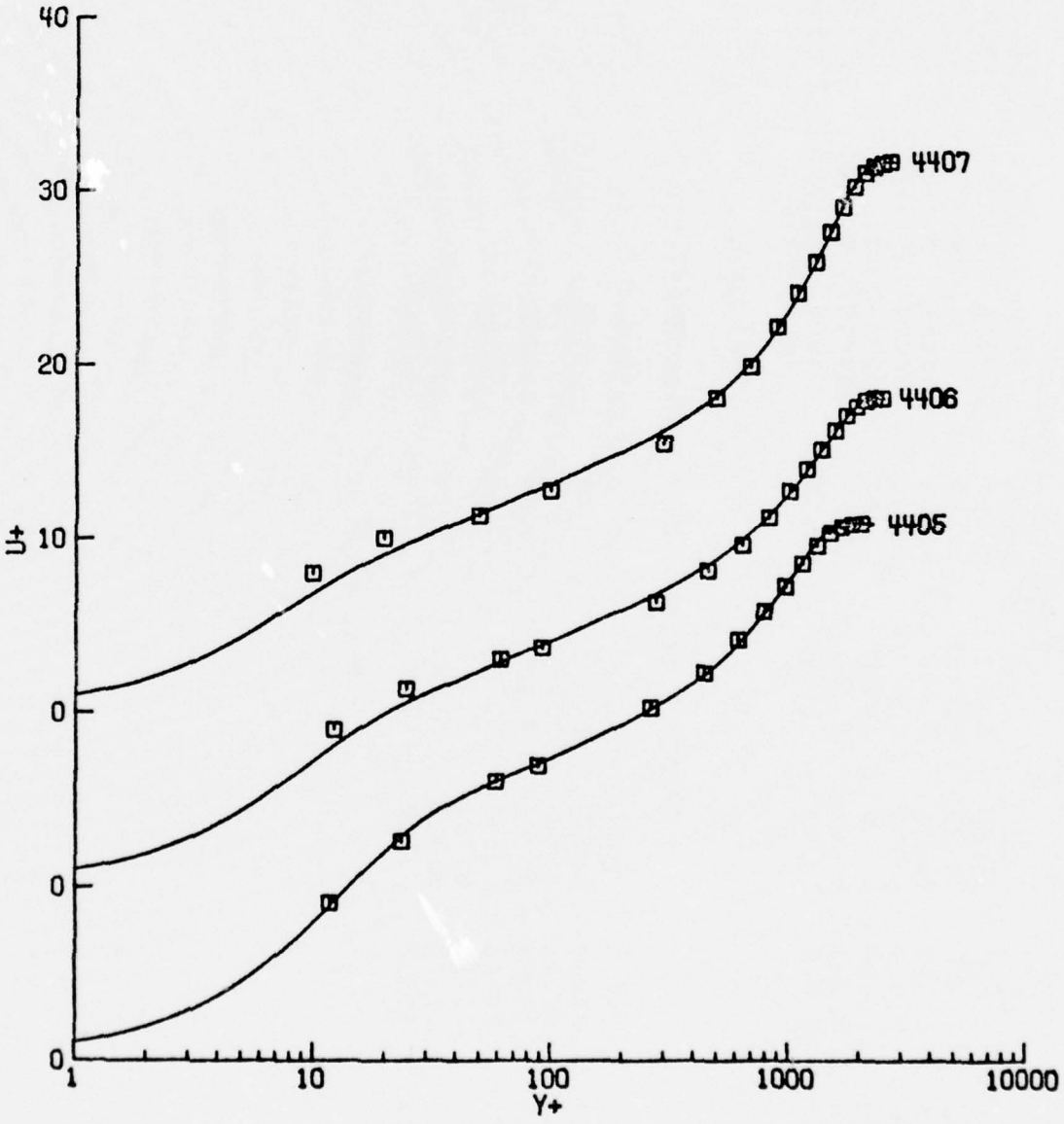

Figure B.15. (Continued).

TABLE B.16: SCHUBAUER AND SPANGENBERG - FLOW B
(ENGLISH UNITS)

NU= 1.650000E-04

EXPERIMENTAL VALUES

ID	XSTA	UE	UTAU	DUEDX	P+	DELTA	DELTA*	THETA
4501	0.000	81.81	3.227	-.40	.00016	.8724	.1363	.0982
4502	1.667	79.25	2.946	-2.40	.00123	1.2026	.1939	.1394
4503	3.333	74.31	2.630	-3.92	.00264	1.6422	.2769	.1984
4504	5.000	67.50	2.077	-4.83	.00600	2.3609	.4813	.3243
4505	6.667	61.04	1.596	-3.85	.00954	3.2554	.8054	.4919
4506	8.333	54.61	1.169	-3.58	.02019	4.4827	1.2768	.7108
4507	10.000	50.47	.727	-2.15	.04660	6.5343	2.3591	1.0604

UNSTEADY + COLES MODEL - FULL PROFILE FIT

ID	P+	UTAU	S	DELTA	EPSILON	Y1+	Ci	PI
4501	.00014	3.339	10.098	.9489	.018525	.3910	4.722	.3658
4502	.00111	3.049	9.677	1.2358	.007723	.4270	4.462	.6386
4503	.00237	2.729	9.829	1.7039	.014112	.3960	4.584	.7618
4504	.00486	2.228	8.858	2.3879	.014112	.4904	3.986	1.4445
4505	.00718	1.754	7.873	3.3143	.010505	.6189	3.387	2.4455
4506	.01133	1.417	5.556	4.5280	.016746	1.0949	2.043	3.4392
4507	.02318	.918	4.803	6.6948	.022515	1.2112	1.704	6.9063

MEAN EPSILON= .014891

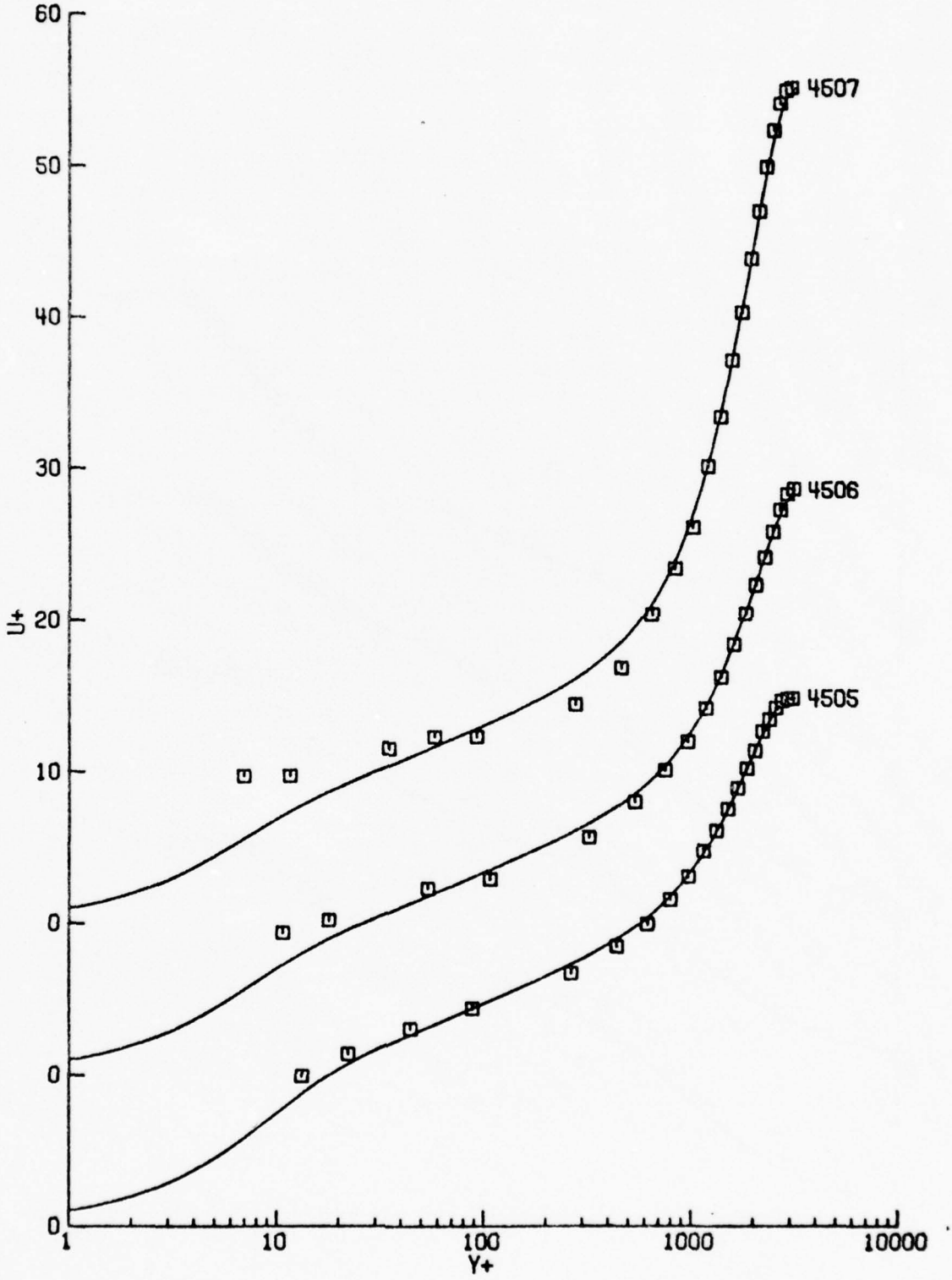

Figure B.16. Schubauer and Spangenbery B. (Note shifted origins on the U^+ axis).

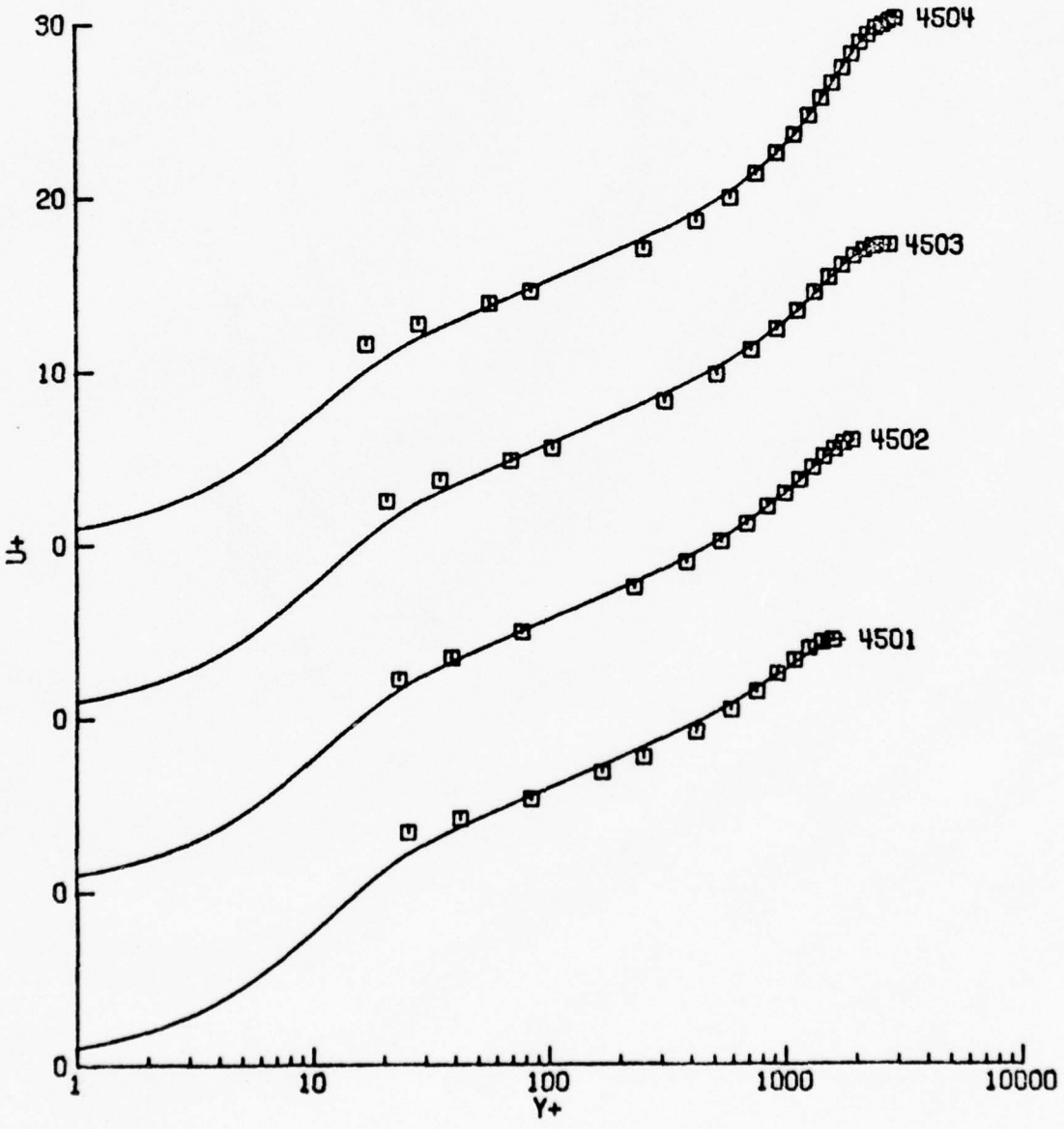

Figure B.16. (Continued).

TABLE B.17: FRASER FLOW A
(ENGLISH UNITS)

NU= 1.690000E-04

EXPERIMENTAL VALUES

ID	XSTA	UE	UTAU	DUEDX	P+	DELTA	DELTA*	THETA
5001	.383	170.00	7.098	10.50	-.00084	.4600	.0519	.0371
5002	.519	171.00	7.092	-15.00	.00122	.5000	.0547	.0395
5003	.691	161.00	6.089	-98.00	.01181	.5800	.0739	.0513
5004	.776	153.00	5.063	-85.50	.01703	.6300	.0948	.0623
5005	.984	138.00	3.730	-56.00	.02517	.7600	.1517	.0887
5006	1.251	126.00	2.598	-37.00	.04493	.9300	.2501	.1255
5007	1.438	120.00	2.096	-29.00	.06387	1.0500	.3408	.1542
5008	1.537	117.00	1.958	-26.50	.06980	1.1700	.3779	.1674
5009	1.715	113.00	1.475	-20.50	.12200	1.3800	.4970	.1931
5010	1.895	110.00	1.270	-17.00	.15428	1.7000	.6068	.2209
5011	2.107	106.00	1.001	-13.00	.23218	1.9500	.7412	.2491

UNSTEADY + COLES MODEL - FULL PROFILE FIT

ID	P+	UTAU	S	DELTA	EPSILON	Y1+	C_i	PI
5001	-.00101	6.679	12.508	.3910	.004741	.2095	6.331	.3393
5002	.00160	6.467	13.437	.4241	.005618	.1417	7.061	.3680
5003	.00825	6.864	6.988	.4447	.008659	.7775	2.851	.5657
5004	.01014	6.018	6.114	.4807	.014592	.9592	2.351	1.0985
5005	.02821	3.591	11.277	.5908	.016573	.1058	6.125	3.1465
5006	.03019	2.966	6.765	.8361	.008641	.6191	2.917	4.5559
5007	.04739	2.315	6.913	1.0515	.007068	.4662	3.168	6.4303
5008	.05170	2.164	6.842	1.1529	.006722	.4534	3.158	6.8780
5009	.09192	1.621	5.997	1.4061	.004560	.4251	2.873	10.1897
5010	.15125	1.278	6.914	1.6594	.017688	.1173	4.050	13.3322
5011	.20104	1.050	6.010	2.0234	.008757	.1408	3.590	16.4776

MEAN EPSILON= .009420

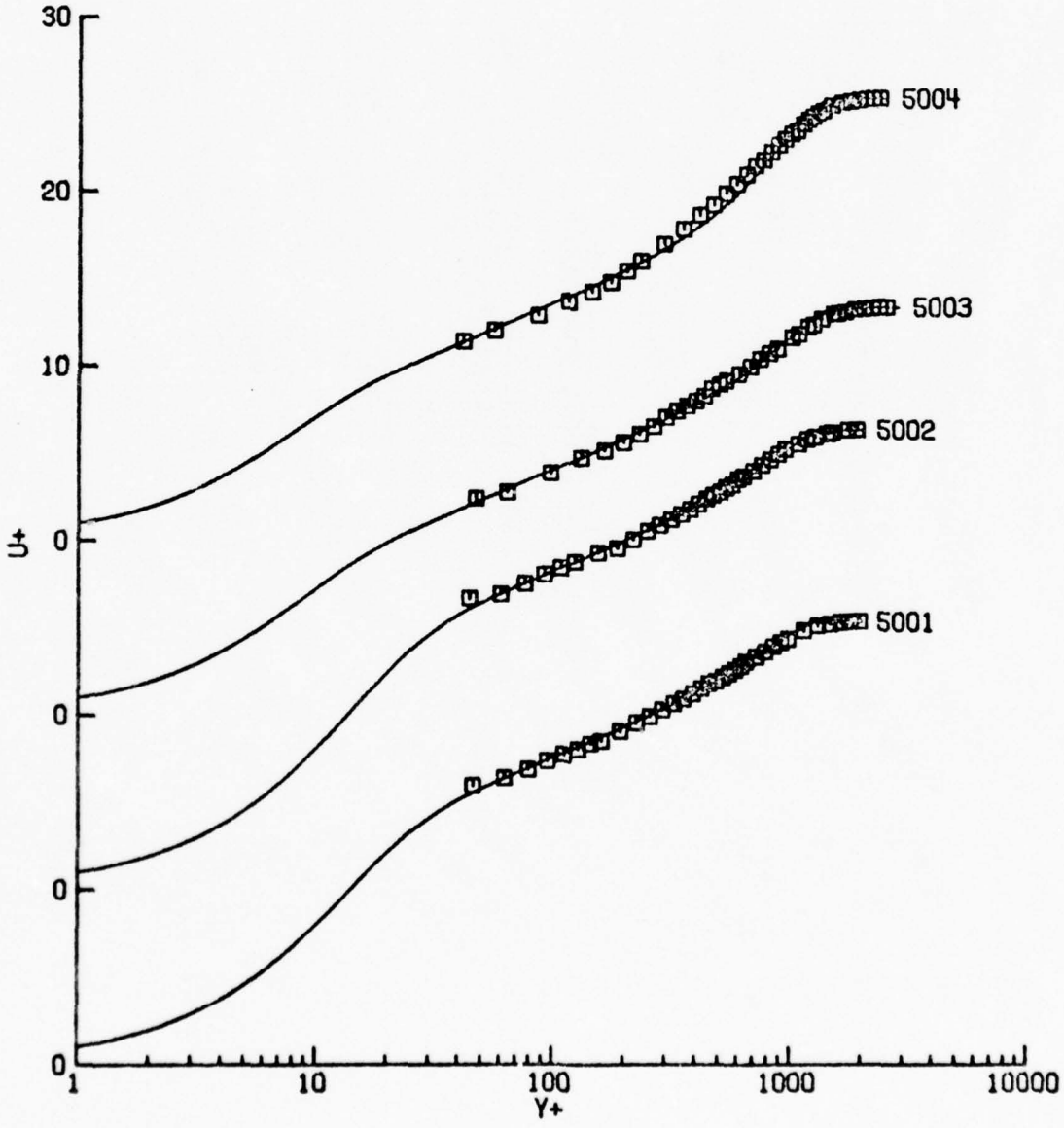

Figure B.17. Fraser Flow A. (Note shifted origins on the U^+ axis).

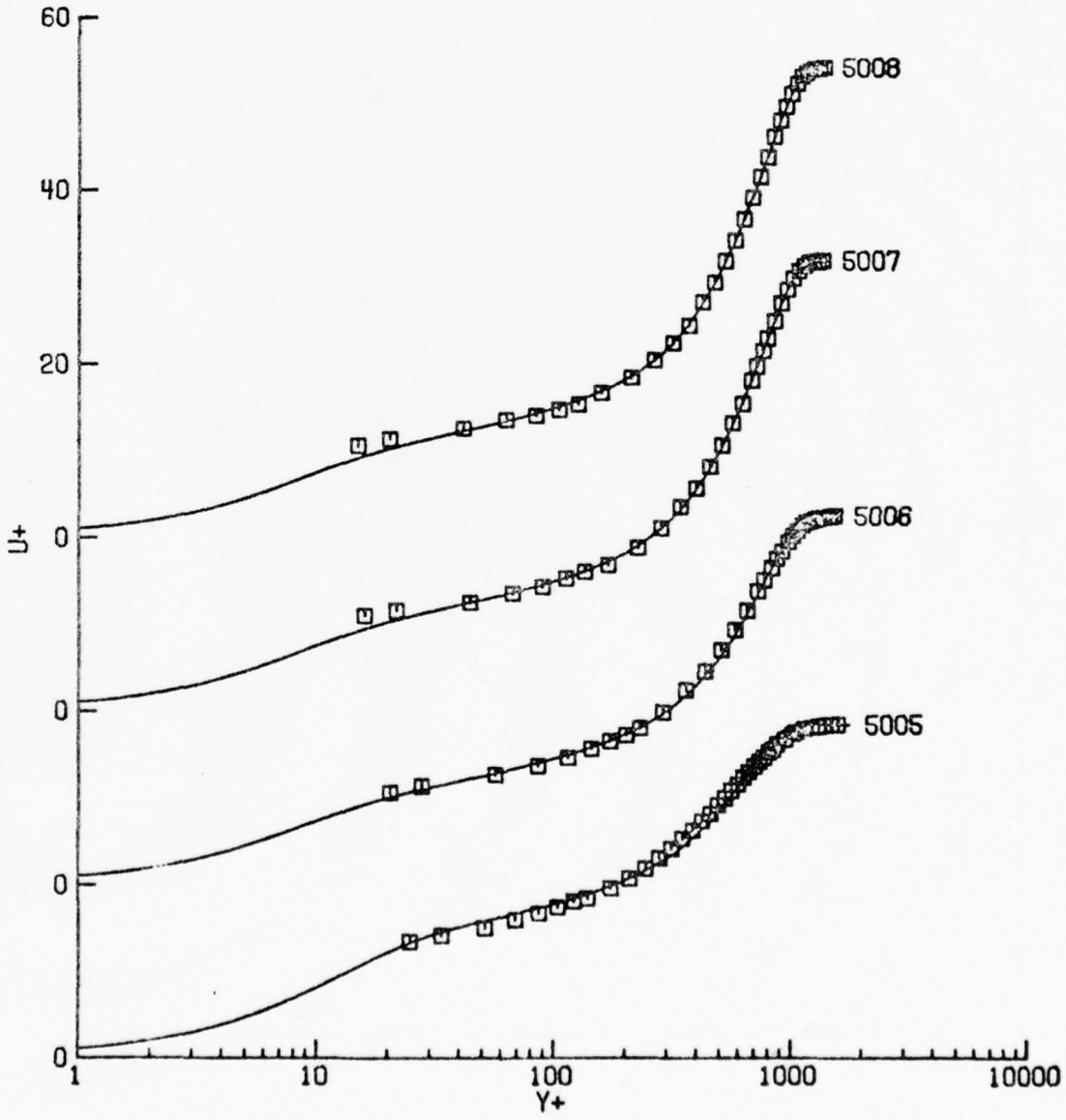

Figure B.17. (Continued).

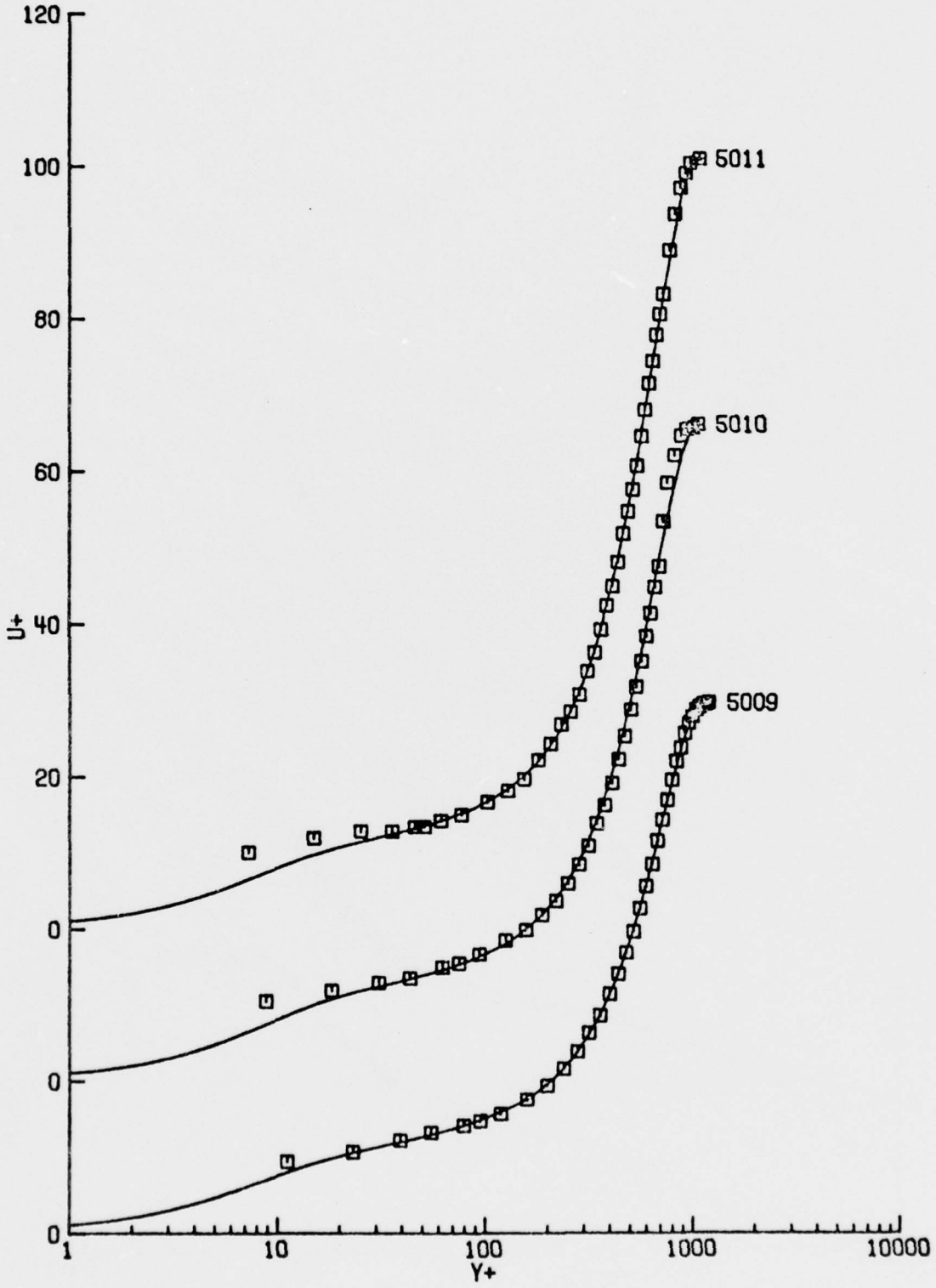

Figure B.17. (Continued).

TABLE B.18: FRASER - FLOW B
(ENGLISH UNITS)

NU= 1.690000E-04

EXPERIMENTAL VALUES

ID	XSTA	UE	UTAU	DUEDX	P+	DELTA	DELTA*	THETA
5101	.383	188.00	7.983	11.50	-.00072	.3400	.0408	.0285
5102	.519	189.00	8.094	-6.00	.00036	.3850	.0425	.0300
5103	.669	179.00	7.089	-124.50	.01057	.4450	.0555	.0385
5104	.776	167.00	5.719	-108.00	.01630	.5100	.0792	.0523
5105	.984	151.00	4.290	-67.50	.02182	.6500	.1265	.0753
5106	1.251	138.00	3.191	-45.00	.03230	.8800	.2111	.1119
5107	1.438	128.00	2.505	-35.50	.04885	.9900	.2947	.1424
5108	1.715	121.00	1.854	-26.50	.08503	1.4000	.4561	.1891
5109	1.903	117.00	1.472	-21.50	.13329	1.7500	.5737	.2196
5110	2.244	111.00	1.005	-16.00	.29569	2.2500	.7993	.2693
5111	2.438	108.00	.695	-13.50	.73399	2.6500	.9664	.2938
5112	2.573	105.00	.467	-12.50	2.17789	2.9500	1.0764	.3018

UNSTEADY + COLES MODEL - FULL PROFILE FIT

ID	P+	UTAU	S	DELTA	EPSILON	Y1+	C	PI
5101	-.00092	7.354	13.064	.3004	.006291	.1784	6.722	.3662
5102	.00045	7.530	12.714	.3261	.005230	.1853	6.514	.2603
5103	.00862	7.589	8.433	.3602	.008689	.5126	3.762	.4609
5104	.00847	7.114	4.467	.3811	.012184	1.4499	1.448	.9166
5105	.01490	4.872	6.980	.5141	.014254	.7100	2.911	2.1980
5106	.02902	3.307	8.777	.7366	.009324	.2987	4.268	4.1341
5107	.04034	2.670	7.999	.9505	.008634	.3296	3.856	5.4710
5108	.08284	1.870	7.078	1.3273	.007397	.2649	3.604	8.9694
5109	.11131	1.563	6.255	1.6128	.008244	.3000	3.198	11.1259
5110	.19288	1.159	4.326	2.1762	.006201	.5295	2.185	15.6258
5111	.39229	.856	2.634	2.5548	.007292	.8244	1.550	22.0427
5112	2.06425	.475	3.936	2.7848	.010061	.0002	6.930	40.6148

MEAN EPSILON= .008650

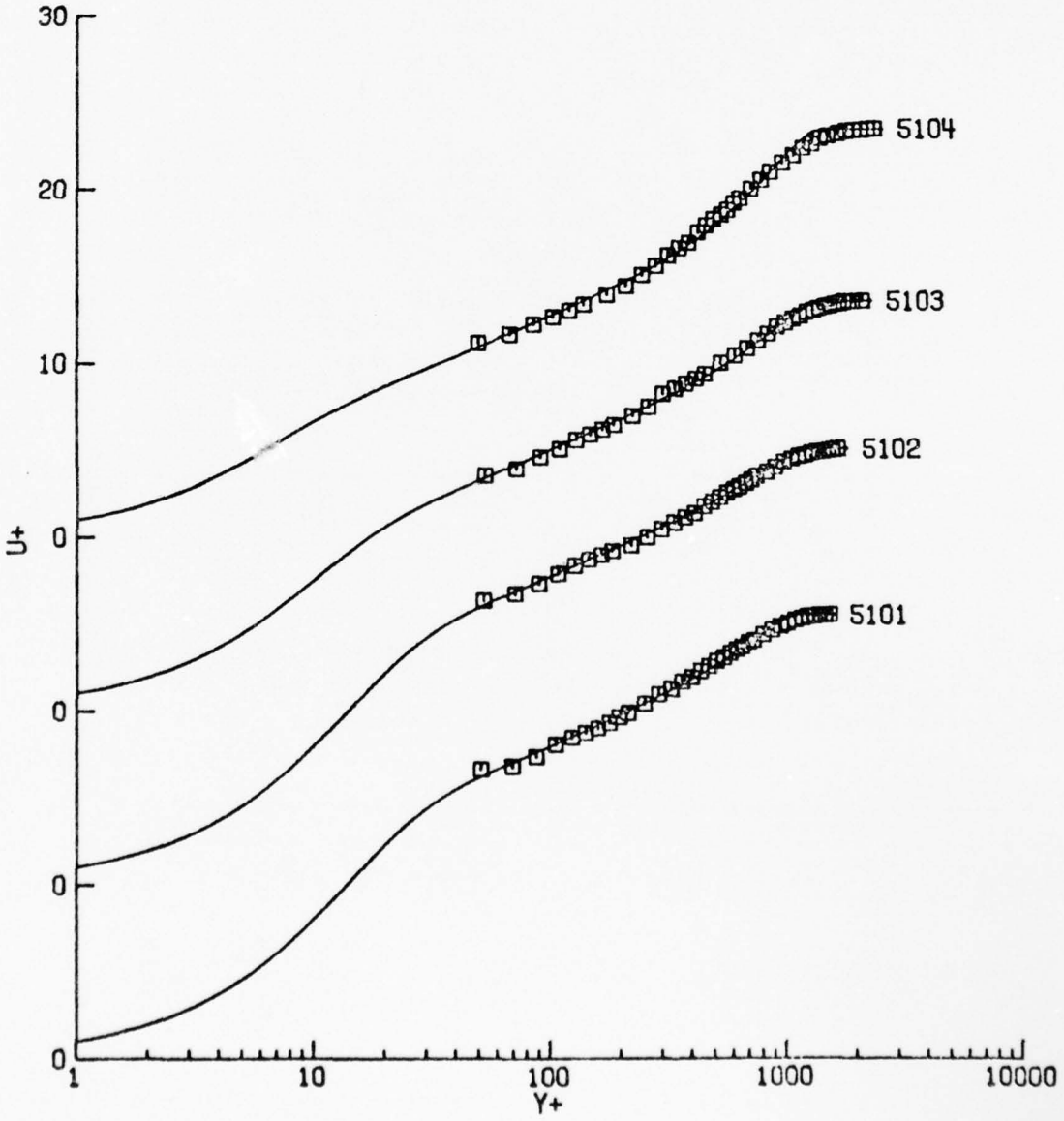

Figure B.18. Fraser Flow B. (Note shifted origins on the U^+ axis).

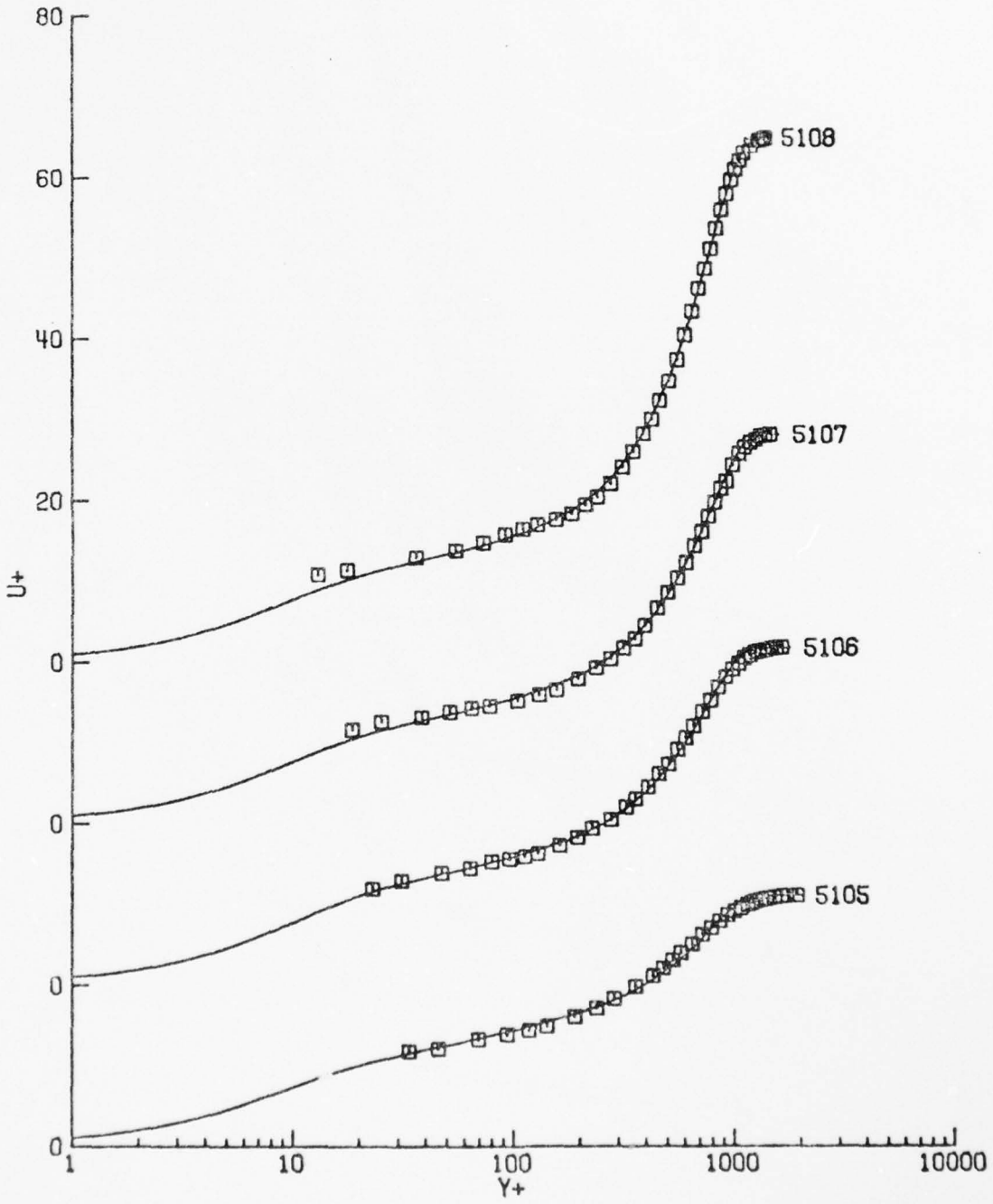

Figure B.18. (Continued).

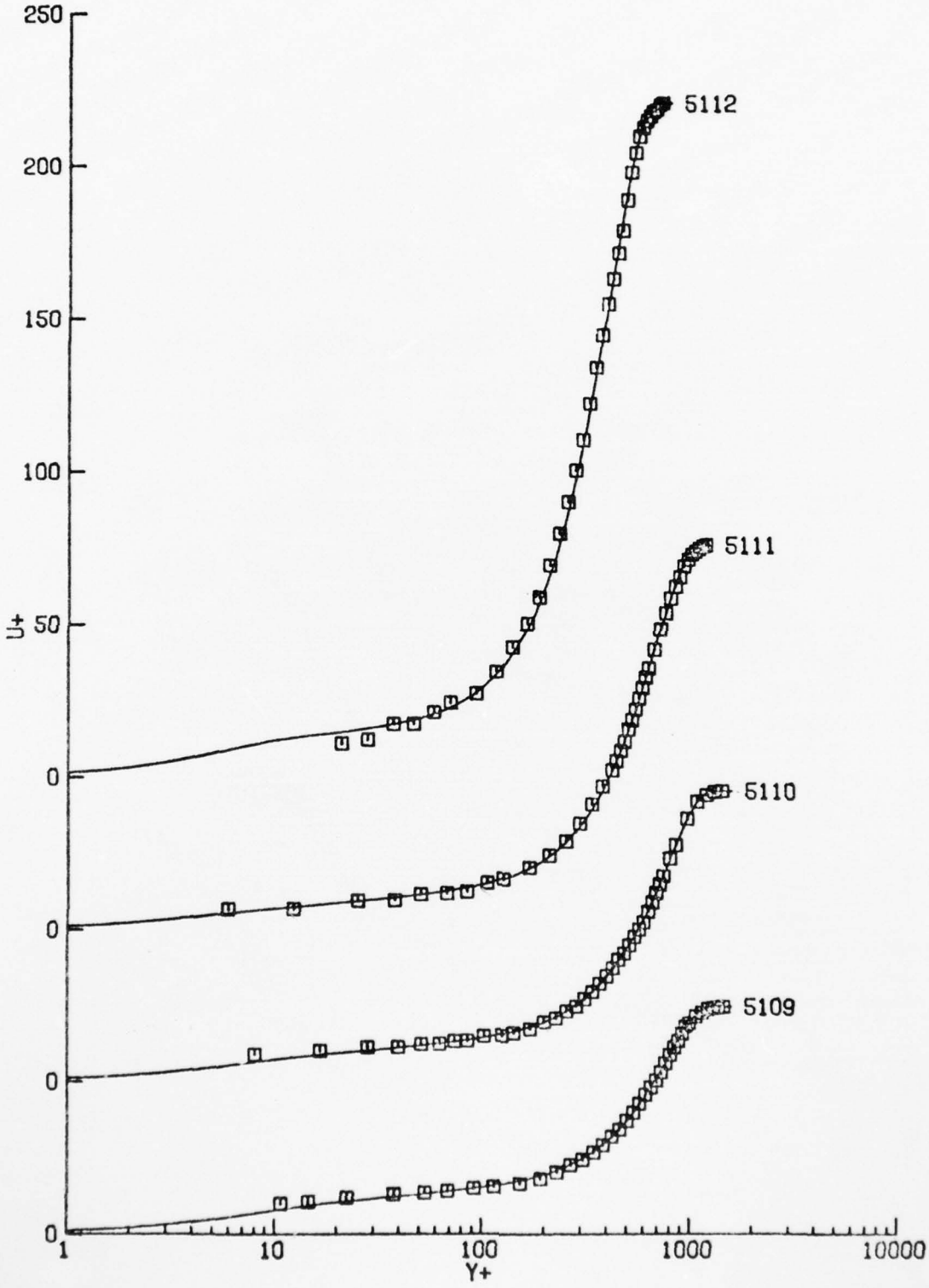

Figure B.18. (Continued).

TABLE B.19: STRATFORD - EXPERIMENT 5
(ENGLISH UNITS)

NU= 1.570000E-04

EXPERIMENTAL VALUES

ID	XSTA	UE	UTAU	DUEDX	P+	DELTA	DELTA*	THETA
5201	2.907	55.00	2.355	-40.00	.02645	.7337	.1092	.0797
5202	2.999	52.06	1.741	-44.00	.06815	.8110	.1492	.0973
5203	3.038	49.83	1.329	-35.00	.11665	.9071	.1974	.1182
5204	3.531	44.07	1.076	-4.60	.02555	1.2325	.3662	.1933
5205	4.103	42.03	1.130	-3.90	.01784	1.4939	.4311	.2402
5206	5.322	37.06	.966	-3.80	.02453	2.1938	.6170	.3484
5207	6.236	34.08	.837	-3.80	.03467	2.9811	.8842	.4852

UNSTEADY + COLES MODEL - FULL PROFILE FIT

ID	P+	UTAU	S	DELTA	EPSILON	Y1+	C_i	PI
5201	.02856	2.295	10.347	.7492	.003513	.1577	5.416	.3932
5202	.18655	1.245	15.647	.7462	.015948	0.0000	16.223	2.1490
5203	.25889	1.019	13.927	.7758	.034897	0.0000	15.740	3.7797
5204	.01478	1.291	5.366	1.1892	.011861	1.1149	1.961	3.2427
5205	.01282	1.261	6.725	1.5476	.012528	.7862	2.736	2.7981
5206	.01591	1.116	6.040	2.2544	.015527	.9195	2.353	2.7278
5207	.02278	.963	5.899	3.0947	.021848	.8917	2.322	3.0967

MEAN EPSILON= .016589

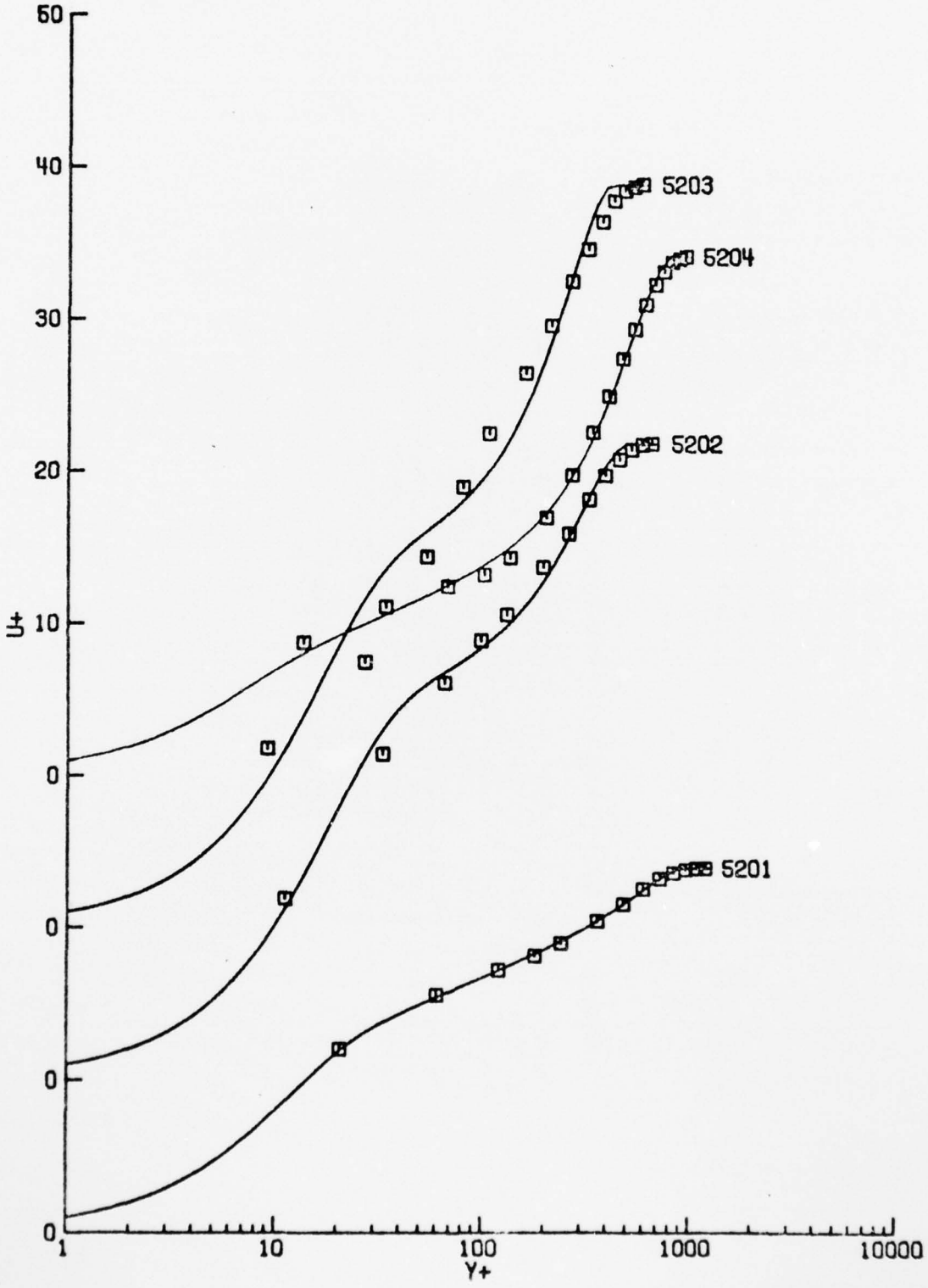

Figure B.19. Stratford 5. (Note shifted origins on the U^+ axis).

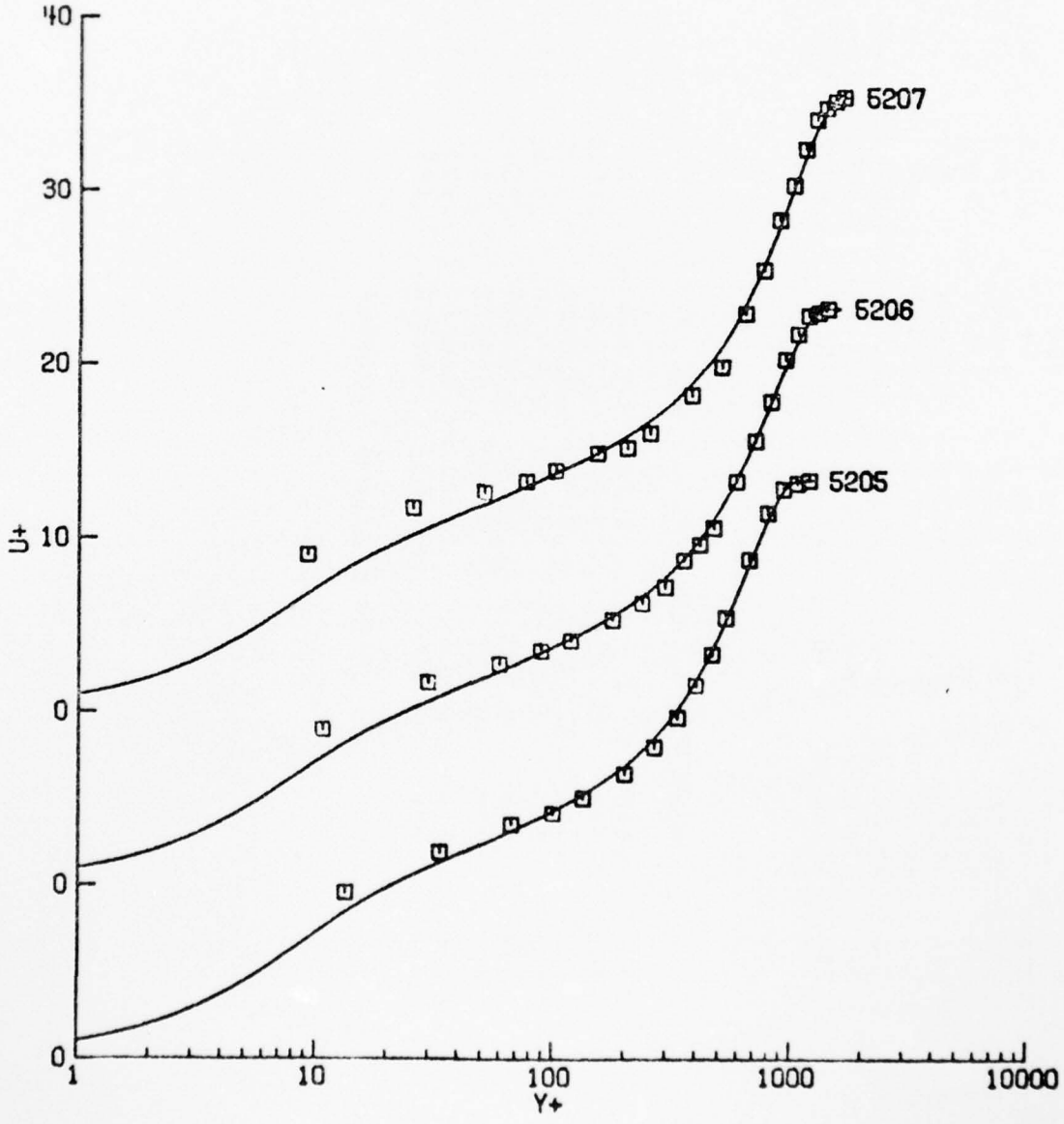

Figure B.19. (Continued).

TABLE B.20: STRATFORD - EXPERIMENT 6
(ENGLISH UNITS)

NU= 1.570000E-04

EXPERIMENTAL VALUES

ID	XSTA	UE	UTAU	DUEDX	P+	DELTA	DELTA*	THETA
5301	2.907	55.00	2.361	-68.00	.04462	.7304	.1070	.0786
5302	2.999	51.54	1.657	-102.00	.18142	.8509	.1572	.1015
5303	3.038	49.19	1.096	-86.00	.50448	.9071	.2181	.1212
5304	3.531	42.64	.709	-7.70	.14463	1.3224	.4952	.2123
5305	4.103	39.32	.642	-5.50	.12831	1.9065	.7162	.3061
5306	5.322	33.72	.431	-3.20	.21159	3.5223	1.4183	.5514
5307	6.236	31.02	.386	-2.40	.20323	4.6957	1.8999	.7404

UNSTEADY + COLES MODEL - FULL PROFILE FIT

ID	P+	UTAU	S	DELTA	EPSILON	Y1+	Ci	PI
5301	.04263	2.397	9.103	.7581	.007561	.1919	4.966	.3047
5302	.77580	1.021	11.029	.7493	.025459	0.0000	21.099	3.0213
5303	3.35032	.583	6.841	.7328	.047697	0.0000	28.957	8.6461
5304	.08764	.838	4.303	1.2977	.011383	.9541	1.742	6.8967
5305	.08827	.727	5.401	1.9163	.007201	.5902	2.438	7.2806
5306	.17336	.461	5.820	3.5811	.016217	.2149	3.253	10.9533
5307	.29278	.342	7.816	4.7160	.016910	.0052	6.344	13.9298

MEAN EPSILON= .018918

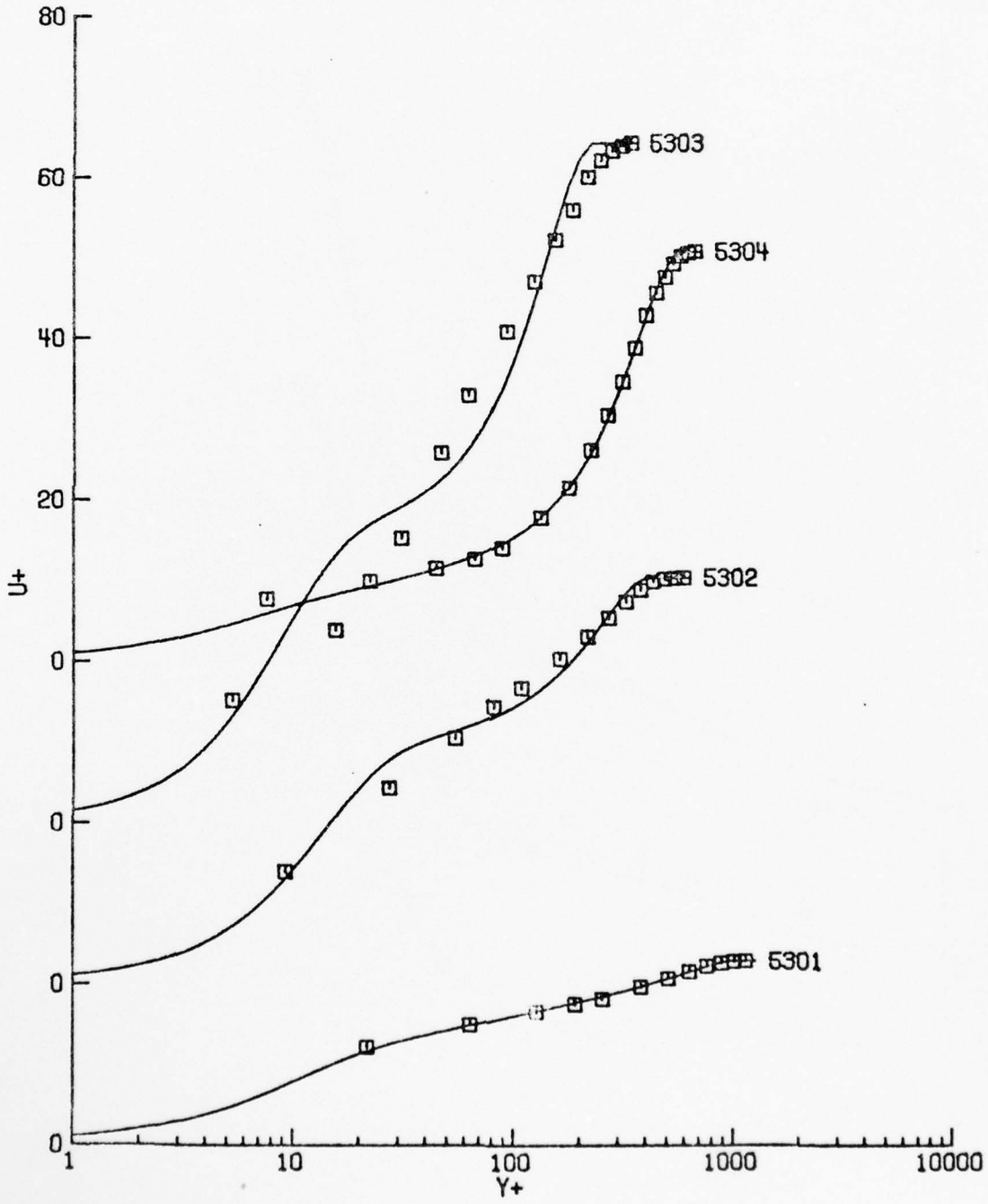

Figure B.20. Stratford 6. (Note shifted origins on the U^+ axis).

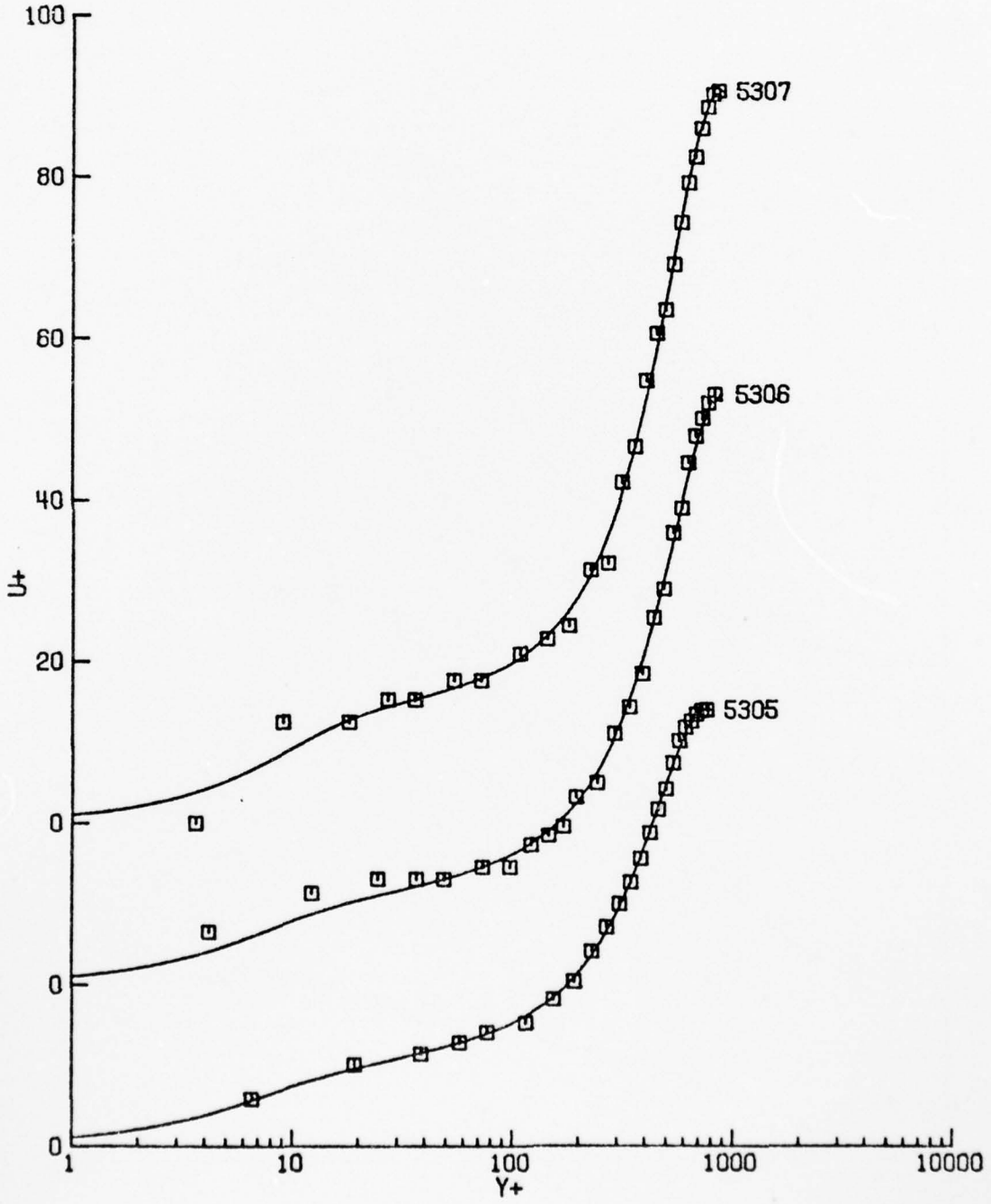

Figure B.20. (Continued).

TABLE B.21: SAMUEL AND JOUBERT
(METRIC UNITS)

NU= 1.550000E-05

EXPERIMENTAL VALUES

ID	XSTA	UE	UTAU	DUEDX	P+	DELTA	DELTA*	THETA
7001	.855	26.49	.984	-.82	.00035	2.4470	.3950	.2840
7002	1.160	26.25	.965	-1.07	.00048	2.9280	.4730	.3400
7003	1.440	25.84	.932	-1.37	.00068	3.1330	.5390	.3880
7004	1.760	25.40	.907	-1.74	.00092	3.6500	.6040	.4350
7005	2.100	24.82	.860	-2.13	.00129	4.3910	.7440	.5310
7006	2.260	24.45	.842	-2.40	.00153	4.6400	.8110	.5750
7007	2.400	24.03	.808	-2.83	.00200	4.9320	.8750	.6120
7008	2.560	23.50	.761	-3.55	.00293	5.3340	1.0200	.7080
7009	2.720	22.90	.724	-4.47	.00418	5.8140	1.1900	.8150
7010	2.870	22.33	.685	-4.68	.00505	6.3650	1.3000	.8780
7011	3.040	21.39	.624	-4.67	.00659	6.9950	1.5100	1.0000
7012	3.400	19.51	.488	-4.02	.01048	8.8240	2.3400	1.4530

UNSTEADY + COLES MODEL - FULL PROFILE FIT

ID	P+	UTAU	S	DELTA	EPSILON	Y1+	C_i	PI
7001	.00041	.937	12.616	2.3860	.005017	.1910	6.444	.8346
7002	.00053	.933	12.207	2.9800	.004412	.2138	6.162	.7572
7003	.00068	.929	11.264	3.4202	.005621	.2782	5.516	.7552
7004	.00102	.875	12.201	3.8990	.004454	.2099	6.171	.8351
7005	.00131	.854	11.508	4.6945	.006883	.2537	5.697	.8629
7006	.00141	.865	10.270	5.1029	.008471	.3596	4.860	.8212
7007	.00195	.815	11.099	5.2953	.006632	.2792	5.431	.9618
7008	.00276	.776	10.620	5.7315	.006814	.3123	5.122	1.1763
7009	.00364	.758	9.834	6.2276	.008595	.3821	4.609	1.2374
7010	.00486	.693	10.672	6.6561	.007352	.2880	5.198	1.5367
7011	.00557	.653	9.838	7.4460	.010704	.3624	4.645	1.7386
7012	.00828	.528	9.094	9.6353	.010786	.4236	4.192	2.6751

MEAN EPSILON= .007145

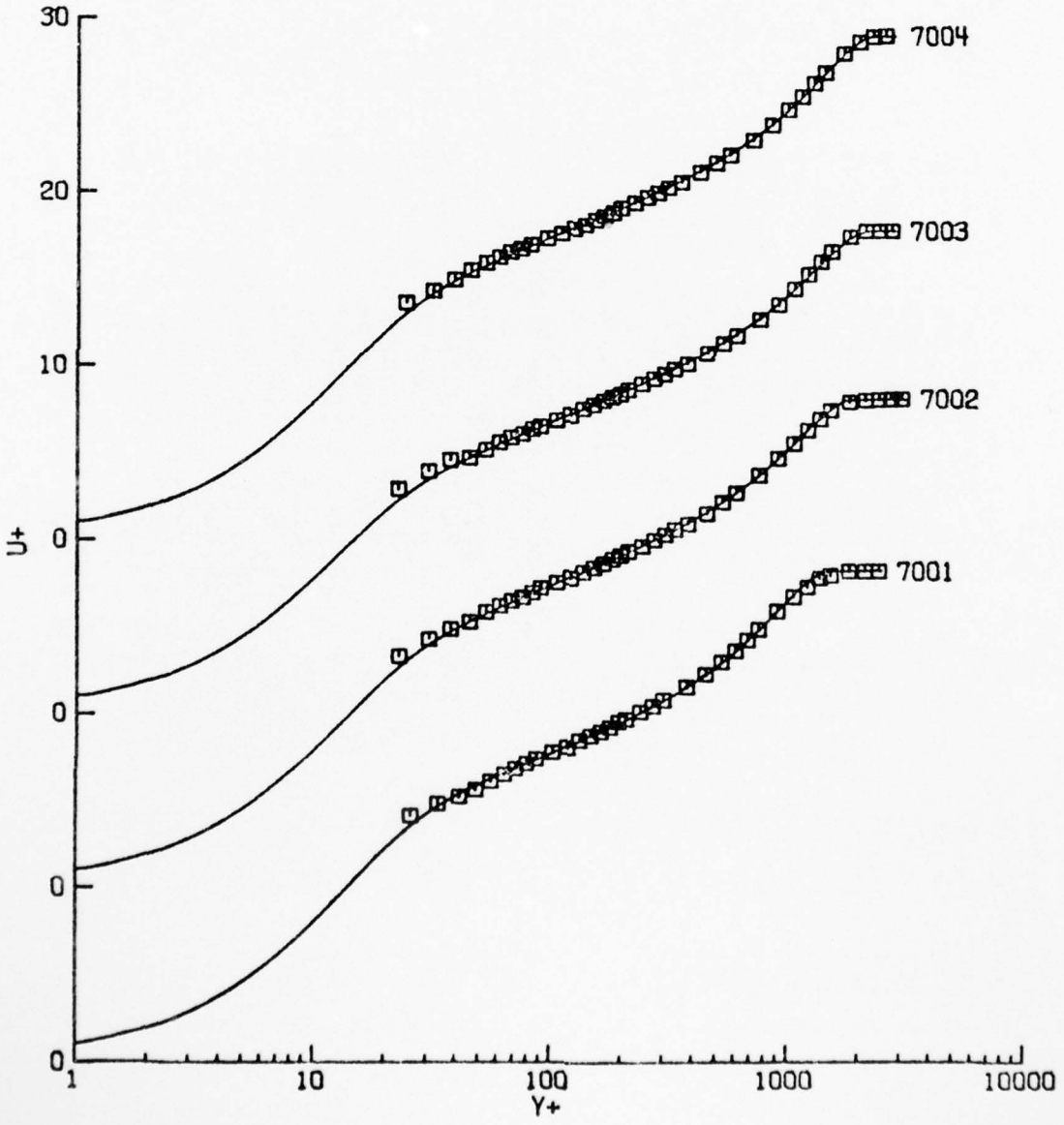

Figure B.21. Samuel and Joubert (1974) adverse pressure gradient flow. (Note shifted origins on the U^+ axis).

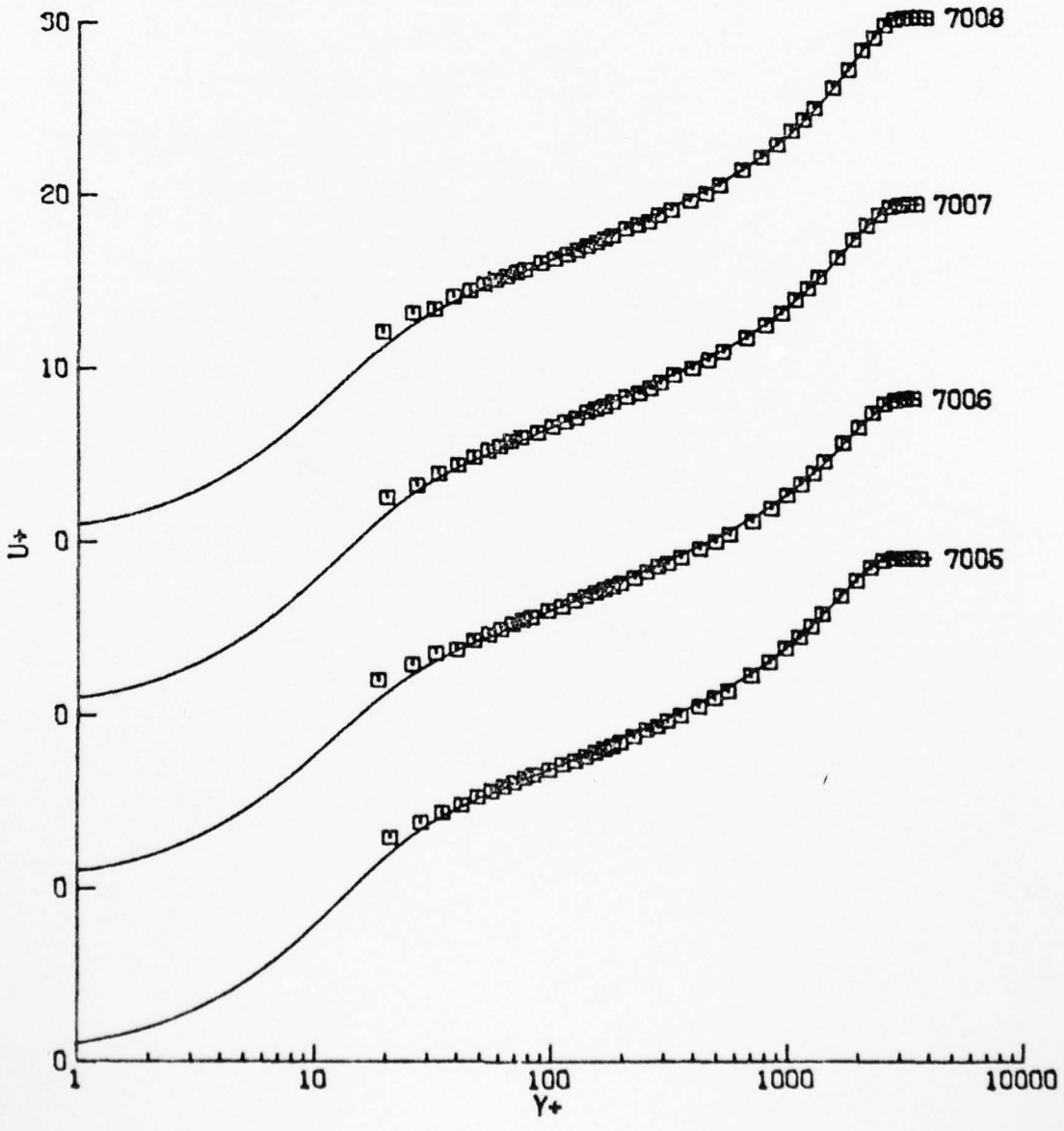

Figure B.21. (Continued).

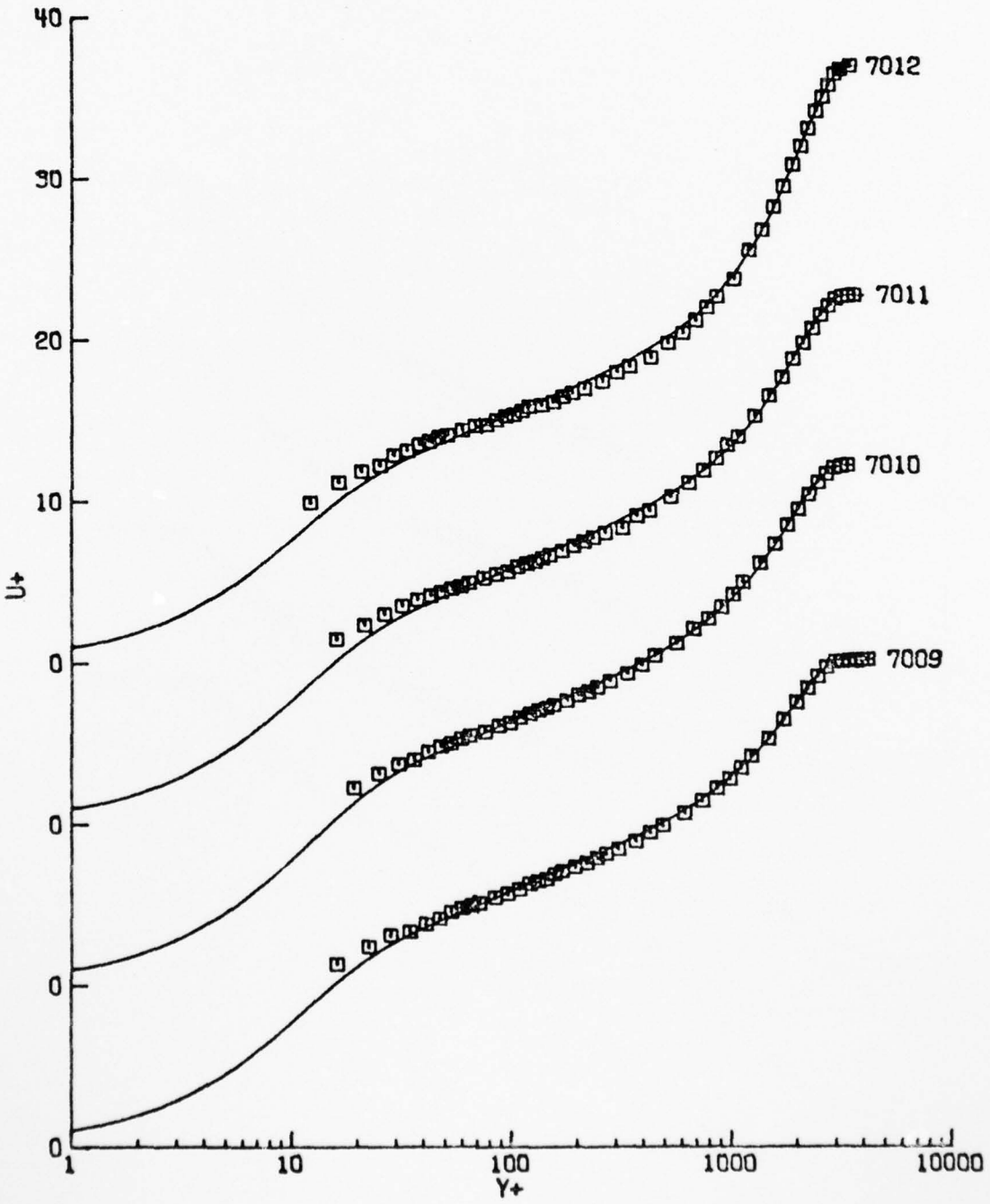

Figure B.21. (Continued).

TABLE B.22: ANDERSEN, KAYS AND MOFFAT - ZERO P. G. - 120771-1
(ENGLISH UNITS)

NU= 1.590000E-04

EXPERIMENTAL VALUES

ID	XSTA	UE	UTAU	DUEDX	P+	DELTA	DELTA*	THETA
8101	.167	31.21	1.557	.01	-.00001	.2871	.0504	.0328
8102	.833	31.13	1.467	.01	-.00001	.4225	.0772	.0521
8103	1.833	31.14	1.400	.01	-.00001	.6242	.1135	.0768
8104	2.833	31.05	1.353	.00	-.00001	.7854	.1412	.0977
8105	3.833	31.04	1.321	.00	-.00000	.9590	.1709	.1185
8106	4.833	31.13	1.298	-.00	.00000	1.1065	.1968	.1375
8107	5.833	31.04	1.272	-.01	.00001	1.2755	.2255	.1584
8108	6.833	31.07	1.254	-.01	.00002	1.4608	.2533	.1794
8109	7.500	31.06	1.246	-.01	.00003	1.5810	.2670	.1902

UNSTEADY + COLES MODEL - FULL PROFILE FIT

ID	P+	UTAU	S	DELTA	EPSILON	Y1+	C_i	PI
8101	-.00001	1.643	9.673	.2991	.005063	.4402	4.441	.2082
8102	-.00001	1.646	7.407	.4604	.004201	.7886	3.019	.2660
8103	-.00001	1.353	11.203	.6740	.008399	.2899	5.460	.5133
8104	-.00001	1.330	10.917	.8687	.005418	.3138	5.266	.5033
8105	-0.00000	1.292	10.861	1.0388	.004217	.3186	5.229	.5738
8106	.00001	1.236	11.927	1.2282	.011198	.2365	5.955	.6011
8107	.00001	1.274	10.274	1.3846	.007307	.3741	4.837	.5882
8108	.00003	1.211	11.546	1.5797	.006156	.2631	5.694	.6386
8109	.00003	1.236	10.722	1.6544	.005259	.3308	5.136	.6103

MEAN EPSILON= .006358

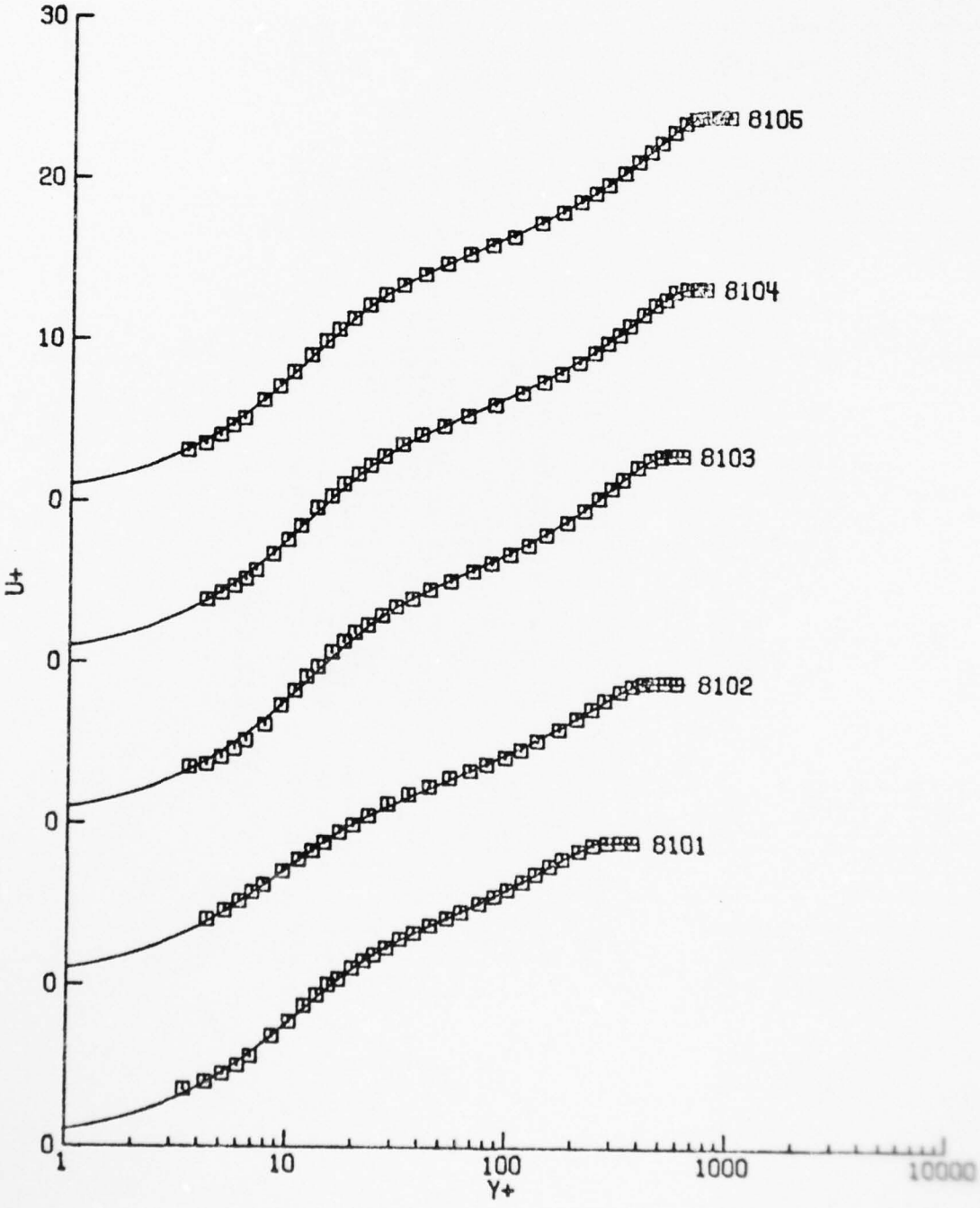

Figure B.22. Constant pressure flow of Andersen et al. (1972). (Note shifted origins on the U^+ axis).

AD-A042 672 PURDUE UNIV LAFAYETTE IND COMPUTATIONAL FLUID MECHAN--ETC F/G 20/4
COMPARISONS OF THEORETICAL PROFILES FOR A TWO-DIMENSIONAL TIME---ETC(U)
JUN 77 R K SCHARNHORST, J D WALKER AF-AFOSR-2707-74

UNCLASSIFIED CFMTR-77-1 AFOSR-TR-77-0877 NL

3 OF 3
ADA042-672

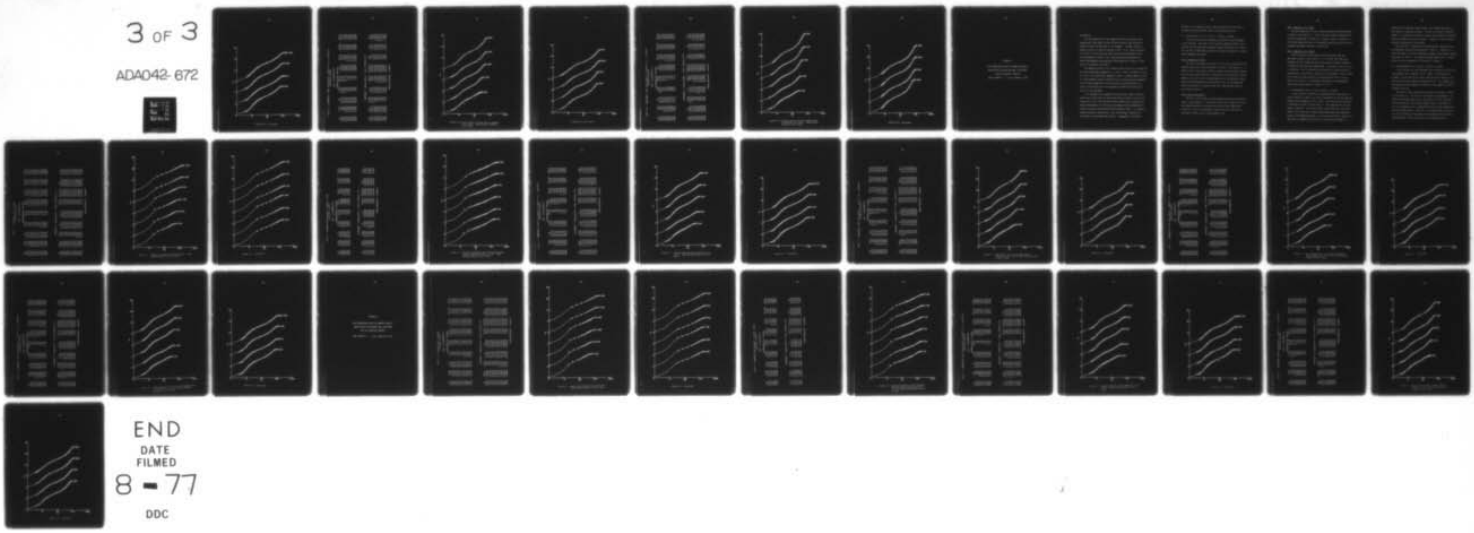

END
DATE FILMED
8 - 77
DDC

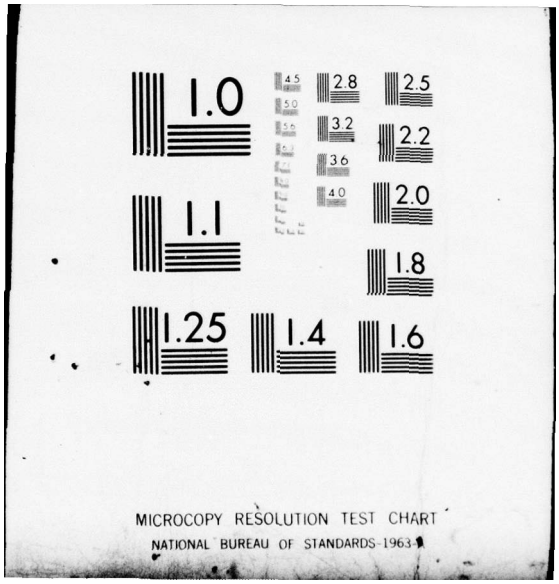
1.0
1.1
1.25
1.4
1.6
1.8
2.0
2.2
2.5
2.8
3.2
3.6
4.0
4.5
5.0
5.6
MICROCOPY RESOLUTION TEST CHART
NATIONAL BUREAU OF STANDARDS-1963-A

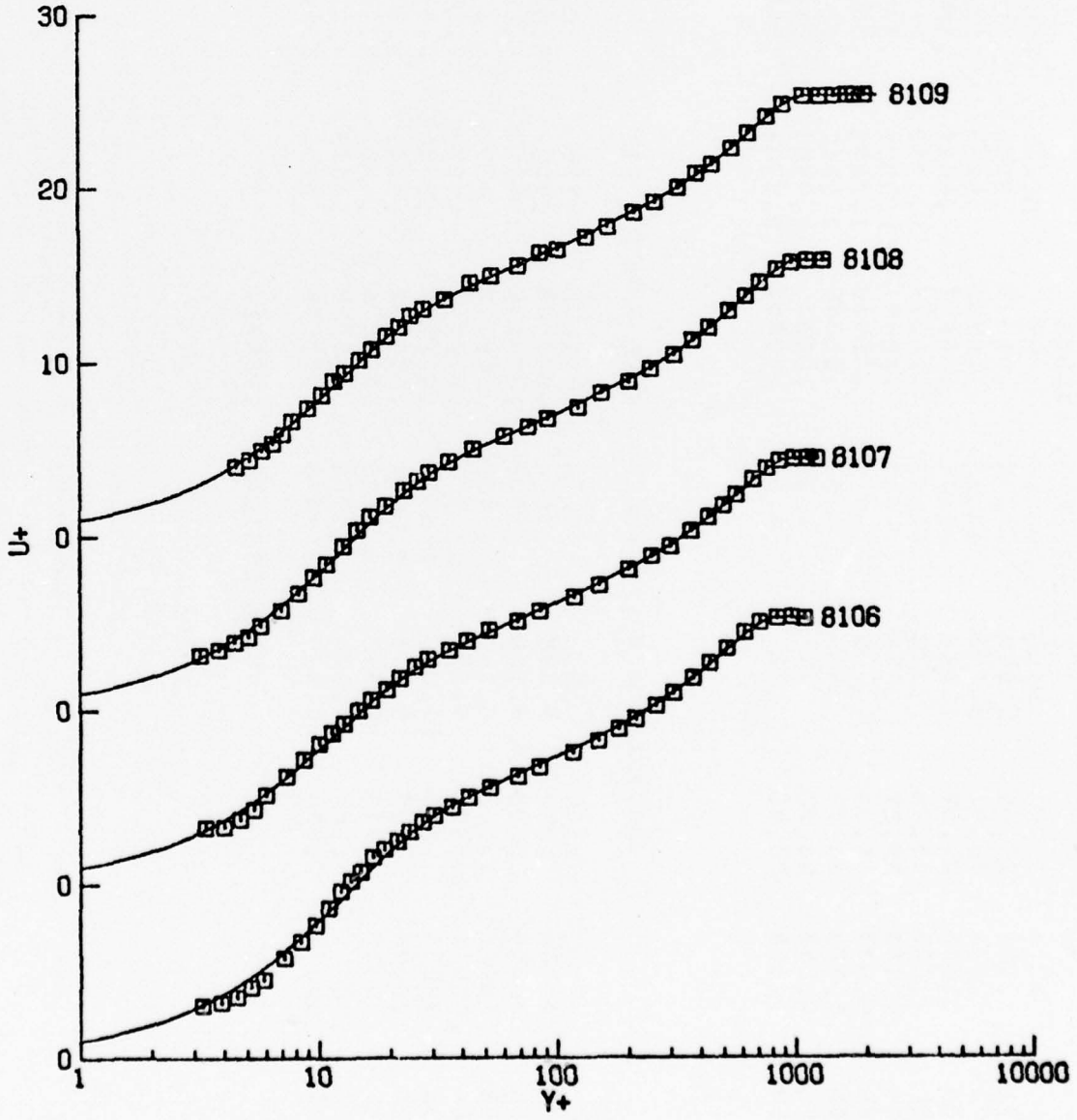

Figure B.22. (Continued).

TABLE B.23: ANDERSEN, KAYS AND MOFFAT - MILD P. G. - 071571-5
(ENGLISH UNITS)

NU= 1.660000E-04

EXPERIMENTAL VALUES

ID	XSTA	UE	UTAU	DUEDX	P+	DELTA	DELTA*	THETA
8201	.167	29.69	1.546	-2.44	.00325	.3081	.0556	.0357
8202	.833	26.93	1.198	-3.79	.00985	.5179	.1138	.0718
8203	1.833	24.57	1.010	-1.76	.00697	.8628	.1936	.1238
8204	2.833	23.26	.910	-1.13	.00579	1.1752	.2616	.1700
8205	3.833	22.27	.848	-.82	.00497	1.5029	.3356	.2176
8206	4.833	21.36	.799	-.63	.00438	1.7870	.3934	.2592
8207	5.833	20.74	.765	-.51	.00392	2.1211	.4610	.3049
8208	6.833	20.35	.742	-.43	.00356	2.4043	.5108	.3419
8209	7.500	20.05	.726	-.41	.00357	2.5701	.5449	.3656

UNSTEADY + COLES MODEL - FULL PROFILE FIT

ID	P+	UTAU	S	DELTA	EPSILON	Y1+	C_i	PI
8201	.00324	1.548	9.397	.3080	.005823	.4372	4.314	.3077
8202	.00959	1.209	8.908	.5509	.004094	.4353	4.087	.8225
8203	.00661	1.028	8.949	.9482	.005710	.4595	4.071	.9679
8204	.00536	.933	9.296	1.2985	.005968	.4274	4.280	1.0253
8205	.00565	.813	11.069	1.6524	.007587	.2485	5.489	1.2358
8206	.00400	.823	9.503	1.9998	.006392	.4164	4.395	1.0576
8207	.00359	.788	9.343	2.3335	.004996	.4403	4.283	1.1026
8208	.00304	.782	9.054	2.6758	.005905	.4836	4.087	1.0172
8209	.00294	.774	8.829	2.8678	.005874	.5156	3.940	.9958

MEAN EPSILON= .005817

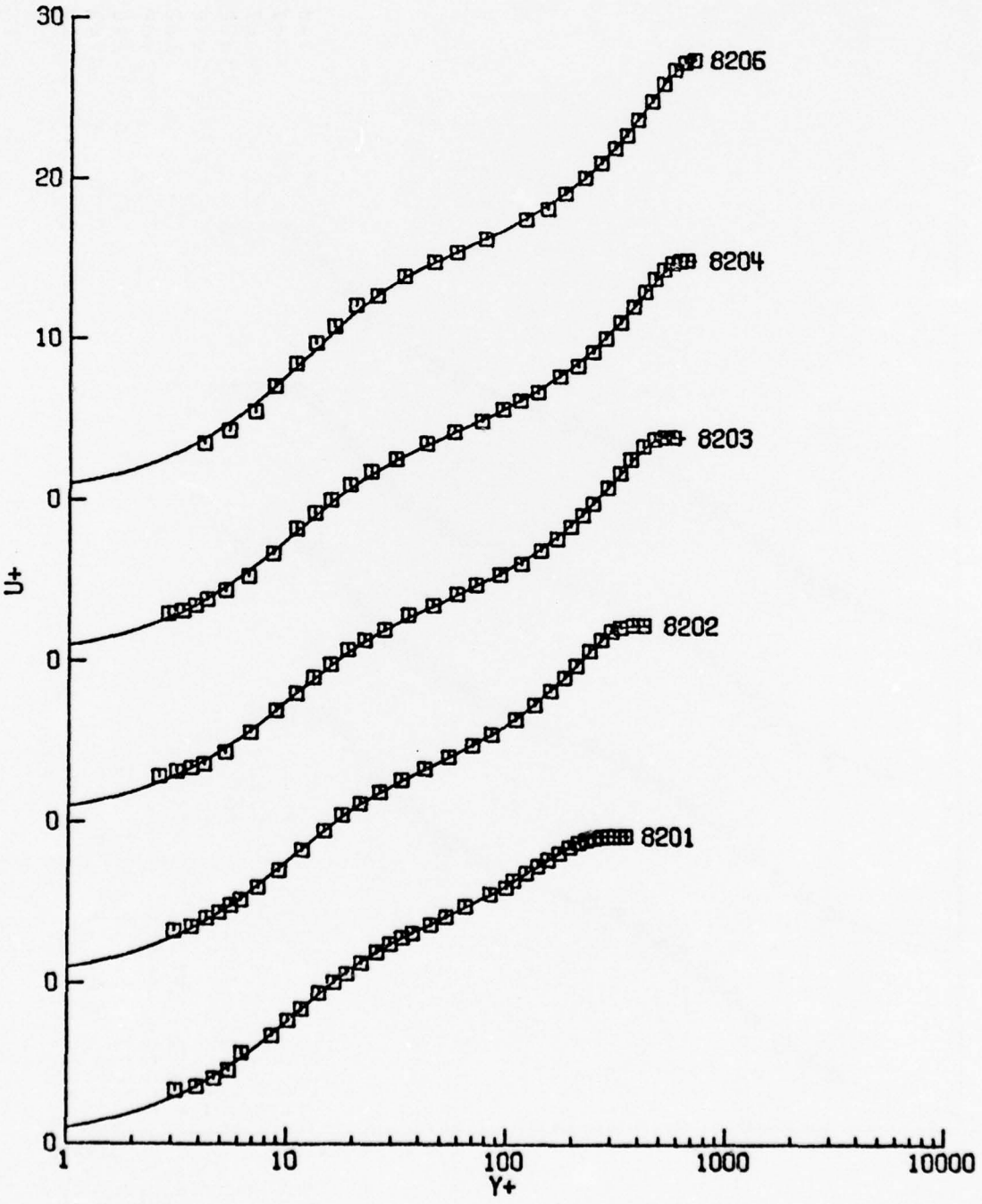

Figure B.23: Mildly adverse gradient flow of Andersen et al (1972). (Note shifted origins on the U^+ axis).

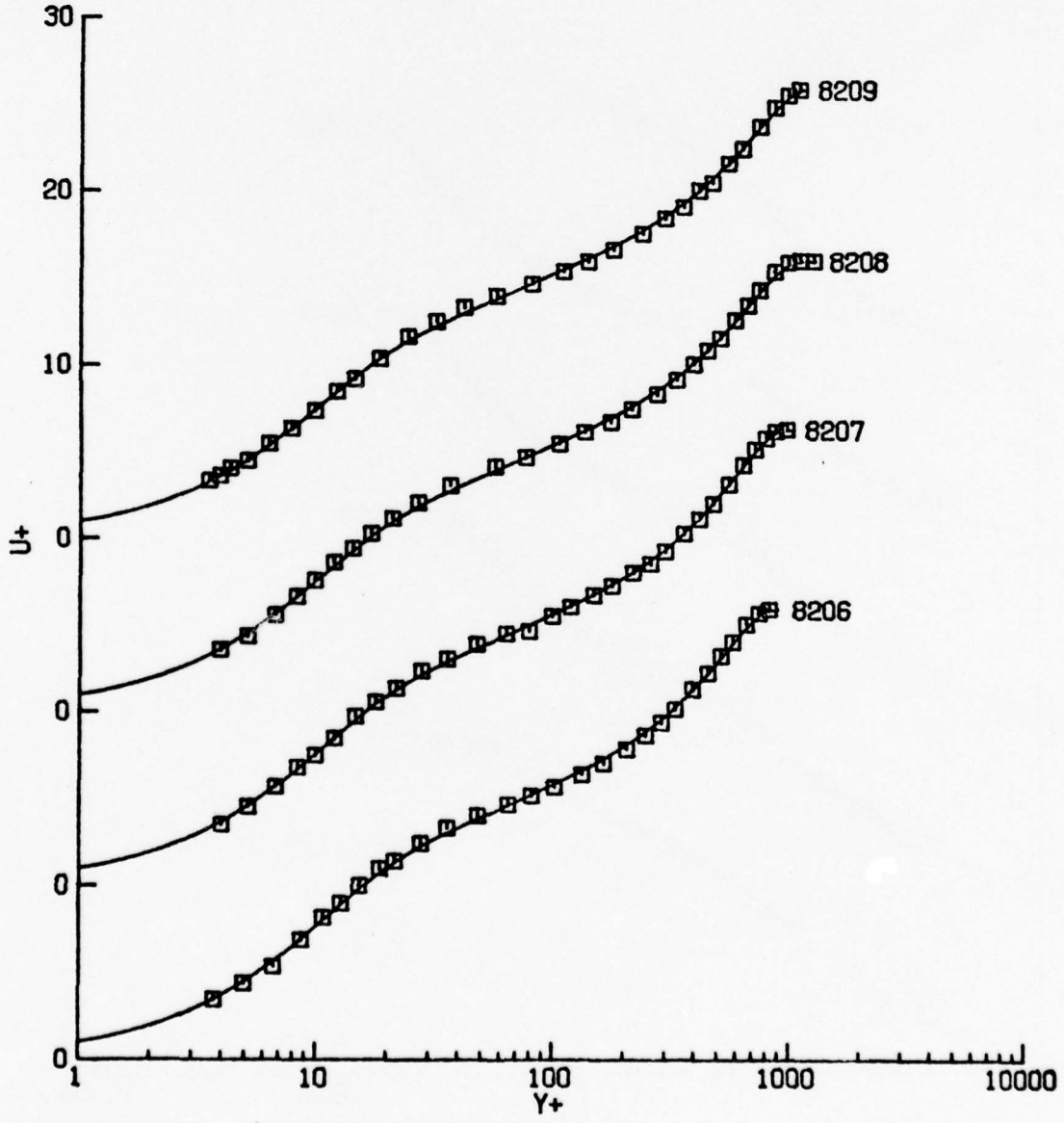

Figure B.23. (Continued).

TABLE B.24: ANDERSEN, KAYS AND MOFFAT - STRONG P. G. - 110971
(ENGLISH UNITS)

NU= 1.610000E-04

EXPERIMENTAL VALUES

ID	XSTA	UE	UTAU	DUEDX	P+	DELTA	DELTA*	THETA
8301	.167	29.13	1.511	-3.68	.00501	.3064	.0561	.0359
8302	.833	25.70	1.072	-5.21	.01750	.5366	.1237	.0770
8303	1.833	22.31	.801	-2.17	.01515	.9542	.2478	.1496
8304	2.833	20.53	.708	-1.32	.01227	1.3935	.3628	.2195
8305	3.833	19.39	.655	-.93	.01029	1.8038	.4663	.2836
8306	4.833	18.55	.615	-.70	.00899	2.1736	.5497	.3406
8307	5.833	17.97	.588	-.57	.00806	2.5570	.6291	.3951
8308	6.833	17.42	.559	-.47	.00753	2.9793	.7263	.4591
8309	7.500	17.10	.543	-.44	.00755	3.3669	.8244	.5174

UNSTEADY + COLES MODEL - FULL PROFILE FIT

ID	P+	UTAU	S	DELTA	EPSILON	Y1+	C_i	PI
8301	.00507	1.505	9.477	.3084	.005699	.4083	4.396	.3272
8302	.01416	1.150	8.079	.5730	.002614	.5136	3.602	.9249
8303	.01336	.836	9.172	1.0520	.005355	.3674	4.320	1.5278
8304	.01140	.726	9.397	1.5330	.007319	.3578	4.442	1.7093
8305	.01075	.645	10.418	1.9779	.005382	.2605	5.137	1.8601
8306	.00855	.626	10.192	2.4163	.007374	.2991	4.939	1.7356
8307	.00665	.627	9.171	2.8163	.005085	.4300	4.218	1.6042
8308	.00655	.586	10.007	3.3021	.007401	.3354	4.776	1.6631
8309	.00653	.570	9.402	3.6398	.005602	.4027	4.369	1.7594

MEAN EPSILON= .005759

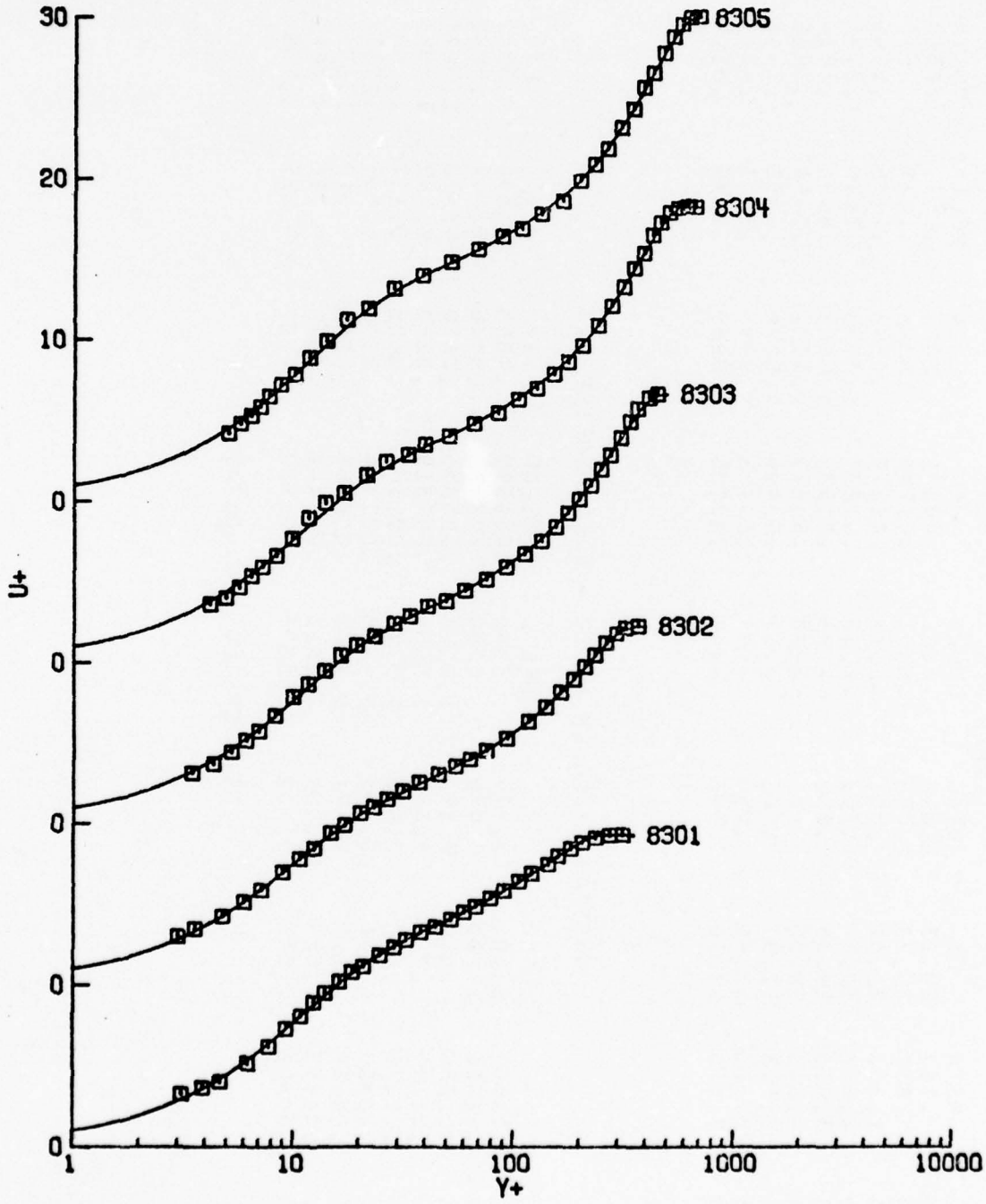

Figure B.24. Strongly adverse pressure gradient flow of Andersen et al (1972). (Note shifted origins on the U^+ axis).

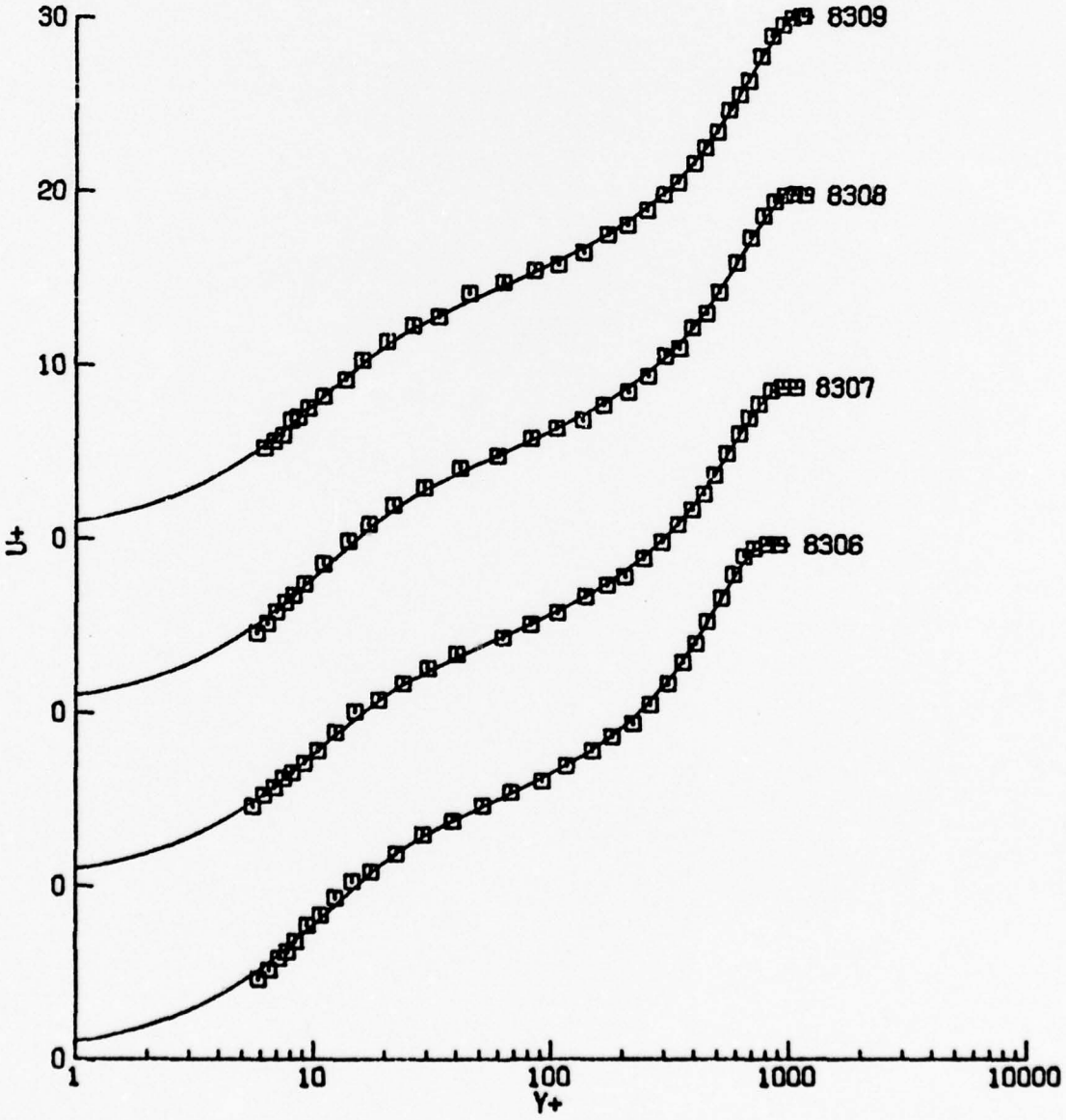

Figure B.24. (Continued).

APPENDIX C

DATA COMPARISONS USING THE COMPOSITE PROFILE CONSISTING OF THE UNSTEADY WALL LAYER MODEL AND THE SIMILARITY PROFILE.

EDDY VISCOSITY: $\varepsilon = \varepsilon_s(\eta)$, equation (5.45).

Introduction

The data comparisons of the composite profile consisting of the unsteady wall layer model and the similarity profile (the solution of equation (5.50)) are described in this appendix. The eddy viscosity formula used here is given by equation (5.45). In all cases the values of δ^* used in the fitting were taken directly from experiment; since the displacement thickness is an integrated quantity obtained from profile measurements the experimental percentage error inherent in this quantity is expected to be small.

The composite profile (5.51) *contains* either implicitly or explicitly the three independent parameters u_τ, κ, and K. With κ set equal to 0.41, as in the Coles (1956) model (Appendix B) and K = 0.0168, equation (5.51) is a one-parameter family of profiles with u_τ being the single parameter. First the data comparisons will be carried out by optimization on u_τ alone; in the latter part of the appendix the effect of varying both κ and K will be considered.

It is worthwhile to re-emphasize that the outer region similarity profile can at best apply to equilibrium flows; moreover in view of the discussion in §5.1, the similarity profile should give a progressively better representation of the data at subsequent stations downstream in constant pressure and favorable pressure gradient flows. In an adverse pressure gradient, applied over a very long distance, separation is anticipated at some downstream location. Consequently a similarity

solution is not expected to give a good representation of the data in an adverse pressure gradient flow at any downstream location.

C.1 One-Parameter Fits (κ = 0.41, K = 0.0168, u_τ varied)

In this section the fits obtained by varying the single parameter u_τ are described. Note that in this case the composite profile (5.51) contains only one adjustable parameter whereas the profile (4.4), which uses the Coles (1956) model and which was treated in Appendix B, contains three independent parameters.

1300 - Ludwieg and Tillman

The fits of the composite profile (5.51) to this favorable pressure gradient equilibrium flow are described in Table C.1 and Figure C.1. In general the fits are good but overall slightly worse than those obtained with the Coles model (Table B.1), particularly at the upstream stations. However, the trend for the root-mean-square error to decrease at subsequent stations downstream is encouraging; in fact, at the downstream station the values of ε become smaller than those obtained with the Coles model (Table B.1).

2700 - Herring and Norbury

The fits to this mildly favorable equilibrium flow are described in Table C.2 and Figure C.2. The quality of the fits is good and the data are represented better on average than with the Coles (1956) model (Table B.6). This is encouraging in view of the fact that the fits described in Table B.6 are three-parameter fits.

8100 - Andersen, et al. (1972)

The data comparisons for this constant pressure flow are described in Table C.3 and Figure C.3. The fits are not as good as obtained with the Coles (1956) model in Table B.22. However, there is a trend for ε to decrease downstream which is encouraging; moreover there are two less adjustable parameters here than in Table B.22.

8200 - Andersen, et al. (1972)

The fits for this mildly adverse pressure gradient flow are described in Table C.4 and Figure C.4. It is clear that these one-parameter fits are rather poor and are not nearly as good as obtained in Table B.23 with the Coles (1956) model. The trend of ε for this case is revealing. This is an equilibrium flow but in an adverse pressure gradient and in view of §5.1, similarity is not expected. This is borne out in Table C.4 where the fits are uniformly poor; that is to say, there is no trend for ε to decrease significantly at the downstream stations which was observed in Tables C.1 to C.3.

C.2 Two-Parameter Fits (κ = 0.41, K varied, u_τ varied)

In this section, the effect of varying the outer region eddy viscosity constant K as well as u_τ will be considered for the zero pressure gradient flow of Andersen, et al. (1972). The result of this procedure is described in Table C.5 and Figure C.5. The motivation for this procedure is two-fold. In the first place, true similarity is not anticipated in this flow until a large distance downstream; thus neglecting $\partial U_1/\partial x$ in the momentum equation is not strictly justified. Varying K is equivalent to attempting to account for the non-similar behavior. A

second and more important reason concerns the ultimate application of this theory in a prediction method. In order to initiate a prediction method it is necessary to be able to obtain a good analytical representation of the data at any initial station. Allowing K to vary provides a convenient mechanism for this purpose.

The trend for K to decrease to an approximately constant value at the downstream stations may be observed in Table C.5. Moreover it is clear from Table C.5 that the additional parameter significantly improves the quality of the fit. The average root-mean-square error is reduced by 38% from the one-parameter fit described in Table C.3.

C.3 Three-Parameter Fits (κ varied, K varied, u_τ varied)

In this section all three parameters were varied for the zero pressure gradient flow of Andersen, et al. (1972). The motivation for allowing κ to vary was that in some of the data sets a skewing of the profile was observed through the logarithmic zone. This tendency may be observed by close inspection of Figure C.5 and suggests a value of κ different from 0.41.

The result of this optimization procedure is described in Table C.6 and Figure C.6. The result of varying the third parameter is to reduce the root-mean-square error from Table C.5 but the reduction is not as substantial as was obtained between Table C.3 and Table C.5. The fits are good and are of comparable quality to that obtained with the Coles (1956) model in Table B.22. The primary source of error in this case originates at the boundary-layer edge where the similarity profile appears to decay too quickly to the mainstream value.

TABLE C.1: LUDWIEG AND TI MANN
(METRIC UNITS)

NU= 1.540000E-05

EXPERIMENTAL VALUES

ID	XSTA	UE	UTAU	DUEDX	BETA	DELTA	DELTA*	THETA
1301	.782	11.52	.553	3.65	-.2640	1.5000	.1920	.1347
1302	1.282	13.38	.628	4.00	-.2778	1.6750	.2047	.1486
1303	1.782	15.61	.711	4.33	-.2899	1.8000	.2168	.1581
1304	2.282	17.85	.796	4.68	-.3106	2.0000	.2356	.1732
1305	2.782	20.20	.875	4.90	-.3343	2.0000	.2586	.1890
1306	3.132	22.07	.939	5.00	-.3339	2.0000	.2668	.1958
1307	3.332	22.90	.975	5.00	-.3199	2.3000	.2656	.1960
1308	3.532	23.70	1.000	4.96	-.3209	2.3000	.2730	.2027
1309	3.732	25.13	1.070	4.86	-.2797	2.3000	.2622	.1963
1310	3.932	25.80	1.060	4.60	-.3128	2.4000	.2961	.2188
1311	4.132	26.40	1.080	4.13	-.2853	2.5000	.3052	.2268
1312	4.332	27.50	1.130	3.50	-.2299	2.5000	.3050	.2274

UNSTEADY + SIMILARITY - FULL PROFILE FIT

ID	BETA	UTAU	S	K	KAPPA	EPSILON	TO+	Ci
1301	-.2575	.545	11.139	.016800	.4100	.013827	.005553	5.429
1302	-.2804	.610	11.737	.016800	.4100	.021665	.003938	5.835
1303	-.2931	.693	11.895	.016800	.4100	.019304	.003549	5.942
1304	-.3289	.759	12.819	.016800	.4100	.007163	.002099	6.582
1305	-.3088	.902	10.196	.016800	.4100	.003574	.009497	4.802
1306	-.3082	.969	10.332	.016800	.4100	.004060	.008790	4.892
1307	-.3083	.984	10.959	.016800	.4100	.003380	.006156	5.308
1308	-.3160	.998	11.515	.016800	.4100	.005158	.004476	5.683
1309	-.3113	1.001	13.367	.016800	.4100	.010060	.001521	6.968
1310	-.2823	1.109	9.894	.016800	.4100	.003541	.011253	4.605
1311	-.2681	1.107	10.513	.016800	.4100	.003495	.007934	5.011
1312	-.2359	1.107	11.620	.016800	.4100	.003235	.004212	5.755

MEAN EPSILON= .008205

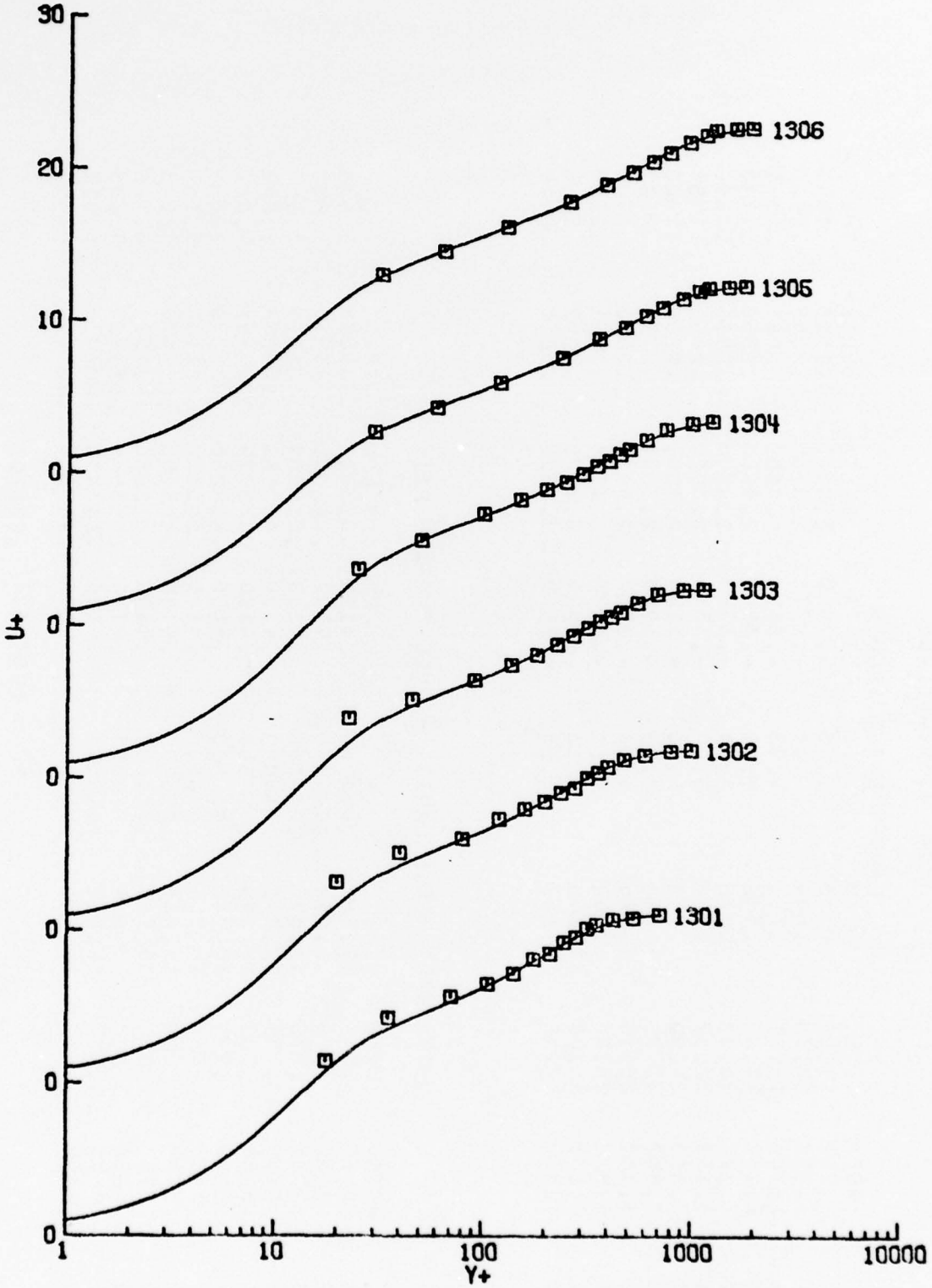

Figure C.1. Ludwieg and Tillman accelerating flow. (Note shifted origins on the U^+ axis).

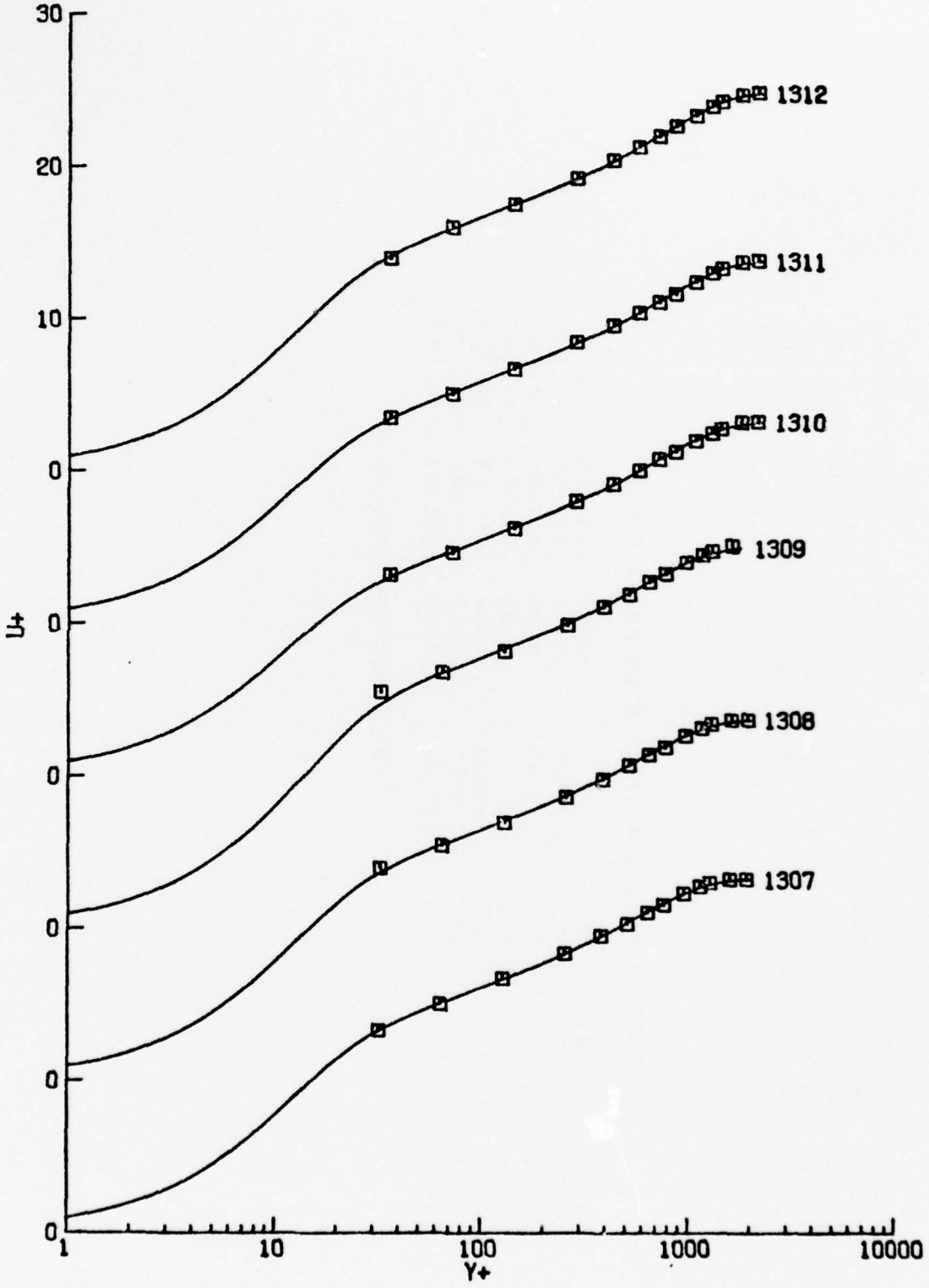

Figure C.1. (Continued).

TABLE C.2: HERRING AND NORBURY - BETA= -0.35
(ENGLISH UNITS)

NU= 1.730000E-04

EXPERIMENTAL VALUES

ID	XSTA	UE	UTAU	DUEDX	BETA	DELTA	DELTA*	THETA
2701	0.000	76.50	3.149	2.65	-.2111	.8500	.1239	.0921
2702	1.000	79.80	3.280	4.90	-.3883	.9000	.1282	.0960
2703	2.000	84.60	3.550	6.13	-.3896	1.0000	.1136	.0875
2704	3.000	90.50	3.798	6.20	-.3598	1.0000	.1110	.0856
2705	4.000	97.10	4.041	6.25	-.3413	1.0000	.1102	.0845
2706	5.000	103.60	4.270	6.25	-.3326	1.0000	.1124	.0860

UNSTEADY + SIMILARITY - FULL PROFILE FIT

ID	BETA	UTAU	S	K	KAPPA	EPSILON	TO+	C_i
2701	-.1946	3.258	9.913	.016800	.4100	.008502	.011133	4.618
2702	-.3266	3.559	8.937	.016800	.4100	.007406	.019195	3.994
2703	-.3666	3.631	10.838	.016800	.4100	.014359	.006597	5.227
2704	-.3491	3.826	11.076	.016800	.4100	.014708	.005759	5.386
2705	-.3322	4.066	11.067	.016800	.4100	.004280	.005788	5.380
2706	-.3197	4.328	10.745	.016800	.4100	.005035	.006954	5.165

MEAN EPSILON= .009048

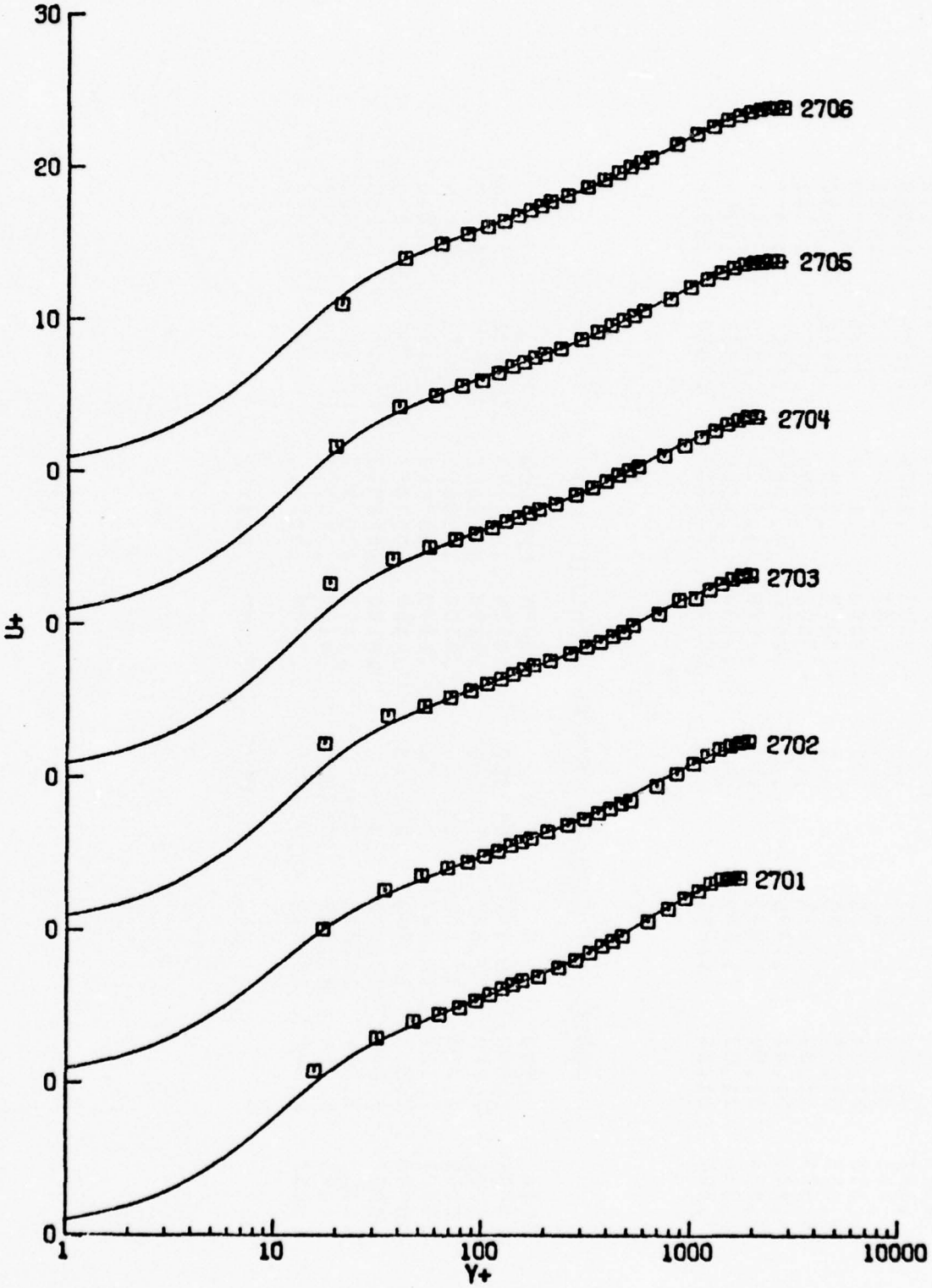

Figure C.2. Herring and Norbury mildly favorable pressure gradient equilibrium flow, β=-0.35. (Note shifted origins on the U^+ axis).

TABLE C.3: ANDERSEN, KAYS AND MOFFAT - ZERO P. G. - 120771-1
(ENGLISH UNITS)

NU= 1.590000E-04

EXPERIMENTAL VALUES

ID	XSTA	UE	UTAU	DUEDX	BETA	DELTA	DELTA*	THETA
8101	.167	31.21	1.557	.01	-.0005	.2871	.0504	.0328
8102	.833	31.13	1.467	.01	-.0007	.4225	.0772	.0521
8103	1.833	31.14	1.400	.01	-.0008	.6242	.1135	.0768
8104	2.833	31.05	1.353	.00	-.0007	.7854	.1412	.0977
8105	3.833	31.04	1.321	.00	-.0002	.9590	.1709	.1185
8106	4.833	31.13	1.298	-.00	.0006	1.1065	.1968	.1375
8107	5.833	31.04	1.272	-.01	.0020	1.2755	.2255	.1584
8108	6.833	31.07	1.254	-.01	.0038	1.4808	.2533	.1794
8109	7.500	31.06	1.246	-.01	.0053	1.5810	.2670	.1902

UNSTEADY + SIMILARITY - FULL PROFILE FIT

ID	BETA	UTAU	S	K	KAPPA	EPSILON	TO+	C_i
8101	-.0004	1.630	8.194	.016800	.4100	.027948	.028896	3.536
8102	-.0006	1.588	7.222	.016800	.4100	.021645	.049006	2.960
8103	-.0009	1.355	11.102	.016800	.4100	.010098	.005673	5.404
8104	-.0007	1.329	10.867	.016800	.4100	.007479	.006458	5.546
8105	-.0002	1.300	10.948	.016800	.4100	.007333	.006196	5.300
8106	.0007	1.243	12.152	.016800	.4100	.012970	.003097	6.119
8107	.0019	1.284	10.348	.016800	.4100	.009537	.008711	4.902
8108	.0040	1.224	11.709	.016800	.4100	.010220	.004003	5.815
8109	.0052	1.247	10.822	.016800	.4100	.007718	.006655	5.216

MEAN EPSILON= .012772

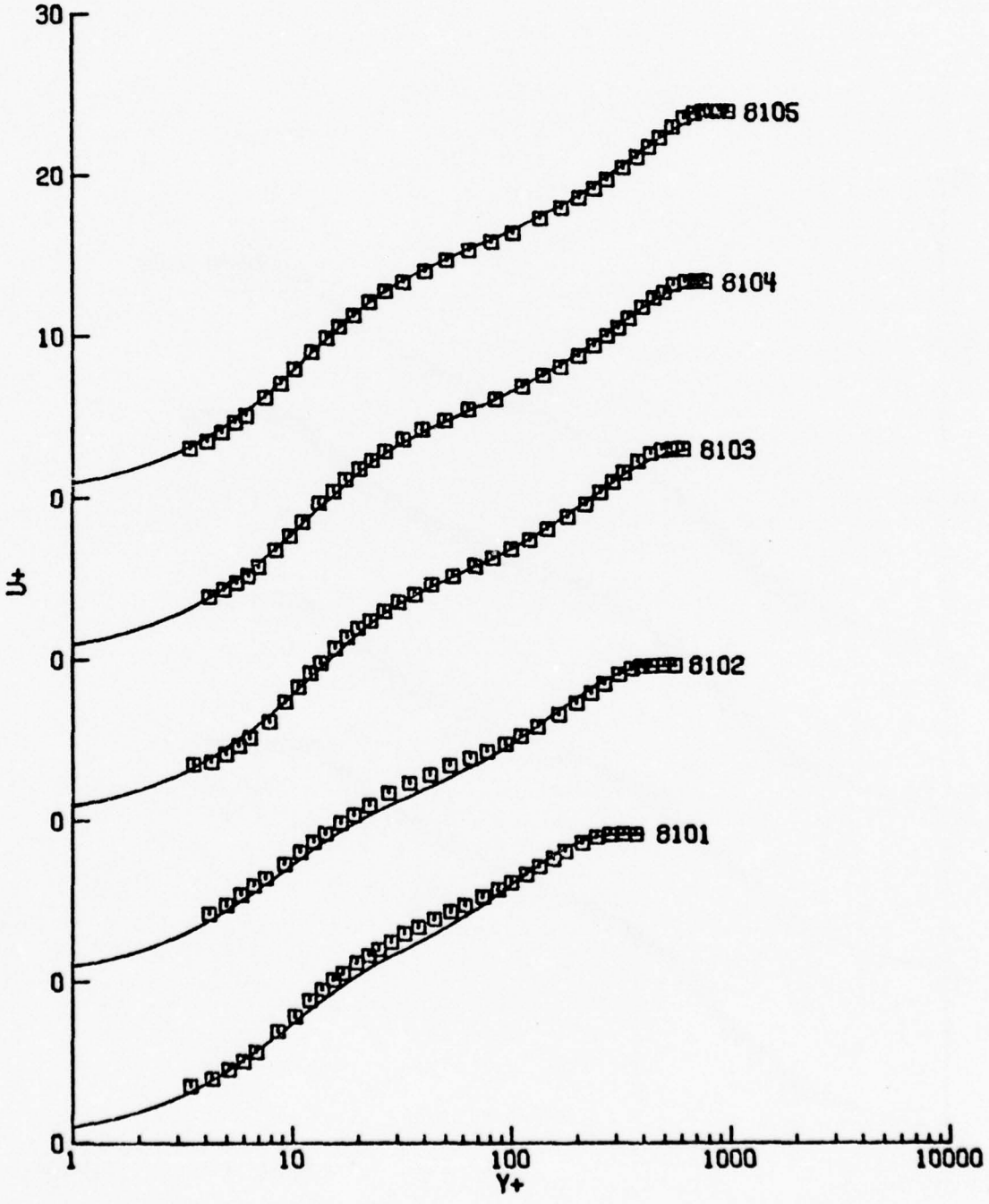

Figure C.3. Constant pressure flow of Andersen et al (1972). (Note shifted origins on the U^+ axis).

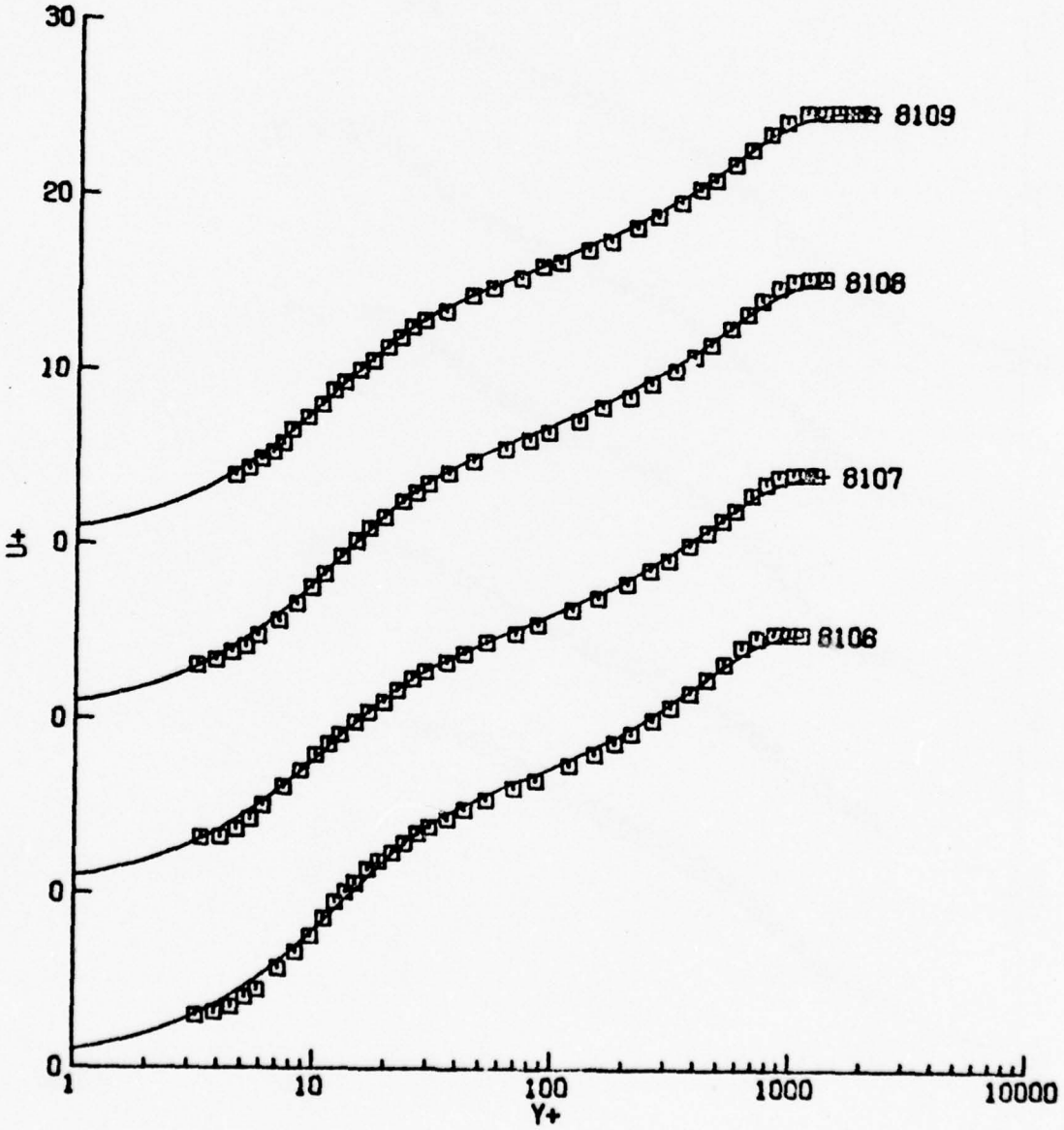

Figure C.3. (Continued).

TABLE C.4: ANDERSEN, KAYS AND MOFFAT - ILD P. G. - 071571-5
(ENGLISH UNITS)

NU= 1.660000E-04

EXPERIMENTAL VALUES

ID	XSTA	UE	UTAU	DUEDX	BETA	DELTA	DELTA*	THETA
8201	.167	29.69	1.546	-2.44	.1404	.3081	.0556	.0357
8202	.833	26.93	1.198	-3.79	.6744	.5179	.1138	.0718
8203	1.833	24.57	1.010	-1.76	.6839	.8628	.1936	.1238
8204	2.833	23.26	.910	-1.13	.6919	1.1752	.2616	.1700
8205	3.833	22.27	.848	-.82	.7102	1.5029	.3356	.2176
8206	4.833	21.36	.799	-.63	.6910	1.7870	.3934	.2592
8207	5.833	20.74	.765	-.51	.6943	2.1211	.4610	.3049
8208	6.833	20.35	.742	-.43	.6765	2.4043	.5108	.3419
8209	7.500	20.05	.726	-.41	.7082	2.5701	.5449	.3656

UNSTEADY + SIMILARITY - FULL PROFILE FIT

ID	BETA	UTAU	S	K	KAPPA	EPSILON	TO+	C_f
8201	.1385	1.525	7.583	.016800	.4100	.026978	.040320	3.170
8202	.6966	1.169	6.682	.016800	.4100	.022952	.065511	2.654
8203	.6880	1.000	7.557	.016800	.4100	.017990	.040892	3.155
8204	.6744	.916	8.066	.016800	.4100	.016262	.031005	3.458
8205	.7625	.812	9.857	.016800	.4100	.015147	.011493	4.581
8206	.6704	.807	8.571	.016800	.4100	.016660	.023499	3.766
8207	.6672	.777	8.448	.016800	.4100	.014312	.025138	3.691
8208	.6316	.765	8.254	.016800	.4100	.016363	.027968	3.572
8209	.6607	.749	8.087	.016800	.4100	.017508	.030645	3.471

MEAN EPSILON= .018241

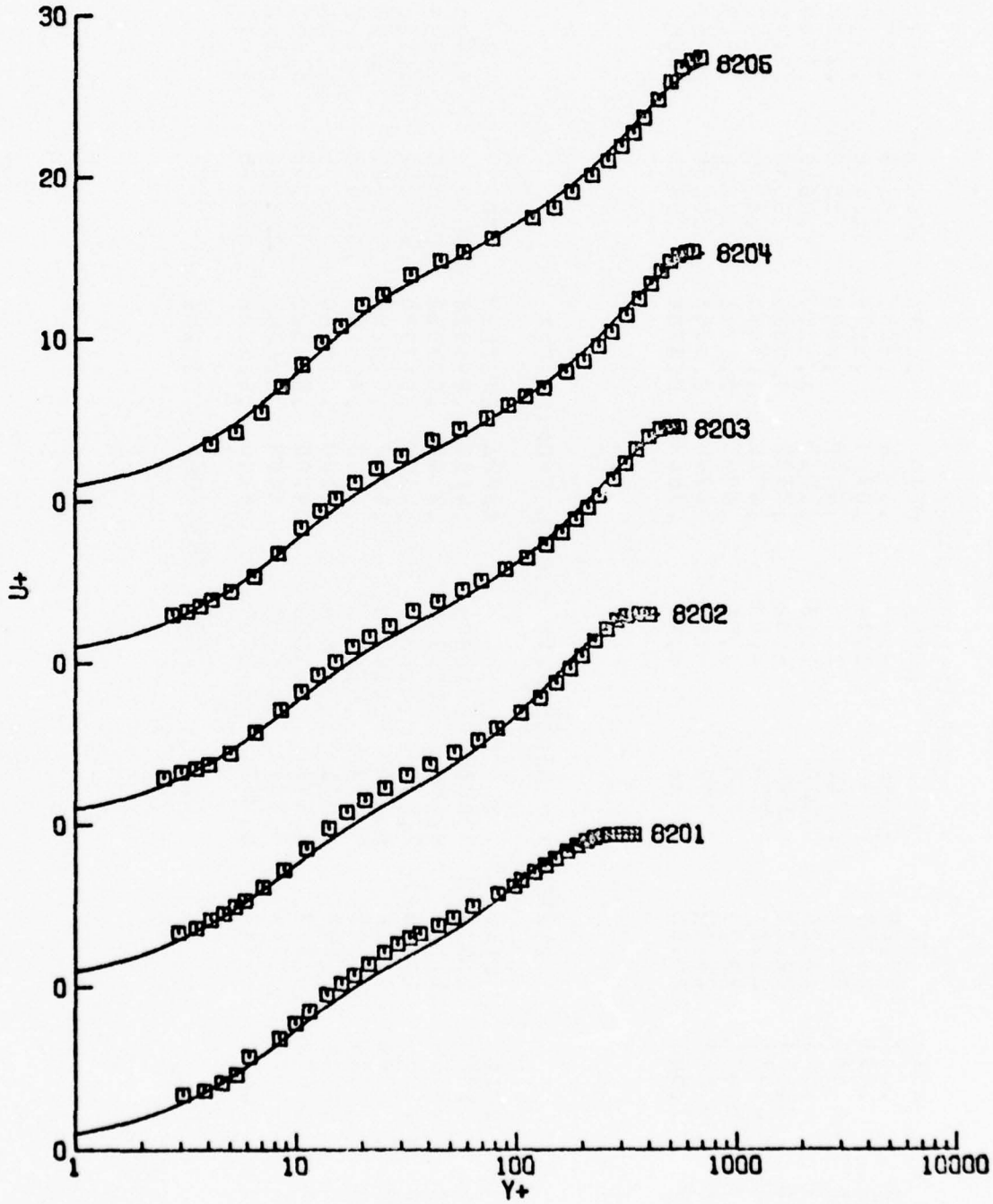

Figure C.4. Mild adverse pressure gradient flow of Andersen, et al. (1972). (Note shifted origins on the U^+ axis).

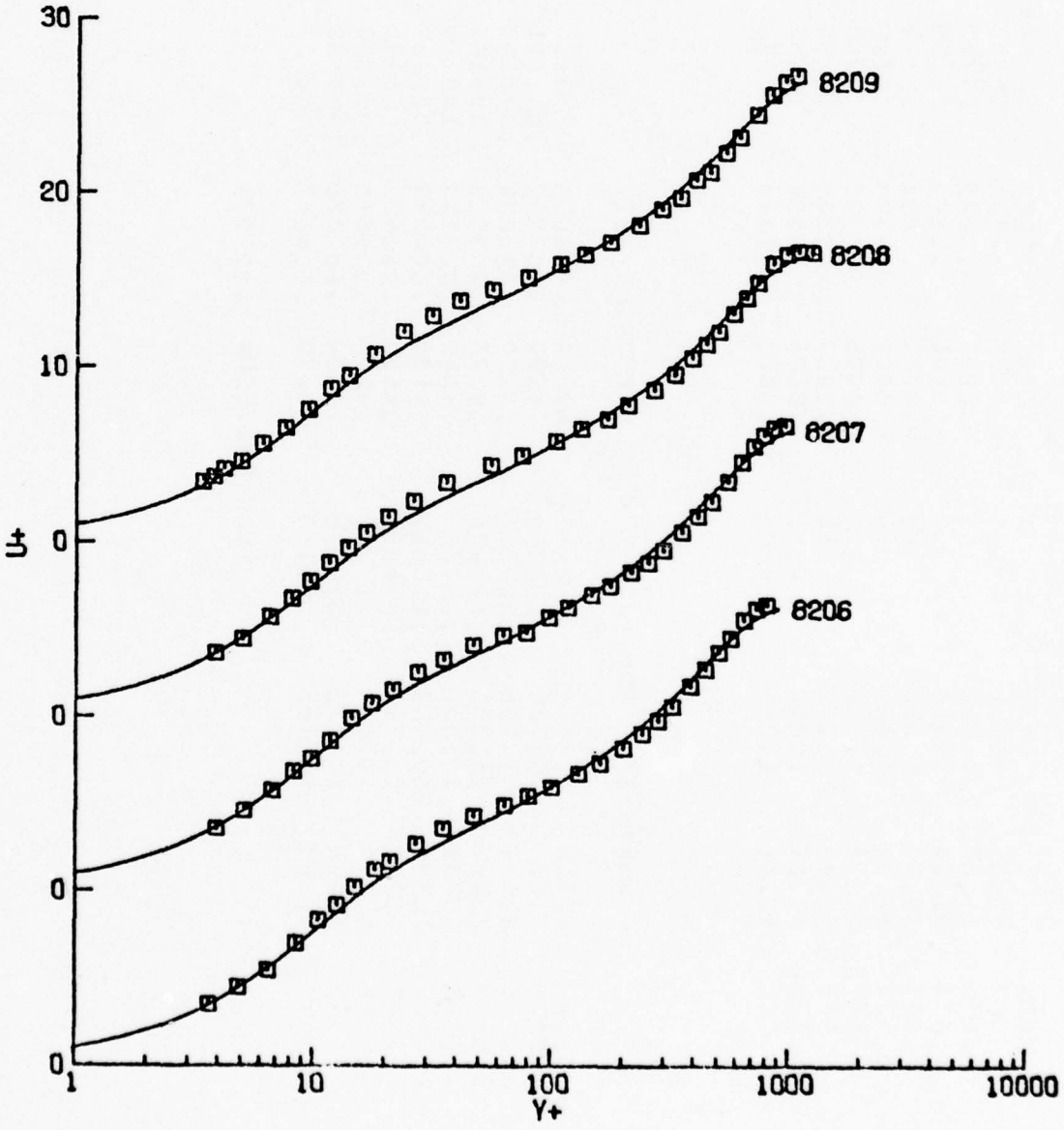

Figure C.4. (Continued).

TABLE C.5: ANDERSEN, KAYS AND MOFFAT - ZERO P. G. - 120771-1
(ENGLISH UNITS)

NU= 1.590000E-04

EXPERIMENTAL VALUES

ID	XSTA	UE	UTAU	DUEDX	BETA	DELTA	DELTA*	THETA
8101	.167	31.21	1.557	.01	-.0005	.2871	.0504	.0328
8102	.833	31.13	1.467	.01	-.0007	.4225	.0772	.0521
8103	1.833	31.14	1.400	.01	-.0008	.6242	.1135	.0768
8104	2.833	31.05	1.353	.00	-.0007	.7854	.1412	.0977
8105	3.833	31.04	1.321	.00	-.0002	.9590	.1709	.1185
8106	4.833	31.13	1.298	-.00	.0006	1.1065	.1968	.1375
8107	5.833	31.04	1.272	-.01	.0020	1.2755	.2255	.1584
8108	6.833	31.07	1.254	-.01	.0038	1.4808	.2533	.1794
8109	7.500	31.06	1.246	-.01	.0053	1.5810	.2670	.1902

UNSTEADY + SIMILARITY - FULL PROFILE FIT

ID	BETA	UTAU	S	K	KAPPA	EPSILON	TO+	C_i
8101	-.0004	1.651	9.734	.028760	.4100	.007937	.012311	4.502
8102	-.0005	1.646	7.536	.024111	.4100	.006004	.041348	3.143
8103	-.0009	1.357	11.201	.017420	.4100	.009895	.005360	5.470
8104	-.0007	1.332	10.938	.017368	.4100	.007257	.006230	5.294
8105	-.0002	1.294	10.862	.015815	.4100	.006549	.006507	5.243
8106	.0007	1.237	11.946	.015379	.4100	.011987	.003490	5.977
8107	.0019	1.274	10.314	.015583	.4100	.006512	.008883	4.880
8108	.0040	1.211	11.572	.014810	.4100	.007375	.004332	5.722
8109	.0053	1.237	10.783	.015493	.4100	.006247	.006807	5.190

MEAN EPSILON= .007974

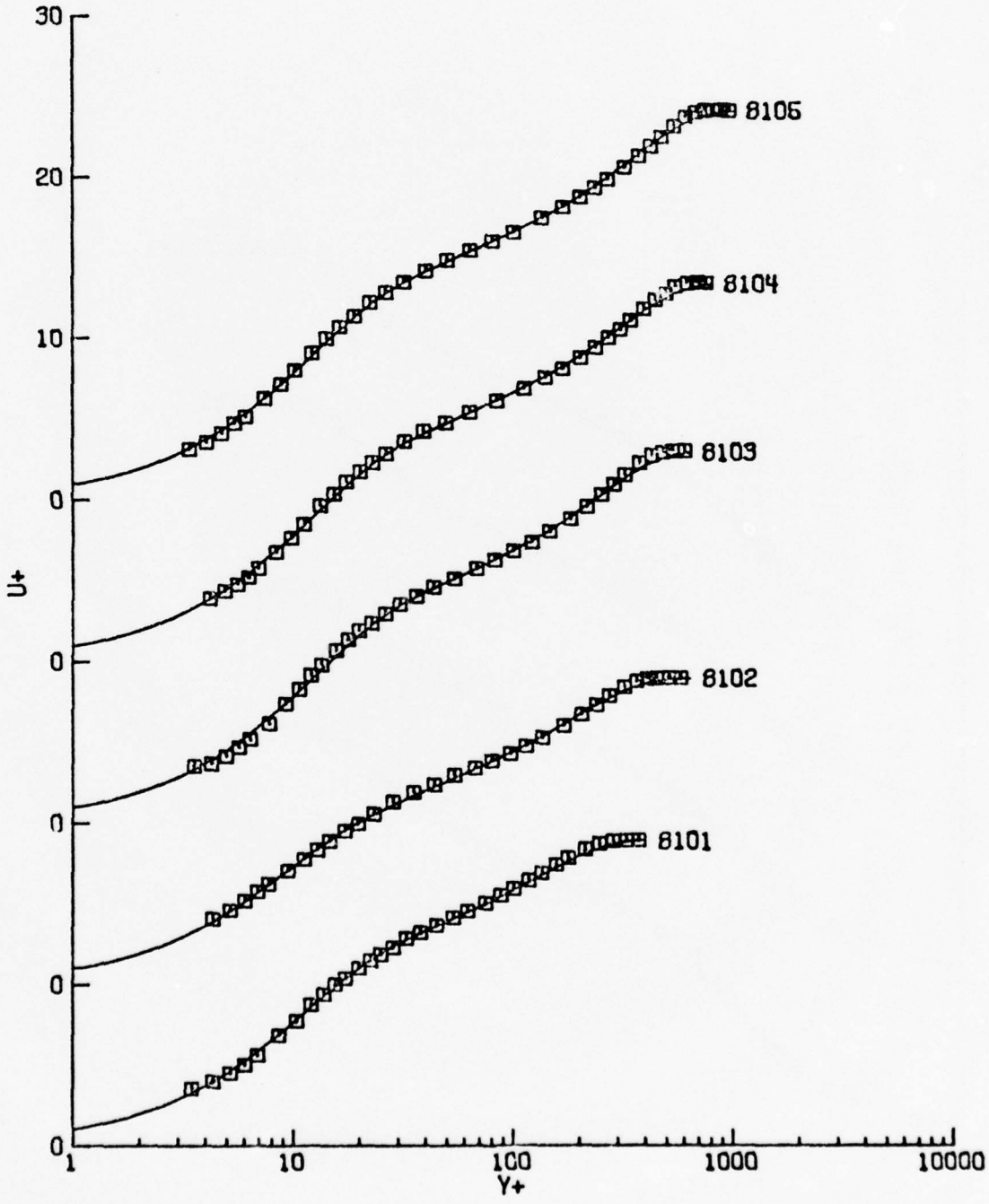

Figure C.5. Two parameter fits to the constant pressure flow of Andersen, et al. (1972). (Note shifted origins on the U^+ axis).

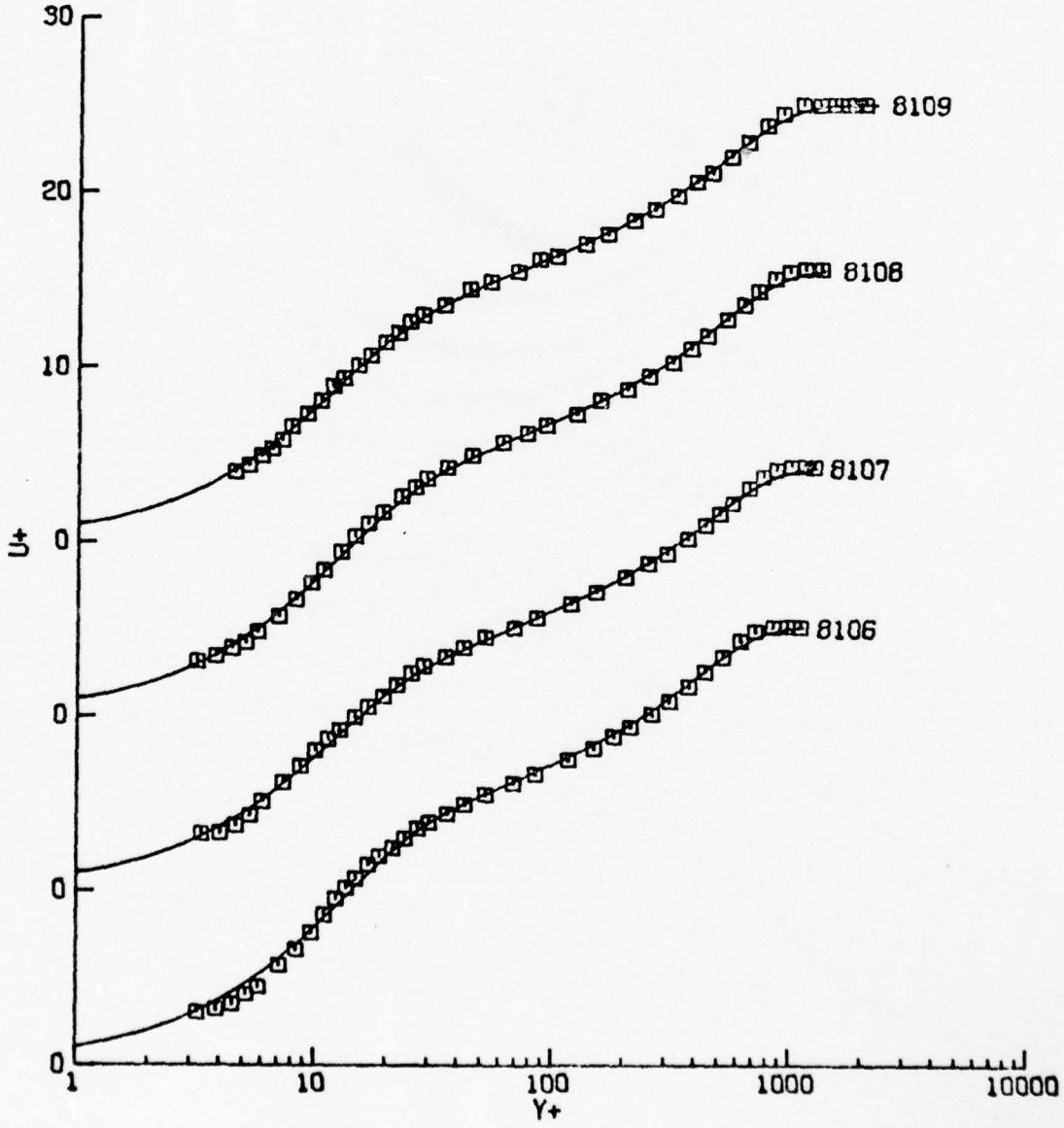

Figure C.5. (Continued).

TABLE C.6: ANDERSEN, KAYS AND MOFFAT - ERO P. G. - 120771-1
(ENGLISH UNITS)

NU= 1.590000E-04

EXPERIMENTAL VALUES

ID	XSTA	UE	UTAU	DUEDX	BETA	DELTA	DELTA*	THETA
8101	.167	31.21	1.557	.01	-.0005	.2871	.0504	.0328
8102	.833	31.13	1.467	.01	-.0007	.4225	.0772	.0521
8103	1.833	31.14	1.400	.01	-.0008	.6242	.1135	.0768
8104	2.833	31.05	1.353	.00	-.0007	.7854	.1412	.0977
8105	3.833	31.04	1.321	.00	-.0002	.9590	.1709	.1185
8106	4.833	31.13	1.298	-.00	.0006	1.1065	.1968	.1375
8107	5.833	31.04	1.272	-.01	.0020	1.2755	.2255	.1584
8108	6.833	31.07	1.254	-.01	.0038	1.4808	.2533	.1794
8109	7.500	31.06	1.246	-.01	.0053	1.5810	.2670	.1902

UNSTEADY + SIMILARITY - FULL PROFILE FIT

ID	BETA	UTAU	S	K	KAPPA	EPSILON	TO+	Ci
8101	-.0004	1.641	8.664	.029030	.3466	.007366	.064864	3.086
8102	-.0005	1.648	7.920	.023885	.4317	.005884	.024069	3.561
8103	-.0009	1.362	12.335	.017107	.5064	.009340	.000327	7.143
8104	-.0007	1.336	12.312	.016721	.5195	.006109	.000250	7.222
8105	-.0002	1.296	11.861	.015342	.4779	.005890	.000854	6.577
8106	.0007	1.241	13.506	.014512	.5387	.011011	.000063	8.241
8107	.0019	1.277	11.430	.014762	.4818	.007667	.001060	6.303
8108	.0040	1.213	12.962	.013962	.5046	.006003	.000214	7.588
8109	.0053	1.237	11.761	.014740	.4670	.005377	.001154	6.413

MEAN EPSILON= .007183

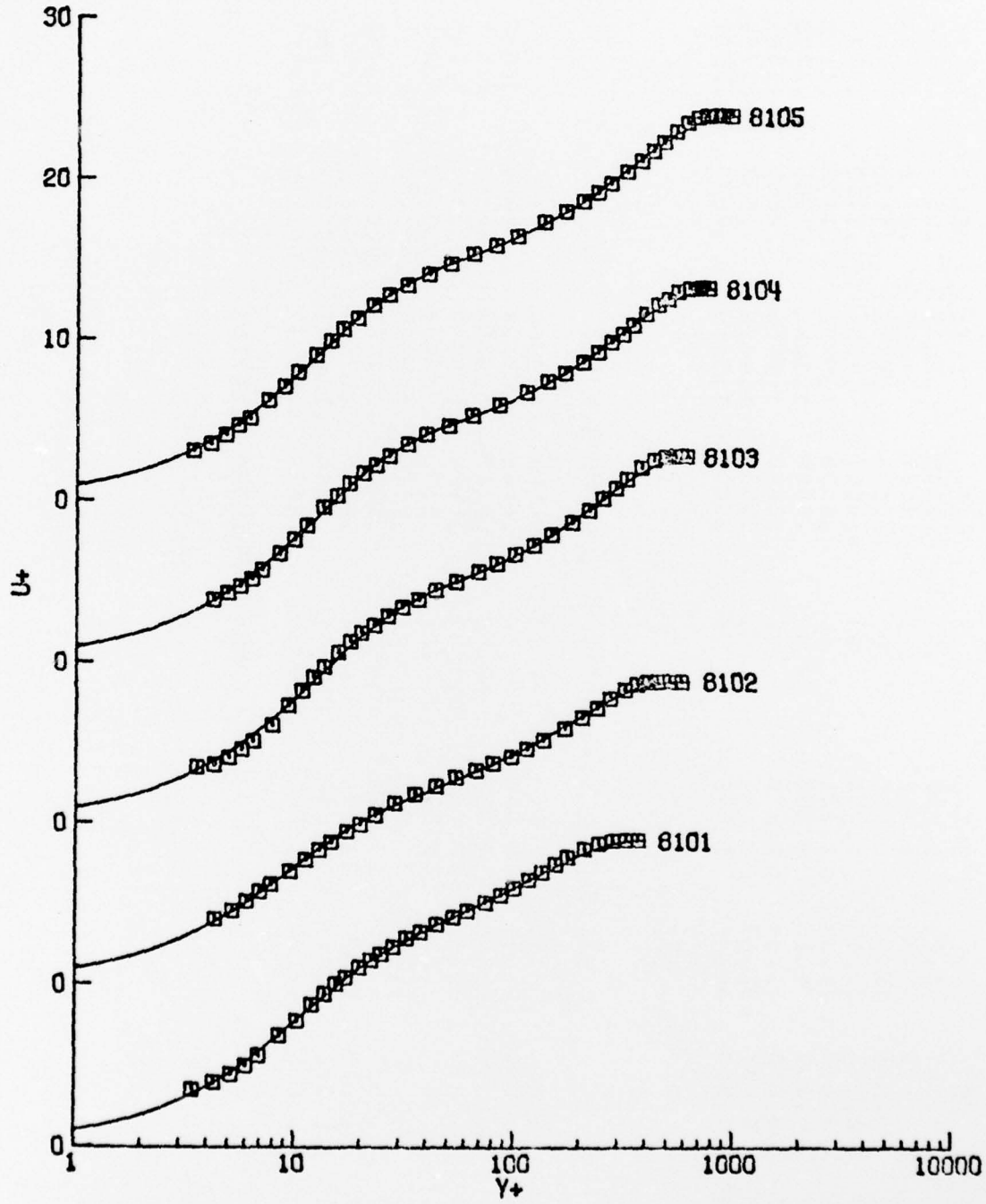

Figure C.6. Three parameter fits to constant pressure data of Andersen, et al. (1972). (Note shifted origins on the U^+ axis).

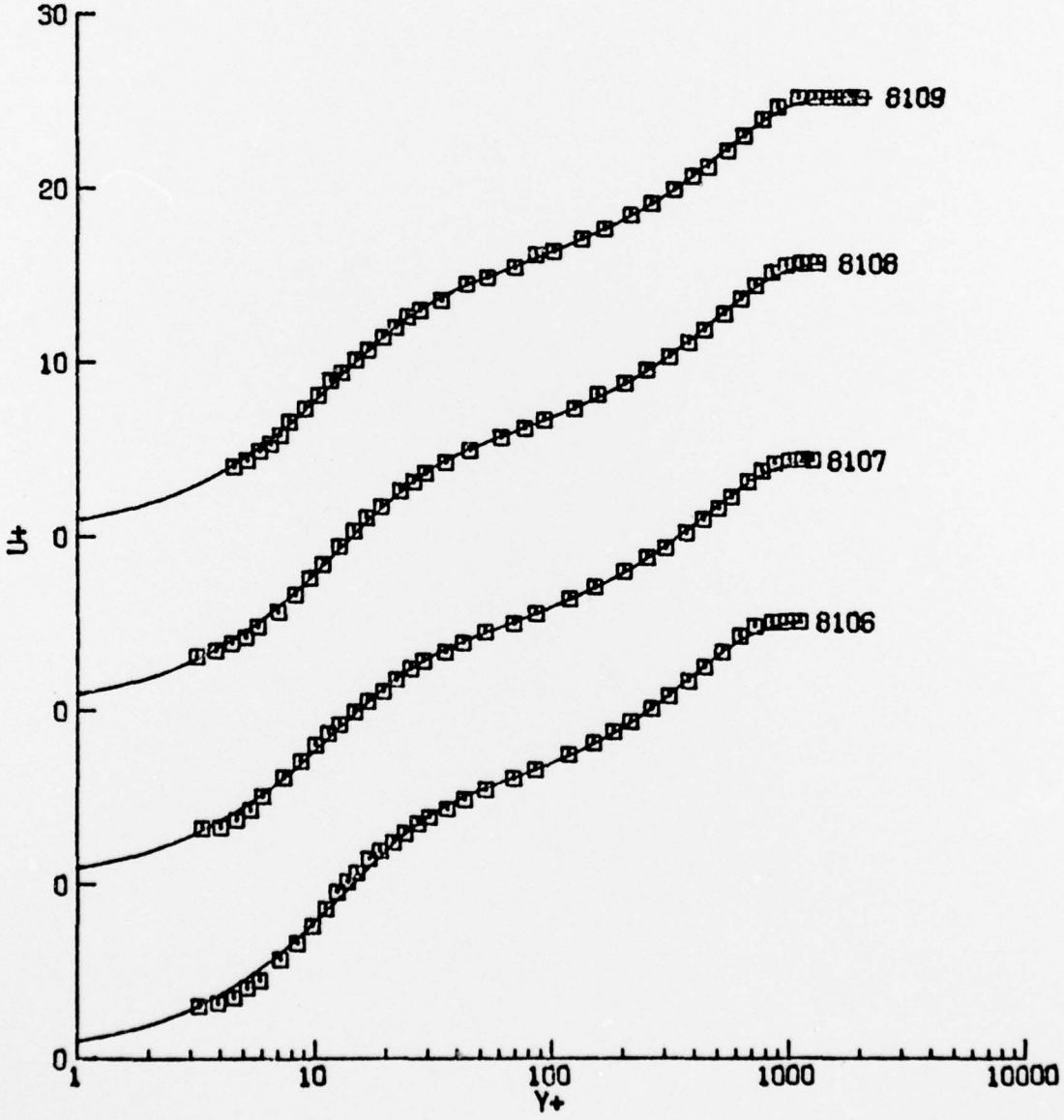

Figure C.6. (Continued).

APPENDIX D

DATA COMPARISONS USING THE COMPOSITE PROFILE CONSISTING OF THE UNSTEADY WALL LAYER MODEL AND THE SIMILARITY PROFILE.

EDDY VISCOSITY: $\varepsilon = \varepsilon_5(\eta)$, equation (5.58).

TABLE D.1: LUDWIEG AND T[illegible]MANN
(METRIC UNITS)

NU= 1.540000E-05

EXPERIMENTAL VALUES

ID	XSTA	UE	UTAU	DUEDX	BETA	DELTA	DELTA*	THETA
1301	.782	11.52	.553	3.65	-.2640	1.5000	.1920	.1347
1302	1.282	13.38	.628	4.00	-.2778	1.6750	.2047	.1468
1303	1.782	15.61	.711	4.33	-.2899	1.8000	.2168	.1581
1304	2.282	17.85	.796	4.68	-.3106	2.0000	.2356	.1732
1305	2.782	20.20	.875	4.90	-.3343	2.0000	.2586	.1890
1306	3.132	22.07	.939	5.00	-.3339	2.0000	.2668	.1958
1307	3.332	22.90	.975	5.00	-.3199	2.3000	.2656	.1960
1308	3.532	23.70	1.000	4.96	-.3209	2.3000	.2730	.2027
1309	3.732	25.13	1.070	4.86	-.2797	2.3000	.2622	.1963
1310	3.932	25.80	1.060	4.60	-.3128	2.4000	.2961	.2188
1311	4.132	26.40	1.080	4.13	-.2853	2.5000	.3052	.2268
1312	4.332	27.50	1.130	3.50	-.2299	2.5000	.3050	.2274

UNSTEADY + SIMILARITY - FULL PROFILE FIT

ID	BETA	UTAU	S	K	KAPPA	EPSILON	TO+	Ci
1301	-.2563	.545	11.547	.016800	.4100	.011975	.004393	5.705
1302	-.2764	.614	11.900	.016800	.4100	.020184	.003585	5.946
1303	-.2879	.699	11.944	.016800	.4100	.018017	.003495	5.976
1304	-.3230	.766	12.804	.016800	.4100	.006870	.002117	6.572
1305	-.3003	.915	9.988	.016800	.4100	.003763	.010678	4.666
1306	-.2998	.983	10.102	.016800	.4100	.004319	.010009	4.741
1307	-.2993	.999	10.716	.016800	.4100	.003961	.007069	5.146
1308	-.3075	1.012	11.291	.016800	.4100	.004270	.005091	5.531
1309	-.3036	1.014	13.191	.016800	.4100	.008670	.001687	6.844
1310	-.2736	1.127	9.619	.016800	.4100	.004000	.013134	4.427
1311	-.2602	1.124	10.223	.016800	.4100	.004308	.009352	4.820
1312	-.2282	1.126	11.276	.016800	.4100	.004064	.005133	5.522

MEAN EPSILON= .007868

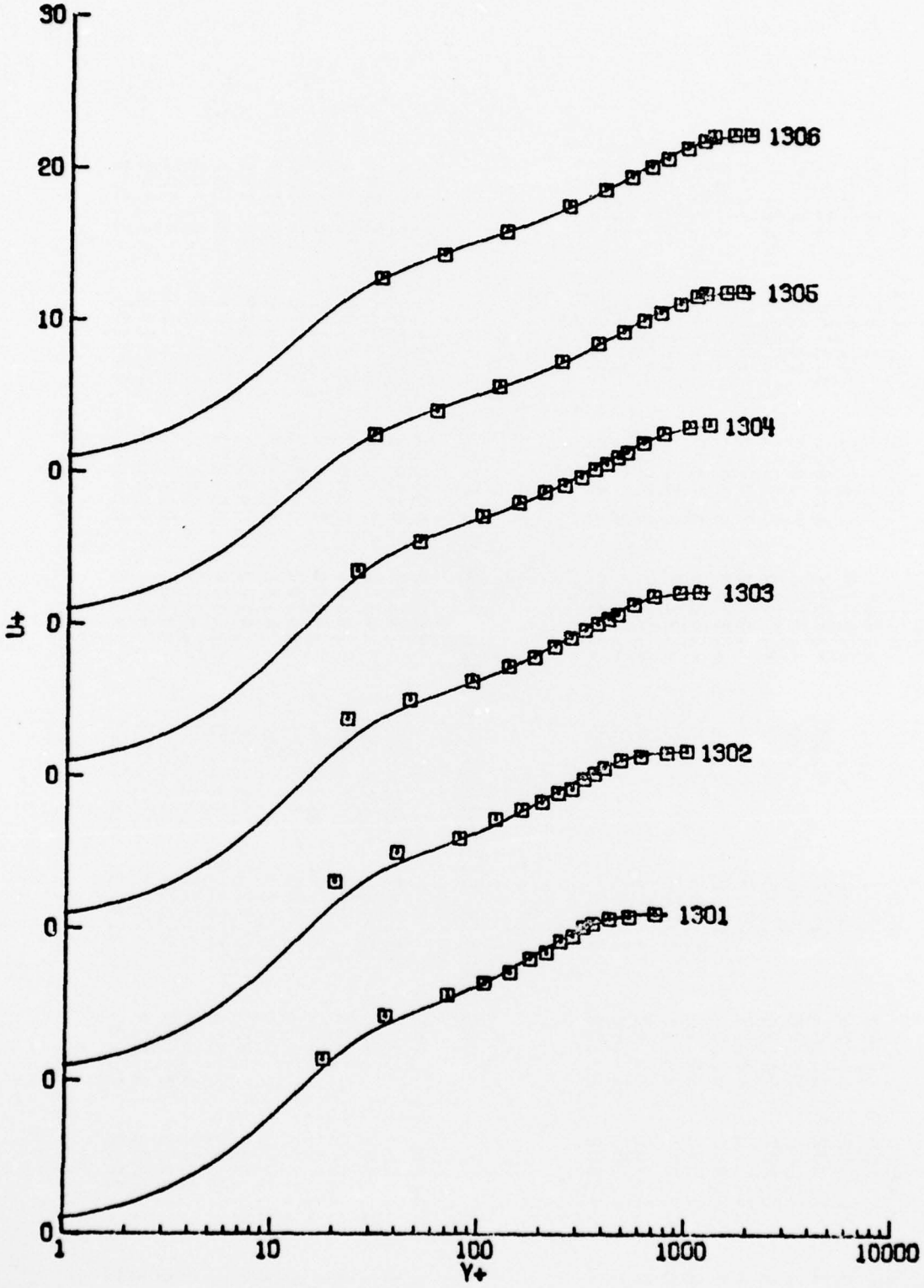

Figure D.1. Ludwieg and Tillman accelerating flow. (Note shifted origins on the U^+ axis).

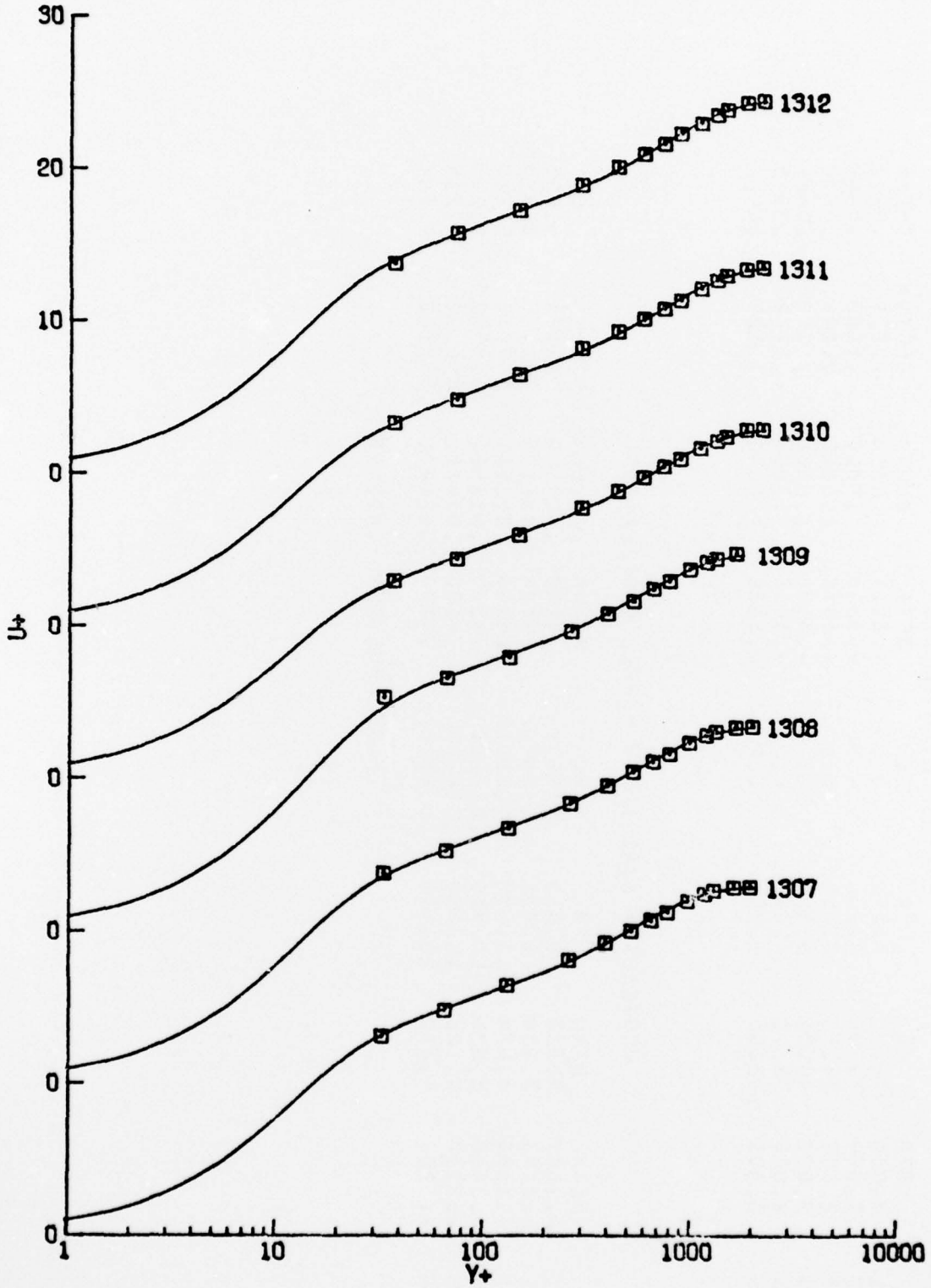

Figure D.1. (Continued).

TABLE D.2: HERRING AND NORBURY - BETA= -0.35
(ENGLISH UNITS)

NU= 1.730000E-04

EXPERIMENTAL VALUES

ID	XSTA	UE	UTAU	DUEDX	BETA	DELTA	DELTA*	THETA
2701	0.000	76.50	3.149	2.65	-.2111	.8500	.1239	.0921
2702	1.000	79.80	3.280	4.90	-.3883	.9000	.1282	.0960
2703	2.000	84.60	3.550	6.13	-.3896	1.0000	.1136	.0875
2704	3.000	90.50	3.798	6.20	-.3598	1.0000	.1110	.0856
2705	4.000	97.10	4.041	6.25	-.3413	1.0000	.1102	.0845
2706	5.000	103.60	4.270	6.25	-.3326	1.0000	.1124	.0860

UNSTEADY + SIMILARITY - FULL PROFILE FIT

ID	BETA	UTAU	S	K	KAPPA	EPSILON	TO+	G
2701	-.1887	3.310	9.662	.016800	.4100	.007229	.012621	4.455
2702	-.3178	3.609	8.711	.016800	.4100	.006523	.021758	3.853
2703	-.3583	3.674	10.675	.016800	.4100	.013147	.007235	5.119
2704	-.3408	3.873	10.910	.016800	.4100	.013561	.006332	5.275
2705	-.3238	4.120	10.656	.016800	.4100	.004101	.006526	5.239
2706	-.3107	4.392	10.476	.016800	.4100	.006431	.008102	4.987

MEAN EPSILON= .008499

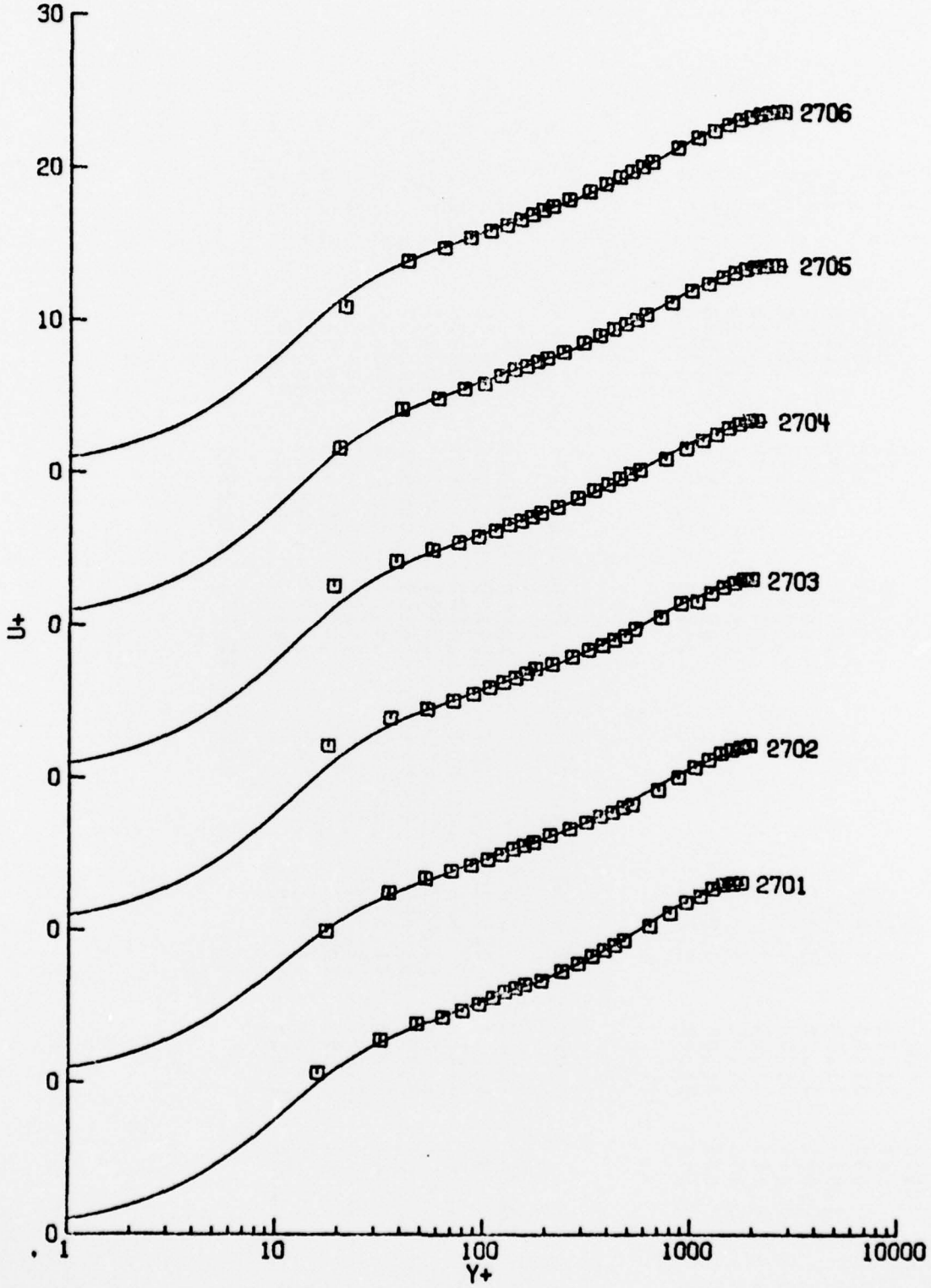

Figure D.2. Herring and Norbury mildly favorable pressure gradient equilibrium flow, β=-0.35. (Note shifted origins on the U^+ axis).

TABLE D.3: ANDERSEN, KAYS AND MOFFAT - ZERO P. G. - 120771-1
(ENGLISH UNITS)

NU= 1.590000E-04

EXPERIMENTAL VALUES

ID	XSTA	UE	UTAU	DUEDX	BETA	DELTA	DELTA*	THETA
8101	.167	31.21	1.557	.01	-.0005	.2871	.0504	.0328
8102	.833	31.13	1.467	.01	-.0007	.4225	.0772	.0521
8103	1.833	31.14	1.400	.01	-.0008	.6242	.1135	.0768
8104	2.833	31.05	1.353	.00	-.0007	.7854	.1412	.0977
8105	3.833	31.04	1.321	.00	-.0002	.9590	.1709	.1185
8106	4.833	31.13	1.298	-.00	.0006	1.1065	.1968	.1375
8107	5.833	31.04	1.272	-.01	.0020	1.2755	.2255	.1584
8108	6.833	31.07	1.254	-.01	.0038	1.4808	.2533	.1794
8109	7.500	31.06	1.246	-.01	.0053	1.5810	.2670	.1902

UNSTEADY + SIMILARITY - FULL PROFILE FIT

ID	BETA	UTAU	S	K	KAPPA	EPSILON	TO+	C_i
8101	-.0004	1.623	8.931	.016800	.4100	.023996	.019265	3.990
8102	-.0006	1.591	7.671	.016800	.4100	.018637	.038434	3.222
8103	-.0009	1.354	11.627	.016800	.4100	.009299	.004197	5.759
8104	-.0007	1.330	11.309	.016800	.4100	.006958	.005037	5.544
8105	-.0002	1.303	11.319	.016800	.4100	.009066	.005010	5.550
8106	.0007	1.244	12.547	.016800	.4100	.014487	.002461	6.392
8107	.0019	1.291	10.568	.016800	.4100	.011370	.007689	5.048
8108	.0039	1.229	11.987	.016800	.4100	.012638	.003408	6.006
8109	.0051	1.253	11.037	.016800	.4100	.009984	.005886	5.361

MEAN EPSILON= .012937

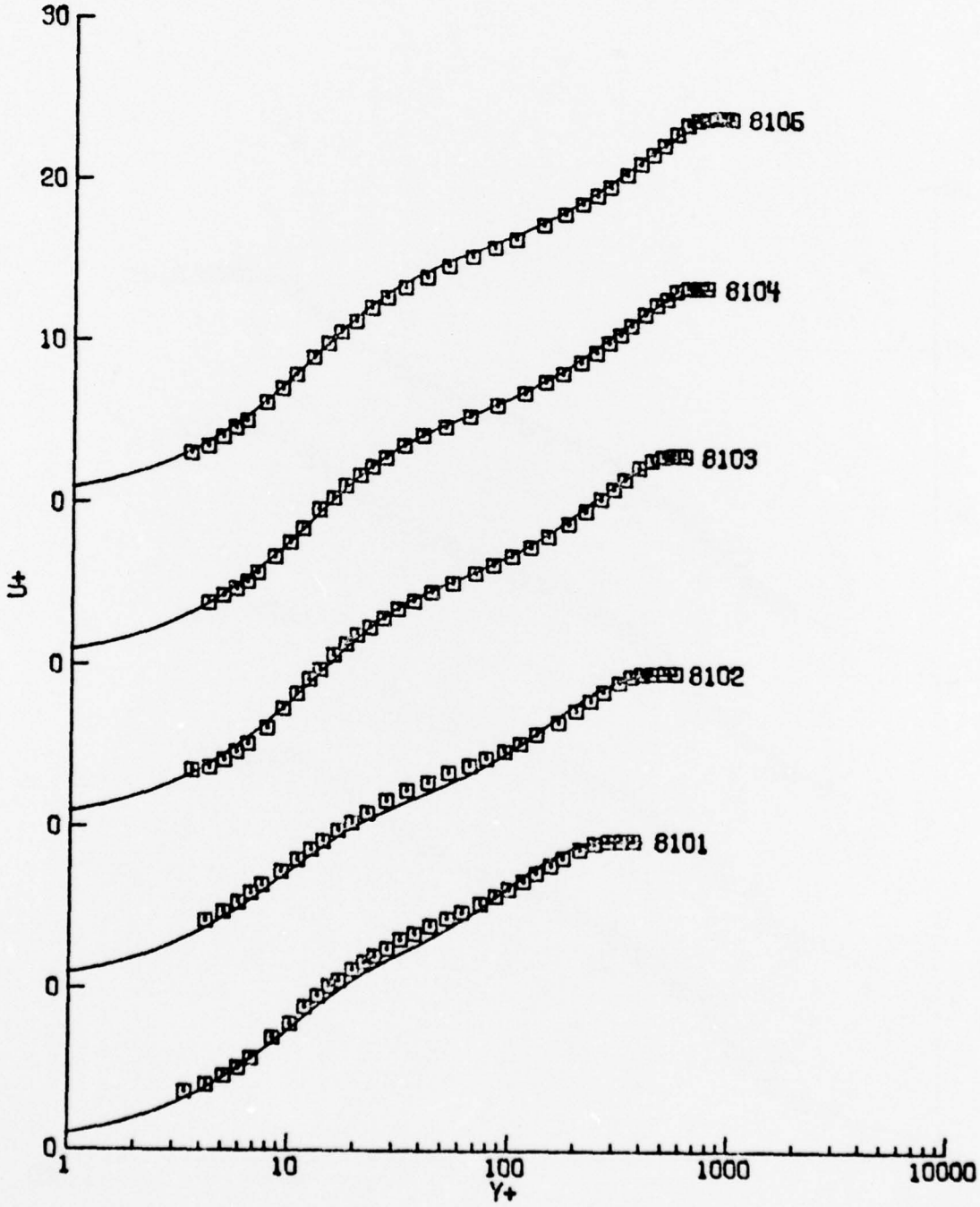

Figure D.3. Constant pressure flow of Andersen, et al (1972). (Note Shifted origins on the U^+ axis).

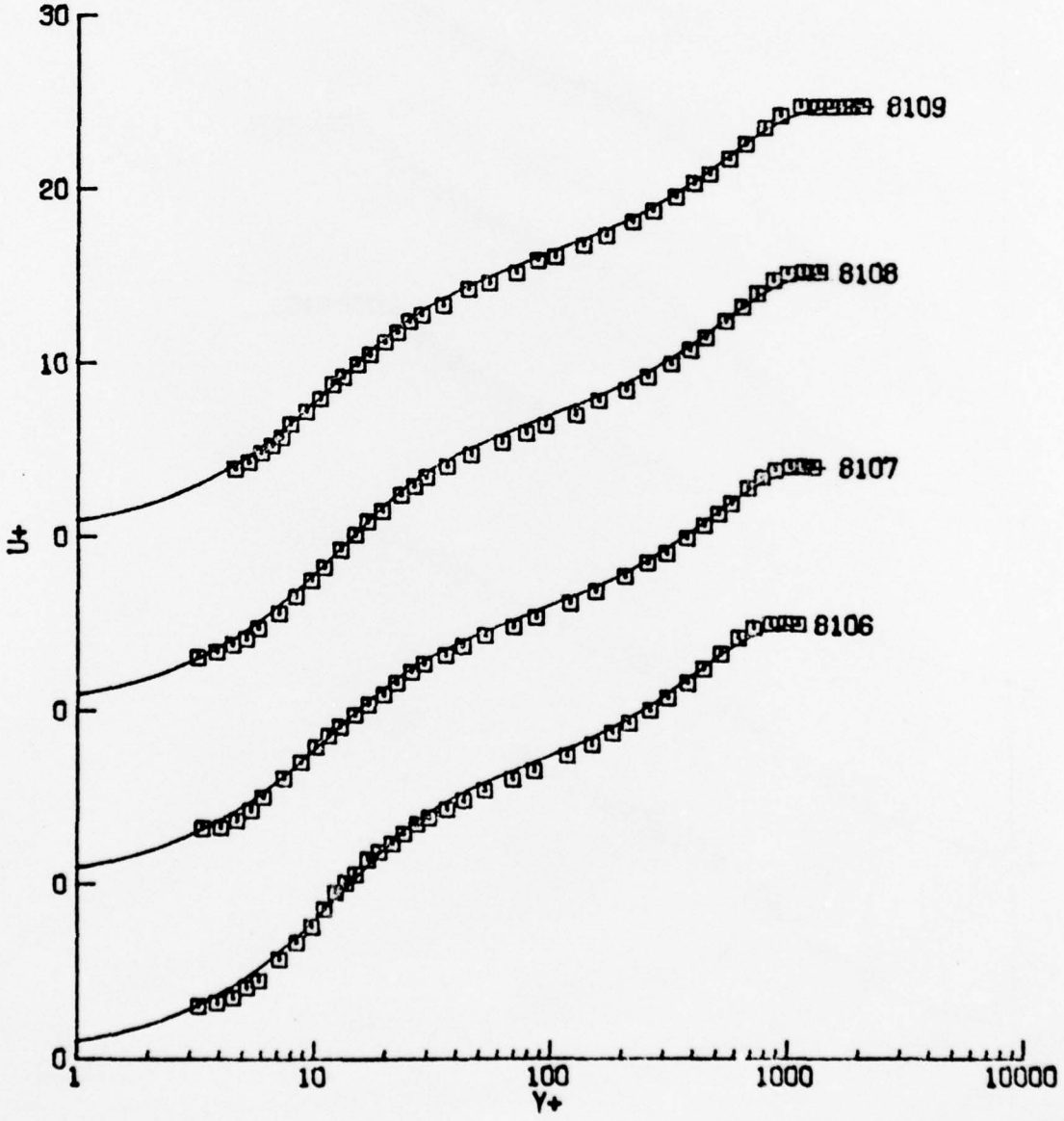

Figure D.3. (Continued).

TABLE D.4: ANDERSEN, KAYS AND MOFFAT MILD P. G. - 071571-5
(ENGLISH UNITS)

NU= 1.660000E-04

EXPERIMENTAL VALUES

ID	XSTA	UE	UTAU	DUEDX	BETA	DELTA	DELTA*	THETA
8201	.167	29.69	1.546	-2.44	.1404	.3081	.0556	.0357
8202	.833	26.93	1.198	-3.79	.6744	.5179	.1138	.0718
8203	1.833	24.57	1.010	-1.76	.6839	.8628	.1936	.1238
8204	2.833	23.26	.910	-1.13	.6919	1.1752	.2616	.1700
8205	3.833	22.27	.848	-.82	.7102	1.5029	.3356	.2176
8206	4.833	21.36	.799	-.63	.6910	1.7870	.3934	.2592
8207	5.833	20.74	.765	-.51	.6943	2.1211	.4610	.3049
8208	6.833	20.35	.742	-.43	.6765	2.4043	.5108	.3419
8209	7.500	20.05	.726	-.41	.7082	2.5701	.5449	.3656

UNSTEADY + SIMILARITY - FULL PROFILE FIT

ID	BETA	UTAU	S	K	KAPPA	EPSILON	TO+	C_i
8201	.1387	1.516	8.429	.016800	.4100	.023585	.025404	3.679
8202	.6935	1.169	7.449	.016800	.4100	.018403	.043348	3.092
8203	.6771	1.007	8.035	.016800	.4100	.013693	.031533	3.439
8204	.6647	.922	8.476	.016800	.4100	.012683	.024763	3.707
8205	.7520	.817	10.300	.016800	.4100	.013957	.008954	4.870
8206	.6538	.817	8.770	.016800	.4100	.013020	.021051	3.690
8207	.6469	.789	8.532	.016800	.4100	.011750	.024008	3.742
8208	.6168	.774	8.415	.016800	.4100	.012742	.025600	3.670
8209	.6449	.758	8.262	.016800	.4100	.013453	.027839	3.577

MEAN EPSILON= .014810

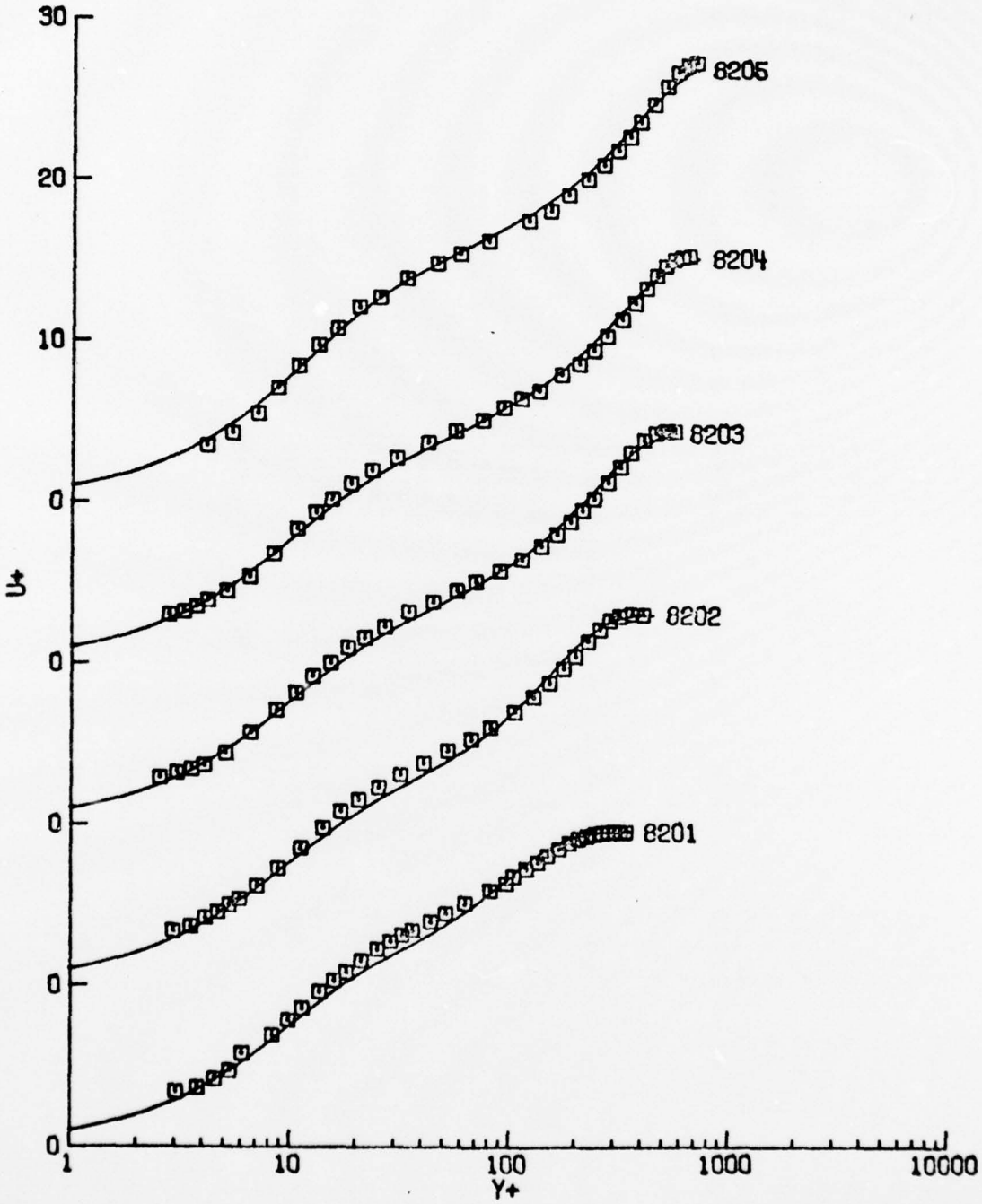

Figure D.4. Mild adverse pressure gradient flow of Andersen, et al. (1972). (Note shifted origins on the U^+ axis).

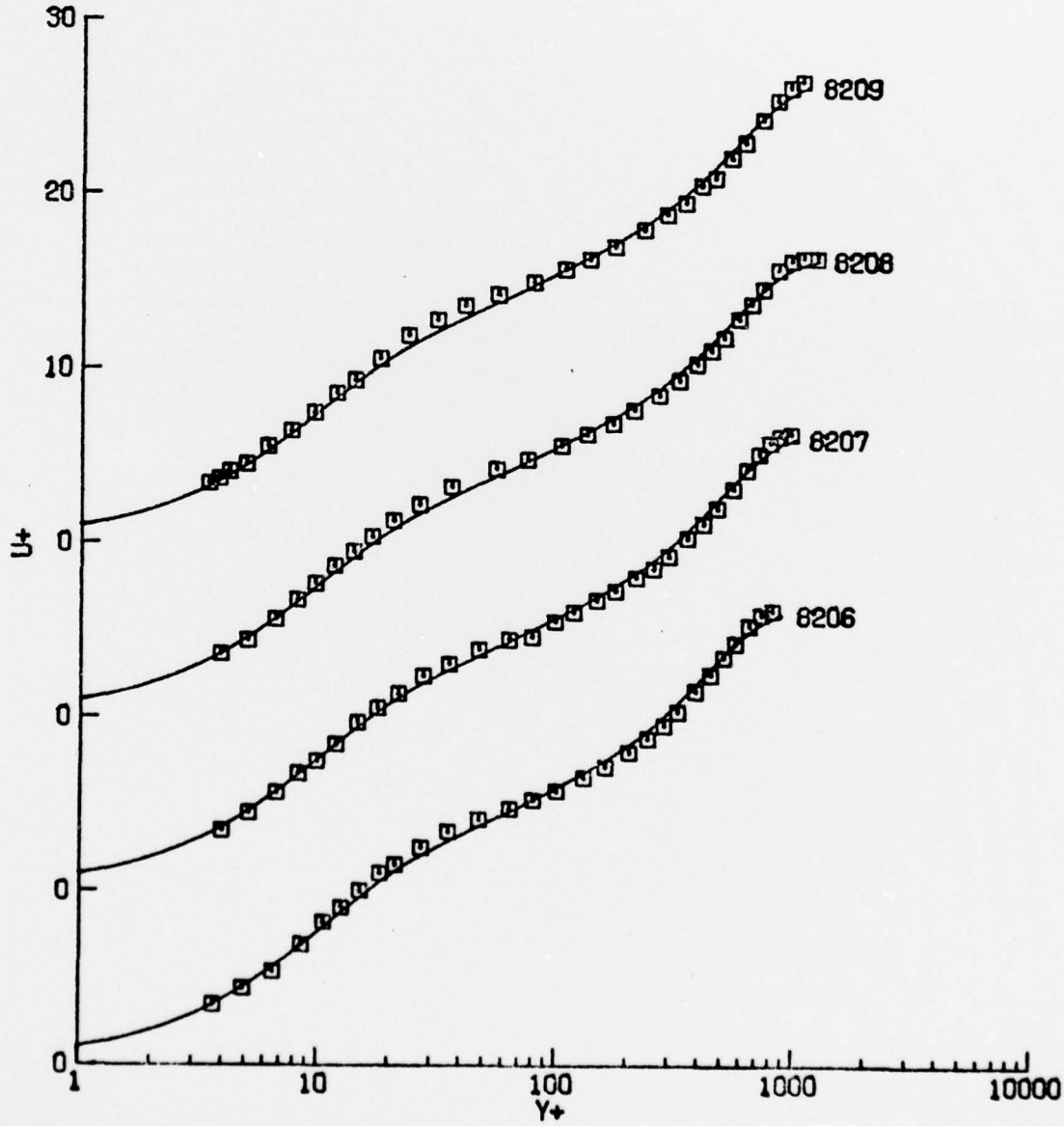

Figure D.4. (Continued).